University of Liège

Faculty of Sciences

Department of Life Sciences

Laboratory of Genetics and Physiology of Microalgae - InBioS

THESIS

Study of photosynthesis and alternative electron pathways in symbiotic cnidarians

Dissertation Submitted by

Félix Vega de Luna

Master in Sciences

in Fulfilment of the Requirements for the Doctorate in Sciences

Academic Year 2022-2023

Thesis jury members :

Claire PERILLEUX, PhD - Physiologie végétale, University of Liège, Belgium
(President)

Pierre CARDOL, PhD - Genetics and Physiology of Microalgae, University of Liège, Belgium
(Supervisor)

Stéphane ROBERTY, PhD - InBioS–Animal Physiology, University of Liège, Belgium
(Secretary)

Gilles LEPOINT, PhD - Ecologie Trophique et Isotropique, University of Liège, Belgium

Benjamin BAILLEUL, PhD - Institut de Biologie Physico Chimique, Sorbonne Université, France

Milán SZABÓ, PhD - Institute of Plant Biology, Eötvös Loránd Research Network, Hungary

European Research Council

List of Publications

Accepted

Vega De Luna F., Dang K. Van, Cardol M., Roberty S. & Cardol P. (2019) Photosynthetic capacity of the endosymbiotic dinoflagellate *Cladocopium sp.* is preserved during digestion of its jellyfish host *Mastigias papua* by the anemone *Entacmaea medusivora*. *FEMS Microbiology Ecology* 95, 1–7.

Vega de Luna F., Córdoba-Granados J.J., Dang K. Van, Roberty S. & Cardol P. (2020) *In vivo* assessment of mitochondrial respiratory alternative oxidase activity and cyclic electron flow around photosystem I on small coral fragments. *Scientific Reports* 10 (1). 1-13.

Gain G., Vega de Luna F., Cordoba J., Perez E., Degand H., Morsomme P., Thiry M., Baurain D., Pierangelini M. & Cardol P. (2021) Trophic state alters the mechanism whereby energetic coupling between photosynthesis and respiration occurs in *Euglena gracilis*. *New Phytologist* 232, 1603–1617.

Submitted

Roberty S., Vega de Luna F., Pierangelini M., Bomhals J., Plumier J.C., Levy O. & Cardol P. (2022) Shallow and mesophotic colonies of the coral *Stylophora pistillata* share regulatory strategies of photosynthetic electron transport but differ in their sensitivity to light.

ABSTRACT

The management of light energy during photosynthesis requires the concerted participation of multiple cellular processes, being the regulation of light absorption and the electron transfer in the photosynthetic machinery in the frontline. Due to the high diversity and divergence of microalgae groups, different molecular components can be found in their photosynthetic molecular machinery. Symbiodiniaceae, a family of dinoflagellates with a secondary-acquired peridinin chloroplast, contains a particular set of attributes. Members of this family perform mutualistic associations with a wide variety of animals, among which cnidarians are the most prominent. These photosynthetic cnidarians, such as the golden jellyfish *Mastigias papua* or the reef-building coral species *Stylophora pistillata*, obtain from their photosynthetic symbionts a variety of molecules to sustain their energetic demands, allowing them to participate as primary producers in marine ecosystems. The photosynthetic activity of these organisms have been documented, but details on the regulation of light absorption and photosynthetic electron transfer along their photosynthetic machinery is not well understood. In this work, the monitoring of the photosynthetic activity was addressed by spectroscopic methods, in order to provide information on the photosynthetic electron transfer activity of Symbidiniaceae in symbiosis with two cnidarians.

With the use of a chlorophyll *a* fluorescence imaging system we tracked the photosynthetic activity of the algal symbionts in the golden jellyfish *M. papua*. This jellyfish, together with its natural predator, the non-photosynthetic anemone *Entacmaea medusivora*, were collected from marine lakes in Palau, West Pacific. A peculiar phenomenon, observed during the field trip, brought a question on the fate of the algal symbiont, *Cladocopium sp.*, when its host was digested by the anemone. The monitoring of the photosynthetic activity revealed that *Cladocopium sp.* was highly resistant to digestion, but it did not form an endosymbiotic association with the anemone. Moreover, the photosynthetic electron transfer activity remained unaffected during the digestion, and even after being expelled with non-digested fractions.

The coral *S. pistillata* was used to standardise a protocol for more specialised spectroscopic methods. Diverse technical problems have been an obstacle for the monitoring of the photochemical process in these organisms due to their calcareous skeleton. This issue was solved by fragmenting coral branches, a process that some corals experience naturally. The coral fragments of colonies grown in aquarium conditions were then used to provide information on the photosynthetic electron transfer process and the alternative electron transfer pathways in Symbiodiniaceae in symbiosis. The occurrence of these alternative pathways was thereafter shown in corals collected at mesophotic and shallow depths from a coral reef in the Gulf of Eilat, Israel. The photosynthetic activity of these coral

colonies was compared, revealing differences in their sensitivity to light intensity and a differential use of the photosynthetic alternative electron pathways and photoprotection mechanisms. As part of the photoacclimation process of this coral species, the resistance of photosystem I to photoinhibition was observed.

Overall, in the symbiotic state, the Symbiodiniaceae species studied here showed a high resistance to harsh conditions, such as digestion of their jellyfish host by other animals, or by the mechanical stress when fragmenting their coral host. The photosynthetic activity of Symbiodiniaceae in symbiosis with *S. pistillata*, was found to present a series of photoacclimation strategies according to their environmental light conditions. Moreover, the photosynthetic activity of these algae include the use of photosynthetic alternative electron pathways. A feature that was found different from the information reported from algal cultures.

RÉSUMÉ DE THÈSE

La gestion de l'énergie lumineuse lors de la photosynthèse nécessite la participation concertée de multiples processus cellulaires, dont la régulation de l'absorption de la lumière et le transfert d'électrons dans la machinerie photosynthétique. En raison de la grande diversité et de la divergence des groupes de microalgues, différents composants moléculaires peuvent être trouvés dans leur machinerie moléculaire. Les Symbiodiniaceae, une famille de dinoflagellés avec un chloroplaste de péridinine acquis secondairement, contient un ensemble particulier d'attributs. Les membres de cette famille effectuent des associations mutualistes avec une grande variété d'animaux, parmi lesquels les cnidaires sont les plus importants. Ces cnidaires photosynthétiques, comme la méduse *Mastigias papua* ou l'espèce de corail constructeur de récifs *Stylophora pistillata*, obtiennent de leurs symbiotes photosynthétiques une variété de molécules pour soutenir leurs besoins énergétiques, leur permettant de participer en tant que producteurs primaires aux écosystèmes marins. L'activité photosynthétique de ces organismes a été documentée, mais les détails sur la consommation d'énergie au sein de leur machinerie photosynthétique ne sont pas bien compris. Dans ce travail, le suivi de l'activité photosynthétique a été abordé par des méthodes spectroscopiques, afin de fournir des informations sur l'activité photosynthétique de transfert d'électrons des Symbidiniaceae en symbiose avec deux cnidaires.

Grâce à l'utilisation d'un système d'imagerie par fluorescence de chlorophylle a, nous avons suivi l'activité photosynthétique des symbiotes algaux chez la méduse *M. papua*. Cette méduse, ainsi que son prédateur naturel, l'anémone non photosynthétique *Entacmaea medusivora*, ont été collectés dans des lacs marins à Palau, dans le Pacifique Ouest. Un phénomène particulier, observé lors de la sortie sur le terrain, a amené à s'interroger sur le devenir du symbiote algal, *Cladocopium sp.*, lorsque son hôte était digéré par l'anémone. Le suivi de l'activité photosynthétique a révélé que *Cladocopium sp.* était très résistante à la digestion, mais elle ne formait pas d'association endosymbiotique avec l'anémone. De plus, l'activité photosynthétique de transfert d'électrons n'est pas affectée pendant la digestion, et même après avoir été expulsée avec des fractions non digérées.

Le corail *S. pistillata* a été utilisé pour standardiser un protocole pour des méthodes spectroscopiques plus spécialisées. Divers problèmes techniques ont été un obstacle pour le suivi du processus photochimique dans ces organismes en raison de leur squelette calcaire. Ce problème a été résolu en fragmentant les branches de corail, un processus que certains coraux subissent naturellement. Les fragments de corail des colonies cultivées dans des conditions d'aquarium ont ensuite été utilisés pour fournir des informations sur le processus de transfert d'électrons photosynthétique et les voies alternatives de transfert d'électrons chez les Symbiodiniaceae en symbiose. L'occurrence de ces voies

alternatives a ensuite été démontrée chez les coraux collectés à des profondeurs mésophotiques et peu profondes d'un récif corallien dans le golfe d'Eilat, en Israël. L'activité photosynthétique de ces colonies coralliennes a été comparée, révélant des différences dans leur sensibilité à l'intensité lumineuse et une utilisation différentielle des voies alternatives photosynthétiques des électrons et des mécanismes de photoprotection. Dans le cadre du processus de photoacclimatation de cette espèce de corail, la résistance du photosystème I à la photoinhibition a été observée.

Globalement, à l'état symbiotique, les espèces de Symbiodiniaceae étudiées ici ont montré une forte résistance aux conditions difficiles, telles que la digestion de leur hôte méduse par d'autres animaux, ou par le stress mécanique lors de la fragmentation de leur hôte corallien. L'activité photosynthétique des Symbiodiniaceae en symbiose avec *S. pistillata* s'est avérée présenter une série de stratégies de photoacclimatation en fonction de leurs conditions d'éclairage environnementales. De plus, l'activité photosynthétique de ces algues comprend l'utilisation de voies d'électrons photosynthétiques alternatives. Une caractéristique qui s'est avérée différente des informations rapportées à partir des cultures d'algues.

List of Abbreviations

α	Quantum yield of O2 evolution
acpPC	Chl a – Chl c_2 – Per Protein Complex
APX	Ascorbate Peroxidase
ATP	Adenosine triphosphate
CA	Carbonic Anhydrase
CBB	Calvin Benson Bassham
CCD	Charge-Coupled Device
CCM	Carbon concentrating mechanism
CEF	Cyclic Electron Flow
Chl a	Chlorophyll a
Chl c_2	Chlorophyll c_2
CO_2	Carbon dioxide
Cyt c_6	Cytochrome c_6
^{3}Chl a	Triplet excited state of chlorophyll a
CN	Cyanide
$\Delta\psi$	Electric field across the thylakoid membrane
DCMU	3-(3,4-dichlorophenyl)-1,1-dimethylurea
Ddx	Diadinoxanthin
Dtx	Diatoxanthin
ECS	Electrochromic Shift
Eo	Gross photosynthetic oxygen evolution
ECS	Electrochromic Shift
FvFm	Maximum quantum yield of PSII
φPo	Maximum quantum yield of PSII
φPSII	Effective quantum yield of PSII
Fd	Ferredoxin
FNR	Ferredoxin NADP Reductase
FQR	Ferredoxin Plastoquinone Reductase
FLV	Flavodiiron protein
HA	Hydroxylamine
HCO_3^-	Bicarbonate ion
Ic	Light-compensation point for oxygen exchange
Ik	Minimum saturating irradiance of the photosynthetic activity
LED	Light Emiting Diode
LHC	Light Harvesting Complex
LHCII	Light Harvesting Complex of PSII
MDAR	Mono-dehydroascorbate reductase
NDH1	Type I NAD(P)H dehydrogenase
NDH2	Type II NAD(P)H dehydrogenase
$^1O_2$	Singlet oxygen species
O_2^-	Superoxide radical
OEC	Oxygen Evoling Complex
P680	Primary electron donor of PSII
P700	Primary electron donor of PSI
PCP	Per – Chl a Protein
Per	Peridinin
PGR5	Proton Gradient Regulator
PGRL1	Proton Gradient Regulator-Like 1
pmf	Proton motive force
PPFD	Photosynthetic photon flux density
PQ	Plastoquinone
PQH_2	Plastoquinol
PSI	Photosystem I
PSII	Photosystem II
PTOX	Plastid Terminal Oxidase
QA	Quinone A
RC	Reaction Centre
Rd	Respiration in dark conditions
rETR	Relative Electron Transfer Rate
ROS	Reactive Oxygen Species
SOD	Superoxide Dismutase
Rubisco	Ribulose 1,5-bisphosphate carboxylase oxygenase
Vo	Net oxygen exchange rate
WWC	Water to Water Cycle

TABLE OF CONTENTS

List of Figures and Tables

CHAPTER 1   Introduction to photosynthetic cnidarians

Coral reefs are found in a nutrient-poor marine environment but are considered to be among the most biodiverse ecosystems on earth (**Reaka-Kudla, 1997**). This counter-intuitive fact is explained by the capacity of coral reef building species to take advantage of sunlight's energy and take part in the reef as primary producers (**Falkowski et al., 1984**). This ability is present in several cnidarian species in other aquatic environments, and it is possible thanks to a specialised intracellular mutualistic relationship with unicellular photosynthetic algae (**Furla et al., 2011**) (**Figure 1**). The algae thus provide their animal hosts with an extraordinary productivity capacity, able to drive the nutritional recycling within an entire coral reef (**Crossland et al., 1991**).

The use of light energy is carried out by photosynthesis, the process by which photosynthetic organisms use light (in the range of 400 to 700 nm) to power their metabolism. This process is based on a complex molecular machinery of pigments and proteins housed in the thylakoid membrane structure located in the chloroplast. The genes coding for this photosynthetic machinery are found in some well-defined groups of organisms. In the dinoflagellate algal symbiont of cnidarians, a complex evolutionary history ended up in a particular set of photosynthetic features (**Dorrel and Howe, 2015**), which differ substantially from the common features found in green algae and plant model organisms.
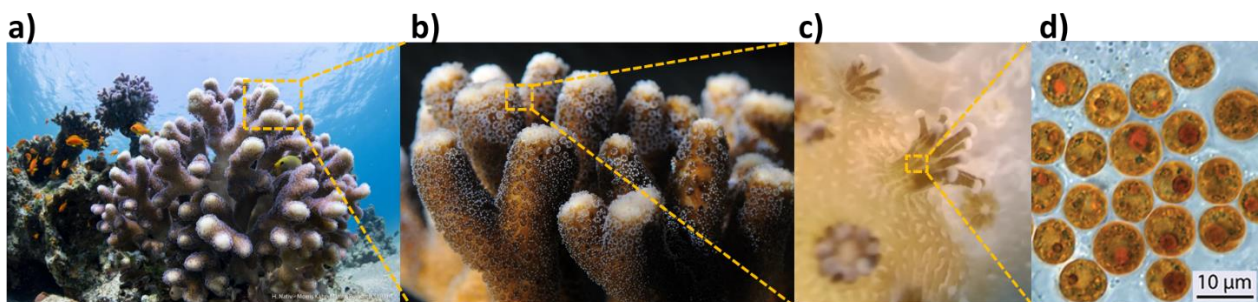
Figure 1. The reef-building coral *Stylophora pistilla*, a photosynthetic cnidarian. **a)** A coral colony of *Stylophora pistillata* found in the reef of shallow waters in the Red Sea and **b)** a zoom in to the terminal tips of its branches (**Karako-Lampert et al., 2014**). **c)** A view of a polyp from a coral fragment at the stereoscopic microscope. **d)** A photomicrograph of cnidarian tissue showing the brownish dinoflagellate algal symbionts, in contrast to the colourless cnidarian cells (image taken from *http://tolweb.org/Symbiodinium/*).

Even though the use of light energy brings a big energetic advantage, it is heavily subjected to its natural variations. Fluctuations of light intensity and environmental conditions at several time spans

are common at any spot of our planet's surface, and are also common in the habitat of photosymbiotic cnidarians (**Roth, 2014**). These provoke temporal variations of energy input, either as a decrease or an increase of energy availability relative to its rate of use. Such strong environmental pressure has promoted that photosynthetic organisms evolved with mechanisms to improve their efficiency of light energy use, but also with mechanisms that prevent the damage to their molecular structures by excessive energy. These regulatory mechanisms have been shown to exist in several photosynthetic species, but most of those descriptions have been done on plants and green algae. Other key ecological species, such as the dinoflagellate symbiont of cnidarians, have been recently recognized for their relevance in marine ecosystems. Understanding those mechanisms in their photosynthetic process allows us to better comprehend the impact of natural or anthropogenically-related environmental variations on the energy management in these species.

Cnidarians and their algal symbiont

Cnidarians are early divergent aquatic invertebrate animals with radial symmetry and a quite simple tissular architecture. Several species of this phylum are well known to perform a mutualistic symbiotic relationship with unicellular photosynthetic algae (**Figure 2**). Their energetic demand is thus satisfied by photosynthetically-fixed carbon by their algal symbionts (photoautotrophy) and by feeding on organic particles such as detritus or microorganisms (heterotrophy) (**Falkowski et al., 1984**). These "photosynthetic cnidarians" live in the photic zone of the water column, from depths close to the surface until depths receiving a fraction of 1 % of surface irradiance, where they have access to light energy used by their photosynthetic symbionts (**Tamir et al., 2019**). They live in tropical marine waters (a good representative is a coral species or a sea anemone), although few others are found in temperate freshwater environments (such as green hydra). There is a good agreement that the common ancestor of cnidarians was not symbiotic, and instead the symbiotic capacity appeared in several cnidarian groups along their evolutionary history (**Kayal et al., 2018**). Two of the three main classes of Cnidaria contain well known groups of symbiotic species that acquired this capacity independently (**Figure 2a**) : Anthozoa (including corals, sea anemones and sea pens; **Kayal et al., 2018; Emery et al., 2021) (Figure 2b and c**) and Medusozoa (including jellyfishes and hydras; **Kayal et al., 2018; Djeghri et al., 2019**) (**Figure 2f and g**). The reef-building species, so-called stony or hard corals, are grouped mainly in the Scleractinian order of Anthozoa, and have a robust symbiotic and colonial story (**Barbeitos et al., 2010**) but a non-symbiotic origin (**Navarro et al., 2020**). Endocnidozoa, the third class of Cnidaria is composed of microscopic parasitic species, and no report exists until now about a possible endosymbiotic past (**Kayal et al., 2018**).

The algal symbionts of photosynthetic cnidarians belong to more restricted clades. The majority of symbiotic cnidarians harbour unicellular dinoflagellate algae from the family Symbiodiniaceae (Suessiales, Dinophyceae), previously known as "zooxanthella". While other few species, such as those of the *Anthopleura* genus in the Anthozoa class, can harbour both Symbiodiniaceae species and Trebouxiophyceae species from the genus *Chlorella* (Trebouxiophyceae, Chlorophyta), also known as "zoochlorella" (**Lewis and Muller-Parker, 2004**). In addition, green *Hydra* species (Hydrozoa) only harbour *Chlorella* species as photosynthetic symbionts (**Kawaida et al., 2013**) (**Figure 2 j and k**).

The Symbiodiniaceae family is currently composed of eleven genera of free-living and facultative symbiotic species (**LaJeunesse et al., 2018; Pochon and LaJeunesse, 2021**). Because of almost null morphological differences, they were previously grouped in clades designated with letters (A, B, C, D, etc) due to genetic differences found at the sequence level (using the internal transcribed spacers ITS1 and ITS2 rRNA gene; **Hume et al., 2018**). After the curation done by **LaJeunesse et al.** in **2018**, Symbiodiniaceae was defined as a family and the clades were recognized as genera (*Symbiodinium*, *Breviolum*, *Cladocopium*, *Durusdinium*, *Effrenium*, *Freudentalidium*, *Fugacium*, *Gerakladium*, *Halluxium*, *Miliolidium* and *Phylozoon*). Species from *Cladocopium* genus are the most widespread and dominant symbionts in corals along the Indo-Pacific region (**LaJeunesse, 2004**), and together with *Breviolum* species they dominate the Caribbean in the Atlantic region (**van Oppen et al., 2008**). While in the open ocean, both *Symbiodinium* and *Cladocopium* free-living species are dominant over the other genera (**Decelle et al., 2018**). The descriptions in this document are centred on the mutualistic symbiosis existing between cnidarians and Symbiodiniaceae.

The cnidarian tissue

The tissular organisation of cnidarians, being diploblastic animals, consists of two cell layers, the ectoderm and the endoderm, separated by an extracellular matrix called mesoglea which contains few cells. This bilayered tissue folds to delimit the animal body creating a compartment called coelenteron and separating the oral and the aboral regions, the regions nearest the mouth and furthest from the mouth, respectively (**Figure 2d, h and l**). The endoderm, also called gastrodermis because it is the cell layer exposed to the gastric cavity, contains the cells that harbour intracellularly the algal symbionts in Anthozoans and Hydrozoa (**Tresguerres et al., 2017; Figure 2e and m**). In Scyphozoans, from the class Medusozoa, these alga-hosting cells originate from the gastrodermis and then migrate to the mesoglea, where they become amoebocytes (**Colley and Trench, 1985; Djeghri et al., 2019**) (**Figure 2i**). The cnidarian reproductive cells do not contain algal symbionts and neither

do their gametes. Instead, the eggs or the larvae acquire the algal symbiont after spawning during sexual reproduction (**Byler et al., 2013**). Only in symbiotic Medusozoa the algal symbiont is obligatorily required for the metamorphosis of polyps into the ephyra stage, a process called strobilation (**Lampert, 2016**).
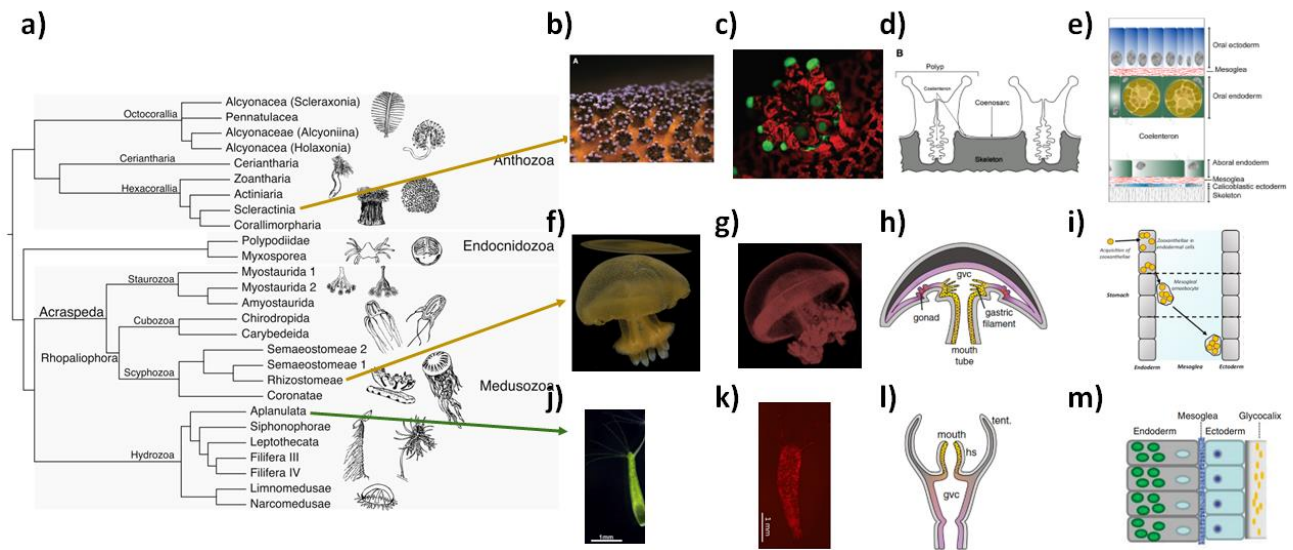
Figure 2. Photosynthetic cnidarians. **a)** Phylogenetic relationship of cnidarian groups (**Kayal et al., 2018**). True colour picture (**b, f and j**) and chlorophyll *a* fluorescence imaging (**c, g and k**) of representative photosymbiotic species. From top to bottom, *Pocillopora damicornis* polyps (**b** and **c**) (**Putnam et al., 2017**), *Mastigias papua* jellyfish (**f** and **g**) (**Vega de Luna et al., 2019**) and *Hydra viridissima* (**j** and **k**) (**Kawaida et al., 2013**; **Ishikawa et al., 2016**). d) The schematic localization of the photosynthetic symbionts in the cnidarian tissue of Hexacorallia (**d** and **e**) (**Tambutté et al., 2011**), Scyphozoa (**h** and **i**) (**Djeghri et al., 2019**) and Hydrozoa (**l** and **m**) (**Bosch and Miller, 2016**) is indicated.

Photosynthetic cnidarians are said to have two strategies of symbiont cell transmission to their progeny, a vertical and a horizontal transmission (**Byler et al., 2013**). The horizontal strategy is the most common and allows the larvae or juveniles to acquire the algal symbiont from the environment, while the vertical transmission consists in the early association, usually when the eggs are released, with the parental algal strain (**Turnham et al., 2021**). With new sequencing technologies, it is now clear that there is a subtle specificity in the cnidaria-Symbiodiniaceae partnership formation, being more specific in those species with vertical transmission, and more generalistic in the horizontal transmission mode (**Fabina et al., 2012**). In addition to this, during their ontological development, cnidarian species, such as corals, may select and stimulate the abundance of a particular population

of Symbiodiniaceae according to their environmental conditions (**Cohen and Dubinsky, 2015**). Many coral species in their adult stage contain few Symbiodiniaceae species, while few others harbour a broader spectrum of them (**Silverstein et al., 2012; Byler et al., 2013**). It is a common thought that the establishment of symbiotic relationships with different Symbiodiniaceae species increases the chances to withstand different kinds of stresses. Some coral species have been reported to shift their Symbiodiniaceae algal community after a stressing period (**Reich et al., 2017; Quigley et al., 2019**). For those corals with a vertical transmission, a mixed strategy (reflecting the capacity of acquiring new algal symbionts at older stages) would allow them to associate with more beneficial Symbiodiniaceae types under unfavourable conditions (**Swain et al., 2018**). On the top of this complexity, the cellular responses of the host to a non-dominant algal species might require gene expression adjustments (**Medrano et al., 2019; Tivey et al., 2020**). It has been observed, for example, some differences in the metabolic activity of *Aiptasia sp.*, when it was associated with a Symbiodiniaceae species different from its natural symbiont (**Starzak et al., 2014**).

The symbiosome

Cnidarians contain a limited diversity of cell types (**Tresguerres et al., 2017**). In the endoderm layer some specialised cells contain the algal symbionts intracellularly within a host-derived vacuole, called symbiosome (**Figure 3a**). The mutualistic *endo*symbiotic relationship in these alga-hosting cells is markedly influenced by cellular events occurring in both symbionts, such as the cell division (**Camaya, 2020; Tivey et al., 2020**). It is particularly impressive the extent of the volume that Symbiodiniaceae occupies within these alga-hosting cells, which can be more than 90 % of the cytosol (**Gates et al., 1992**).

The establishment of the symbiotic relationship can occur during the larval and the adult stage of the animal (**Byler et al., 2013; Mies et al., 2017**), but the details of this process at the molecular level remain vastly unknown. No excreted signalling molecules have been reported so far in cnidarians that may attract their potential algal symbiont. By contrast, it has been proven that motile free-living Symbiodiniaceae can be attracted by the fluorescence emission of corals (**Aihara et al., 2019**). Although the function of host-derived fluorescent proteins in corals is not yet clear, their abundance has been reported to be more evident after the loss of their photosynthetic symbionts during a bleaching event (**Bollati et al., 2020**).

The cellular recognition relies on cell surface components, such as lectins and glycoproteins, on both host and symbiont (**Fransolet et al., 2012**). Interestingly it has recently been proven that photosynthetic activity is not a requirement for the establishment of the intracellular allocation of the

algae (**Jinkerson et al., 2022**). The infectivity of Symbiodiniaceae to artificially-induced non-symbiotic *Aiptasia sp*., and to juvenile polyps of *Acropora tenuis*, was shown to correlate with the algal cell size, with large Symbiodiniaceae cell strains (>10 μm of diameter) being less or not infective (**Biquand et al., 2017**). This feature, however, was shown to not be determinant for the retention of the alga, thus indicating that downstream steps in the symbiosis establishment depend on different processes. After the gastrodermal cells engulf the algae, they allocate them within the phagosome, and are not digested but undergo a still-unclear pathway to originate the symbiosome (**Davy et al., 2012**). This step is accompanied by transcriptional changes that might regulate the immune response of the host, with similar patterns in *Aiptasia* and the coral *Acropora* (**Mohamed et al., 2016**). In this way, the symbiosome consists of a subcellular structure delimited by an animal cell membrane of cytoplasmic origin, containing the alga (**Figure 3b**).

Within the symbiosome, Symbiodiniaceae cells are found as non-motile spherical cells. In culture, the free-living cells can be found in two morphological stages, one is a motile, also referred as gymnodinioid morphology or mastigote form, and the other is the non-motile spherical, also called coccoid form (**Figure 3c**). The two morphological types alternate during a diurnal cycle in culture (**Fitt and Trench, 1983**) and possess differences in the thickness and structure of their cell wall (**Yamashita and Koike, 2015**) (**Figure 3d**). The dinoflagellate cell wall is described as a structure called amphiesma, where the cellulosic thecal plates are surrounded by the plasma membrane and accompanied by vesicles in the mastigote (**Wang et al., 2011**) (**Figure 3e**), whereas the coccoid contains a thick pellicle layer (**Yamashita and Koike, 2015**) (**Figure 3d**). Although this structure has not been well studied in Symbiodiniaceae, it has been proposed that it gives origin to a multiple membrane layers structure within the symbiosome through a series of rearrangements once the alga localises in the phagosome (**Wakefield et al., 2000**) (**Figure 3f**). The symbiosome, thus, contains additional membrane layers of algal origin that are located between the algal cell wall and the host vacuolar membrane.
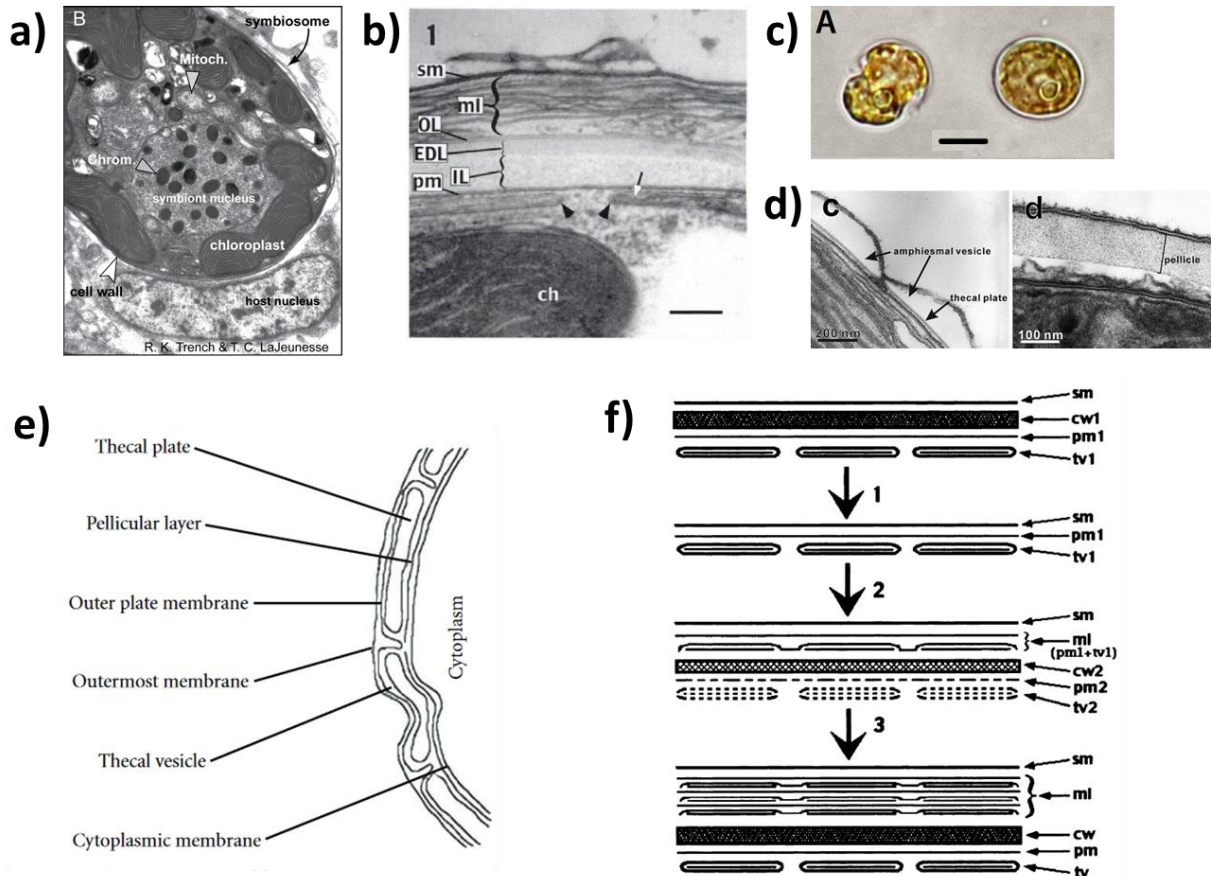
Figure 3. Symbiosome structure in cnidarians. **a)** Symbiodiniaceae as found in symbiosis with reef-building corals (image taken from http://tolweb.org/Symbiodinium/). Subcellular structures are indicated, such as the alga-hosting cell's nucleus (host nucleus) and the symbiosome, as well as the algal symbiont's cell wall, nucleus, chromosomes (Chrom), chloroplast and mitochondria (Mitoch). **b)** Detailed view of the symbiosome limiting membranes. sm- symbiosome membrane, ml- multiple membrane layers, OL- membranous outer layer, EDL- electron dense cell wall layer, IL- inner cell wall layer, pm- algal cell plasma membrane, ch- chloroplast, arrowheads indicate thecal vesicles and the bar indicates 100 nm (**Wakefield et al., 2000**). **c)** Photomicrograph of *Symbiodinium microadriaticum* in culture showing the mastigote (left) and coccoid (right) morphology (**LaJeunesse, 2017**), the bar indicates 5 μm. **d)** Transmission electron microscopy image of Symbiodiniaceae CS-156 in culture showing the cell wall details of the mastigote (left) and coccoid (right) (**Yamashita and Koike, 2015**), left and right bar indicate 200 and 100 nm, respectively. **e)** Schematic detail of the amphiesma structure in the motile dinoflagellate *Alexandrium catenella*, Gonyaulacales, Dinophyceae (**Wang et al., 2011**), indicating the membrane arrangement and the thecal plates. **f)** Hypothetic transformation of the amphiesma structure into the multiple membrane layers in the symbiosome

(**Wakefield et al., 2000**) The numbers refer to two intermediate steps of the transformation of the amphiesma into the membrane layers during two consecutive removal of the cell wall. sm: surface of symbiosome membrane; cw: cell wall; pm: symbiont plasma membrane; tv: thecal vesicles; ml: multiple layers of membrane.

The environment inside the symbiosome, surrounding the algal symbiont, has been poorly characterised, but it has been found to be acidic with a pH value of approximately 4, as the result of an active pumping of H^+ by a host's vacuolar and an algal P-type H^+-ATPase (**Figure 4**; **Bertucci et al., 2010**; **Barott et al., 2015a**). Despite the peculiar structural complexity of the membranes in the symbiosome, it is postulated that such acidic conditions allows bicarbonate ions (HCO_3^-) to be dehydrated by carbonic anhydrases (CA), in order to enrich with CO_2 the algal environment (**Barott et al., 2015a**; **Raven et al., 2020**).
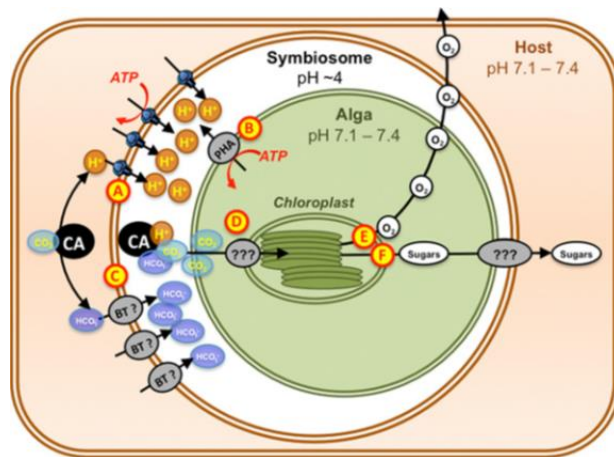
Figure 4. Symbiosome lumen acidification by the action of a H^+ pumping and its postulated role in the inorganic carbon assimilation (image taken from **Barott et al., 2015a**). The vacuolar H^+ ATPase (A) and the algal P-type ATPase (B) actively pump H^+ into the symbiosome lumen. HCO_3^- is transported by a bicarbonate transporter located in the vacuolar membrane of the symbiosome (C). The action of carbonic anhydrase (CA) is also depicted. The resulting CO_2 might diffuse or be transported by an unknown mechanism (D) to reach the carbon fixation sites within the algal chloroplast. As photosynthetic products, oxygen (O_2) diffuses out of the cells (E) and sugars are transported to the cnidarian host (F).

Despite the lack of a better picture on the symbiosome, it can be said that its peculiarities impose a radically different environment to the algal symbiont in comparison to the free-living conditions. Alga-hosting cells, on the other hand, must also regulate the metabolite exchange between the animal neighbouring cells and Symbiodiniaceae.

Nutritional interactions in the cnidarian-Symbiodiniaceae symbiosis

The translocation of photosynthates from Symbiodiniaceae to the cnidarian host has been shown to constitute an important fraction of the algal productivity (**Figure 5**). In the Scleractinian coral *Stylophora pistillata*, less than 5 % of the net fixed carbon is used by the algal symbiont for cell growth and respiration, and the translocated photosynthates represent more than 120 % of the host's daily demand for growth and respiration (**Muscatine, 1984**). Similar values were reported for the Scyphozoan jellyfish *Mastigias sp*. (**McCloskey et al., 1994**). In the coral *Pocillopora damicornis*, the photosynthetically-derived molecules can be stored as lipid droplets and starch granules in the alga, and are distributed in the cnidarian tissues where they can, in turn, be stored as lipid droplets in the oral gastrodermis and as glycogen granules in the oral epidermis (**Kopp et al., 2015**).
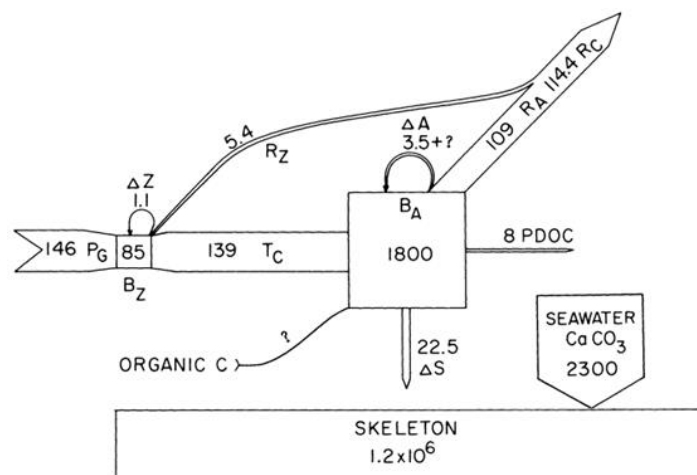
Figure 5. Carbon fluxes model in *Stylophora pistillata* living in shallow depths (image taken from **Falkowski et al., 1984**). Flux values (in $\mu g\ C\ cm^{-2}\ d^{-1}$) are indicated for gross photosynthesis (P_G), carbon translocated from algae to animal (T_C), algae respiration (R_Z), algal growth (ΔZ), animal respiration (R_A), whole coral respiration (R_C), particulate and dissolved organic carbon excreted by the coral (PDOC), animal growth (ΔA) and skeleton growth (ΔS). Biomass values (in $\mu g\ C\ cm^{-2}$) are indicated for algae (B_Z) and animal tissue (B_A).

In the sea anemone *Aiptasia pallida*, the soft corals *Discosoma sp*. and *Cladiella sp*., and the Scleractinian coral *Acropora millepora*, the major carbon-containing molecule exported from Symbiodiniaceae has been found to be glucose (**Burriesci et al., 2012**). A set of cnidarian glucose transporters (GLUT), as well as putative algal ammonium (AMT) and nitrate transporter (NTR2) were identified as potential symbiosis specific in genomic and transcriptomic databases (**Sproles et**

al., 2018). However, the cellular location of GLUT8, one of the glucose transporter candidates, was also found in the non-symbiotic stage of the anemone *Exaiptasia diaphana* (**Mashini et al., 2022**). The algal symbiont also provides carbon skeletons for amino acids synthesis (**Ferrier-Pagès et al., 2021**), and may contribute with the synthesis of those amino acids that are made in small quantities by the cnidarian host (**Fitzgerald and Szmant, 1997**). A variety of lipids, such as fatty acids and sterols, have also been shown to be provided by the alga (**Papina et al., 2013**). This metabolic integration, although still under research, has brought many more questions related to the capacity of both symbionts to regulate the metabolite trafficking.

The cnidarian host is believed to control or stimulate the release of photosynthates through the use of a substance that affects the algae. A soluble crude extract of cnidarian tissues has been shown to propitiate this effect, inducing the release of photosynthetic products from freshly isolated algal symbionts (**Gates et al., 1995**). This extract, considered to contain the "cnidarian host release factor", is able to induce changes in the metabolism of free-living Symbiodiniaceae (**Stambler, 2011**). Such an effect has been also achieved by an artificial mixture of selected amino acids (**Biel et al., 2007**), but the mechanism by which this factor induces the release of photosynthetic products is far from being clear.

The host eventually makes use of the photosynthates for its cellular activities, although an important fraction can be excreted in the form of coral mucus (**Xu et al., 2022**). This has been calculated to represent up to 40 % of the photosynthetically-fixed carbon in *Acropora acuminata* (**Crossland et al., 1980**). The coral mucus is a mix of glycoproteins and lipids low in nitrogen content, with a carbon to nitrogen ratio of approximately 12 (**Naumann et al., 2010**). The function of this mucus is to form a protective barrier, but it also constitutes the coral-derived organic carbon contributing to trophic relations in the coral reef (**Naumann et al., 2012**).

Due to the limited diffusion of soluble molecules across membranes, and the intracellular location of the algal symbionts, the mobilisation of inorganic ions (such as HCO_3^-, ammonium (NH_4^+) and phosphate (PO_4^{3-})) and soluble photosynthates is facilitated by molecule transporters located in the membranes of both Symbiodiniaceae and alga-hosting cells (**Figure 6**). The complex array of the multiple membranes in the symbiosome constitutes a challenging structure to isolate for proteomic analysis purposes (**Peng et al., 2010**). This constraint has limited the precise recognition of the transporters in the symbiosome membranes. Immunolocalization has been used to show that the cnidarian sterol transporter NPC2 (Niemann-Pick type C) was located in symbiosome membranes of the anemones *Anemonia viridis* and *Aiptasia sp*. (**Dani et al., 2017**). Other non-canonical NPC2 sterol transporters found in *Aiptasia sp*. were proposed to be adapted to the acidic environment of the symbiosome, binding different types of sterols (**Hambleton et al., 2018**). Cnidarians are known to

be sterol auxotrophs (**Gold et al., 2016**), and they must acquire it from their diet or their symbionts. Symbiodiniaceae, on the other hand, may have a different set of sterols among the different algal genera (**Lu et al., 2020**). A metabolic profile on cultured Symbiodiniaceae species from *Symbiodinium*, *Breviolum* and *Durusdinium* genera, that perform symbiosis with corals, showed that they have a marked difference in the production of sterols, sugars and inositol (**Klueter et al., 2015**).
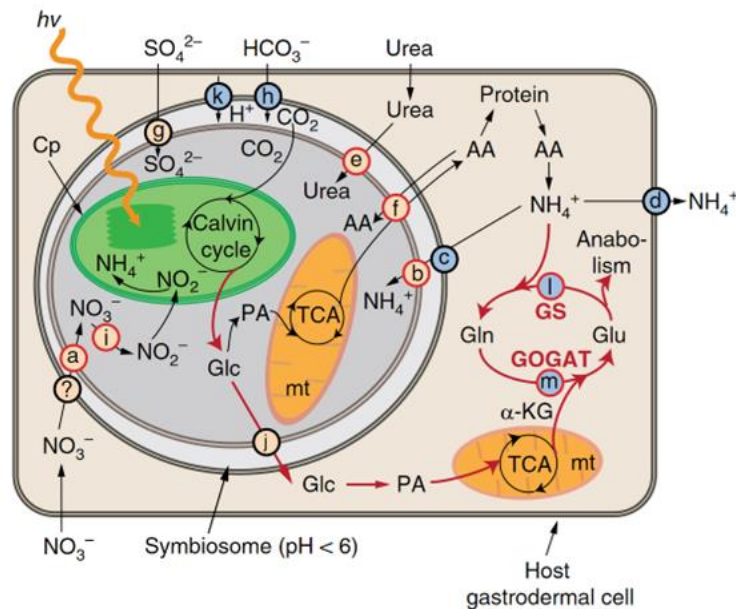
Figure 6. Metabolic interactions within the alga-hosting cell and the Symbiodiniaceae algal symbiont (image taken from **Xiang et al., 2020**). The membrane transporters indicated with letters are those which have been identified, except for the nitrate transporter (indicated with a question mark - ?). AA- amino acids; Cp- chloroplast; Glc-glucose; Gln- glutamine; Glu- glutamate; α-KG- alpha ketoglutarate; mt- mitochondria; PA- pyruvate; TCA- tricarboxylic acid cycle.

Proteomics approaches have found in the symbiotic anemone *Aiptasia* sp., a higher expression of proteins related to lipid, nitrogen and inorganic carbon transport than in its aposymbiotic state (**Oakley et al., 2016**). Recently, a single cell transcriptomic analysis in the coral *Stylophora pistillata*, showed that alga-hosting cells, in comparison with other cell lineages, overexpress enzymes for galactose and lipid metabolism, together with some key antioxidant enzymes, carbonic anhydrases and ammonium and amino acid transporters (**Levy et al., 2021**). On the other hand, a large set of potential transporters for amino acids, lipids, glycerol, as well as for carbon and nitrogen acquisition, have been found to be encoded in the genomes of *Symbiodinium microadriaticum*, *Breviolum minutum*, and *Fugacium kawagutii*, reflecting their adaptation to the symbiotic lifestyle (**Aranda et al., 2016**). A transcriptome profiling of *B. minutum* cultured and in symbiosis with *Exaiptasia*

diaphana, showed that bicarbonate, ammonium, sugar, phospholipid and amino acid transporters were more expressed in the algae in symbiosis, while the host downregulates phosphate, ammonium and amino acid transporters in comparison to non-symbiotic anemones (**Lehnert et al., 2014; Maor-Landaw et al., 2019**). The missing localisation of these transporters along the different cell membranes (e.g. vacuolar or plasma membrane), makes the understanding of their roles in uptaking and distributing the photosynthates an open question.

Nitrogen metabolism in the cnidaria-Symbiodiniaceae relationship has been shown to play an important role in the symbiosis. In the upside-down jellyfish *Cassiopea sp.*, its algal symbiont *Symbiodinium sp*. assimilates efficiently ammonium, but not nitrate (**Lyndby et al., 2020**). While the coral *Pocillopora damicornis*, in symbiosis with a *Symbiodinium* species, is able to assimilate ammonium, nitrate and aspartic acid, and can be incorporated into a crystalline structure of uric acid in the algal cytosol (**Kopp et al., 2013**). In the free-living alga these deposits of uric acid serve as nutrient storage and may work as photoreceptors (**Yamashita et al., 2009**). The ammonium assimilation pathway, glutamine synthetase (GS)-glutamine 2-oxoglutarate aminotransferase (GOGAT), is present in both Symbiodiniaceae (**Anderson and Burris, 1987**), and cnidarians (**Pernice et al., 2012**), although these last ones might also use glutamate dehydrogenase (GDH) (**Wang and Douglas, 1998**). It has been shown that after a pulse of ammonium, the alga can be more than ten times faster in its assimilation than the animal host (**Pernice et al., 2012**). Contrastingly, differences in the relation of nitrogen to carbon content, lower in Symbiodiniaceae in symbiosis than in free-living and the host tissue, were early recognized. It was found that during symbiosis, Symbiodiniaceae experience nutrient (nitrogen) limitation (**Rees, 1991**). This was recently corroborated by gene expression profiles, indicating that the host exerts a nutritional control on the algal population (**Cui et al., 2022**). However, the growth rate of Symbiodiniaceae in hospite has been shown to depend on its density within the host. Comparable growth rates were observed in Symbiodiniaceae when free-living in culture and when they started to populate a bleached anemone *Aiptasia pulchella*, but the growth rate in symbiosis decreased to 5 % when its density was the one of a normal symbiotic anemone (**Berner et al., 1993**). The growth rate of free-living *B. minutum* was found, by gene expression profile, to correlate with nitrogen availability in the medium, but in symbiosis it was observed to present a nitrogen limitation profile when it approached the maximum density in *Exaiptasia pulchella* (**Xiang et al., 2020**). Nitrogen limitation has a well-known effect in reducing photosynthesis in different types of microalgae (**Berges et al., 1996**). However, Symbiodiniaceae in hospite does not show signs of impairment in their photosynthetic activity (**Rees, 1991; Xiang et al., 2020**). In free-living conditions, *B. minutum* (SSB01) shows a lower photosynthetic activity in response to nitrogen limitation, but when found in hospite these cells

maintained a photosynthetic activity comparable to the nitrogen repleted culture (**Xiang et al., 2020**). Free living cultures of a sun adapted species (*Symbiodinium pilosum*) and a shade adapted species (*Fugacium kawagutii*), showed a marked impact on the photosynthetic activity when grown under nitrogen limitation conditions (**Rodríguez-Román and Iglesias-Prieto, 2005**). Under nitrogen limitation, cultures of *Breviolum sp.* isolated from *A. pulchella*, accumulated cytosolic lipid droplets, containing triacylglycerol, cholesterol ester and polyunsaturated fatty acids, together with a decrease in the growth rate (**Jiang et al., 2014**).

This intriguing phenomenon indicates a decoupling of nitrogen-limitation and photosynthesis existing in Symbiodiniaceae in symbiosis. The energetic relations within the alga in symbiosis are thus a particular problem that has not been addressed properly. Several studies aiming to understand the photosynthetic capacity of Symbiodiniaceae, and its regulatory mechanisms, have been conducted on cultures, a condition that does not consider the integration of the algal cells into the symbiosome environment.

Symbiodiniaceae and its photosynthetic machinery

Slight morphological differences exist among species of the distinct Symbiodiniaceae genera, for example the amount of cell thecal plates (**LaJeunesse et al., 2018**). Some *Symbiodinium* and *Durusdinium* species have the capacity to synthesise Mycosporine-like amino acids (MAAs; secondary metabolites with the capacity to absorb UV light), but *Breviolum* and *Cladocopium* species have lost a gene cluster related to its biosynthesis (**Shoguchi et al., 2020**). Other studies have shown, after comparing dinoflagellate genomes, that the distinct Symbiodiniaceae genera hold a relatively high sequence and structural genomic divergence (**Bi et al., 2019; González-Pech et al., 2021**). These differences, could be also observed among some species of the *Symbiodinium* genus with different symbiotic lifestyles, such as the free-living *S. natans* and the symbiotic *S. tridacnidorum* species (**González-Pech et al., 2021**). This led the authors of that study to propose the symbiotic lifestyle as the responsible of such genomic divergence (**González-Pech et al., 2021**).

The chloroplast of Symbiodiniaceae

As in all photosynthetic eukaryotes, the photosynthetic activity occurs in the chloroplast. In dinoflagellates, it is well accepted that the peridinin chloroplast, present in the core group of dinoflagellates, was acquired through a secondary endosymbiosis event with a member of the red algal lineage (**Ishida and Green, 2002**). This event could have occurred in an ancestor shared by dinoflagellates, apicomplexans and heterokonts, as postulated after the analysis of plastid genome

sequences (**Janouškovec et al., 2010**). The peridinin chloroplast of dinoflagellates is delimited by three membranes (**Yoon et al., 2002**). In Symbiodiniaceae, the chloroplast has a reticulated shape and is distributed at the cell periphery, an arrangement proposed to be the result of an optimization of the light absorption capacity (**LaJeunesse et al., 2010**) (**Figure 7a and b**). It contains a peripheral pyrenoid surrounded by a cytosolic plate of starch, and invaginated by the chloroplast envelope, but not penetrated by thylakoids (**Yamashita et al., 2009; Camaya, 2020**). Another distinctive feature of peridinin-dinoflagellates is the presence of small plasmid-like DNA minicircles in the chloroplast, encoding core subunits of the photosynthetic complexes (**Barbrook et al., 2014**). In Symbiodiniaceae, the content of chloroplast-encoded genes is highly reduced in comparison with other microalgae, but it has been the result of a massive transfer of the typical red-algal chloroplast-encoded genes to the nucleus (**Mungpakdee et al., 2014**).

The Rubisco type II

Carbon fixation evaluated in freshly-isolated Symbiodiniaceae from *Acropora formosa* showed that it follows a common C3 pathway, where glycerate-3-phosphate was the main molecule marked after incubation with [^{14}C]-bicarbonate in the seconds time range (**Streamer et al., 1993**). CO_2 fixation is carried out by a type II Rubisco (Ribulose-1,5-bisphosphate carboxylase oxygenase), whose gene in Symbiodiniaceae is nuclear encoded and expressed as a polyprotein (**Rowan et al., 1996**). This gene was, most likely, acquired by horizontal gene transfer, as it shares 65 % identity with the type II Rubisco of *Rhodospirillum rubrum* (Alphaproteobacteria) (**Rowan et al., 1996**). This enzyme might be localized in the pyrenoid matrix (**Jenks and Gibbs, 2000**), but it is labile when extracted from Symbiodiniaceae cells (**Lilley et al., 2010**), limiting the study of its kinetic and catalytic properties. An in silico analysis suggested that Rubisco from *Symbiodinium sp*. might form trimers of homodimers (**Rydzy et al., 2021**) (**Figure 7c**). The gene expression was shown to follow a circadian rhythmicity when the cells were in free-living conditions, but when in symbiosis with *Aiptasia pulchella* the protein level did not show changes along the diurnal cycle (**Mayfield et al., 2014**). A difference in the molecular mass of this protein was observed when it was extracted from algal cultures (60 kDa) than from algae in symbiosis with *Aiptasia pallida* (62 kDa), the authors suggested that this difference might be due to a post-translational modification as part of a regulatory mechanism (**Stochaj and Grossman, 1997**). It is also a common observation that the content of Rubisco is higher in cultured cells than in symbiosis (**Mayfield et al., 2014; Stochaj and Grossman, 1997**). Moreover, two cultured Symbiodinium species, originally isolated from reef-forming corals, were found to contain similar Rubisco levels but different chlorophyll content, and, interestingly, their maximal

photosynthetic activity (Pmax) and the growth rate were more in accordance with the chlorophyll content than the Rubisco content (**Brading et al., 2013**).

The antenna complexes

During the light reactions of photosynthesis, photons are absorbed by the pigment-protein complexes located in the chloroplast thylakoids which divert the exciton energy to the photosystem reaction centres. The main pigments found in these peridinin dinoflagellates are chlorophyll *a* (Chl *a*) chlorophyll c_2 (Chl c_2), and the carotenoids peridinin (Per) and diadinoxanthin (Ddx). The light harvesting complex (LHC) in these organisms consists of two antenna types. The main type is the membrane-embedded Chl *a*-Chl c_2-Per Protein Complex (acpPC) of 18 kDa, containing a pigment ratio of 4/6/6/1 (Chl *a*/Chl c_2/Per/Ddx) (**Niedzwiedzki et al., 2014**). *Cladocopium sp*. was found to contain a high diversity of acpPC genes encoded in the nuclear genome, from which some are expressed as polycistronic transcripts and the resulting polyproteins, after being transported across the chloroplast membranes, are cut to yield three-transmembrane LHC subunits (**Boldt et al., 2012**; **Maruyama et al., 2015**) (**Figure 7d**). Phylogenetic analysis of these acpPC genes showed that they can be grouped in three LHC lineages, the two most diverse are LHCR type (conserved among red algae and secondary algae containing chloroplasts of red algae origin, and whose protein product is associated with PSI) and LHCF type (grouped with genes coding for fucoxanthin-Chl *a*-Chl *c* binding proteins of diatoms), while a third minor group (**Boldt et al., 2012**; **Maruyama et al., 2015**). This antenna has been isolated in a trimeric state from *Fugacium kawagutii* (**Jiang et al., 2014**) but higher oligomeric states might be also present in the cultured algae (**Niedzwiedzki et al., 2022**). In *Symbiodinium tridacnidorum* in free-living conditions, the abundance of acpPC was found to be increased after incubation at low light intensity (**Supasri et al., 2021**). In this antenna, both Per and Chl c_2 showed an efficient exciton energy transfer to Chl *a*, but a low capacity to quench its excited state (**Niedzwiedzki et al., 2014**). Ddx, on the other hand, might function in the photoprotection mechanism called xanthophyll cycle. This photoprotection mechanism is addressed later.

The second antenna type is an external and soluble Per-Chl *a* Protein (PCP) Complex, which might be located in the thylakoid lumen (**Norris and Miller, 1994**). The pigment content in PCP consists of four Per per Chl *a* (**Jiang et al., 2012**). In cultured cells of *Symbiodinium pilosum* the PCP complex has been found as a homodimer of two proteins of about 15 kDa, while in *Fugacium kawagutii* it has been found as a monomeric antenna of about 35 kDa consisting of two PCP domains, but *Symbiodinium microadriaticum* was found to possess both (**Iglesias-Prieto et al., 1991**) (see a model structure of PCP from the dinoflagellate *Amphidinium carterae* in **Figure 7e**). In *Symbiodinium bermudensis* cultured cells, a 14 kDa PCP was found more abundant than a 35 kDa PCP, while in

28

symbiosis with *Aiptasia pallida* the 35 kDa PCP was more abundant (**Stochaj and Grossman, 1997**). The PCP antenna seems to have an efficient mechanism of photoprotection, based on the capacity of Per to rapidly quench the triplet state of Chl *a* (^{3}Chl *a*), avoiding the formation of singlet oxygen species ($^1O_2$) (**Niedzwiedzki et al., 2013**). The regulation mechanism on the abundance of the two antenna types in Symbiodiniaceae in symbiosis remains vastly unknown despite being considered as an important part of its photoacclimation strategy (**Gierz et al., 2016; Supasri et al., 2021**).
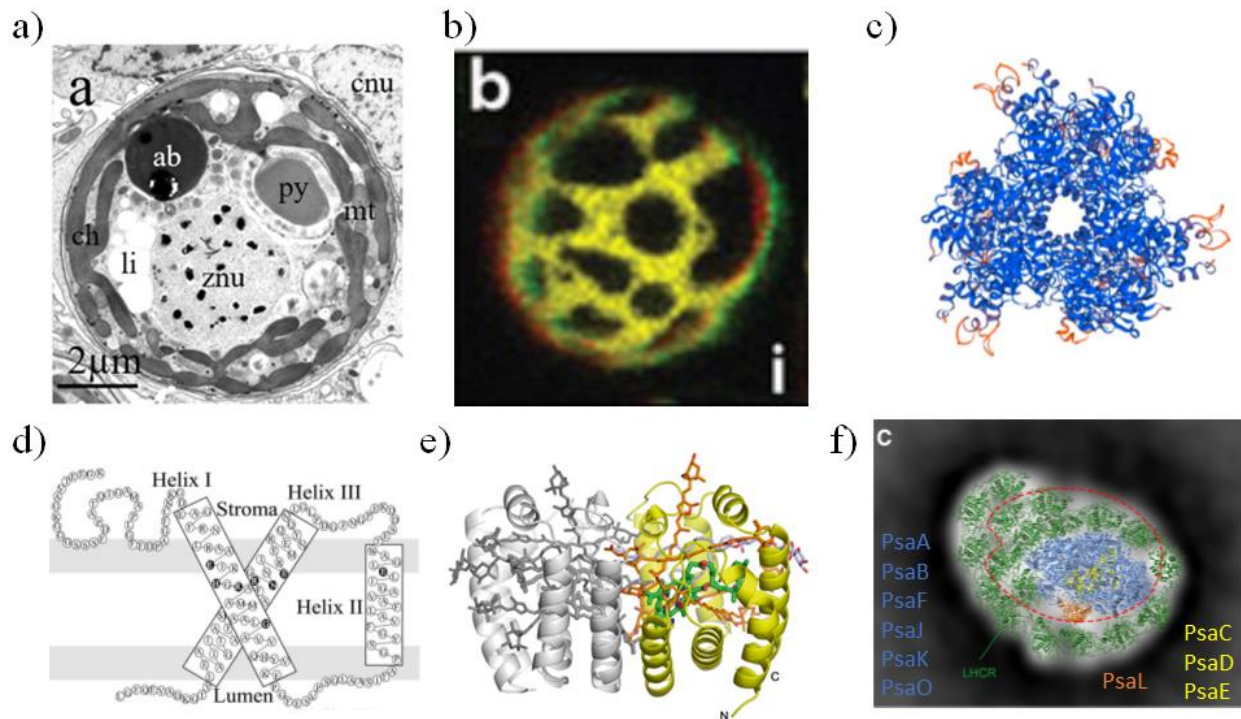
Figure 7. Photosynthetic components in the chloroplast of Symbiodiniaceae. **a)** Photomicrograph of a Symbiodiniaceae cell in symbiosis with *P. damicornis* (**Camaya, 2020**). Symbiodiniaceae nucleus (znu), mitochondria (mt), chloroplast (chl), pyrenoid (py), accumulation bodies (ab), lipid vacuoles (li), and the nucleus of the cnidarian alga-hosting cell (cnu) are indicated. **b)** Reticulated chloroplast imaged by confocal laser scanning of Chl *a* fluorescence of a coccoid form of *Symbiodinium sp*. (**LaJeunesse et al., 2010**). **c)** Model structure of a trimer of homodimers of Rubisco type II of *Symbiodinium sp*. (**Rydzy et al,. 2021**). **d)** Schematic representation of the transmembrane topology of an acpPC antenna (**Boldt et al., 2012**). **e)** Homodimeric structure model of a PCP antenna from the motile dinoflagellate *Amphidinium carterae* (Gymnodiniales, Dinophyceae) (**Políkva and Hofmann, 2014**). Chl *a* is shown in green, Per is shown in orange. **f)** PSI supercomplex structure found in *Breviolum minutum* (**Kato et al., 2020**). Protein structures from *Cyanidioschyzon merolae* were superimposed on the

negative stained image, in green the LHCR antenna, in blue and yellow the core subunits as indicated in the image.

Photosynthetic complexes and electron transfer

In oxygenic photosynthetic organisms, the structure and function of the photosynthetic complexes are highly conserved. The photosynthetic light reactions occur in the reaction centre (RC) of both photosystem II (PSII) and photosystem I (PSI). Each RC contains a pair of Chl *a* molecules known as P680 and P700, in PSII and in PSI respectively, that are held by two transmembrane proteins. In PSII these are PsbA (also called D1) and PsbD (also called D2), and in PSI the proteins are PsaA and PsaB. In Symbiodiniaceae the genes encoding these subunits are found in the minicircles of the chloroplast genome. Although these genes are usually highly conserved among photosynthetic eukaryotes, a striking divergence has been observed in their coding sequences in dinoflagellates (**Barbrook et al., 2014**). They are also submitted to post-transcriptional edition to retain the highly conserved amino acid residues (**Mungpakdee et al., 2014**). Another interesting difference with other eukaryotes was found in a low-resolution structure of the PSI of *Breviolum minutum*, where the core complex is surrounded by an unusually large amount of antenna subunits (**Kato et al., 2020**) (**Figure 7f**).

During the functioning of the photosystems, the exciton energy funnelling towards the RCs allows the photochemical reactions to happen, promoting the excited state of the pigments at the RC and the consequent reduction of the downstream redox centres. This results in the reduction of the electron acceptors within both photosystems, in PSII is a quinone A (QA), and in PSI is a 4Fe-4S cluster. The electron carriers are then reduced, in PSII plastoquinone (PQ) is reduced to plastoquinol (PQH_2) with the acceptance of two consecutive electrons and two protons from the stromal side, and in PSI Ferredoxin (Fd) is reduced with the transfer of one electron. The oxidised RCs of PSII ($P680^+$) and PSI ($P700^+$) are reduced by their respective donor side, in PSII by the Oxygen Evolving Complex (OEC), and in PSI by the thylakoid lumen protein Cytochrome c_6 (Cyt c_6). The OEC is able to bind two molecules of H_2O at the same time, which can provide four consecutive electrons after four consecutive photochemical reactions. One molecule of O_2 and four H^+ are then released into the thylakoid lumen, and the four electrons can reduce two PQ molecules.

The Cytochrome b_6f complex couples the electron movement occurring in both PSII and PSI, in a mechanism known as Q cycle (**Malone et al., 2021**). This mechanism consists in the oxidation of one PQH_2, the reduction of two Cyt c_6, and the translocation of four H^+ into the thylakoid lumen. Briefly, during the first half of the cycle, one PQH_2 is bound to the Qo site in the complex, which is situated close to the lumenal side of the thylakoid membrane. There, the oxidation of PQH_2 results in the

release of the two H$^+$ into the lumen, while the two electrons are transferred through the cytochromes of the complex, one is directed to the reduction of one Cyt c$_6$, and the other is directed to the Qi site in the complex, close to the stromal side of the thylakoid membrane. In this site, one PQ is bound and is reduced by two consecutive electrons, avoiding the formation of a semiquinone (PQ$^-$) form. In the second half of the Q cycle, another PQH$_2$ is bound and the same reactions occur with the reduction of another Cyt c$_6$, the release of other two H$^+$ into the thylakoid lumen, and the electron guided towards the Qi site completely reduces PQ$^-$, with two H$^+$ from the stromal side, into PQH$_2$. The balance of the Q cycle indicates that the two PQH$_2$ produced after the oxidation of two H$_2$O molecules at PSII would be used to reduce four Cyt c$_6$ and result in the translocation of eight H$^+$ into the lumen of the thylakoid. These four Cyt c$_6$ provide electrons to PSI along four consecutive photochemical reactions that lead to the reduction of four Fd. These last ones are then used by the stromal enzyme Ferredoxin-NADP$^+$ Reductase (FNR) to yield two NADPH (**Figure 8**).
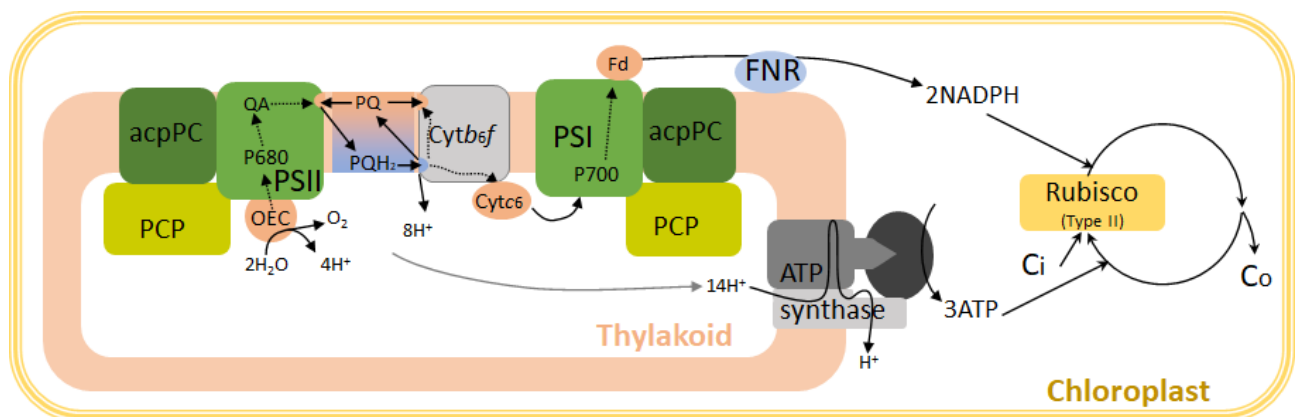
Figure 8. Major components of the photosynthetic electron transfer chain in Symbiodiniaceae. The antenna system (acpPC- Chl *a*-Chl *c$_2$*-Per Protein Complex, and PCP-Per-Chl *a* Protein), the photosynthetic complexes (PSII-photosystem II, Cyt b$_6$f-cytochrome b6f, and PSI-photosystem I), and the intermediate electron carriers (PQ-plastoquinone, Cyt c6-cytochrome c6, and Fd-ferredoxin) are outlined. The oxygen evolving complex (OEC) in the PSII, and the Ferredoxin NADP Reductase (FNR) are also shown. The H$^+$ accumulated within the thylakoid lumen and its use by the ATP synthase is indicated for the synthesis of 3 ATP, while the electron movement along the photosynthetic chain is indicated for the synthesis of 2 NADPH. Inorganic carbon (Ci) and organic carbon (Co) are indicated for the activity of the CBB cycle.

The electron movement and the accumulation of H$^+$ in the thylakoid lumen generates a proton motive force (*pmf*) across its membrane that is used to drive the synthesis of ATP in the stroma of the

chloroplast by the ATP synthase complex. This complex consists of a membrane-immersed rotative sector, also called rotor. The complete rotation of this sector induces conformational changes in three ADP+Pi binding sites of an hexameric sector of the complex located in the stromal side of the thylakoid membrane. These two sectors are stabilised by a peripheral stalk. In the chloroplasts of green microalgae and plants, the rotative sector of the ATP synthase usually contains 14 H^+ binding sites (**Davies and Kramer, 2020**), which are required to accomplish one turn, and by consequence the synthesis of three ATP. Assuming that this structure is conserved in Symbiodiniaceae, the 12 H^+ accumulated at the thylakoid lumen after the synthesis of two NADPH, may yield less than three ATP (2.57 moles of ATP every 12 moles of H+). However, the energetic requirement for carbon fixation along the Calvin–Benson-Bassham (CBB) cycle consists of three ATP and two NADPH per CO_2 fixed. This indicates that the ATP and NADPH production are regulated during the photosynthetic activity in order to constantly provide a stoichiometric ratio of these energetic molecules for carbon fixation.

On the energetic requirement for carbon fixation

The theoretical energetic consumption in the CBB cycle after fixing six CO_2 for the production of one hexose phosphate and the regeneration of six ribulose-1,5-bisphosphate, is 18 ATP and 12 NADPH. In the CBB cycle, ATP is used by Phosphoglycerate Kinase, converting glycerate-3-phosphate into glycerate-1,3-bisphosphate, and by Phosphoribulokinase to convert ribulose-5-phosphate into ribulose-1,5-bisphosphate. The NADPH in the CBB cycle is used by Glyceraldehyde-3-phosphate Dehydrogenase (GAPDH) for the conversion of glycerate-1,3-bisphosphate into glyceraldehyde-3-phosphate.

A theoretical value of the quantum requirement for CO_2 fixation, considering the energetic requirements in the CBB cycle and the photosynthetic linear electron transfer activity, results in eight mols of photons absorbed per mol of CO_2. This can also be expressed as four photosynthetically-derived electrons per fixed CO_2, reflecting the efficiency of the photosynthetic machinery in the use of light for carbon fixation. This value is an important parameter in studies aiming to better comprehend the productivity of photosynthetic organisms. However, the experimental determination of these parameters in a variety of cultured marine microalgae has shown ratios higher than the theoretical reference (**Suggett et al., 2009**). In cultures of Symbiodiniaceae the electron requirement for carbon fixation has shown to be variable, in *Symbiodinium sp.* it was reported a value of about 5 (**Brading et al., 2013**), in *Cladocopium goreaui* it was reported a value of 7, while in *Durusdinium trenchii* it was up to 10.7 electrons per CO_2 (**Hughes et al., 2021**).

This experimentally-determined parameter has shown an inverse correlation with the growth rate in some algal groups (**Hughes et al., 2021**). Nonetheless, the reasons for the difference with the theoretical value might lie in both technical and theoretical assumptions (e.g. lack of tools to monitor key energetic processes involved in the energy flow, or underestimation of important electron and ATP sinks). The variability in this parameter in microalgal species could be also related to environmental factors, such as light and nutrients availability in the open ocean (**Lawrenz et al., 2013**).

The theoretical minimum value of four electrons per fixed CO_2 might also be exceeded with the inclusion of key light-related pathways that use NADPH and ATP with a different stoichiometry than the CBB cycle. This is the case of photorespiration, where, after Rubisco carries out the oxygenation of ribulose-1,5-bisphosphate, 3.5 ATP and 2 NADPH are consumed with the release of CO_2. In this respect, the cnidarian host has shown to be able to uptake bicarbonate from the medium to supply inorganic carbon to its algal symbiont (**Goiran et al., 1996**). The matrix of the pyrenoid also contains a Carbonic Anhydrase that might assist to increase the CO_2 level in the Rubisco subcellular environment (**Loussert-Fonta et al., 2020**), decreasing the probability of photorespiration in the algal symbiont. Despite photorespiration intermediate molecules were not detected during isotopic chasing in freshly isolated algae from the coral *Acropora formosa* (**Streamer et al., 1993**), *S. pistillata* corals have displayed a positive dependence on bicarbonate and NH_4^+ availability in the medium (**Roberty et al., 2020**). In the Symbiodiniaceae symbiont of *A. formosa*, the expression of Phosphoglycolate Phosphatase, the enzyme that dephosphorylates the toxic Rubisco's oxygenation product glycolate-2-phosphate into glycolate, was decreased after a four days incubation of the coral in a tank with an atmospheric CO_2 concentration of 1100 ppm (resulting in a pH of 7.6 and a HCO_3^- concentration of 2.17 mM), suggesting that this condition could have affected the photorespiratory capacity of the coral (**Crawley et al., 2010**).

Another prominent pathway coupled to the photosynthetic activity by the consumption of energetic molecules, is NO_3^- assimilation, whose reduction into amino acids requires approximately 12 ATP. Fatty acid synthesis in the chloroplast might require large amounts of NADPH, while starch, nucleic acids and protein synthesis within the chloroplast, are well known for their high requirements of ATP. Moreover, in the green alga model species *Chlamydomonas reinhardtii*, the production of glycerate-3-phosphate by the carboxylation activity of Rubisco, was shown to be required for the synthesis of the D1 protein of PSII under photo-inhibition conditions (**Takahashi and Murata, 2006**). Overall, clearly indicating a high complexity in the relation of the chloroplast-localised processes with the photosynthetic reactions.

Photosynthetic alternative electron pathways

Microalgae contain a diversity of mechanisms aiming to regulate the photosynthetic electron transport under dynamic conditions (**Cardol et al., 2011**). The so-called alternative electron pathways re-route the photosynthetically-derived electrons along the chain, resulting in an adjustment in the stoichiometric production of NADPH and ATP. The alternative electron pathways modifying the production of ATP and NADPH in the photosynthetic chain consist of two main mechanisms, a cyclic electron flow (CEF) and a pseudo-cyclic electron flow, also known as the water to water cycle (WWC).

CEF consists in the usage of electrons generated by the photochemical reaction of PSI to reduce back $P700^+$. This involves the reduction of PQ and the Cytochrome b_6f complex activity, and results in the movement of H^+ into the thylakoid lumen. The redox centres used during CEF around PSI have been a matter of research and debate in the last decades (**Nawrocki et al., 2019a**), and four distinct electron routes have been described (**Figure 9**). One consists in the oxidation of Fd by a proton-pumping analogue of the mitochondrial complex I (NDH1) located in the thylakoid membranes of plants, and able to couple the pump of two H^+ with the transfer of one electron from Fd to PQ (**Strand et al., 2017**). Unicellular algae do not contain the genes coding for that protein complex, but they have a type II NADPH dehydrogenase (**Peltier et al., 2016**). This protein, also called NDH2, is not a proton-pumping component but can couple the oxidation of NADH to the reduction of PQ. Another main route occurs through the couple of Protein Gradient Regulator 5 (PGR5) and Protein Gradient Regulator-Like 1 (PGRL1), which were found to participate in the regulation of the *pmf* in green photosynthetic eukaryotes, and were proposed to perform the function of Fd-PQ reductase (FQR) (**Hertle et al., 2013**). An additional route considered as a potential path of electrons during CEF, is the direct electron transfer from Fd to the Qi site of the Cytochrome b_6f complex when binding FNR (**Nawrocki et al., 2019a; Kanazawa et al., 2020**). The activity of CEF through the NDH1 path in plants results in a higher yield–of ATP synthesis per electron transferred through PSI, due to the amount of H^+ translocated per pair of electrons, than the other routes present in microalgal species. Still, the other routes of CEF are thought to contribute to the production of additional *pmf* to complement the required ATP for the functioning of the CBB cycle. In Symbiodiniaceae, the genes coding for PGR5 and PGRL-1 (FQR), and for NDH2 have been found (**Roberty et al. 2014**; **Aihara et al. 2016**), but their contribution to the photosynthetic process has been barely mentioned when the alga is in symbiosis.
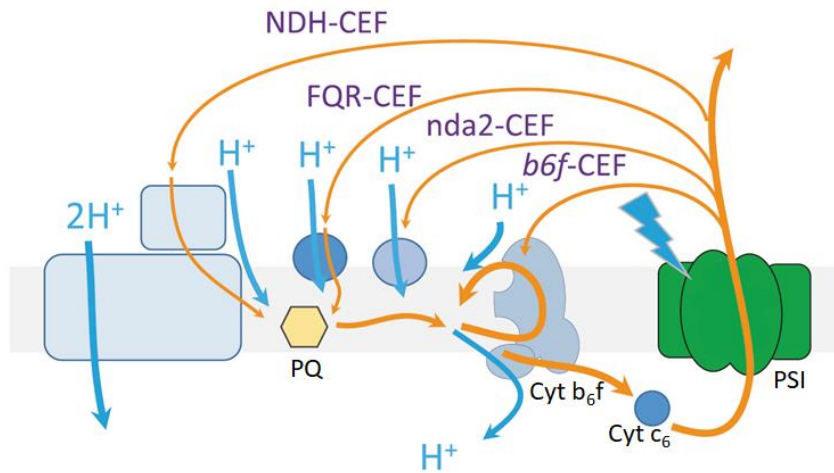
Figure 9. Electron transfer routes during the functioning of CEF (image taken from **Kanazawa et al., 2020**). Orange arrows indicate the electron transfer during CEF, while blue arrows indicate the H^+ movement concurrently to each electron path. The light driven activity of PSI is indicated by the lightning symbol on PSI, and PQ indicated the plastoquinone pool participating in these pathways.

The WWC is described as the use of electrons derived from the photochemical oxidation of H_2O by PSII, for the reduction of O_2 back into H_2O (**Curien et al., 2016**). Different sites of this reaction can be present along the photosynthetic machinery (**Figure 10**). One of these consists in the transfer of four electrons from the Fd pool, at the acceptor side of PSI, directly to O_2 by the activity of Flavodiiron proteins (FLV). These proteins are present in green photosynthetic organisms such as cyanobacteria, green microalgae and plants, but not in angiosperms nor in red algae (**Alboresi et al., 2018**). In Symbiodiniaceae, one *FLV* gene has been found expressing a polycistronic product that is cut to yield two proteins, and its activity was shown to be present in symbiosis (**Shimakawa et al., 2022**). Another mechanism of the WWC consists of the Mehler-Asada pathway. This pathway begins with the non-catalysed photoreduction of O_2 at the A1 site (phylloquinone) of PSI, producing the superoxide radical (O_2^-) (**Kozuleva et al., 2021**). This radical is then scavenged enzymatically by Superoxide Dismutase (SOD) in the chloroplast stroma, producing one O_2 and one H_2O_2 from two O_2^-. In the next step H_2O_2 is reduced by Ascorbate Peroxidase (APX) producing two H_2O with ascorbate as reductant. Mono-dehydroascorbate reductase (MDAR) then uses NADPH, produced by the photosynthetic electron transfer chain, to regenerate ascorbate (**Asada, 2000**). The activity of the WWC pathways also results in the formation of additional *pmf* without the net production of NADPH, contributing to balance the stoichiometric production of ATP and NADPH. The WWC allows the

active consumption of O_2, a molecule with negative impacts on the photosynthetic carbon fixation, limiting its excessive accumulation in comparison the photosynthetic electron transfer activity.

In Symbiodiniaceae, the Mehler-Asada pathway, also called Mehler reaction, was found to be the main alternative electron pathway when cultures were subjected to a transient increase of light intensity (**Roberty et al., 2014**). The activity of the enzymes participating in the Mehler-Asada pathway have been detected in cultures of *Symbiodinium sp.*, and were found to increase upon exposure to high light intensity (**Roberty et al., 2015**).
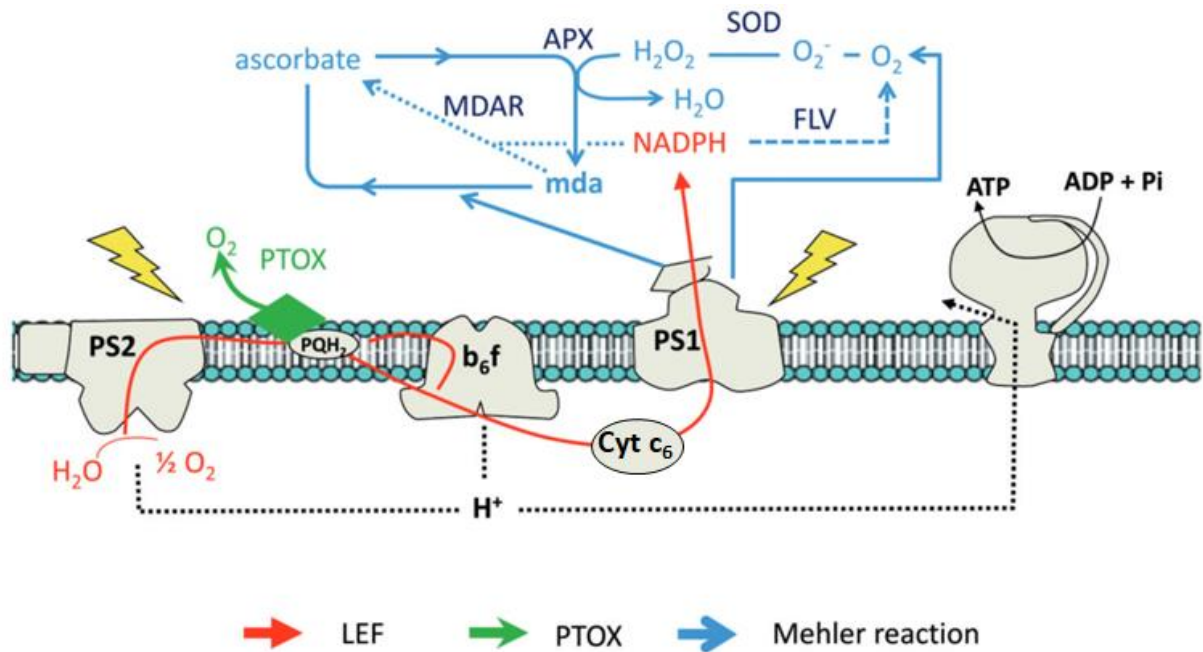
Figure 10. The pathways of electrons during the WWC. The linear electron flow (LEF) is indicated by red lines, while the WWC is indicated by blue lines. The activity of Flavodiiron proteins (FLV) is indicated with a blue dashed line. The Mehler-Asada pathway is indicated with the blue continuous lines. This includes the non-enzymatic production of the superoxide radical (O_2^-), its scavenging by Superoxide Dismutase (SOD) into hydrogen peroxide (H_2O_2) and its further conversion into water (H_2O) by Ascorbate Peroxidase (APX). The blue dotted line indicates the use of NADPH to reduce monodehydroascorbate (mda) by Monodehydroascorbate Reductase (MDAR). Additionally, the Plastid Terminal Oxidase (PTOX) pathway is indicated by the green line. Adapted from **Curien et al., 2016**.

Another route contributing to the WWC is through the coupling of PSII with the Plastid Terminal Oxidase (PTOX), this last is a peripheral thylakoid membrane enzyme that transfers electrons from PQH_2 to O_2. PTOX is usually described to be coupled with the oxidation of stromal NADH by NDH2

in darkness or very low light conditions in microalgae, with a low impact on the photosynthetic electron transfer, a pathway called chlororespiration (**Nawrocki et al., 2015**). Interestingly, a mutant of the green microalga *Chlamydomonas reinhardtii* deficient in PTOX2, the major isoform, showed a dysregulation of the photosynthetic electron transfer, in favour to the CEF activity when the alga was submitted to intermittent light (**Nawrocki et al., 2019**). This phenotype shows the importance of this enzyme in the adjustment of the electron transfer. Under nitrogen limiting conditions *C. reinhardtii* has been reported with an increased chlororespiratory activity, as shown by a lower PSII activity and Cytochrome b_6f abundance, a higher PQH_2 oxidation and O_2 consumption (**Peltier and Schmidt, 1991**). Despite the nitrogen limitation experienced by Symbiodiniaceae in symbiosis, this phenotype has not been reported so far. In free-living conditions, Symbiodiniaceae may have a low chlororespiratory activity (**Roberty et al., 2014**). However, in a Caribbean dominant coral species, a prominent non-photochemical reduction of the PQ pool has raised the attention for its relation to coral resilience under environmental stressing conditions (**Claquin et al., 2021**).

Taken together, these photosynthetic alternative electron pathways participate in the optimization of the photosynthetic activity. However, even in the best studied model organisms their role is still a matter of study. A common problem during the experimental determination of the photosynthetic activity is the correct recognition of the multiple alternative pathways. Novel experimental strategies have been developed and tested on Symbiodiniaceae in free-living conditions, although few less in symbiosis (**Reynolds et al., 2008**; **Roberty et al., 2014**; **Mohammad Aslam et al., 2022**). These strategies that include a better resolution of key traits during *in vivo* monitoring and the concurrent monitoring of multiple parameters, are aimed to advance and to unveil the contribution and occurrence of the alternative pathways and their relevance under stressing conditions causing coral bleaching. Some of these methods are further explained in the **Chapter 2**.

Photosynthetic control and photoprotection mechanisms

Situations where the photosystems activity can overtake the rate of regeneration of the energy carrying molecules (i.e. ADP and $NADP^+$), include CO_2 limitation and changes in light intensity (**Tikkanen et al., 2012**). In symbiosis with cnidarians, due to their intracellular location, Symbiodiniaceae is highly dependent on the host's inorganic carbon supply, which, despite not being completely understood, is robust enough to sustain the photosynthetic activity (**Raven et al., 2020**). Light intensity fluctuation, on the other hand, is common in the aquatic environment of symbiotic cnidarians, and can range from milliseconds to annual seasons (**Roth, 2014**).

An ADP limitation in the stroma of the chloroplast can bring down the activity of the ATP synthase, and by consequence, a decrease of H^+ conductance across the enzyme. In plants, a point mutation on the regulatory subunit of the ATP synthase, the gamma subunit, revealed that this enzyme may participate regulating the acidification level of the thylakoid lumen under low CO_2 and fluctuating light conditions (**Kanazawa et al., 2017**). A strong decrease of pH in the thylakoid lumen has a negative impact on the oxidation rate of PQH_2 at the Qo site of the Cytochrome b_6f, leading to a higher reduced state of the PQ pool, and limiting the electron transfer at the Qi site (**Foyer et al., 1990; Tikhonov, 2014**). The limitation of $NADP^+$ at the PSI acceptor side, on the other hand, potentially favours the reduced state of the whole photosynthetic chain, limiting the electron transfer to the acceptor side in both photosystems. This blockage of electrons results in a decreased rate of de-excitation of Chl a, propitiating the appearance of its triplet excited state (^{3}Chl a), and promoting the production of ROS, such as singlet oxygen ($^1O_2$) or O_2^- (**Khorobrykh et al., 2020**). The downregulation of the Cytochrome b_6f complex and the photosynthetic electron transfer rate by ADP and $NADP^+$ limitation is known as photosynthetic control, and may occur in the millisecond time range once the disequilibrium is set (**Colombo et al., 2016**; **Johnson and Berry, 2021**).

During the disbalance between the electron transfer rate and the ADP and $NADP^+$ availability, the highly reduced state of PQ and the acidification of the thylakoid lumen activate a set of photoprotection mechanisms commonly known as non-photochemical quenching (NPQ). These mechanisms allow the increased capacity of light energy dissipation and the redistribution of exciton funnelling from the antennas to both photosystems. These are widely known as NPQ (non photochemical quenching) because experimentally they are observed as a decrease of the maximum fluorescence yield of Chl a at PSII, indicating a lower quantum yield for PSII light absorption. The increased acidification of the thylakoid lumen activates an energy-dependent NPQ (qE), which in many organisms is present with the concomitant activation of the xanthophyll cycle. In peridinin dinoflagellates and diatoms, this consists in the de-epoxidation of diadinoxanthin (Ddx) into diatoxanthin (Dtx) by the luminal enzyme Diadinoxanthin de-epoxidase, which is activated by a decrease of pH, and the reversed reaction (Dtx to Ddx) catalysed by the stromal enzyme Diatoxanthin epoxidase during the darkness or at higher pH (**Goss and Lepetit, 2015**). Dtx might function as a quenching site by thermally dissipating the exciton energy transferred from Chl a (**Kagatani et al., 2022**). In the coral *Goniastrea aspera*, the abundance of Dtx was found to parallel the irradiance intensity, but it was inverse to the photosynthetic quantum yield of PSII along the diurnal cycle, indicating its main role as a photoprotection mechanism (**Brown et al., 1999**). In other coral species it was observed that the response of Dtx production under high light intensity might be variable among the different Symbiodiniaceae species (**Warner and Berry-Lowe, 2006**). qE occurs in the antenna

system attached to PSII (LHCII complex) in plants (**Ruban and Wilson, 2020**), and in Symbiodiniaceae it does in the acpPC antenna (**Kanazawa et al., 2014**). In *Breviolum minutum*, the antenna system associated with PSI was found to contain an important amount of Ddx that could be transformed to Dtx after a high light intensity treatment (**Kato et al., 2020**). In the plant *Arabidopsis thaliana*, PSI does not carry out qE through the xanthophyll cycle-pigment zeaxanthin, corresponding to Dtx, because both P700 and P700$^+$ possess a high quenching capacity (**Tian et al., 2017**). In the red-alga diverged species *Chromera velia* (Chromerida, Alveolata) and *Phaeodactylum tricornutum* (Bacillariophyceae, Heterokonta), a short PSI fluorescence lifetime was reported to correspond to a higher photochemical efficiency than the one reported for plants and green algae (**Belgio et al., 2017**). Although this feature has not been reported in peridinin-dinoflagellates or Symbiodiniaceae, an exciton energy funnelling from PSII to PSI, a mechanism called *energy spillover*, has been reported in *Cladocopium sp*. in culture (**Slavov et al., 2016**). According to this study, about half of the PSII pool in control conditions could participate in this mechanism relying on the capacity of P700$^+$ to quench exciton energy, but it increased with the exposition of the cells to combined light and temperature stress (**Slavov et al., 2016**). Interestingly, in the phycobilisome-containing red macroalgae *Chondrus crispus* (Florideophyceae, Rhodophyta), the spillover mechanism was reported to be triggered by the reduced state of the PQ pool (**Kowalczyk et al., 2013**).

In plants and green algae, the reduced state of the PQ pool activates a kinase enzyme associated to the Cytochrome b$_6$f (called STN7 in plants and STT7 in green algae), which phosphorylates LHCII protein components and promotes its association with PSI, a mechanism called state transitions (**Minagawa, 2011**). A similar mechanism was initially proposed to exist in Symbiodiniaceae to explain fluorescence spectral changes in the antenna system upon exposure to high light intensity. It was suggested that under high light conditions, either the PCP antenna complex (**Reynolds et al., 2008**) or the acpPC antenna complex were physically dissociated from photosystems (**Hill et al., 2012**), but no evidence of phosphorylation or regulation was provided. It was shown later, by time-resolved spectroscopy, that this phenomenon was rather due to activation of NPQ by high light intensity, but PCP maintained an efficient energy transfer to acpPC and to PSI (**Kanazawa et al., 2014**).

The link between photosynthesis and the bleaching phenomenon

Current climate changing conditions and its linked periods of extreme temperature, are associated with the more-often events of mass coral bleaching (**Hughes et al., 2018**). Coral bleaching, consisting in the loss of the algal symbionts from the cnidarian tissue, is usually augmented under high

temperature and high solar radiation (**Brown, 1997**). The high mortality associated with mass coral bleaching events occurs differently among coral species (**Harriott, 1985**), and can also occur in a variety of aquatic communities including photo-symbiotic jellyfish living in tropical marine lakes (**Martin et al., 2006; Maas et al., 2020**). The impact of the bleaching phenomenon has been of big concern due to its consequences, ranging from loss of local productivity to loss of biodiversity (**van Oppen and Lough, 2018**).

With the loss of algae during bleaching, the non-colored tissue of the cnidarian host, and the white skeleton in the case of corals, is then exposed, giving to this phenomenon the name of coral or cnidarian bleaching. At the cellular level, this can occur through some not well-understood mechanisms, including *in situ* algal degradation, expulsion of the algal symbiont, detachment of alga-hosting cells from cnidarian tissue, or death of alga-hosting cells (**Bieri et al., 2016**).

The disruption of symbiosis during the events of high temperature and light intensity, has been proposed to have its origin in a disbalance between the antioxidative capacity of the holobiont and the production of reactive oxygen species (ROS) (**Lesser, 1997**). In this hypothesis, the photosynthetic activity in the thylakoid membranes, being the main source of ROS in photosynthetic organisms, was also considered to be the source of ROS in Symbiodiniaceae (**Tchernov et al., 2004**; **Smith et al., 2005**; **Richier et al., 2005**). During the bleaching episodes the impairment of the photosynthetic activity, reflected in the decline of the quantum yield of PSII, has been a common observation (**Hill et al., 2004**; **Kemp et al., 2014**). Cultures of Symbiodiniaceae also develop damage in their photosynthetic activity by the combined effect of elevated temperature and high light intensity (**Iglesias-Prieto et al., 1992**; **Lesser, 1996; Robison and Warner, 2006; Suggett et al., 2008**). Heat stress has shown to decrease the antenna protein synthesis and the loss of pigments in Symbiodiniaceae in free-living conditions (**Takahashi et al., 2008**). In the coral *S. pistillata*, elevated temperature and high light intensity was shown to trigger an increased response of the antioxidative system that most likely was overtaken by the ROS production (**Roberty et al., 2015**). Following this hypothesis, the bleaching response to excessive production of ROS would be triggered by at least two paths, the signalling by ROS particles, or the oxidative damage caused by oxidative stress (reviewed in **Szabó et al., 2020**). In a more recent study with the anemone *Exaiptasia diaphana*, the role of ROS in the bleaching phenomenon has been challenged. In that study, externally supplied antioxidants (ascorbate, catalase and mannitol) could avoid the anemone bleaching, but not the ROS production (**Dungan et al., 2022**).

Although the impact of bleaching conditions has been difficult to assess on Rubisco activity, due to its instability *in vitro*, it has been proposed that the affection leading to symbiosis disruption could be located in the Symbiodiniaceae carbon fixation capacity (**Figure 11**). The analysis of expelled algal

symbionts from the coral *Cyphastrea serailia* incubated at 33 °C, found a comparable photosynthetic electron transfer capacity than the symbionts in non-treated corals (**Ralph et al., 2001**). This study suggested that coral bleaching could reside in the disruption of a different process than the photosynthetic electron transfer impairment. In another study it was shown that the inhibition of the CBB cycle by the external addition of glycolaldehyde, an inhibitor of Phosphoribulokinase, led to an affection of protein synthesis during the PSII repair mechanism in *S. pistillata* (**Bhagooli, 2013**). In this case, the authors proposed that an affection to the CBB cycle could give origin to a fast development of photoinhibition and bleaching. Other evaluations on the capacity to acquire inorganic carbon for its fixation by photosynthesis, showed that cultured Symbiodiniaceae contain a robust carbon concentrating mechanism (CCM) under high temperature conditions (**Oakley et al., 2014**). This was also observed in Symbiodiniaceae isolated from a symbiotic clam (**Leggat et al., 2004**). Contrastingly, the inhibition of the CBB cycle by glycolaldehyde, did not promote bleaching of the coral *Pocillopora damicornis* under thermal stress, as it did cyanide, an inhibitor of Rubisco but with a broader spectrum of targets (**Hill et al., 2014**).
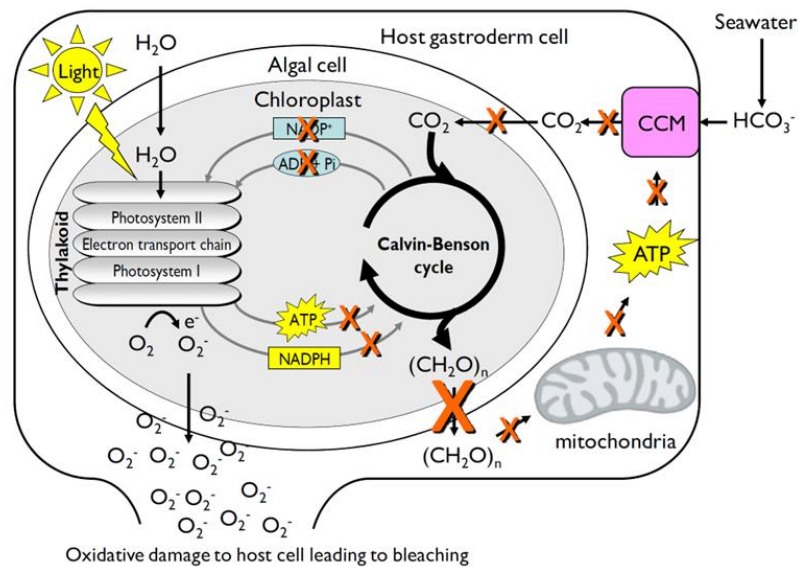
Figure 11. Metabolic disruption during a bleaching event affecting the photosynthetic activity in Symbiodiniaceae. Impairment in the activity of the inorganic carbon supply (CCM-carbon concentrating mechanism) of the algae-hosting cell (referred as Host gastroderm cell in the image) can be originated in an decreased availability of energy (ATP) or carbohydrates provided by the algal cell ($(CH_2O)_n$). This scenario results in the disruption of the photosynthetic capacity of its algae due to a lack of CO_2 within the chloroplast. The lack of ADP and $NADP^+$ recycling, and the continuous irradiance have the potential to bring the photosynthetic apparatus to an excessive oxidative damage production. Image taken from **Wooldridge, 2013**.

Some coral species showed a sensitive phenotype to thermal stressing conditions when they hosted a thermal sensitive Cladocopium species, but were more tolerant when hosted a temperature tolerant Durusdinium species (**Rowan, 2004**; **Shahhosseiny et al., 2011**). Other corals, harbouring *Symbiodinium* species, have shown to be able to withstand high light conditions (**LaJeunesse, 2002; Arrigoni et al., 2016**). These observations, however, should be considered as subjected to a species-specific association, as some sensitive Symbiodiniaceae species have shown to confer tolerance to high light intensity and high temperature conditions to juveniles of different coral species (**Abrego et al., 2008**) and to larvae of other photo-symbiotic animals (**Mies et al., 2018**).

Aim and Objectives of this Thesis

Considering the differences in the cellular environment and the nutritional relationships of Symbiodiodiniaceae in symbiosis compared to their free living condition, diverse questions stand on the nature of their photosynthetic activity. Photosynthesis is, without a doubt, the main metabolic contribution of this algae to the symbiotic association, and so, a better understanding of its regulation *in vivo* is vitally important to picture its functioning. Diverse studies have been conducted to demonstrate the presence of the regulatory and photoprotective mechanisms in the symbiotic condition. However, in the case of corals, the use of spectroscopic techniques has not been common due to a lack of suitable protocols to manage the samples. Because of these considerations, the aim in this work was to provide evidence on the occurrence of the regulatory mechanisms and the photosynthetic electron transfer chain in Symbiodiniaceae in symbiosis with cnidarian species by spectroscopic methods.

In order to pursuit the general photosynthetic process in these cnidarians and to overpass technical constraints during the manipulation, the initial objective consisted in the use of Chl *a* fluorescence imaging, to track the symbiotic algae in a diverse set of photosynthetic cnidarians, such as the golden jellyfish *Mastigias papua*, and a variety of reef-building corals. The natural process that this jellyfish faces, its capture and digestion by a non-symbiotic anemone, was used to unveil the fate and changes of Symbiodiniaceae by spectroscopy. These observations were complemented with the monitoring of oxygen evolution and light-induced absorption changes. This information provided clues on the photosynthetic capacity of Symbiodiniaceae in symbiosis, and its resistance to digestion.

A second objective consisted in the use of the coral model species *Stylophora pistillata* to standardise a protocol for the use of coral fragments in absorption spectroscopy measurements. We evaluated, through Chl *a* fluorescence imaging, the survival and photosynthetic capacity of the fragments in the following two days. The coral fragments from *S. pistillata* were then used to acquire photosynthetic parameters and to compare them with previous reports in order to prove their reliability at informing of *in vivo* processes. Moreover, the coral fragments were used to carry out physiological comparisons under increasing light conditions to deduce the presence of CEF and the WWC.

The protocol was then used to evaluate the photosynthetic electron transfer in corals collected in mesophotic and shallow depths from a coral reef in the Gulf of Eilat, Israel. Diverse physiological measurements were carried out in order to better differentiate their acclimation, such as pigment content and oxygen exchange capacity, to demonstrate the occurrence of the alternative electron pathways. The genetic identification of the Symbiodiniaceae population harboured by corals from

both depths was also obtained. Finally, a short exposure of corals to a different light regime was then evaluated through physiological parameters to evidence the relevance of the alternative pathways during photoacclimation.

CHAPTER 2   Methodological aspects

The experimental strategies employed during this study were addressed to monitor the *in vivo* photosynthetic activity of the algal symbionts of cnidarians, and thereafter to evidence the participation of the photosynthetic alternative electron pathways. The techniques used consisted of the monitoring of oxygen concentration in solution, and spectroscopic methods as the monitoring of Chl *a* fluorescence and light-induced absorption changes of photosynthetic pigments.

Oxygen measurements

During the photosynthetic activity, the oxygen molecules (O_2) produced at the OEC in PSII, constitute an easy target for monitoring. O_2 diffuses out of the thylakoids and the organisms and can be homogeneously distributed within the monitoring chamber, which in turn can be detected with amperometric electrodes (such as the Clark electrode, Hansatech Instruments, UK) or optical sensors (such as the fluorescence probes commercialized by PyroScience, Germany). This allows the monitoring of oxygen exchange rates to obtain, for example, the rate of respiration in dark conditions (Rd), or, during a period of illumination, the net oxygen exchange rate (Vo), reflecting the combined effect of gross photosynthetic oxygen evolution rate (Eo) and respiration. The use of increasing light intensities during the period of illumination, commonly reported as a light-response curve, allows the acquisition of classical photosynthetic parameters, such as the maximum photosynthetic capacity for oxygen evolution (Max Eo), the quantum yield of O_2 evolution (α), the light-compensation point for oxygen exchange (Ic) or the minimum saturating irradiance of the photosynthetic activity (Ik) (**Osinga et al., 2011**).

The monitoring of oxygen evolution in photosynthetic animals, compared to plant leaves or free-living microalgae, has a set of challenging features. One being the multiple tissue layers of the animals or the presence of coral mucus, influencing the diffusion rate of O_2 and the time-resolution accuracy during the monitoring. The natural movement of the animals within the monitoring chamber or the contraction of the animal body during the measurements, have the potential to modify the exposure area of the animal to light or the correct diffusion of O_2. In some cases this problem can be solved by immobilizing these marine organisms with an anaesthetic compound, such as $MgCl_2$ (**Arossa et al., 2022**) or eugenol, a phenolic derivative from clove extracts (**Cruz et al., 2012**) among other. However, some of these compounds can display toxicity with undesired effects on photosynthesis (**Cruz et al., 2012**). Another important consideration, which is usually overlooked in most of the studies, is the changes in the animal metabolic activity during the period of illumination. In most of

the cases this phenomenon can be noticed in the post-illumination period of the measurement (Respiration Post-I), if the change in the metabolic activity relaxes to the dark acclimated values with a considerable time to be detected.

Chl a fluorescence

The analysis of Chl *a* fluorescence emission in oxygenic photosynthetic organisms is as a powerful tool to investigate, in a non-invasive way, the electron transfer and other processes related to the activity of PSII (**Baker, 2008**). The phenomenon of Chl *a* fluorescence emission results from the de-excitation process of Chl *a* molecules located in PSII. When light absorption occurs in these pigments, they have the capacity to transfer its energy as excitons towards the RC, where the special pair of Chl *a* molecules are able to trigger the photochemical reactions, transferring one electron to QA. However, other two routes of energy de-excitation of these pigments may occur : (i) the thermal dissipation, in which the energy is dissipated as heat, and (ii) the Chl *a* fluorescence, consisting of the radiative dissipation of the energy of excited Chl *a* molecules (**Roháček and Barták 1999**). In the conditions where QA is able to accept the electron released, such as in dark acclimated conditions, the photochemical reaction constitutes the main de-excitation mechanism, and the other two represent a small fraction. In these conditions, it is commonly said that the RCs are open, and a short pulse of light is used to detect a signal of minimum fluorescence (Fo). When QA is reduced, for example due to a previous photochemical reaction, and is not able to accept the electron, the energy dissipation of excited Chl *a* molecules occurs through the thermal dissipation and the Chl *a* fluorescence. This condition can be reached by illumination with a flash of saturating light (usually lasting less than 1 s), and it is said that the RCs turn closed. A short pulse of light in these conditions then yields a signal of maximum fluorescence (Fm). At intermediate conditions, when not all the PSII RCs are open, but neither closed, the Chl *a* fluorescence level (F) varies according to the redox state of QA.

Such behaviour of the Chl *a* fluorescence, responding to the PSII photochemical capacity, is the basis for the calculation of the maximum quantum yield of PSII (φPo = Fm-Fo/Fm = Fv/Fm) (**Kitajima and Butler, 1975**). The maximum quantum yield of PSII in plants growing in optimal conditions is usually found around 0.83 (**Pfündel et al., 2013**). In diverse groups of photosynthetic organisms this value can be different, for example in the green microalga *Chlamydomonas reinhardtii* this can be between 0.65 to 0.75 (**Bonente et al., 2012**), but in some red-algae species it has been found between 0.52 to 0.66 (**Schubert and García-Mendoza, 2008**). In free-living Symbiodiniaceae, this parameter has been also been shown to vary among species ranging from 0.4 to 0.6 (**Rodríguez-Román and Iglesias-Prieto, 2005; Hennige et al., 2009; Dang et al., 2019**), and in reef building corals a diurnal variation of this parameter has also been observed (**Hoegh-Guldberg and Jones, 1999**).

In a different approach, the increase of the Chl *a* fluorescence level from Fo to Fm, can also be studied. It describes a polyphasic rise called OJIP curve (**Tóth et al., 2007**). The analysis of these OJIP curves in photosynthetic cnidarians has been more limited, but has been helpful to determine the effect of environmental (**Ulstrup et al., 2005**) or chemical (**Hill et al., 2014**) agents on the redox state of the PQ pool.

When a photosynthetic organism is light acclimated, a steady level of Chl *a* fluorescence is usually obtained (Fs). With this, the activation of other processes different that the photochemical reactions (such as the photoprotection mechanisms discussed before), may affect the fluorescence yield levels. The closure of the RCs by a saturating pulse of light in these light conditions, yields a maximum of Chl *a* fluorescence (Fm') usually different than Fm. These fluorescence values are used to calculate the effective quantum yield of PSII (φPSII = Fm'-Fs/Fm') (**Maxwell and Johnson, 2000**) for a determined light intensity. This parameter was shown to linearly correlate with the quantum yield for CO_2 fixation under non-photorespiratory conditions in plants (**Genty et al., 1989**). Because of this, the effective quantum yield of PSII has been used to deduce the activity of the photosynthetic linear electron transfer rate (ETR) by considering the fraction of photosynthetic photon flux density of the light condition (PPFD; with units of μmol photons m^{2-} s^{-1}) that is absorbed (Abs) by the fraction of PSII (PSII/PSI+PSII) present in the sample analysed (ETR = φPSII x PPFD x Abs x (PSII/PSI+PSII)) (**Baker et al., 2008**). The analysis of the Chl *a* fluorescence quenching during the light acclimation has been also used to identify the non-photochemical quenching fraction due to these processes (collectively called NPQ), and it is calculated from maximum fluorescence values (NPQ = Fm-Fm'/Fm') (**Maxwell and Johnson, 2000**).

Among the different instruments used to acquire the Chl *a* fluorescence signal (for a review see **Huot and Babin, 2010**), the time-resolved fluorescence camera has been shown to be highly versatile (**Johnson et al., 2009**). The imaging system used in this study consists of an array of LED, providing red actinic light and blue detecting light, it is electronically controlled and coupled to a CCD camera protected by a long-pass red filter (SpeedZeen Camera, BeamBio, France). This system allows to image Chl *a* fluorescence values that can be used to calculate the quantum yields on the surface of animals, but also allows the simultaneous monitoring of multiple samples.

Monitoring of P700$^+$

The activity of PSI is assessed through the monitoring of the redox state of its primary electron donor (P700). It is commonly used to calculate the photosynthetic quantum yield of PSI (Y(I)), as well as the PSI-related electron transfer rate (PSI-ETR) (**Klughammer and Schreiber, 2008**). This is achieved by the monitoring of absorption changes in the near-infrared region of the light spectrum.

In photosynthetic oxygenic species, P700 is characterised by an ample decrease in light absorption capacity (expressed as $\Delta I/I$) when it turns into its oxidised form (P700$^+$), the negative peak of absorption is centred around 700 nm (**Witt et al., 2003**). Experimentally, the absorption changes of P700 are induced with red actinic light. In this study, this was carried out with a Joliot-Type Spectrophotometer (JTS-10, BioLogic, France) controlled by a custom-made unit (BeamBio/API, France), and by applying weak beam flashes of 10 µs of duration.

Due to the presence of other photosynthetic components that develop their own kinetics of absorption in the near-infrared region, such as Plastocyanin or Ferredoxin in green plants and algae (**Klughammer and Schreiber, 2016**) a deconvolution of the signal is usually necessary. This is achieved by the simultaneous monitoring at different wavelengths, with the objective of removing their contribution to their signal measured at around 700 nm (**Schreiber, 2017**). Interestingly, the absence of Plastocyanin from red-algae and from secondary-chloroplast containin algae, such as dinoflagellates and diatoms (with the exception of the diatom *Thalassiosira oceanica*; **Peers and Price, 2006**), decreases the contamination of other components to the P700 kinetics at 705 nm. With this consideration the monitoring of absorption changes in Symbiodiniaceae in symbiosis with cnidarians, could be improved, avoiding the subtraction of values to the recordings.

Due to the position of PSI in the photosynthetic electron transfer chain, and its role both in the linear and in the cyclic electron transfer, the determination of the PSI activity has the potential to be determinant in the assessment of CEF activity (**Fan et al., 2016**).

ElectroChromic Shift (ECS) spectra

The electrochromic shift (ECS) is a phenomenon described as a consequence of the electric field present along the thylakoid membranes ($\Delta\psi$), which is generated in response to the photosynthetic activity (**Witt 1979**). The electric field is generated by both the pumping of protons and the charge separations generated at PSII, PSI and Cytochrome b_6f. The phenomenon of ECS results from changes in the light absorption capacity of carotenoids in the yellow region of the spectrum. As carotenoids are large molecules, they are influenced by the magnitude of the electric field present along the thylakoid membrane, and so their absorption spectrum (**Bailleul et al., 2010**).

Among distinct applications of the ECS technique in photosynthetic organisms, it can be mentioned its sensitivity to the pigment composition of the thylakoid membranes of different organisms (**Bailleul et al., 2010**). It can also be used to determine the photosynthetic activity through photochemical rates (**Mathiot and Alric, 2021**), or it can be used to determine the presence of photosynthetic components such as the Cyt c_6 and Plastocyanin in certain organisms through the comparison of ECS spectra (**Viola et al., 2021**). In our case, we used this technique to compare the ECS spectra of

Symbiodiniaceae in symbiosis with the symbiotic jellyfish *Mastigias papua*, or after being released with non-digested material from the gastric cavity of *Entacmaeae medusivora* (**Chapter 3 and Annex B**), and also in a free-living culture of *Symbiodinium microadriaticum* in comparison to its form in symbiosis with the coral *Stylophora pistillata*, and other coral species (**Chapter 4**). These comparisons, although not well understood, have the potential to reveal differences in the composition and functioning of the pigments present in their thylakoids. Another application of ECS that we made use of, was the determination of the relative abundance of active PSII centers in relation to the abundance of active PSI reaction centers (**Chapter 4**).

Experimentally, the ECS can be followed in a spectrophotometer with enough resolution and with the appropriate filters in the region of 500 to 600 nm. In this study we made use of the Joliot-Type Spectrophotometer (JTS-10, BioLogic, France). This set up creates a baseline of light absorption in the dark. A saturating single-turnover flash (of about 7 nanoseconds of duration) is then triggered to induce one charge separation in the photosystems present in the sample, and is continuously monitored in the following milliseconds. The absorption changes (expressed as $\Delta I/I$), due to the saturating single-turnover flash, correspond to one charge separation in the total PSII and PSI active reaction centers. The consecutive addition of specific inhibitors of PSII, 3-(3,4-dichlorophenyl)-1,1-dimethylurea (DCMU) and hydroxylamine (HA), to the sample, prevents charge separations in this photosystem. The changes in absorption then observed correspond only to PSI active reaction centres (**Cardol et al., 2008**).

Assessing the Water to Water Cycle

The analysis of the photosynthetic activity in response to increases of light intensity, can be enriched through the comparison of the photosynthetic electron transfer activity (ETR) and the oxygen exchange rates (Eo). Such comparison provides the proportion of oxygen production rate in comparison to linearly-transferred electrons along the chain. A linear proportion between the data of these two curves is expected. This, however, does not discard the presence of WWC activity in the data that maintains a linear proportion, but rather indicates that the increase of light intensity corresponds to an increase in linear electron flow. In the case of activation of WWC, or any other light-dependent oxygen consumption processes, the relationship between the oxygen exchange rate and electron transfer rate would become modified (**Roberty et al., 2014**). In such case, the linear proportion of the plot at low light intensities is modified in favour of the electron transfer activity. These plots usually show a change in trend of the relationship from the values obtained at low light intensity to a different relation at high light intensities.

Assessing the CEF

The assessment of the activity of CEF in *in vivo* conditions is an area of continuous research due to a bunch of technical considerations (**Fan et al., 2016; Mohammad Aslam et al., 2022**). Because the physiologically relevant activity of CEF is present in continuous light conditions, when the linear electron transfer also occurs, its activity is not easily deduced from there. Certainly, the function of CEF in the regulation of ATP and NAPDH production for CO_2 fixation, leads to observe that the experimental modification in the linear electron transfer pathway impacts the activity of CEF (**Alric, 2014**). In this work we carry out comparisons of the PSII- and PSI-related electron transfer measurements along the light-response curve, in order to compare the magnitude of their changes. The monitoring of both photosystems is carried out under similar experimental conditions, providing an adequate tool to compare the relative activity of both photosystems. A linear proportion in the electron transfer activity of PSII and PSI, in response to an increase of light intensity, is indicative of the increase of the linear electron transfer. However, any deviation in favour of PSI activity, can be assigned to an increase of the CEF activity (**Roberty et al., 2014**).

CHAPTER 3   The monitoring of the photosynthetic activity of Symbiodiniaceae in symbiosis with *Mastigias papua* demonstrates its extraordinary resistance to digestion

The photosynthetic activity of the Symbiodiniaceae alga *Cladocopium sp*. in symbiosis with the golden jellyfish *Mastigias papua*, is addressed in this chapter. This jellyfish was collected from marine lakes in Palau, West Pacific, together with its natural predator, the non-symbiotic anemone *Entacmaea medusivora*. Chl *a* fluorescence imaging was used to track the localisation of the algae within the body of the jellyfish as well as during its engulfment by the anemone.

During the digestion of a symbiotic jellyfish, the anemone is constantly exposed to large amounts of the symbiotic alga *Cladocopium sp*. While the genus *Entacmaea* contains symbiotic species, it has been reported that *E. medusivora* does not take Symbiodiniaceae as endosymbionts. Algal species of the same genus are widely known to perform symbiosis with other hosting cnidarian species. Because the acquisition of the photosynthetic algal symbionts by cnidarians begins with the close contact between both partners, we formulated a question on the fate of Symbiodiniaceae when in close contact with the non-symbiotic anemone. The digestive system of cnidarians is not well studied, but in the Scleractinian coral *Stylophora pistillata*, digestion is carried out importantly in the mesenterial filaments where enzymes involved in this process are present (**Raz-Bahat et al., 2017**). While in the coral *Galaxea fascicularis*, this has been described a slight acidic (with pH in the range of 6.5 to 7.2) with a bacterial community different than the one found on the external surface of the animal (**Agostini et al., 2012**).

Observations on the feeding activity of the anemone with the fluorescence imaging system allowed us to demonstrate that the photosynthetic activity was maintained even until the non-digested algae were expelled from the gastric cavity of the anemone.

We also made use of a Joliot-Type Spectrophotometer (JTS-10, BioLogic, France) in order to obtain light-dependent absorption changes in the green-orange region of the light spectrum. These absorption changes occur during the formation of an electric potential across the thylakoid membrane due to photosynthetic activity (**Bailleul et al., 2010**). A spectrum of absorption changes in response to a pulse of light, inducing charge separations, was obtained in order to demonstrate the intactness of the thylakoid membranes in the *Cladocopium sp*. during its digestion. Two ECS values at 546 and 554 nm were not included in the published version of the **Figure 4a** of this Chapter, but are included as an additional Figure in the **Annex B**.

Title of publication : Photosynthetic capacity of the endosymbiotic dinoflagellate *Cladocopium sp.* is preserved during digestion of its jellyfish host *Mastigias papua* by the anemone *Entacmaea medusivora*.

Authors : Félix Vega de Luna, Kieu-Van Dang, Mila Cardol, Stéphane Roberty, Pierre Cardol.

Journal : *FEMS Microbiology Ecology*, 95 (10) 2019 https://doi.org/10.1093/femsec/fiz141.

My contribution in this publication consisted in the acquisition of chlorophyll *a* fluorescence images during the experiment, the preparation of the figures and the writing of the manuscript.

Title

Photosynthetic capacity of the endosymbiotic dinoflagellate *Cladocopium sp.* is preserved during digestion of its jellyfish host *Mastigias papua* by the anemone *Entacmaea medusivora*

Running Title

Photosynthesis upon digestion of *M. papua* by *E. medusivora*

Authors

Vega de Luna Félix, Dang Kieu-Van, Cardol Mila, Roberty Stéphane, Cardol Pierre*

Affiliation

Inbios / Phytosystems, Université de Liège, Belgium

*to whom correspondence should be addressed

Pierre Cardol, pierre.cardol@uliege.be, +32 43 66 38 40, 4 chemin de la vallée, Institut de Botanique, Université de Liège 4000 Liège, Belgique

Abstract

The sea anemone *Entacmaea medusivora* (Actiniaria, Anthozoa) commonly feeds on the golden jellyfish *Mastigias papua* (Rhizostomeae, Scyphozoa) which harbours endosymbiotic dinoflagellate of the genus *Cladocopium* (Symbiodiniaceae). In this study, we monitored the photosynthetic activity of the endosymbiotic microalgae while their host jellyfish were ingested and digested by starved medusivorous anemones. By analyzing the photosynthetic yield of Photosystem II, we observed that *Cladocopium* cells remain photosynthetically competent during the whole digestion process, thus confirming the exceptional resistance of Symbiodiniaceae to digestive enzymes. In the gastric cavity of *E. medusivora*, *Cladocopium* cells release oxygen, which could broadly stimulate the gastric microbiotic flora of the sea anemone. Ultimately, *E. medusivora* is not able to retain *Cladocopium* cells more than few days and physiologically-unaltered cells are therefore expelled in faecal pellets. The potential contribution of *E. medusivora* to maintain a reservoir of *Cladocopium* symbionts and its role in the life cycle of *M. papua* is discussed.

Introduction

Dinoflagellates from the Symbiodiniaceae family have the capacity to establish an endosymbiotic relationship with many species of cnidarians (*i.e.* corals, sea anemones and jellyfish) (LaJeunesse *et al*. 2018). The establishment of symbiosis implies a multistep process involving the host and the endosymbiont, the very first step being the physical interaction between both partners. The recognition mechanisms are similar to those acting in the recognition of pathogenic organisms and imply the production of pattern recognition receptors (PRR) able to bind to specific microbial compounds (named microbe-associated molecular patterns or MAMPs). In the case of Cnidarian-Dinoflagellate symbiosis, the PRR are carbohydrate-binding proteins (*e.g.* lectins) that are either secreted or present at the surface of the host, while the MAMPs are glycans harbored on the cell surface of the symbionts (Davy *et al*. 2012; Fransolet *et al*. 2012). Initial contacts between algae and animal host cells, and the subsequent phagocytosis of algal cells lead to the sorting of the symbionts engulfed in functional structures known as symbiosomes (Fransolet *et al*. 2012). On the other hand, many cnidarians such as the actiniarian anemone *Nematostella vectensis (*Hand and Uhlinger 1992), the hydrozoan jellyfish *Clytia hemisphaerica* (Houliston *et al*. 2010), the scyphozoan jellyfish *Aurelia aurita* (Hernroth and Gröndhal 1983), some strains of the freshwater-living polyp *Hydra vulgaris* (Ishikawa *et al*. 2016), and even some scleractinian corals (Daly *et al*. 2007; Barbeitos *et al*. 2010) are asymbiotic.

In the Palau's Archipelago, the meromictic saline lake of the Eil Malk Island (commonly known as Jellyfish Lake) comprises an upper layer (up to 15 m deep) of oxygenated, nutrient-poor and brackish water where cnidarians inhabit (Hamner *et al*. 1982). Those include the asymbiotic sea anemone *Entacmaea medusivora* (Fautin and Fitt 1991) and the golden jellyfish *Mastigias papua* (De Souza and Dawson 2018). In Palau, *M. papua* usually lives in symbiosis with dinoflagellates from the genus *Cladocopium* (formerly Clade C) (Krueger *et al*. 2015; LaJeunesse *et al*. 2018). About 10% of the jellyfish protein biomass corresponds to endosymbiotic *Cladocopium* cells that reside within the mesoglea of the coelenterate (Muscatine *et al*. 1986). Because of this symbiotic relationship, *M. papua* is responsible for about 20% of the carbon primary production of the lake (Hamner *et al*. 1982). These jellyfish swim horizontally close to the surface following the sun position to the shadow line (Dawson and Hamner 2003) and avoid reaching the shoreline where the sea anemone *E. medusivora*, its natural predator, lives (Fautin and Fitt 1991).

E. medusivora is considered as asymbiotic (Fautin and Fitt 1991). However, given that this sea anemone feeds on symbiotic jellyfish, its gastric cavity is exposed to a large amount of *Cladocopium* cells. The fate of these algae upon digestion is not yet known. However, it has been documented in

some symbiotic cnidarian-eating parrotfishes or sea stars that Symbiodiniaceae algae survive digestion and are present in faeces (Castro-Sanguino and Sánchez 2012; Bachman and Parker 2007). In this report, we studied the photosynthetic capacity and distribution of *Cladocopium* cells during digestion of golden jellyfish by the sea anemone *E. medusivora*.

Methods

Biological materials

During a sampling campaign conducted in January 2018, six specimens of *E. medusivora* were collected from Jellyfish Lake (Ongeim'l Tketau, OTM) on the island of Eil Malk (Mecherchar) in the Republic of Palau. Because population of golden jellyfish *Mastigias papua etpisoni*, dropped to zero in OTM since May 2016 (the causes are most likely similar to causes of a previous event of disappearance in 1998; see Dawson et al. 2001), *M. papua remeliiki* were sampled in Uet era Ngermeuangel lake (NLK) on January 17th, 2018, or Ngerchaol cove (NCK) on January 19th, 2018 (Figure 1A-E), under the permit n° 027 delivered by the Koror State Government. Four specimens were obtained from each site, 1.5-2 cm diameter and 1.5-2 g fresh weight. One specimen of each site was genotyped by T. Lajeunesse at Pennsylvania State University (according to LaJeunesse *et al*. 2018). Both correspond to *Cladocopium sp.* (unpublished data). Sea anemones and jellyfish were maintained at the Palau International Coral Research Center (PICRC) for 10-14 days in 70% seawater for specimens from NLK and OTM or natural seawater for jellyfish from NCK. Sea anemone *E. medusivora* were maintained individually in 100 mL cylindrical glass jars. They were starved for at least 7 days before being fed with one or two anemones (see result section). Light intensity was low, with a maximum of 100 µmol photons m-2 s-1 reached at noon. Water temperature was maintained at 30 ± 1°C (day-night variations). This temperature corresponds to the average temperature of different Lakes in Palau (Dawson *et al*. 2001) and to the sea surface temperature of western Pacific Ocean (Locarnini *et al*. 2010) in january. The physiological state of sampled golden jellyfish was monitored in the laboratory every day by evaluating their motility and their maximum quantum yield of photosystem II (FV/FM) by fluorescence imaging (Figure 1 F-H). Measurements were performed in standard 12-well plates.
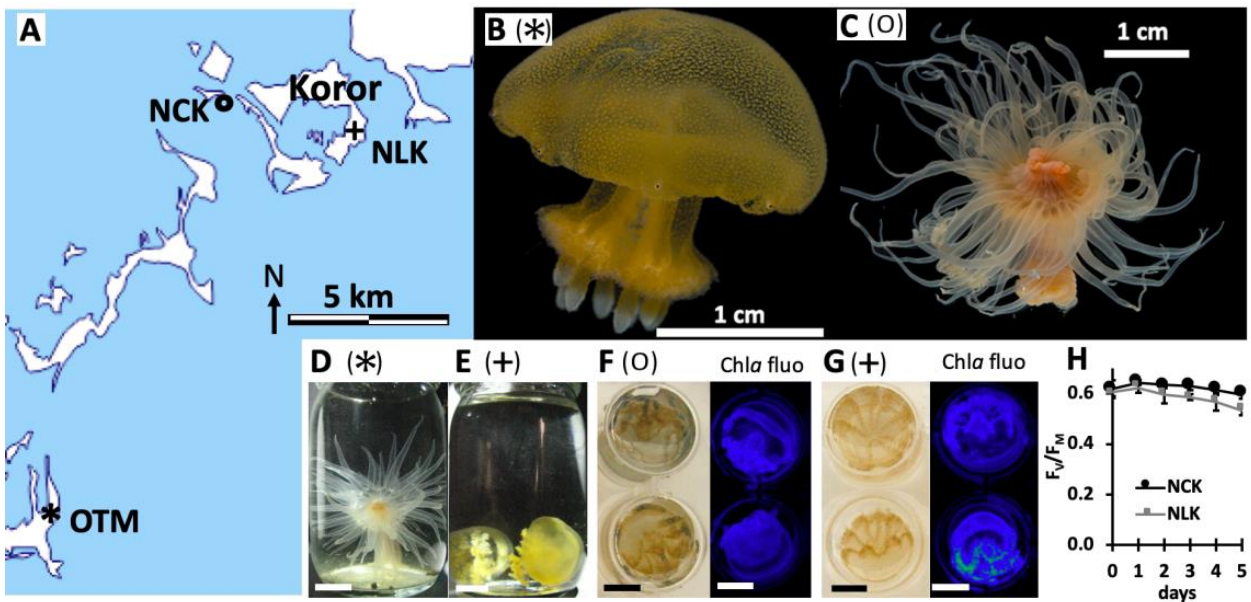
Figure 1. Geographic origin, aspect and size of golden jellyfish *Mastigias papua* and medusivorous anemone *Entacmaea medusivora* from Palau used in this study. **A.** Partial map of Palau's archipelago indicating the sampling sites (**∗**) Ongeim'l Tketau in Mecherchar (OTM, Jellyfish Lake), 7°09'40.2"N 134°22'35.0"E; (**+**) Uet era Ngermeuangel lake in Koror (NLK), 7°19'28.5"N 134°30'31.6"E; (**o**) Ngerchaol cove in Koror (NCK), 7°20'17.6"N 134°27'04.6"E. Map was obtained at https://dmaps.com/carte.php?num_car=3326. **B,F.** *Mastigias papua* from NCK. **C,D.** *Entacmaea medusivora* from OTM. **E,G.** *Mastigias papua remeliiki* from NLK. **H.** Maximal PSII quantum yield (FV/FM) at day 0 (after sample harvesting) and during 5 days in aquariums. Measurements were performed by chlorophyll fluorescence imaging of jellyfish in standard 12-well plates (mean of 4 jellyfish with standard errors). Scale bars on panels B-G correspond to 1 cm.

In vivo chlorophyll fluorescence imaging

True-colour pictures along with chlorophyll *a* fluorescence imaging were used to monitor the distribution of symbiotic microalgae and overall shape during the feeding and digestion events by anemones. Distribution of chlorophyll *a* fluorescence yield in jellyfish and anemones was determined at room temperature with a fluorescence imaging system (SpeedZen, BeamBio/API, France). Chlorophyll *a* fluorescence was excited by an array of blue LEDs (450-470 nm), filtered with a long pass red filter and recorded by a CCD camera (UI-3240CP-NIR-GL Rev.2, IDS, Obersulm, Germany). The anemones change their overall shape during digestion and move inside the glass containers, so the geometry of the fluorescence imaging system is different from one image to

another. Accordingly, it was not possible to quantitatively compare the overall amount of fluorescence at the different time points.

To determine if algal cells were photosynthetically active, we measured the relative electron transfer rate of photosystem II (rETR-PSII) at different continuous actinic light intensities (up to 1000 μmol photons m^{-2} s^{-1}) by a LED array emitting at 660 nm, also delivering 200 ms 6000 μmol photons m^{-2} s^{-1} saturating pulses. The maximum quantum yield of photosystem II was measured as FV/FM, where FV = FM - FO, FO is the initial fluorescence level in dark-adapted sample, and FM is the maximum fluorescence level after a saturating pulse of light (Kitajima and Butler 1975). After acclimation to different light intensities, FS and FM' (stationary fluorescence level in continuous light and maximum fluorescence emission induced by saturating pulse of light, respectively) were measured and the effective quantum yield of photosystem II at steady state (φPSII = (F$_M$'-F$_S$)/F$_M$', Genty *et al.* 1989) was calculated. The relative electron transfer rate (rETRPSII) was calculated as the product of φPSII by the actinic light intensity (Ralph and Gademann 2005). Because rETR-PSII value is proportional to a ratio of fluorescence measurements, its value is much less affected by the geometry of our experimental setup and the data can be quantitatively compared.

Polarographic measurements of oxygen

Measurements of light-dependent oxygen release of *M. papua* and *E. medusivora* (24 h after having being fed with one jellyfish) were carried out by using a Clark type electrode in a 2.5 mL chamber (Oxygraph+, Hansatech, UK). The translucent acrylic chamber (DW1, Hansatech, UK) was set next the SpeedZen camera, which was accommodated in a horizontal position. The same red actinic light intensity used to perform fluorescence measurements was used to monitor oxygen exchange. Measurement of light intensity was performed using a Submersible Spherical Micro Quantum Sensor (Walz, Germany) connected to a LI-250A light meter (Li-Cor, USA).

Electrochromic shift spectra

The response of photosynthetically competent microalgae to actinic radiation was also assessed by electrochromic shift signal (ECS) detection using a JTS-10 LED pump-probe spectrophotometer (Biologic, France). ECS occurs only in response to an electric potential across the thylakoid membrane (Bailleul et al. 2010). The shape of the ECS spectrum also reflects the membrane pigment composition and is therefore different between various photosynthetic eukaryote lineages (Bailleul *et al.* 2010). Spectral characteristics of ECS were determined from *M. papua* and *E. medusivora* 24 h after being fed with one NLK jellyfish. Absorbance changes were measured in glass visible spectrometer cuvette cell (Path Length 1 cm), from 480 to 540 nm each 10 nm using BrightLine (Semrock) single-band bandpass filters (full width at half maximum bandwidth of about 15 nm). They were determined during 4 ms after a short saturating pulse of red light (9000 μmol photons m-2 s-1,

660nm), as previously described for cultured *Symbiodinium* (formerly temperate Clade A) cells (Roberty *et al*. 2014).

Results

Specimens of the sea anemone *E. medusivora* collected on the shores of Jellyfish Lake (Ongeim'l Tketau, OTM) in the Republic of Palau presented on average the same size, about 3 cm high when individuals were fully extended (Figure 1 D). Before being fed, the anemones did not show any chlorophyll *a* fluorescence signal (Figure 2 B.1, C.1 & D). We first fed an anemone with small *M. papua* jellyfish collected at Uet era Ngermeuangel lake (NLK). From the moment when a jellyfish was caught by anemone tentacles, it took approximately 5 minutes for *E. medusivora* to fully ingest their prey (Figure 2 B.2, C.2 & C.3). The shape of the jellyfish could be distinguished up to one hour after ingestion inside the sea anemone column (Figure 2 B.3). From three hours after ingestion, the shape of the jellyfish was no longer distinguishable and chlorophyll *a* fluorescence was distributed in mesenteries of the anemone (Figure 2 B.4 & C.5), indicating that the jellyfish have been dislocated and digestion has occurred. The overall trend was a decrease in the chlorophyll fluorescence (Figure 2A & 2B) that fully disappeared after 3-4 days (data not shown).

To determine if these fluorescence signals corresponded to photosynthetically active microalgae upon digestion, light saturation curves of the relative electron transfer rate of photosystem II (rETR-PSII) were established. When comparing the light curve obtained with free jellyfish, ingested jellyfish (5 min - 1 h) and mesenteries of anemones (from 3 h to 24h after digestion), no significant differences were found both in the maximum rate of rETR-PSII and in the initial slope of the light curve (Figure 2 B.6 & C.6). These results strongly suggest that an important fraction of *Cladocopium* cells remain photosynthetically competent during the digestion process of symbiotic jellyfish by *E. medusivora*.

We also collected faecal pellets expelled by these anemones 12 to 18 h after feeding with jellyfish (Figure 2 B.5 & C.4). These excretions were fluorescent (see B.5 & C.4 in Figure 2 E.1). In contrast, faeces from another anemone fed with mussel flesh, or waste matters from a starved specimen were not fluorescent (see D& F in Figure 2 E.1). rETR-PSII of the fluorescent faecal matters (Figure 2 E.2) were similar to the one of intact or digested jellyfish. These results indicate that *Cladocopium* cells can resist digestive enzymes of *E. medusivora*.
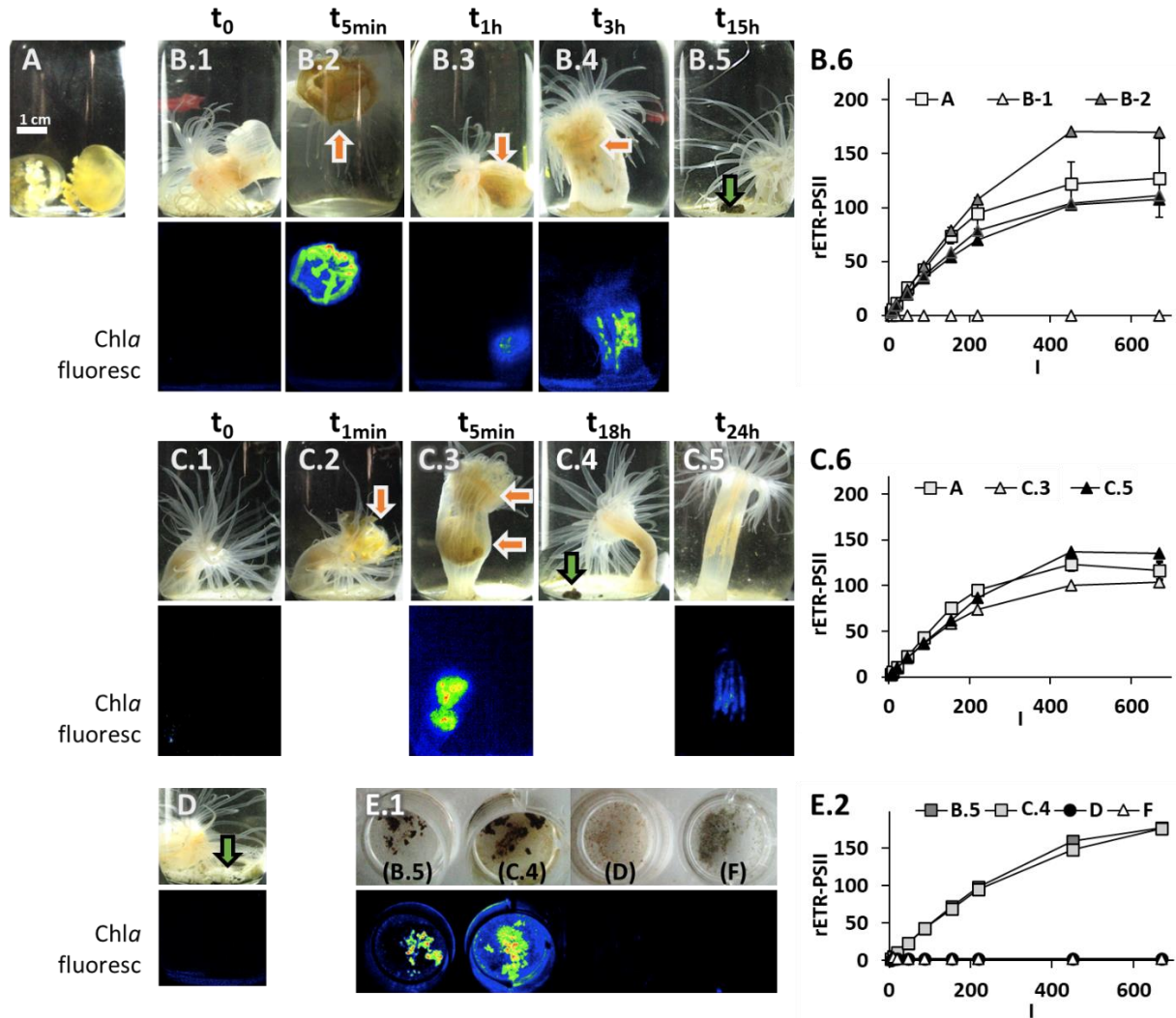
Figure 2. Photosynthetic activity of *Cladocopium* upon digestion of its host golden jellyfish *M. papua NLK* by the anemone *E. medusivora*. A. *M. papua* from Uet era Ngermeuangel lake in Koror (NLK; see Figure 1 for details). A starved *E. medusivora* was fed with one (**B.1-5**) or two (**C.1-5**) NLK jellyfish. Orange arrows point to jellyfish whose shape is still visible inside the anemone. **D**. *E. medusivora* was fed with (non-photosynthetic) mussel flesh collected on the shore of Ongeim'l Tketau (OTM, JellyFish lake). **E.1**. Faeces from anemones (**B.5, C.6, & D**; green arrows) and waste matters at the bottom of the glass pot of a starved anemone (**F**) were transferred in standard 12-well plates. Imaging of the maximal yield of chlorophyll fluorescence (FM, **Chl*a* Fluo**) is shown for selected pictures: before ingestion of jellyfish (**B.1, C.1**); at various moments during digestion of jellyfish (**B.2-4, C.3, C.5**); after feeding with mussels (**D**) and for waste matters (**F**). **B.6, C.6, E.2**. Relative electron transfer rates of PSII (rETR-PSII) as a function of the actinic light intensity (I, μmol photons m^{-2} s^{-1}) was calculated from

chlorophyll fluorescence signals of intact jellyfish (A, n=3) and anemones from B & C series (n=1). Scale bar on panels A corresponds to 1 cm.

When *M. papua* oceanic subspecies collected in Ngerchaol cove (NCK, Figure 1 B & F) was used to feed another starved anemone, the same set of events was observed, meaning that the jellyfish is digested and *Cladocopium* cells stay photosynthetically active during digestion (Figure 3 A). Because chlorophyll fluorescence is emitted in all directions and may therefore diffuse into the animal tissues, we could not fully exclude that some *Cladocopium* cells are not located outside the mesenteries. For instance, tentacles were faintly fluorescent in some pictures (see for instance Figure 3 A.1). No chlorophyll *a* fluorescence was however detected in separated tentacles. All anemones fed only once with jellyfish (NLK or NCK) were also starved thereafter. No remaining fluorescence was detected in these animals after 3 days (data not shown).
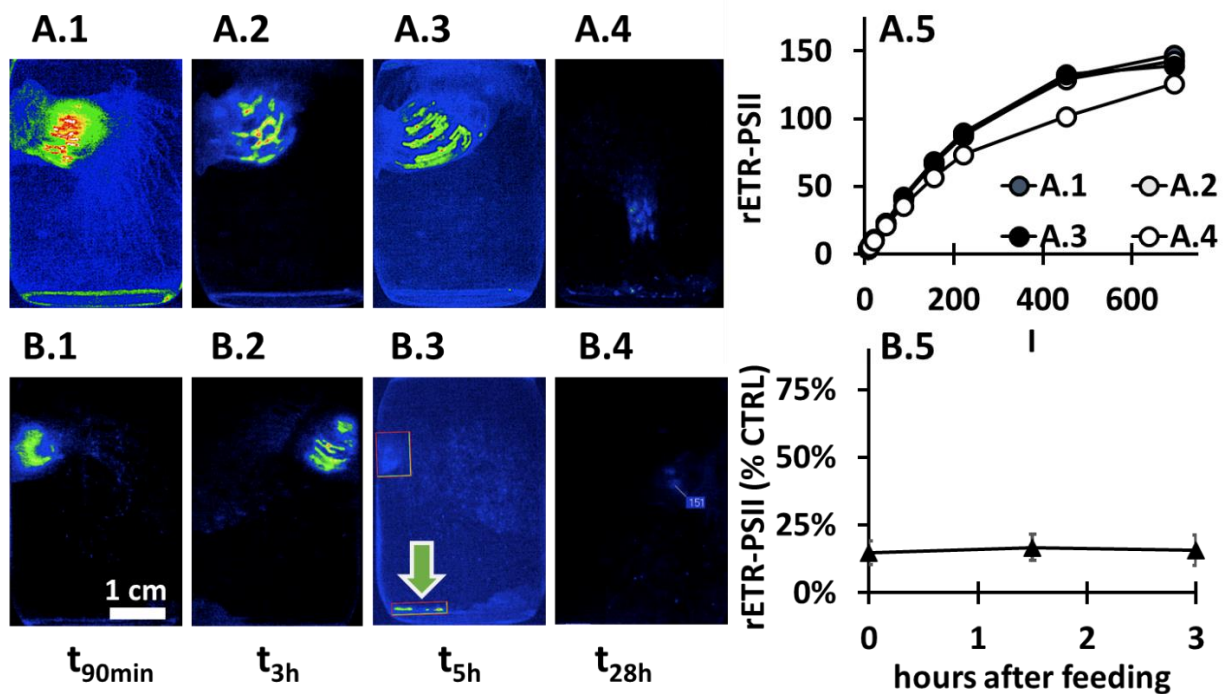
Figure 3. Comparison of photosynthetic activity in DCMU-poisoned and unpoisoned *Cladocopium* during digestion of *M. papua* NCK by *E. medusivora*. (**A.1-4**) A starved *E. medusivora* was fed with *M. papua* jellyfish (from Uet era Ngerchaol cove in Koror, NCK; see Figure 1 for details). Pictures were obtained by *in vivo* fluorescence imaging of the maximal yield of chlorophyll fluorescence at various moments (from 90 min to 28h) during digestion of the jellyfish. (**A.5**) Relative electron transfer rates of PSII (rETR-PSII) as a function of the actinic light intensity (I, μmol photons m-2 s-1) was calculated

from chlorophyll fluorescence signals of A series (n=1). (**B.1-4**) A starved *E. medusivora* was fed with NCK *M. papua* jellyfish poisoned by DCMU 20 μM during 5 min prior ingestion. (**B.5**) Ratio between rETR-PSII from DCMUtreated (B series) and control experiment (A series) (n=1). A green arrow indicates faecal pellets. Averaged values and standard deviations were calculated from values at 8 different light intensities. Scale bar on panel B.1 corresponds to 1 cm.

In parallel, another *E. medusivora* was fed with an oceanic NCK jellyfish poisoned with DCMU, a potent inhibitor of Photosystem II. Although rETR-PSII of the ingested jellyfish was initially less than 10% of the control (Figure 3 B.5), the same temporal set of events occurred. The overall amount of fluorescence however decreased rapidly in the DCMU-poisoned experiment, being very low 5 h after feeding (compare Figures 3 B.3 & A.3). This suggests that DCMU-poisoned *Cladocopium* cells lost their fluorescence due to damages to the photosynthetic apparatus and might have been digested, or died and have been expelled with excrements (green arrow in Figure 3 B.3).

To confirm that *Cladocopium* cells were still photosynthetically active inside the anemone one day after being fed with unpoisoned jellyfish, we examined if an electrochromic shift signal (ECS) could be measured. A similar ECS spectrum could be determined for both types of golden jellyfish as well as for an anemone fed with a jellyfish from NLK (Figure 4 A). These ECS spectra of *Cladocopium* are similar to those of cultured *Symbiodinium* (formerly Clade A) cells, which are characterized by a maximum at 510 nm and a minimum at 550 nm (Roberty *et al*. 2014). These results confirm that *Cladocopium* cells were still photosynthetically active in the mesenteries and that membrane pigments responsible for ECS were not impaired.

Finally, net oxygen exchange rate (VO2) of this latter anemone was compared with VO2 values of an intact golden jellyfish (Figure 4 B). The dark respiratory rate per animal of both cnidarians was similar. For both organisms, a light-dependent oxygen evolution was observed. Because the experiment was performed only once we cannot comment on the absolute values. Still, this result is another confirmation that *Cladocopium* cells are able to perform photosynthesis inside the gastric cavity of the anemone.
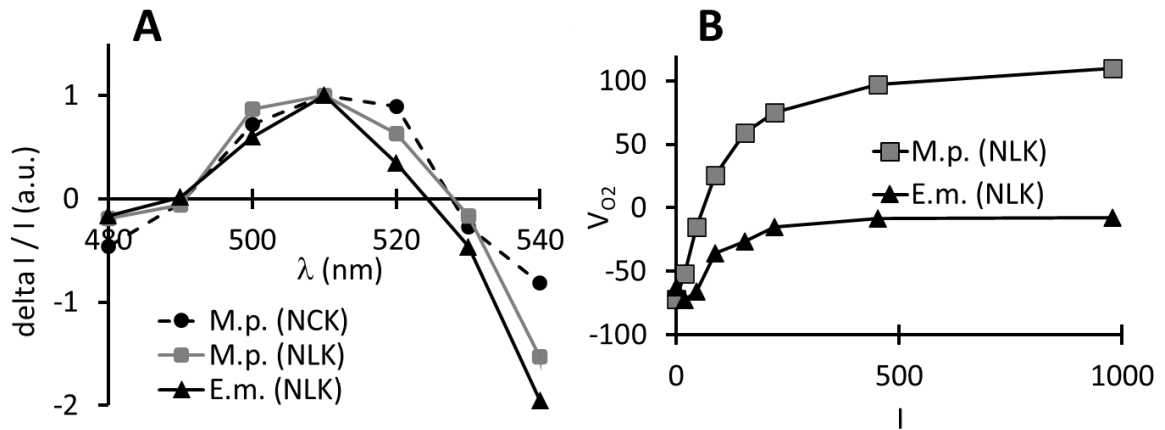
Figure 4. **Comparison of photosynthetic features from golden jellyfish *Mastigias papua* and *Entacmaea medusivora* 24h after feeding with NLK golden jellyfish**. **A**. Electrochromic shift (ECS) spectra upon 4 ms of illumination. **B**. Net oxygen exchange rate (VO2; 10-1 nmol O2 s-1 per animal, n=1) as a function of light intensity (I, μmol photons m-2 s-1, 3 min steps). M.p. (NLK), M.p. (NCK): *Mastigias papua* from NLK lake and NCK lake respectively. E.m. (NLK): *Entacmaea medusivora* fed with NLK golden jellyfish.

Discussion

Overall, our observations indicate that a significant fraction of *Cladocopium* cells are not altered and remain photosynthetically active from ingestion of symbiotic jellyfish *M. papua* to expulsion of excrements by the sea anemone *E. medusivora*. The sea anemone *E. medusivora* has been found so far only in Jellyfish Lake located on Eil Malk island in Palau (Fautin and Fitt 1991) and in Kakaban Lake in Indonesia (Hoeksema *et al.* 2015). These anemones notably feed on various jellyfish species such as *Aurelia aurita* (the moon jellyfish), *M. papua* (golden jellyfish) and *Cassiopea sp.* (upside-down jellyfish) (Fautin and Fitt 1991; Hoeksema *et al.* 2015). These two last species live in symbiosis with photosynthetic dinoflagellates of the Symbiodiniaceae family (LaJeunesse *et al.* 2018). In Palau, the population of *M. papua etpisoni* disappeared from Jellyfish Lake (OTM) in 2016 following a strong El Niño - southern oscillation event, and began recovering towards the end of 2018 (Coral Reef Research Foundation, personal communication). Therefore, *E. medusivora* sampled in January 2018 had been deprived of photosynthetic jellyfish for several months. Upon digestion of *M. papua* by starved *E. medusivora*, the vast majority of *Cladocopium* chlorophyll fluorescence is distributed in areas that most likely correspond to mesenteries, where digestive enzymes are present. Despite this

high amount of algae that remain photosynthetically active from ingestion of their host jellyfish to expulsion with undigested matters, *E. medusivora* does not establish stable symbiosis with photosynthetic *Cladocopium* cells. The lack of chlorophyll fluorescence measured *in vivo* on individuals just after sampling, or several days after feeding with *M. papua*, confirms that *E. medusivora* is asymbiotic. This is in good agreement with a previous study that failed to identify dinoflagellates cells using electron microscopy (Fautin and Fitt 1991). But this contrasts with the fact that this sea anemone belongs to a genus containing symbiotic species, such as the bubble-tip anemone *Entacmaea quadricolor* (Scott and Harrison 2007). Several assumptions can explain why ingested *Cladocopium* do not establish endosymbiosis: 1) the absence of a recognition mechanism between the two species; 2) the sea anemone recognizes *Cladocopium* as a prey; 3) *Cladocopium* is recognized and then phagocytized but the phagosome does not maturate into a symbiosome and fuses with lysosomes. In this respect Fautin and Fitt (1991) suggested that some Symbiodiniaceae are phagocytosed into host digestive cells when introduced with *Artemia* nauplii, but do not remain in the *E. medusivora* digesting cavities for more than one week. Few cases of non-photosynthetic anemones capable of establishing a symbiotic relationship with algae have been however documented. For instance, asymbiotic strains of *Hydra vulgaris* (Hydrozoa) may establish endosymbiosis with *Chlorococcum* green algae under laboratory conditions (Ishikawa *et al*. 2016).

Although *E. medusivora* is unable to establish a lasting relationship with *Cladocopium*, it is tempting to suggest that the transient presence of large amount of photosynthetically active Symbiodiniaceae inside its digestive cavity may have a positive impact on the physiology of the anemone. As the body of *E. medusivora* is translucent, *Cladocopium* cells located inside the gastric cavity perform photosynthesis and release O2. Carbon fixed by photosynthesis may also be exported by the microalgae. Indeed, it has been previously reported that isolated Symbiodiniaceae from the sea anemone *Exaiptasia* released approximately 5% of their photosynthates. This proportion even increased to 14-25 % in response to extracts of host tissue (host-release factor; Davy and Cook 2001). Therefore, we suggest that the release of photosynthetic products may directly contribute to the metabolism of *E. medusivora*. This needs to be further investigated by the use of stable isotope tracers of Carbon or Nitrogen, with labelling of the microalgae before ingestion by anemones (Cleveland *et al.,* 2011). The effect may also be indirect through the stimulation of the bacterial community inhabiting the gastric cavity (Agostini *et al*. 2011; Cleary *et al*. 2016).

Our study also demonstrates that expelled *Cladocopium* from *E. medusivora* after digestion of *M. papua* are still photosynthetically competent. Similar results have been previously reported in other corallivorous organisms. For instance, some parrot fishes can carry Symbiodiniaceae algae in their digestive system and expel them alive within their faeces (Castro-Sanguino and Sánchez 2012). The

faeces of the sea star *Dermasterias imbricata* fed with the symbiotic anemone *Anthopleura elegantissima* also contains almost physiologically-unaltered symbiotic microalgae (Bachman and Parker 2007). These observations in three different species indicate a general resistance capacity of Symbiodiniaceae to the digestion process of various animals. This is not really surprising since a method aiming to isolate intact and viable Symbiodiniaceae from host tissues requires the use of 1M NaOH (Zamoum and Furla 2012). Such a resistance to host lysosomal enzymes could be considered as a fundamental prerequisite to the establishment of a symbiotic relationship (*e.g.* Kodama and Fujishima 2014).

Similarly to *Cassiopea* (Lampert 2016), a Rhizostomeae jellyfish closely related to the golden jellyfish, the transmission of endosymbiotic dinoflagellates in *M. papua* occurs horizontally. Indeed, eggs, testicular vesicles and planula larvae of both species are free of endosymbionts, and only scyphistomae (polyps) acquire them during growth (Sugiura 1964; Hoffman et al., 1996). The colonization of the polyps is even required to initiate the strobilation and the production of symbiont-containing ephyra larvae and adults of *M. papua* (Sugiura 1964). Consequently, the Symbiodiniaceae community hosted by the jellyfish necessarily originates from an environmental reservoir of free-living symbionts present in sediments and in the water column. This reservoir can be constituted by the release of Symbiodiniaceae (1) from *Mastigias* polyps, ephyra and adults into the surrounding water (Sugiura 1964), release that could be constant as in symbiotic corals (Hoegh-Guldberg *et al*. 1987); (2) from the degradation of dead adult jellyfish; (3) from predators feeding on cnidarians (Muller-Parker 1984; Castro-Sanguino and Sánchez 2012; Bachman and Parker 2007).

Based on the results presented in this report, we propose that, by feeding on *M. papua*, the medusivorous anemone could significantly contribute to increase the speed of algal release. Because *Mastigias* scyphistomae and *E. medusivora* are living in close vicinity to each other in the Jellyfish Lake (Dawson 2005), this could participate to maintain an environmental reservoir of free-living *Cladocopium*. Hence, by eating some jellyfish, and participating to microalgal cycling, *E. medusivora* would play a key role in the life cycle of *M. papua*.

Acknowledgments

Reference

Agostini S, Suzuki Y, Higuchi T *et al.* Biological and chemical characteristics of the coral gastric cavity. *Coral Reefs* 2012;**31**:147–56.

Bachman S, Muller-Parker G. Viable algae released by the sea star Dermasterias imbricata feeding on the symbiotic sea anemone *Anthopleura elegantissima*. *Mar Biol* 2007;**150**:369–75.

Bailleul B, Cardol P, Breyton C *et al.* Electrochromism: A useful probe to study algal photosynthesis. *Photosynth Res* 2010;**106**:179–89.

Barbeitos MS, Romano SL, Lasker HR. Repeated loss of coloniality and symbiosis in scleractinian corals. *Proc Natl Acad Sci* 2010;**107**:11877–82.

Castro-Sanguino C, Sánchez JA. Dispersal of *Symbiodinium* by the stoplight parrotfish *Sparisoma viride*. *Biol Lett* 2011;**2**:282–6.

Cleary DFR, Becking LE, Polónia ARM *et al.* Jellyfish-associated bacterial communities and bacterioplankton in Indonesian Marine lakes. *FEMS Microbiol Ecol* 2016;**92**:1–14.

Cleveland A, Verde EA, Lee RW. Nutritional exchange in a tropical tripartite symbiosis: direct evidence for the transfer of nutrients from anemonefish to host anemone and zooxanthellae. *Mar Biol* 2011;**158**:589-602.

Daly M, Brugler MR, Cartwright P *et al.* The phylum Cnidaria: A review of phylogenetic patterns and diversity 300 years after Linnaeus. In: Zhang, Z.-Q. & Shear, W.A. (Eds) Linnaeus Tercentenary: Progress in Invertebrate Taxonomy. *Zootaxa* 2007;**1668**:127–182.

Davy SK, Allemand D, Weis VM. Cell Biology of Cnidarian-Dinoflagellate Symbiosis. *Microbiol Mol Biol Rev* 2012;**76**:229–61.

Davy SK, Cook CB. The influence of 'host release factor' on carbon release by zooxanthellae isolated from fed and starved *Aiptasia pallida* (Verrill). *Comp Biochem Physiol Part A* 2001;**129**:487–94.

Dawson MN. Five new subspecies of *Mastigias* (Scyphozoa: Rhizostomeae:Mastigiidae) from marine lakes, Palau, Micronesia. *J Mar Biol Assoc United Kingdom* 2005;**85**:679–94.

Dawson MN, Martin LE, Penland LK. Jellyfish swarms, tourists, and the Christ-child. *Hydrobiologia* 2001;**451**:131–144.

Dawson MN, Hamner WM. Geographic variation and behavioral evolution in marine plankton: The case of *Mastigias* (Scyphozoa, Rhizostomeae). *Mar Biol* 2003;**143**:1161–74.

Fautin DG, Fitt WK. A jellyfish-eating sea anemone (Cnidaria, Actiniaria) from Palau: *Entacmaea medusivora* sp. nov. *Hydrobiologia* 1991;**216**–**217**:453–61.

Fransolet D, Roberty S, Plumier JC. Establishment of endosymbiosis: The case of cnidarians and *Symbiodinium*. *J Exp Mar Bio Ecol* 2012;**420**–**421**:1–7.

Genty B, Briantais JM, Baker NR. The relationship between the quantum yield of photosynthetic electron transport and quenching of chlorophyll fluorescence. *Biochim Biophys Acta - Gen Subj* 1989;**990**:87–92.

Hamner WM, Gilmer RW, Hamner PP. The physical, chemical, and biological characteristics of a stratified, saline, sulfide lake in Palau. *Limnol Oceanogr* 1982;**27**:896–909.

Hand C, Uhlinger KR. The culture, sexual and asexual reproduction, and growth of the sea anemone *Nematostella vectensis*. *Biol Bull* 1992;**182**:169–76.

Hernroth L, Gröndahl F. On the biology of aurelia aurita (L.) 1. Release and growth of *Aurelia aurita* (L.) ephyrae in the gullmar fjord, Western Sweden, 1982-83. *Ophelia* 1983;**22**:189–99.

Hoegh-Guldberg O, McCloskey LR, Muscatine L. Expulsion of zooxanthellae by symbiotic cnidarians from the Red Sea. *Coral Reefs* 1987;**5**:201–4.

Hoeksema BW, Tuti Y, Becking LE. Mixed medusivory by the sea anemone *Entacmaea medusivora* (Anthozoa: Actiniaria) in Kakaban Lake, Indonesia. *Mar Biodivers* 2015;**45**:141–2.

Hofmann DK, Fitt WK, Fleck J. Checkpoints in the life-cycle of *Cassiopea* spp.: control of metagenesis and metamorphosis in a tropical jellyfish. *Int J Dev Biol* 1996; **40**:331-338.

Houliston E, Momose T, Manuel M. *Clytia hemisphaerica*: A jellyfish cousin joins the laboratory. *Trends Genet* 2010;**26**:159–67. Ishikawa M, Shimizu H, Nozawa M *et al.* Two-step evolution of endosymbiosis between hydra and algae. *Mol Phylogenet Evol* 2016;**103**:19–25.

Kitajima M, Butler WL. Quenching of chlorophyll fluorescence and primary photochemistry in chloroplasts by dibromothymoquinone. *BBA – Bioenerg* 1975;**376**:105–15.

Kodama Y, Fujishima M. Symbiotic *Chlorella variabilis* incubated under constant dark conditions for 24 hours loses the ability to avoid digestion by host lysosomal enzymes in digestive vacuoles of host ciliate *Paramecium bursaria*. *FEMS Microbiol Ecol* 2014;**90**:946–55.

Krueger T, Fisher PL, Becker S *et al.* Transcriptomic characterization of the enzymatic antioxidants FeSOD, MnSOD, APX and KatG in the dinoflagellate genus *Symbiodinium* Genome evolution and evolutionary systems biology. *BMC Evol Biol* 2015;**15**:1–20.

LaJeunesse TC, Parkinson JE, Gabrielson PW *et al.* Systematic Revision of Symbiodiniaceae Highlights the Antiquity and Diversity of Coral Endosymbionts. *Curr Biol* 2018;**28**:2570–2580.e6.

Locarnini RA, Mishonov AV, Antonov JI *et al.* World Ocean Atlas 2009, Volume 1: Temperature. In: Levitus S (ed). NOAA Atlas NESDIS 68, U.S. Washington, DC: Government Printing Office, 2010, 184 pp.

Muller-Parker GT. Dispersal of Zooxanthellae on Coral Reefs by Predators on Cnidarians. *Biol Bull* 1984;**167**:159–67.

Muscatine L, Wilkerson FP, McCloskey LR. Regulation of population density of symbiotic algae in a tropical marine jellyfish (*Mastigias* sp.). *Mar Ecol Prog Ser* 1986;**32**:279–90.

Ralph PJ, Gademann R. Rapid light curves: A powerful tool to assess photosynthetic activity. *Aquat Bot* 2005;**82**:222–37.

Roberty S, Bailleul B, Berne N *et al.* PSI Mehler reaction is the main alternative photosynthetic electron pathway in *Symbiodinium* sp., symbiotic dinoflagellates of cnidarians. *New Phytol* 2014;**204**:81–91.

Scott A, Harrison PL. Embryonic and larval development of the host sea anemones *Entacmaea quadricolor* and *Heteractis crispa*. *Biol Bull* 2007;**213**:110–21.

De Souza MR, Dawson MN. Redescription of *Mastigias papua* (Scyphozoa, Rhizostomeae) with designation of a neotype and recognition of two additional species. *Zootaxa* 2018;**4457**:520–36.

Sugiura Y. On the life-history of Rhizostomae medusae. II Indispensability of zooxanthellae for strobilation in *Mastigias papua*. *Embryologia (Nagoya)* 1964;**8**:223–33.

CHAPTER 4   Coral fragments to study photosynthesis in hard corals

The evaluation of the photosynthetic activity in symbiotic animals has represented a challenge due to their complex morphology and behaviour. In this chapter we evaluated the feasibility of using coral fragments, obtained by the mechanical breaking of *S. pistillata* branches, for the acquisition of photosynthetic parameters. These fragments were obtained from healthy coral colonies maintained in aquarium conditions and were monitored during three days. In the frame of our study, we made use of spectroscopic methods to unveil the photosynthetic reactions along the photosynthetic chain of Symbiodiniaceae in symbiosis with these coral fragments.

Spectroscopic techniques have been preferred because they give fine details on the functioning of key processes *in vivo* in diverse photosynthetic organisms, such as plants and microalgae. These processes are light responding, and the use of light saturating curves have been the choice of study. This approach has the advantage of unveiling the dynamic response of the photosynthetic chain (**Ralph and Gademann, 2005**). The prominent *in vivo* Chl *a* fluorescence signal arising from the chlorophylls attached to PSII, provides details of the electron transfer with the PSII as the pivotal source of information. However, few studies have intended to provide information of the PSI activity during the *in vivo* monitoring of coral photosynthesis. This photosynthetic complex roughly represents half of the photosystems in plants and microalgae but is much less studied due to technical constraints. Because PSI participates in the photosynthetic alternative electron pathways, its activity determination is important for the deduction of the alternative pathways activity.

We carried out comparisons of photosynthetic parameters from light response curves in order to deduce the presence of light-dependent oxygen consumption and the CEF activity. These measurements, together with measurements in other coral species, allowed us to demonstrate the presence of CEF in corals by the direct comparison of both photosystems activity. Additional measurements of oxygen exchange and the use of respiration inhibitors demonstrated the potential of coral fragments to withdraw *in vivo* details of the bioenergetic processes in corals.

In this publication, my contribution consisted in the designing of the joint measurements, the acquisition of coral fragments for its manipulation, the experimental acquisition of data and its analysis, the preparation of the figures and the writing of the manuscript.

Title :

***In vivo* assessment of mitochondrial respiratory alternative oxidase activity and cyclic electron flow around photosystem I on small coral fragments**

Authors :

Vega de Luna Félix, Córdoba-Granados Juan José, Dang Kieu-Van, Roberty Stéphane*, Cardol Pierre*

Inbios/PhytoSystems, Université de Liège, Liège 4000, Belgium

*Corresponding authors pierre.cardol@uliege.be and sroberty@uliege.be

ABSTRACT

The mutualistic relationship existing between scleractinian corals and their photosynthetic endosymbionts involves a complex integration of the metabolic pathways within the holobiont. Respiration and photosynthesis are the most important of these processes and although they have been extensively studied, our understanding of their interactions and regulatory mechanisms is still limited. In this work we used chlorophyll-*a* fluorescence, oxygen exchange and time-resolved absorption spectroscopy measurements on small and thin fragments (0.3 cm²) of the coral *Stylophora pistillata*. We showed that the capacity of mitochondrial alternative oxidase accounted for ca. 25% of total coral respiration, and that the high-light dependent oxygen uptake, commonly present in isolated Symbiodiniaceae, was negligible. The ratio between photosystem I (PSI) and photosystem II (PSII) active centers as well as their respective electron transport rates, indicated that PSI cyclic electron flow occurred in high light in *S. pistillata* and in some branching and lamellar coral species freshly collected in the field. Altogether, these results show the potential of applying advanced biophysical and spectroscopic methods on small coral fragments to understand the complex mechanisms of coral photosynthesis and respiration and their responses to environmental changes.

INTRODUCTION

Coral reefs owe most of their high diversity and productivity to energetic relationships occurring in Scleractinian corals [1]. Coral symbiotic nature is characterized by a complex metabolism integration between the cnidarian host and its photosynthetic endosymbiont (Symbiodiniaceae, dinoflagellate)

[2, 3]. The coral physiology is thus determined by multiple metabolic traits [4] from which respiration and photosynthesis are the utmost driving processes [5]. Coral bioenergetics has been investigated through gas exchange analysis thanks to the development of different systems which allow measurements *in situ* (e.g. [6, 7]) or in laboratory (*e.g.* [8, 9]). Coral respiration is largely fuelled by photosynthetically-derived carbon molecules [10], by active heterotrophy [11], and by oxygen released during photosynthesis [12]. It is carried out in both animal and algal mitochondria by the respiratory complexes (Complex I, II, III, IV and F_1F_O ATP synthase) which fulfils most of the cellular ATP demands. Host mitochondrial electron transport activity is directly related to respiratory substrates availability [13]. However, it has been suggested that the way in which corals consume storage molecules, as lipids, may be related to their sensitivity to bleaching conditions [14]. In the model sea anemone *Exaiptasia pallida*, thermal stress causes a decrease in gene expression of cytochrome *c* and ATP synthase subunit *a*, and ultimately to mitochondria degradation and apoptosis [15]. Cnidarian cellular physiology seems to be intimately linked to mitochondrial redox state [16]. Beyond this, the role of non-proton pumping (and consequently non-ATP yielding) alternative respiratory enzymes, such as alternative NADH dehydrogenases and alternative ubiquinol oxidase (AOX) which genes are present in the cnidarian genome [17, 18], is still unknown. Differently from the host, Symbiodiniaceae mitochondria lack the canonical NADH:ubiquinone oxidoreductase (Complex I) but possess an AOX [19, 20]. Understanding the contribution of all these components to regulation of symbiont and host respiration will help to understand the physiological responses of corals to natural oxygen variations in the reefs and its interaction with stress [21].

Coral photosynthesis is carried out by Symbiodiniaceae algae only. Light absorption occurs in the thylakoid antenna system, which in peridinin plastid-containing algae as Symbiodiniaceae consists of a membrane embedded chlorophyll *a*-chlorophyll c_2-peridinin protein complex (acpPC) and a water soluble peridinin-chlorophyll a-protein complex (PCP) [22]. These antennas transfer energy to photosystem II (PSII) and photosystem I (PSI) reaction centers, allowing charge separation, and a linear electron flow (LEF) from oxidation of water molecules at the PSII donor side to reduction of NADP at the PSI acceptor side. The intermediate Cytochrome b_6f complex oxidises the plastoquinol pool (electron acceptor of PSII) and reduces cytochrome c_6 (cyt c_6; electron donor of PSI), meanwhile translocating protons to the lumenal side of the thylakoid. This transmembrane electrochemical proton gradient is then used by the ATP synthase complex. The availability of NADPH and ATP for CO_2 fixation depends largely on a complex balance between the different processes producing and consuming the electrochemical proton gradient, ATP and NADPH. An alternative cyclic electron flow (CEF), involving PSI and Cytochrome b_6f, may work to balance the energetic requirements for CO_2 fixation. CEF activity, by contributing to increase the electrochemical proton gradient,

71

accomplishes two main functions that are driving the synthesis of extra ATP and inducing a non-photochemical quenching (NPQ) dissipation mechanism that may prevent PSII photoinhibition [23]. CEF has been poorly studied in Symbiodiniaceae and its role under steady physiological conditions, both in culture and in hospite, is not clear.

Carbon fixation is carried out by a type II Rubisco which is characterized by a low CO_2-O_2 selectivity factor, and requires the presence of an efficient CO_2 concentrating mechanism [24, 25] largely controlled by the host [26, 27] that limits the occurrence of the photorespiratory pathway [24]. After accomplishing carbohydrate synthesis, an important amount of photosynthetic products is transported to the host [28] thanks to the expression of membrane transporters [29]. The photosynthetic activity of corals is dynamic at different levels of time and space scales in coral reefs [30], and it has been shown to be highly coupled with nutrients [31] and water flow [7]. The delicate balance of symbiosis in corals can be disrupted as a consequence of affections in the photosynthetic activity. For instance, a decrease in the electron transfer at the PSII acceptor side in heat sensitive species, leads to damage in thylakoid membranes and potentially to bleaching [32]. Altogether, this points out the importance of studying Symbiodiniaceae photosynthesis *in hospite*.

At the cellular level, different regulatory mechanisms of photosynthetic electron flow help to balance the light energy absorbed and the energetic requirements for carbon fixation in microalgae [33]. The characterization of these mechanisms has been achieved through *in vivo* PSII-related chlorophyll *a* fluorescence [34]. This technique has shown that different Symbiodiniaceae isolates show diverse photobiological responses to light changes [35]. For instance, the presence of CEF has been suggested to occur in *Symbiodinium* genus (formerly Clade A) both free-living and in symbiosis [36]. The combination of chlorophyll *a* fluorescence and oxygen exchange measurements also showed that *Symbiodinium* sp. in culture activates a light-enhanced dark respiration during photosynthesis [8]. A more detailed characterization through the combination of various techniques (O_2 exchange, PSII chlorophyll *a* fluorescence emission, PSI primary electron donor [P700] absorbance change in the far-red spectrum, and analysis of the thylakoid transmembrane electric field), revealed that an oxygen-dependent reduction at the acceptor side of PSI occurs as photoprotective mechanism in *Symbiodinium* isolates [37, 38].

Spectrophotometric measurements of PSI activity performed in the anemone model species *Exaiptasia pallida* harboring *Breviolum* sp. (formerly Clade B) revealed that exposure to high temperature can stimulate the CEF capacity [23]. However, on corals such studies are still scarce because: 1) their morphology is not suitable for most spectroscopic apparatus that accomodate 1 cm^2 cuvette; 2) the thickness and nature of their calcareous skeleton makes coral branches or nubbins not homogenous spectroscopic objects, scattering and poorly transmitting detecting light; 3) actinic light

cannot be delivered in a homogenous manner on all sides of the coral specimens even in simple systems, like in oximeter chambers.

The simultaneous monitoring of *in vivo* PSI and PSII activity in corals has been attempted by using the pulse-amplitude-modulation technique (Dual-PAM, Walz, Germany) which records variable chlorophyll *a* fluorescence and P700 photo-oxidation. Hoogenboom et al. [39] analyzed the laminar coral *Turbinaria reniformis* and concluded that PSI was not a major site for damage during thermal stress. They also suggested the existence of CEF at high light intensities because of a decoupling between PSII and PSI activity was observed, but no clear results were obtained from the branching coral *S. pistillata*. In contrast, a recent study using improved settings of the Dual-PAM in reflectance mode, in combination with chlorophyll *a* fluorescence kinetics, showed a strong sensitivity of PSI to a Calvin cycle inhibitor and thermal stress in the plate-like coral *Pavona decussata* [40]. This highlights the lack of knowledge on PSI activity in corals in response to environmental changes.

Coral skeleton is composed by aragonite depositions which has a low light absorption capacity and diffuses and scatters light through its structure [41]. Other works have used small coral fragments to better characterize biophysical properties of the coral skeleton [41] or coral pigments through spectroscopic kinetics [42]. Consequently, coral fragments might be good spectroscopic objects but, despite this, they have not been studied by advanced biophysical and spectroscopic methods commonly applied for other photosynthetic organisms to study photosynthesis (and more generally bioenergetics). In this work we challenged thin and small coral fragments to classical physiological and highly specialized spectroscopic measurements of respiration and photosynthesis, and we aim to propose them as reliable sources of *in vivo* information.

METHODS

Biological material

Coral colonies of *Stylophora pistillata* variety Milka were obtained from DeJong Marinelife (Netherlands), and maintained in a 300 L capacity aquarium filled with artificial seawater prepared at 34 PSU (Coral Pro Salt, Red Sea Fish LTD). Temperature was set to 26°C and light was provided by a LED spot light (A360W tuna Blue, Kessil, USA) at 100 μmol photons m^{-2} s^{-1} in a light-dark cycle of 12h:12h. Corals were fed two or three times per week with freshly hatched artemia. Some measurements reported here were also conducted on coral colonies of *Pachyseris speciosa*, *Pocillopora damicornis*, *Acropora formosa* and *Pavona cactus*. These colonies were collected by SCUBA diving in the area of Malakal in the Palau Archipelago (7°19'28.3"N 134°28'01.6"E), during a sampling campaign conducted in January 2018. After collection, colonies were transferred to the facilities of the Palau International Coral Reef Center (PICRC) and suspended from a nylon wire

inside a tank supplied with running filtered natural seawater. Temperature in the tank was $30 \pm 1°C$ and the maximum Photosynthetic Photon Flux Density (PPFD) at noon was about 100 μmol photons $m^{-2} s^{-1}$.

Symbiodinium microadriaticum culture (CCMP 2467) originally isolated from shallow water coral *S. pistillata* from the Red Sea, was kindly provided by Prof. Oren Levy (Bar Ilan University, Israel). The culture was maintained in 250 mL Fernbach flasks containing 75 mL of artificial sea water (Coral Pro Salt, Red Sea Fish LTD) at 34 PSU and enriched with Guillard's (F/2) Marine Water Enrichment Solution (Sigma-Aldrich). The culture was grown under cool white fluorescent lamps at 75 µmol photons $m^{-2} s^{-1}$ on a 12h:12h light:dark cycle and it was subcultured weekly. For spectroscopic measurements cells were adjusted to 10 µg of total chlorophyll per mL and supplemented with 10 % (w/v) of Ficoll to avoid sedimentation.

Coral fragment preparation

Square fragments of about 5 by 5 mm (**Figure 1a**) were cut from various coral colonies with a Dremel 8220 (Dremel, USA) equipped with a diamond disk. For the branching corals *S. pistillata* and *A. formosa*, two transversal cuts were done close to the end of similar terminal branches, one to remove the growing white tip, and the other which determine the length of the fragment (*i.e.* approximately 5 mm). A third longitudinal cut determined the thickness of the fragment. The longitudinal cut in the arbustive coral *P. damicornis* was made in the skeleton regions thicker than 3 mm. Laminar corals *P. speciosa* and *P. cactus* were cut perpendicularly to the plane of the skeleton. This procedure was performed out of the aquarium and took less than 30 s per fragment, after which it was rapidly immersed in another sea water container to remove debris. Coral fragments were analysed within one hour after being cut (termed 'day 0') or thereafter maintained in the same aquarium conditions as their parent colony.
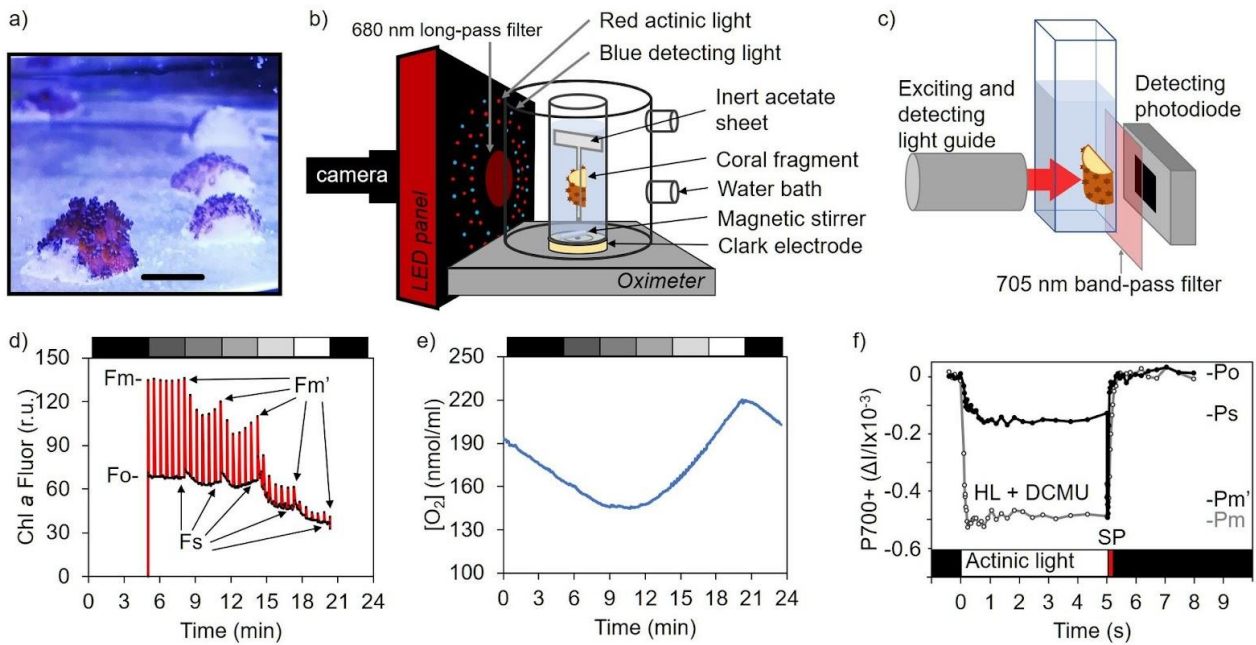
Figure 1. Experimental setup and representative experiments on small and thin coral fragments. **a)** Picture of recently obtained *S. pistillata* fragments settled back in the aquarium; the black bar indicates 5 mm. **b)** Schematic representation of the setup used for simultaneous analyses of chlorophyll *a* fluorescence yield and oxygen exchange. **c)** Disposition and orientation of a coral fragment into a 1 cm^2 glass cuvette relative to the light guide and the detecting photodiode in the JTS-10 spectrophotometer. **d,e)** Representative records of chlorophyll *a* fluorescence yield measurements and oxygen concentration changes. Each light step (represented by the upper bar with a grey scale) lasted three minutes and saturating pulses were given each 30 seconds (r.u. = relative units). **f)** Representative record of Photosystem I primary donor (P700) photo-oxidation upon five seconds of illumination (210 µmol photons m^{-2} s^{-1}) followed by a saturating pulse of light (SP), in presence of PSII inhibitor (DCMU at 20 µM).

Chlorophyll *a* fluorescence measurements

In vivo chlorophyll *a* fluorescence images were obtained by a SpeedZen imaging system (BeamBio/API, France). An array of blue LEDs (450-470 nm) was used to excite chlorophyll *a* during 400 µs, and images were obtained by a CCD camera (UI-3240CP-NIR-GL Rev.2, IDS, Obersulm, Germany) filtered by a long pass red filter (680 nm) (**Figure 1b**). After incubating samples in darkness for at least 15 min, minimal chlorophyll *a* fluorescence yield (Fo) image was acquired. A saturating red actinic light pulse (3000 µmol photons m^{-2} s^{-1}), provided by a LED array (660 nm), was applied

for 200 ms and maximal chlorophyll *a* fluorescence yield (Fm) was acquired. Maximum quantum yield of photosystem II was calculated as Fv/Fm = (Fm-Fo)/Fm [43].

Coral fragments were exposed to different PPFD (15, 68, 172, 354 and 755 µmol photons m^{-2} s^{-1}, provided by the same red LED array than the saturating pulse) during three minutes and fluorescence (Fs) was recorded every five seconds (**Figure 1d**). A saturating red actinic light pulse was applied to obtain the maximum fluorescence yield under light acclimation (Fm') every 30 s, and the effective quantum yield of PSII at steady state was calculated as ɸPSII = (Fm'-Fs)/Fm'. The relative electron transfer rate through PSII (rETR-PSII) was then calculated as ɸPSII x PPFD, and the non-photochemical quenching of chlorophyll a fluorescence (NPQ) as (Fm-Fm')/Fm' [43].

Fast induction curves of chlorophyll *a* fluorescence were recorded with a Handy PEA fluorometer (Hansatech Instruments, UK), by illuminating the sample during 10 s with a strong red light pulse (peak wavelength of 650 nm) of 2000 µmol photons m^{-2} s^{-1}. This fluorescence rise is characterized by a sudden increase from a basal fluorescence level (O), with two intermediate inflections (J and I), to a maximum fluorescence level (P) commonly referred as OJIP transient (see Chapter 12 in [34]). O phase is taken at 50 µs, J appears at 2 ms, while I appears after 50 ms and P after 2 s in corals. Each coral fragment was set in the bottom of a standard spectrophotometer cuvette facing the head sensor and filled with 2 mL of artificial seawater and maintained in darkness for 15 min before the measurement.

Light-induced absorption changes

All measurements were performed with a JTS-10 spectrophotometer (BioLogic, France) piloted by a BeamBio/API (France) electronic device. When necessary, the final size of the coral fragments was adjusted to fit into standard 45 mm × 12.5 mm × 12.5 mm (H x W x D) glass spectrophotometer cuvette, *i.e.* with a pathlength of 10 mm. Each coral fragment was held in the cuvette with the side containing most polypes facing the light source and the skeleton exposed area (when applicable) in front of the detecting photodiode (**Figure 1c**). This guaranteed a controlled illumination of the sample. In the photosynthetic electron transport chain of peridinin chloroplast-harboring dinoflagellates cyt c_6 is the electron donor to PSI instead of Plastocyanin (PC) [44]. For this reason, light-induced absorption changes of P700 were directly measured at 705 nm [45] by applying µs detecting flashes during short intervals of dark pulses (as described in [46]). Continuous actinic light at different intensities (25, 85, 210, 380, 670 and 1400 µmol photons m^{-2} s^{-1}) was provided during 5 s (3 min for field coral specimens) by a LED array (640 nm). When coral fragments were exposed to continuous light, a stable negative change in absorbance at 705 nm (due to the formation of oxidized P700) [47] was obtained and recorded as Ps (**Figure 1f**). A strong saturating pulse of light (9000 µmol photons m^{-2} s^{-1}) was applied to obtain a more negative absorbance signal corresponding to maximum photo-

oxidation of P700 as Pm', while after a dark period of 1 s absorbance was recorded as Po. Maximum absorbance change (Pm) was estimated by adding the potent photosystem II inhibitor DCMU (3-(3,4-dichlorophenyl)-1,1-dimethylurea) at 20 µM (**Figure 1f**). Photosystem I quantum yield was calculated as Y(I) = (Pm'-Ps)/(Pm-Po), quantum yield of non-photochemical energy dissipation due to donor side limitation as Y(ND) = (Ps-Po)/(Pm-Po), and the quantum yield of non-photochemical energy dissipation due to acceptor side limitation as Y(NA) = (Pm-Pm')/(Pm-Po) [48]. The relative electron transfer rate through PSI (rETR-PSI) was calculated as the product of Y(I) and PPFD.

Absorbance changes of some pigments in the green region of the visible spectrum occur in response to light-induced changes of the trans-thylakoid electric field. This so-called electrochromic shift (ECS) is a useful way to determine photosynthetic parameters such as stoichiometry of active PSI and PSII in photosynthetic eukaryotes [49], including Symbiodiniaceae [37]. ECS spectra were determined by measuring light-absorption changes in response to 2 ms continuous illumination, each 10 nm using light band-pass filters from 480 to 600 nm, as previously described [50].

The ratio between active PSII and PSI centers can be quantified because the ECS signal responds linearly to the intensity of the electric field [37]. ECS signal at 554 nm was followed by applying a saturating single-turnover flash of 5 ns provided by a Nd:YAG Laser (Minilite II, Continuum) and its amplitude was considered as PSI+PSII reaction centers contribution. PSII inhibitors DCMU (20 µM, from a stock dissolved in ethanol) and hydroxylamine (1 mM, from a stock dissolved in distilled water) were added simultaneously and incubated in darkness during 10 min, another single-turnover flash was given and the resulting ECS amplitude accounted for PSI contribution. Ten consecutive repetitions, separated by 5 s in darkness, were averaged per measurement.

Oxygen exchange

Oxygen consumption (respiration) or evolution (photosynthesis) were measured with an Oxygraph+ System (Hansatech, UK). Oxygen concentration calibration was carried out at two points with 0.2 µm-filtered f/2 medium either saturated in oxygen after vigorous shaking, or depleted in oxygen by addition of sodium dithionite (Sigma-Aldrich).

Coral fragments were held suspended into a DW1 oximeter chamber (Hansatech, UK) by an inert piece of acetate sheet. This enabled the adequate stirring of the medium by the magnetic bar (**Figure 1b**). Each fragment was dark acclimated for at least 15 min with the chamber opened before closing it to monitor oxygen consumption in the dark for 5 min. After this dark period, illumination was provided by the Chlorophyll *a* fluorescence imaging system, so during fluorescence recording oxygen concentration was simultaneously acquired (**Figure 1e**).

Chlorophyll content and coral surface determination

Pigments were extracted by incubating coral fragments in cold methanol during at least 12 h in darkness at 4°C. For *S. microadriaticum*, cells were resuspended in cold methanol and vortexed in presence of 500 µL of acid-washed and autoclaved glass beads (710–1,180 µm; Sigma-Aldrich) for 2 minutes at 30 Hz with a TissueLyser II (QIAGEN). Pigment extracts were centrifuged at 16000 g for 10 min to remove debris, and chlorophyll *a* and c_2 concentrations were calculated according to [**51**] from absorption measurements at 632 and 665 nm. Tissue-containing surface of coral fragments was calculated from conventional real color pictures of each fragment by using the software ImageJ (version 1.51j8).

Symbiodiniaceae genotyping

Small fragments of each species (n = 3) were removed from independent colonies and immediately processed or preserved in RNA*later* (Invitrogen). Fresh or preserved fragments were washed with filtered artificial sea water and coral tissues were extracted by airbrushing the fragments into sterile PBS. DNA from the microalgal fraction was then extracted by using a DNeasy Plant mini kit (QIAGEN) according to the manufacturer's instructions, with slight modifications. The PCR amplification of the ITS2 gene marker was performed using primers pair SYM_VAR_5.8S2 and SYM_VAR_REV as detailed in [**52**]. The amplicons library was constructed using the Nextera XT kit (Illumina, Inc., San Diego, CA, USA) and sequencing was carried out on the Illumina MiSeq platform with 2 x 250 bp read configuration. The ITS2-type profiles were obtained by using the SymPortal analytical framework [**53**].

RESULTS

Whole *S. pistillata* coral colonies containing *S. microadriaticum* exhibited a homogeneous pigmentation (as illustrated in **Figure 2a**). Chlorophyll *a* fluorescence imaging indicated a maximum quantum yield of photosystem II (Fv/Fm) of 0.53 ± 0.03 (**Figure 2b,d**). Small half-cylinder shape fragments were cut from these colonies. They were covered with about 35 mm^2 of coral tissue with an average total chlorophyll content (Chl *a*+c_2) of 30.5 ± 7.6 µg cm^{-2}, a Chl *a*/c_2 ratio of 2.39 ± 0.11 and 61 ± 11 polypes cm^{-2} (n = 16). These values remained stable up to 2 days after cutting and no visual sign of tissue necrosis was observed during this period (**Figure 2c**). Although there was a positive correlation ($R^2=0.41$, $p=0.007$) between Fv/Fm and fragment thickness (from 1.5 to 5 mm), the slope of the linear regression is very small so that the difference between a 2 mm fragment and a 5 mm fragment is less than 6% (**Figure 2e**). In addition, the average of Fv/Fm values of coral fragments is not significantly different to the Fv/Fm value of coral colonies (one-way ANOVA $F(3,20)=2.14, P=0.13$) (**Figure 2d**). The fast polyphasic chlorophyll *a* fluorescence rise (*i.e.* OJIP

curves) was obtained from freshly cut coral fragments and from 1- or 2-days old fragments (**Figure 2f**) and no changes in the relative amplitude or presence of phases were observed.
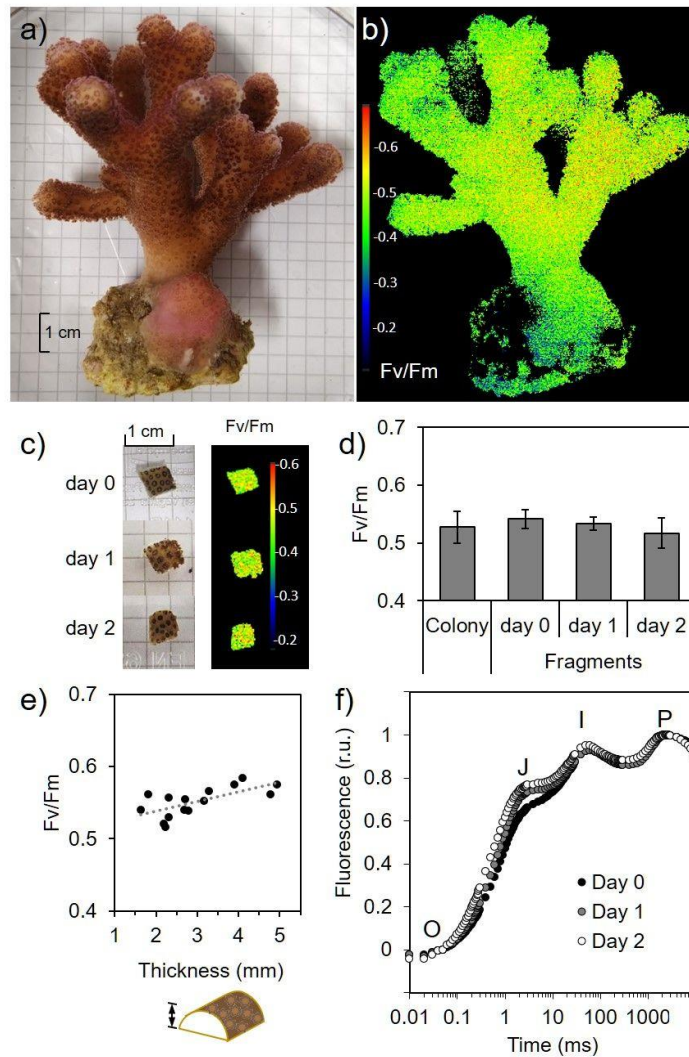
Figure 2. Maximum photosynthetic quantum yield of photosystem II (Fv/Fm) is not altered in thin fragments of the coral *S. pistillata*. **a)** Picture of one *S. pistillata* colony maintained in aquarium conditions. **b)** False-color picture of Fv/Fm obtained by chlorophyll *a* fluorescence imaging of Fo and Fm. **c)** Representative coral thin fragment monitored during two days and its related Fv/Fm false-color image. **d)** Fv/Fm measured on the apical region of coral colonies where coral fragments were sampled and coral fragments monitored two days after sampling. **e)** Fv/Fm of coral fragments of variable thickness after one day of sampling. **f)** Polyphasic chlorophyll *a* fluorescence rise from dark adapted coral fragments was normalized to 0 at 50 µs ('O' phase) and to 1 at the plateau ('P' phase) (r.u. = relative units). The two typical inflections, phase J and I, are indicated (n=6 for d) and f).

To further test the good health of coral fragments, we determined respiratory and photosynthetic oxygen exchange rates from 3 mm thick fragments. Dark oxygen consumption (Rd) was on average 13.9 ± 2.1 nmol O_2 cm^{-2} min^{-1} over the three days and remained stable (**Figure 3a, inset**). Net oxygen evolution as a function of the light intensity (**Figure 3a**) was obtained simultaneously with fluorescence-based calculation of relative electron transport rate of PSII (rETR-PSII) (**Figure 3b**). Both parameters showed a similar light dependency as indicated by the fact that rETR-PSII linearly correlated to oxygen evolution rates ($R^2=0.98$, $p=0.002$) (**Figure 3c**). Moreover, non-photochemical quenching (NPQ) capacity was similar in coral fragments (**Figure 3d**).
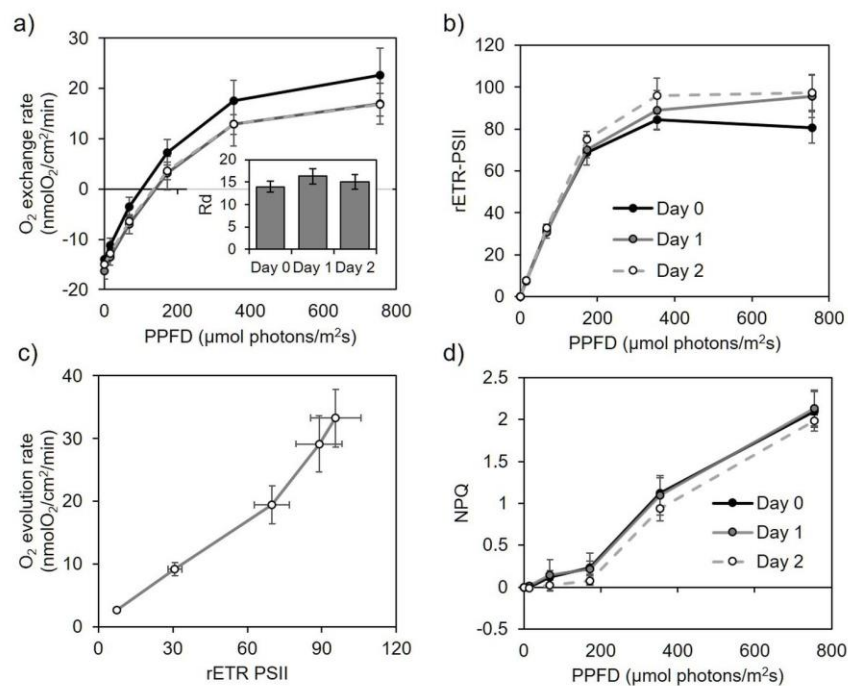
Figure 3. *In vivo* measurement of respiration and photosynthesis in *S. pistillata* coral fragments. **a**) inset : Oxygen consumption in the dark (Rd, nmol O_2 cm^{-2} min^{-1}). **a-b)** Light-dependent oxygen exchange and relative electron transport rate (rETR-PSII) were obtained simultaneously. **c)** Relationship between rETR-PSII and oxygen evolution. **d)** Non photochemical quenching of fluorescence (NPQ) is shown for three minutes light-acclimated coral fragments. Vertical bars in a-d) represent standard deviation, n=6.

Altogether, these data indicated that the global photosynthetic and respiratory activities of the coral fragments remained stable after cutting. In addition, most of the coral fragments showed the same

potential to regenerate the tissue and the coral skeleton, as already shown for fragments of similar size [**54**].

We then tested the effect of two classical inhibitors on respiration: potassium cyanide (KCN), a potent inhibitor of mitochondrial cytochrome *c* oxidase complex (Complex IV), and salicylhydroxamic acid (SHAM), an inhibitor of mitochondrial alternative oxidase (AOX). Addition of 1 or 2 mM KCN reduced Rd to 50% after five minutes (**Figure 4a**). Addition of 2 mM SHAM further decreased the remaining cyanide-insensitive oxygen consumption to 26% of total Rd (**Figure 4b**), and higher concentrations of SHAM (4 or 6 mM) did not suppress this residual oxygen consumption (data not shown). In contrast, addition of SHAM up to 2 mM alone did not have an impact on Rd during the 20 min of exposure to the inhibitor (**Figure 4a**).
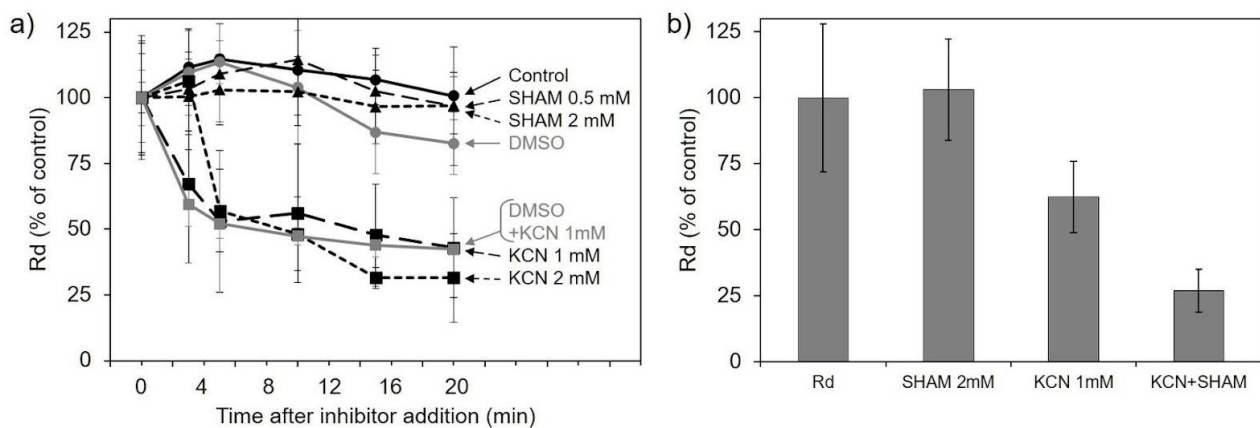
Figure 4. Impact of SHAM and KCN on dark respiration of *S. pistillata* coral fragments. **a)** Respiratory rates of dark adapted coral fragments were monitored up to 20 minutes in dark conditions, n=3. Cyanide (KCN dissolved in deionized H_2O) at 1 or 2 mM, n=4. SHAM (dissolved in DMSO) at 0.5 or 2 mM, n=4. DMSO at 2 %, n=4. DMSO at 2 % plus KCN at 1 mM, n=6. **b)** Mitochondrial dark respiration rate (Rd) and the effect of SHAM 2 mM, KCN 1mM or SHAM 2 mM + KCN 1mM (KCN+SHAM). Respiratory rates were measured 5 minutes after the addition of inhibitors, n=10.

We then tested the potential of coral fragments to monitor light-induced absorption changes of PSI primary electron donor (P700) in the far-red region of the visible spectrum (705 nm) (**Figure 1f**). These absorption changes corresponding to P700 photo-oxidation are fully consistent with previous observations in plant leaves or algae [**48**] and allowed us to calculate PSI quantum yield [Y(I)] and both PSI donor and acceptor side limitations [Y(ND) and Y(NA), respectively] at different light intensities (**Figure 5a**). In addition, relative electron transport rates of PSI (rETR-PSI) were

calculated from Y(I) values and a typical photosynthesis-light curve was obtained (**Figure 5b**). We also observed a positive correlation (R^2=0.40, p=0.01) between absorbance changes upon a saturating pulse of light in presence of DCMU (Pm values) and chlorophyll *a* content per coral fragment (**Figure 5c**). In contrast, thickness of coral fragments did not correlate (R^2=0.06, p=0.36) to the maximum amplitude of P700 absorbance change (Pm) (**Figure 5d**). This indicates that the coral skeleton did not interfere significantly with our measurements.
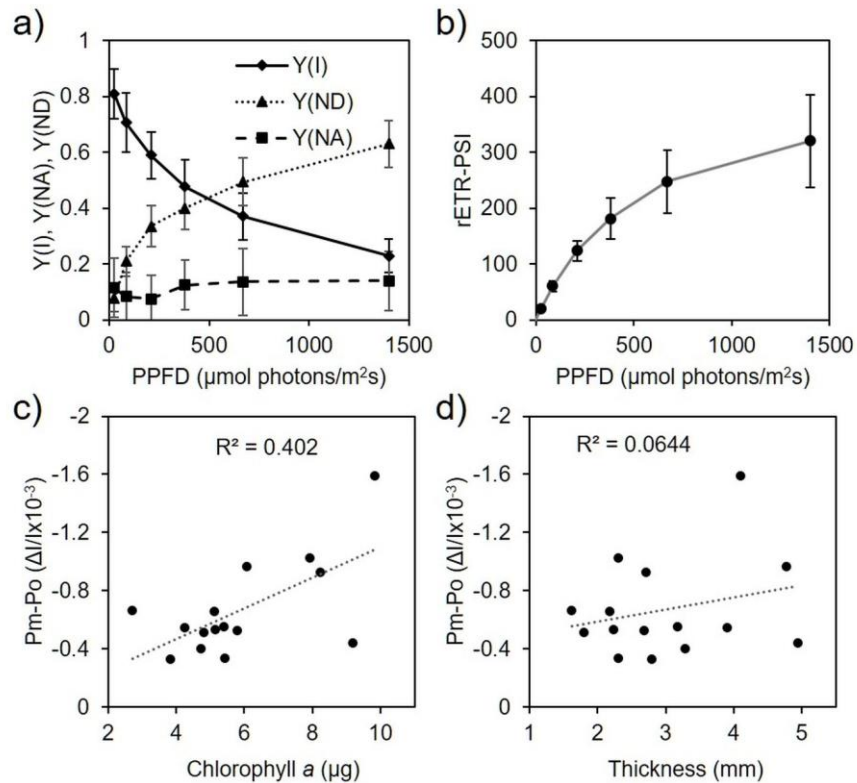
Figure 5. Light-dependent P700 oxidation measurement and PSI activity in *S. pistillata* coral fragments. **a)** PSI quantum yield (Y(I), acceptor and donor side limitations (Y(NA) and Y(ND), respectively) as a function of PPFD). **b)** Relative electron transport rate through PSI (rETR-PSI) calculated as the product of Y(I) and PPFD. **c-d)** Maximum P700 absorbance change in the presence of DCMU 20 µM at high light (Pm) in function of its chlorophyll *a* content (**c**) or in function of its skeleton thickness (**d**). A correlation factor (R^2) obtained from a linear trendline is shown for c) and d). n=13 for a) and b).

We next quantified the fraction of active PSI and PSII centers in coral fragments by monitoring the electrochromic shift signal (ECS), a technique previously used in various algal species, including Symbiodiniaceae [37, 49]. The overall shape of the ECS spectrum of *S. pistillata* was similar to the one of its isolated symbiotic algae (*S. microadriaticum*), with a maximum and a minimum observed at 510 nm and around 560 nm, respectively (**Figure 6a**). However, the ratio between maximum (510

nm) and minimum (560 nm) values was smaller in coral fragments than in isolated algae. We then assessed the amplitude of the fast ECS (< 1 ms) at 554 nm in response to a saturating single turnover flash (**Figure 6b**). Under these conditions, the amplitude of the ECS is proportional to the amount of active PSI+PSII (reviewed in [**49**]). Addition of Hydroxylamine (HA) and DCMU, two PSII inhibitors, halved the amplitude of the ECS both in coral fragments of *S. pistillata* and isolated *S. microadriaticum* (**Figure 6b**), indicating that PSI to PSII ratio is about 1 in both cases.

The four different coral species collected from Palau harbored the same *Symbiodiniaceae* genus (*Durusdinium* sp), which is a dominant algal genotype of inshore corals in this region [**55**]. For them, a similar ECS spectrum was obtained (**Figure 6c, d**). It was not possible to test PSI:PSII stoichiometry in these coral species because a saturating flash laser was not available at that time of analysis.
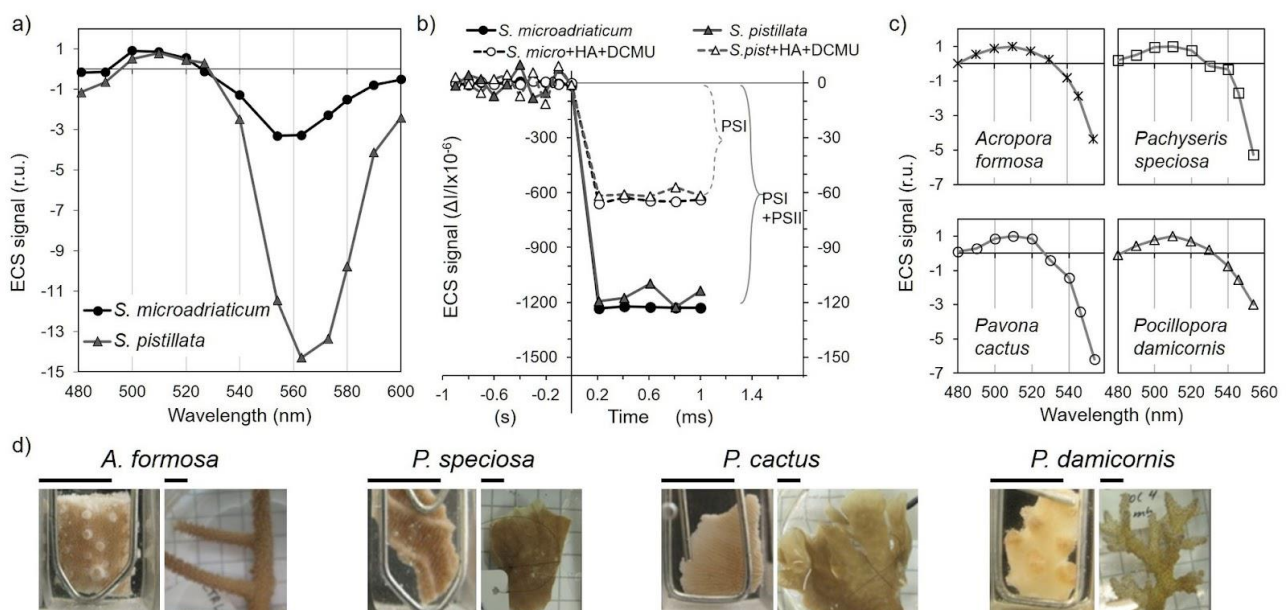
Figure 6. Electrochromic shift (ECS) signal from different Symbiodiniaceae sources. **a)** ECS signal is compared between isolated and *in hospite S. microadriaticum* cells normalized to ECS at 510 nm (r.u. = relative units normalized to ECS signal at 510 nm). **b)** PSI and PSII contribution to ECS signal at 554 nm was assessed by addition of PSII inhibitors hydroxylamine (HA, 1 mM) and DCMU (20 µM). Note the different scale magnitude for ECS signal between *S. microadriaticum* (left axis) and *S. pistillata* (right axis) acquisition. Time scale shows different units for negative and positive values. **c)** ECS signal obtained from four different scleractinian corals species freshly sampled in the field (r.u. = relative units normalized to ECS signal at 510 nm). **d)** True colour pictures of the coral fragments used to obtain ECS spectrum and a representative picture of the corals collected. The black bar stands for 5 mm. n = 3 for a) and b).

Spectroscopic-based photosynthesis activity measurements allowed us to compare different parameters obtained from small coral fragments. In *S. pistillata*, rETR-PSII linearly correlated (R^2=0.999, *p*=0.0005) to rETR-PSI up to the minimum saturating light intensity (around 200 µmol photons m^{-2}s^{-1}), after which PSI activity continued increasing compared to PSII (**Figure 7a**). Corals from the field revealed different responses when PSI and PSII activities were compared (**Figure 7b**). A linear response was obtained from the two branching corals *A. formosa* (R^2=0.95, *p*=0.004) and *P. damicornis* (R^2=0.96, *p*=0.003) along with the different light intensities tested, but the laminar corals *P. cactus* and *P. speciosa* exhibited a disrupted relationship when light intensity was higher than 200 µmol photons m^{-2}s^{-1}.
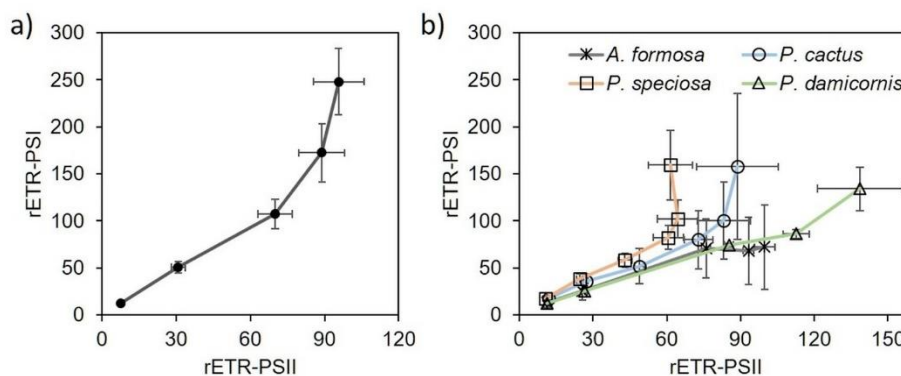
Figure 7. Relationship between rETR-PSI and rETR PSII in *S. pistillata* (**a**) and in four reef-building corals species freshly collected in the field (**b**). Each light step was 3 minutes. n=6 for a), n=5 for b).

DISCUSSION

Coral survival to fragmentation is a well known and broadly documented phenomenon (*e.g.* [**56**]). In the case of *S. pistillata*, a robust scleractinian coral species, small nubbins survive after fragmentation as well [**54**] and have been used in skeleton calcification observations [**57**]. In this work, we demonstrate that thin coral fragments (30 mm^2) can be used to study various bioenergetics traits which so far have not been assessed in reef-building coral species.

The chlorophyll *a* fluorescence-based photosynthetic parameter Fv/Fm, which accounts for the maximum quantum yield of PSII, has been used to track damages on the photosynthetic capacity and health in photosynthetic organisms, including corals (e.g. [**58**]). On the other hand, OJIP chlorophyll fluorescence rise has been used to reveal alterations of the PSII reaction center in Symbiodiniaceae cultures [**59**] and changes in the redox state of PSII acceptor side in corals [**60**]. The fact that we did

not observe any significant modification neither of the Fv/Fm value nor in OJIP chlorophyll *a* fluorescence kinetics up to 48 h after fragmentation in small coral fragments (**Figure 2**), indicates the absence of structural or functional disturbance in the photosynthetic electron transfer chain. Moreover, our coral fragments exhibited a photoprotection capacity (NPQ; Figure 3d) comparable to values registered from branches of *S. pistillata* collected from shallow waters in the Red Sea [**61**] and from colonies maintained in aquarium conditions for several years [**31**]. Respiration measured in our coral fragments (Rd = 13.9 $\pm$ 2.1 nmol O_2 cm^{-2} min^{-1}; **Figure 3a**) was in agreement with previous studies on 2 cm long nubbins or 10 to 15 cm long branches from *S. pistillata* collected in the Red Sea (11 nmol $\pm$ 4 O_2 cm^{-2} min^{-1} in average) [**12, 62**]. Maximum gross photosynthetic rate (Pgmax = 33 $\pm$ 4.7 nmol O_2 cm^{-2} min^{-1}; **Figure 3a**) was also similar to values measured in coral branches of this species either maintained in aquarium conditions or freshly collected from the sea (20 - 35 nmol O_2 cm^{-2} min^{-1}) [**31, 62**]. Rd and Pgmax values can be used to roughly calculate an extrapolated daily photosynthesis to respiration ratio (Pgmax/Rd*2) [**63**]. In our thin coral fragments of *S. pistillata* this ratio is 1.23 $\pm$ 0.16, a value in good agreement with *S. pistillata* branches (10 to 15 cm long) collected in summer from the Gulf of Aqaba (1.4) [**56**], or from nubbins (2 to 3 cm long) prepared from *S. pistillata* coral colonies grown in aquarium conditions (1.1 to 1.5) [**63**]. Similarities between our results and data from the literature show that values measured on small thin fragments give reliable information on energetic relationships as those measured from bigger pieces of corals.

Alternative electron transport pathways in mitochondria and chloroplasts are described as regulators of the redox poise in the main electron transfer chains, and more generally are known for their influence on the energetic state of the cell [**64**]. By measuring oxygen consumption rates in *S. pistillata* in presence of inhibitors (**Figure 4**), we evidenced, for the first time, the presence of a cyanide-insensitive but SHAM-sensitive mitochondrial alternative oxidase (AOX) activity in coral. In several algal species, AOX contributes to dissipate excess of redox equivalents produced in the chloroplast during photosynthetic activity (*i.e.* NAD(P)H) (*e.g.* [**66**]). The capacity of the AOX pathway measured in *S. pistillata* was 24% of Rd and is in the range as values previously reported for different species of *Symbiodiniaceae* grown in culture [**20, 65**]. The observed lack of effect of the AOX inhibitor (i.e. SHAM) addition to fully respiring coral fragments demonstrates a high capacity of mitochondrial respiration through Complex IV. However, further studies are needed to determine the extent of both the cnidarian and photosymbionts AOX contribution to whole holobiont respiration and to elucidate the role of AOX under control and stress conditions.

Besides, in several species of Symbiodiniaceae in culture, a high light-dependent oxygen uptake was found to occur at the acceptor side of PSI through a Mehler-type reaction [37, 38]. As illustrated in **Figure 3**, the linear relationship between rETR-PSII and oxygen evolution observed in *S. pistillata* suggests that the photosynthetic electron transfer rate in high light does not depend on an alternative electron pathway to oxygen reduction as it does in free living cultures [*e.g.* 37, 67]. This result may be explained by a lower CO_2 limitation for symbionts in hospite compared to those isolated in culture [26, 37], but does not exclude that a different strategy operates under high light intensities. In this respect, PSI-dependent CEF is another alternative photosynthetic pathway that has been suggested to play an important role in the energetic balance in Symbiodiniaceae [36, 23]. The most recommended way to assess CEF *in vivo* is to compare PSI and PSII activities [68] (**Figure 7**). Despite the fact that calculation of absolute electron transport was not assessed [69] in the present study, our results indicate the occurrence of CEF in high light in *S. pistillata* and in two laminar corals from the field (*P. cactus* and *P. speciosa*). In contrast, we found that light influenced at the same proportion the relative electron transport rate of both photosystems in *A. formosa and P. damicornis*, two branching coral species, indicating that CEF is neglectable in high light (**Figure 7**). It is worth to notice that these last four corals species harbour the same *Durusdinium* genus. A previous study, based on chlorophyll *a* fluorescence Serial Irradiation Pulses (SIP) method, indicated the absence of CEF in isolates of *Durusdinium* genus (referred as Clade D) [36]. Altogether, this highlights that involvement of photosynthetic alternative electron flows may strongly differ between corals harboring Symbiodiniaceae from the same genus.

Contrastingly to PSII, the role of PSI on photoacclimation has just started to be revealed in Symbiodiniaceae dinoflagellates [70]. PSI has been the target of very few studies on coral photosynthesis due to technical constraints. An indirect determination made on freshly extracted algae from *S. pistillata* showed a higher PSI content in coral colonies in symbiosis with *Symbiodinium* sp. (referred as Clade A) than *Cladocopium* sp. (referred as Clade C) [61], suggesting that PSI content can be determinant for coral photosynthesis adaptation to changing light regimes. Other studies, aiming to assess *in vivo* PSI activity in nubbins from other coral species were performed by following changes in light reflectance of 820 or 830 nm, and correcting the signal at 870 nm with a pulse-amplitude-modulated Dual-PAM instrument (Walz, Germany) [39, 40]. With this method a correction at 870 nm is commonly implemented in PSI activity determination to deconvolute PC contribution in the far-red region [48]. However, due to the absence of PC in peridinin chloroplasts [44] we consider that this correction is not necessary in photosynthetic corals, and light-induced absorption change at 705 nm can be used (Figure 1f), as it commonly yields a high negative value in

plants [**46**] and green algae [**71**]. In the case of Symbiodiniaceae isolates, absorbance change at 705 nm has been used with no major differences in kinetics of P700 photo-oxidation when a correction at 740 nm was applied (personal observation, [**37, 38**]). Assuming that the molar attenuation coefficient of P700 at 705 nm of Symbiodiniaceae is in the range of values determined for P700 in green photosynthetic organisms (*i.e.* 64 mM^{-1} cm^{-1} in spinach) [**72**] and 105 mM^{-1} cm^{-1} in *Chlamydomonas reinhardtii* [**47**]), we estimated the number of P700 per chlorophyll *a* to be between 1/720 to 1/1180 in *S. pistillata*. This range of values is in good agreement with values reported for several Symbiodiniaceae isolates [**35, 37**]. Despite missing a molar absorption coefficient of P700 for peridinin plastids, our results indicate that spectroscopy-based measurement in thin coral fragments is a reliable and accurate strategy to ascertain PSI activity of coral endosymbionts (e.g. **Figure 5**).

As thin coral fragments enabled spectroscopy-based measurements, ECS spectrum could be acquired. The presence of an ECS signal allows a direct measure of the electric field across algal thylakoid membranes [**49**]. The ECS spectrum measured in *S. pistillata* showed a small ratio between maximum (510 nm) and minimum (560 nm) ECS values in comparison to in culture Symbiodiniaceae (**Figure 6a**; [**37**]). On the other hand, field coral specimens showed different ECS signal amplitudes at 554 nm compared to 510 nm, despite harbouring the same Symbiodiniaceae genera *Durusdinium* (**Figure 6c**). In general, this difference can be attributed to pigment composition, distribution and orientation along the thylakoid membranes [**49**], but we cannot exclude that other effects such as differences in coral tissue or skeleton optical properties contribute to this difference. ECS-based measurements of PSI to PSII active center ratio in coral fragments gave comparable values to those previously reported in *Symbiodiniaceae* isolates (**Figure 6b**; [**37, 38**]).

In conclusion, *in vivo* monitoring of photosynthesis and respiration, as well as PSI and PSII activities, of *S. pistillata* coral fragments resulted in robust and reliable information. We thus consider that coral fragments are good spectroscopic objects to obtain reliable information about coral photosynthesis. This approach does not consume large amounts of coral colonies or nubbins allowing to limit the loss of living samples when destructive measures are taken. This work paves the way towards a better understanding of the role of bioenergetics processes in coral symbiosis establishment and persistence.

REFERENCES

1.   Falkowski, P. G., Dubinsky, Z., Muscatine, L. & Porter, J. W. Light and the bioenergetics of a symbiotic coral. *Bioscience* **34**, 705–709 (1984).

2.   Morris, L. A., Voolstra, C. R., Quigley, K. M., Bourne, D. G. & Bay, L. K. Nutrient availability and metabolism affect the stability of coral–symbiodiniaceae symbioses. *Trends Microbiol.* **27**, 678–689 (2019).

3.   LaJeunesse, T. C. *et al.* Systematic revision of symbiodiniaceae highlights the antiquity and diversity of coral endosymbionts. *Curr. Biol.* **28**, 2570–2580.e6 (2018).

4.   Cunning, R., Silverstein, R. N. & Baker, A. C. Symbiont shuffling linked to differential photochemical dynamics of Symbiodinium in three Caribbean reef corals. *Coral Reefs* **37**, 145–152 (2018).

5.   Muscatine, L., Falkowski, P. G., Porter, J. W. & Dubinsky, Z. Fate of photosynthetic fixed carbon in light- and shade-adapted colonies of the symbiotic coral *Stylophora pistillata. Proc. R. Soc. B Biol. Sci.* **222**, 181–202 (1984).

6.   Porter, J. W. Primary productivity in the sea: Reef corals in situ. in *Primary Productivity in the Sea. Environmental Science Research* (ed. Falkowski, P. G.) **19**, 403–410 (Springer Boston, 1980).

7.   Patterson, M. R., Sebens, K. P., Olson, R. O. In situ measurements of flow effects on primary production and dark respiration in reef corals. *Limnol. Oceanogr.* **36**: 936-948 (1991).

8.   Wangpraseurt, D. *et al.* Spectral effects on Symbiodinium photobiology studied with a programmable light engine. *PLoS One* **9**, (2014).

9.   Kühl, M. *et al*. Microenvironment and photosynthesis of zooxanthellae in scleractinian corals studied with microsensors for O_2, pH and light. *Mar. Ecol. Prog. Ser.* **117**, 159–172 (1995).

10. Burriesci, M. S., Raab, T. K., & Pringle, J. R.. Evidence that glucose is the major transferred metabolite in dinoflagellate-cnidarian symbiosis. *J. Exp. Biol.* **215**, 3467–3477 (2012).

11. Houlbrèque, F. & Ferrier-Pagès, C. Heterotrophy in tropical scleractinian corals. *Biol. Rev.* **84**, 1–17 (2009).

12. Holcomb, M., Tambutté, E., Allemand, D. & Tambutté, S. Light enhanced calcification in *Stylophora pistillata*: Effects of glucose, glycerol and oxygen. *PeerJ*, 2:e375 (2014).

13. Agostini, S., Fujimura, H., Hayashi, H. & Fujita, K. Mitochondrial electron transport activity and metabolism of experimentally bleached hermatypic corals. *J. Exp. Mar. Bio. Ecol.* **475**, 100–107 (2016).

14. Imbs, A. B. & Yakovleva, I. M. Dynamics of lipid and fatty acid composition of shallow-water corals under thermal stress: and experimental approach. *Coral Reefs* **31**, 31-41 (2012).

15. Dunn, S. R., Pernice, M., Green, K., Hoegh-Guldberg, O. & Dove, S. G. Thermal stress promotes host mitochondrial degradation in symbiotic cnidarians: Are the batteries of the reef going to run out? *PLoS One* **7**, (2012).

16. Blackstone, N. Mitochondria and the redox control of development in cnidarians. *Semin. Cell Dev. Biol.* **20**, 330–336 (2009).

17. McDonald, A. E., Vanlerberghe, G. C. & Staples, J. F. Alternative oxidase in animals: Unique characteristics and taxonomic distribution. *J. Exp. Biol.* **212**, 2627–2634 (2009).

18. McDonald, A. E. & Gospodaryov, D. V. Alternative NAD(P)H dehydrogenase and alternative oxidase: Proposed physiological roles in animals. *Mitochondrion* **45**, 7–17 (2019).

19. Raven, J. A. & Beardall, J. Consequences of the genotypic loss of mitochondrial Complex I in dinoflagellates and of phenotypic regulation of Complex I content in other photosynthetic organisms. *J. Exp. Bot.* **68**, 2683–2692 (2017).

20. Oakley, C. A., Hopkinson, B. M. & Schmidt, G. W. Mitochondrial terminal alternative oxidase and its enhancement by thermal stress in the coral symbiont Symbiodinium. *Coral Reefs* **33**, 543–552 (2014).

21. Nelson, H. R. & Altieri, A. H. Oxygen: The universal currency on coral reefs. *Coral Reefs* 38, 177-189 (2019).

22. Iglesias-prieto, A. R., Govind, N. S. & Trench, R. K. Isolation and characterization of three membrane bound chlorophyll-protein complexes from four dinoflagellate species. *Philos. Trans. R. Soc. London. Ser. B Biol. Sci.* **340**, 381–392 (1993).

23. Aihara, Y., Takahashi, S. & Minagawa, J. Heat induction of cyclic electron flow around photosystem I in the symbiotic dinoflagellate Symbiodinium. *Plant Physiol.* **171**, 522–529 (2016).

24. Leggat, W., Badger, M. & Yellowlees, D. Evidence for an inorganic carbon-concentrating mechanism in the symbiotic dinoflagellate Symbiodinium sp. *Plant Physiol.* **121**, 1247-1255 (1999).

25. Raven, J. A., Suggett, D. J. and Giordano, M. (2020), Inorganic carbon concentrating mechanisms in free-living and symbiotic dinoflagellates and chromerids. *J. Phycol.* doi:10.1111/jpy.13050 (2020).

26. Barott, K. L. *et al.* Coral host cells acidify symbiotic algal microenvironment to promote photosynthesis. *Proc. Natl. Acad. Sci. U. S. A.* **112**, 607–612 (2015).

27. Mayfield, A. B., Hsiao, Y. Y., Chen, H. K. & Chen, C. S. Rubisco expression in the dinoflagellate *Symbiodinium* sp. is influenced by both photoperiod and endosymbiotic lifestyle. *Mar. Biotechnol.* **16**, 371–384 (2014).

28. Tremblay, P., Grover, R., Maguer, J. F., Legendre, L. & Ferrier-Pagès, C. Autotrophic carbon budget in coral tissue: A new 13C-based model of photosynthate translocation. *J. Exp. Biol.* **215**, 1384–1393 (2012).

29. Maor-Landaw, K., van Oppen, M. J. H. & McFadden, G. I. Symbiotic lifestyle triggers drastic changes in the gene expression of the algal endosymbiont *Breviolum minutum* (Symbiodiniaceae). *Ecol. Evol.* **10**, 451–466 (2020).

30. Roth, M. S. The engine of the reef: Photobiology of the coral-algal symbiosis. *Front. Microbiol.* **5**, 1–22 (2014).

31.   Roberty, S., Béraud, E., Grover, R. & Ferrier-Pagès, C. Coral productivity is co-limited by bicarbonate and ammonium availability. *Microorganisms* **8**, (2020).

32. Tchernov, D. et al. Membrane lipids of symbiotic algae are diagnostic of sensitivity to thermal bleaching in corals. *Proc. Natl. Acad. Sci. U. S. A.* **101**, 13531-13535 (2004).

33.   Cardol, P., Forti, G. & Finazzi, G. Regulation of electron transport in microalgae. *Biochim. Biophys. Acta - Bioenerg.* **1807**, 912–918 (2011).

34.   Papageorgiou, G. C. & Govindjee. *Chlorophyll a fluorescence. A signature of photosynthesis.* **19**, (Springer Netherlands, 2004).

35.   Hennige, S. J., Suggett, D. J., Warner, M. E., McDougall, K. E. & Smith, D. J. Photobiology of Symbiodinium revisited: Bio-physical and bio-optical signatures. *Coral Reefs* **28**, 179–195 (2009).

36.   Reynolds, J. M. C., Bruns, B. U., Fitt, W. K. & Schmidt, G. W. Enhanced photoprotection pathways in symbiotic dinoflagellates of shallow-water corals and other cnidarians. *Proc. Natl. Acad. Sci. U. S. A.* **105**, 17206 (2008).

37.   Roberty, S., Bailleul, B., Berne, N., Franck, F. & Cardol, P. PSI Mehler reaction is the main alternative photosynthetic electron pathway in *Symbiodinium* sp., symbiotic dinoflagellates of cnidarians. *New Phytol.* **204**, 81–91 (2014).

38.   Dang, K. V., Pierangelini, M., Roberty, S. & Cardol, P. Alternative photosynthetic electron transfers and bleaching phenotypes upon acute heat stress in *Symbiodinium* and *Breviolum* spp. (Symbiodiniaceae) in culture. *Front. Mar. Sci.* **6**, 1–10 (2019).

39.   Hoogenboom, M. O., Campbell, D. A., Beraud, E., DeZeeuw, K. & Ferrier-Pagès, C. Effects of light, food availability and temperature stress on the function of photosystem II and photosystem I of coral symbionts. *PLoS One* **7**, (2012).

40.   Szabó, M. *et al.* Non-intrusive assessment of photosystem II and photosystem I in whole coral tissues. *Front. Mar. Sci.* **4**, (2017).

41.   Enríquez, S., Méndez, E. R. & Iglesias-Prieto, R. Multiple scattering on coral skeletons enhances light absorption by symbiotic algae. *Limnol. Oceanogr.* **50**, 1025–1032 (2005).

42.   Gilmore, A. M. *et al.* Simultaneous time resolution of the emission spectra of fluorescent proteins and zooxanthellar chlorophyll in reef-building corals. *Photochem. Photobiol.* **77**, 515 (2003).

43.   Maxwell, K. & Johnson, G. N. Chlorophyll fluorescence-a practical guide. *J. Exp. Bot.* **51**, 659–668 (2000).

44.   Sandmann, G., Reck, H., Kessler, E. & Böger, P. Distribution of plastocyanin and soluble plastidic cytochrome c in various classes of algae. *Arch. Microbiol.* **134**, 23–27 (1983).

45.   Schreiber, U. Redox changes of ferredoxin, P700, and plastocyanin measured simultaneously in intact leaves. *Photosynth. Res.* **134**, 343–360 (2017).

46.   Joliot, P. & Joliot, A. Quantification of cyclic and linear flows in plants. *Proc. Natl. Acad. Sci. U. S. A.* **102**, 4913–4918 (2005).

47.   Witt, H. *et al.* Species-specific differences of the spectroscopic properties of P700: Analysis of the influence of non-conserved amino acid residues by site-directed mutagenesis of photosystem I from Chlamydomonas reinhardtii. *J. Biol. Chem.* **278**, 46760–46771 (2003).

48.   Klughammer, C. & Schreiber, U. An improved method, using saturating light pulses, for the determination of photosystem I quantum yield via P700+-absorbance changes at 830 nm. *Planta* **192**, 261–268 (1994).

49.   Bailleul, B., Cardol, P., Breyton, C. & Finazzi, G. Electrochromism: A useful probe to study algal photosynthesis. *Photosynth. Res.* **106**, 179–189 (2010).

50.   Vega De Luna, F., Dang, K. Van, Cardol, M., Roberty, S. & Cardol, P. Photosynthetic capacity of the endosymbiotic dinoflagellate *Cladocopium* sp. is preserved during digestion of its jellyfish host *Mastigias papua* by the anemone *Entacmaea medusivora*. *FEMS Microbiol. Ecol.* **95**, 1–7 (2019).

51.   Ritchie, R. J. Consistent sets of spectrophotometric chlorophyll equations for acetone, methanol and ethanol solvents. *Photosynth. Res.* **89**, 27–41 (2006).

52.   Hume, B. C. C. *et al.* An improved primer set and amplification protocol with increased specificity and sensitivity targeting the Symbiodinium ITS2 region. *PeerJ*, 6:e4816 (2018).

53.   Hume, B. C. C. *et al.* SymPortal: A novel analytical framework and platform for coral algal symbiont next-generation sequencing ITS2 profiling. *Mol. Ecol. Resour.* **19**, 1063–1080 (2019).

54.   Shafir, S., Van Rijn, J. & Rinkevich, B. Nubbing of coral colonies: A novel approach for the development of inland broodstocks. *Aquarium Sci. Conserv.* **3**, 183–190 (2001).

55.   Hoadley, K. D. *et al.* Host–symbiont combinations dictate the photo-physiological response of reef-building corals to thermal stress. *Sci. Rep.* **9**, 1–15 (2019).

56.   Heyward, A. J. & Collins, J. D. Fragmentation in *Montipora ramosa*: the genet and ramet concept applied to a reef coral. *Coral Reefs* **4**, 35–40 (1985).

57.   Raz-Bahat, M., Erez, J. & Rinkevich, B. In vivo light-microscopic documentation for primary calcification processes in the hermatypic coral *Stylophora pistillata. Cell Tissue Res.* **325**, 361–368 (2006).

58.   Warner, M. E., Fitt, W. K. & Schmidt, G. W. Damage to photosystem II in symbiotic dinoflagellates: A determinant of coral bleaching. *Proc. Natl. Acad. Sci. U. S. A.* **96**, 8007–8012 (1999).

59.   Rehman, A. U. *et al. Symbiodinium* sp. cells produce light-induced intra- and extracellular singlet oxygen, which mediates photodamage of the photosynthetic apparatus and has the potential to interact with the animal host in coral symbiosis. *New Phytol.* **212**, 472–484 (2016).

60.   Hill, R. & Ralph, P. J. Dark-induced reduction of the plastoquinone pool in zooxanthellae of scleractinian corals and implications for measurements of chlorophyll a fluorescence. *Symbiosis* **46**, 45–56 (2008).

61.   Einbinder, S. *et al.* Novel adaptive photosynthetic characteristics of mesophotic symbiotic microalgae within the reef-building coral, *Stylophora pistillata. Front. Mar. Sci.* **3**, 1–9 (2016).

62.   Mass, T. *et al.* Photoacclimation of *Stylophora pistillata* to light extremes: Metabolism and calcification. *Mar. Ecol. Prog. Ser.* **334**, 93–102 (2007).

63.   Ferrier-Pagès, C., Gattuso, J. P., Dallot, S., & Jaubert, J. Effect of nutrient enrichment on growth and photosynthesis of the zooxanthellae coral Stylophora pistillata. *Coral Reefs* **19**:103-113 (2000).

64.   Peltier, G., Tolleter, D., Billon, E. & Cournac, L. Auxiliary electron transport pathways in chloroplasts of microalgae. *Photosynth. Res.* **106**, 19–31 (2010).

65.   Pierangelini, M., Thiry, M. & Cardol, P. Different levels of energetic coupling between photosynthesis and respiration do not determine the occurrence of adaptive responses of Symbiodiniaceae to global warming. *New Phytol.* doi:10.1111/nph.16738 0–2 (2020). doi:10.1111/nph.16738

66.   Bailleul, B. *et al.* Energetic coupling between plastids and mitochondria drives CO2 assimilation in diatoms. *Nature* **524**, 366–369 (2015).

67.   Badger, M. R. *et al.* Electron flow to oxygen in higher plants and algae: Rates and control of direct photoreduction (Mehler reaction) and rubisco oxygenase. *Philos. Trans. R. Soc. B Biol. Sci.* **355**, 1433–1446 (2000).

68.   Fan, D. Y. *et al.* Obstacles in the quantification of the cyclic electron flux around photosystem I in leaves of C3 plants. *Photosynth. Res.* **129**, 239–251 (2016).

69.   Szabó, M. *et al.* Effective light absorption and absolute electron transport rates in the coral *Pocillopora damicornis*. *Plant Physiol. Biochem.* **83**, 159–167 (2014).

70.   Kato, H. *et al.* Characterization of a giant photosystem I supercomplex in the symbiotic dinoflagellate Symbiodiniaceae. *Plant Physiol.* pp.00726.2020 (2020). doi:10.1104/pp.20.00726 (2020).

71.   Alric, J. Cyclic electron flow around photosystem I in unicellular green algae. *Photosynth. Res.* **106**, 47–56 (2010).

72.   Melis, A. & Jeanette, J. S. Stoichiometry of system I and system II reaction centers and of plastoquinone in different photosynthetic membranes. *Proc. Natl. Acad. Sci. U. S. A.* **77**, 4712–4716 (1980).

CHAPTER 5   The photosynthetic activity of Symbiodiniaceae in symbiosis with *S. pistillata* under stressing conditions

Derived from the previous observations, the question of the occurrence of photosynthetic alternative electron pathways in corals found in a coral reef was addressed. *S. pistillata* is known to be a depth-generalist species, living from shallow, close to the surface, to mesophotic depths, receiving 1 % of surface irradiance, in the coral reef of the Gulf of Aqaba-Eilat, in Israel. Bigger depths represent a change in the light environment for aquatic organisms. During a field trip to the Inter-University Institute for Marine Sciences, in Eilat, Israel, coral colonies of *S. pistillata* were collected from shallow (10 m) and mesophotic (45 m) depths. We expected that this coral presented a series of photoacclimation strategies. Some of those closely link to the light absorption capacity, and by consequence with the use of photosynthetic alternative electron pathways. We carried out photosynthetic measurements on coral fragments, and included the genetic determination of the Symbiodiniaceae symbionts harboured by this coral species from both depths.

Photoacclimation of the reef-building coral *S. pistillata* to both shallow and mesophotic depths in the Gulf of Eilat/Aqaba, includes adjustments of, at least, both animal host and algal symbiont (**Falkowski and Dubinsky, 1981**). Photoacclimation in the host includes changes of its coral skeleton morphology, pigment production, symbiont cell density, symbiont type proliferation, and metabolic activity. While the photosynthetic symbiont is able to adjust its pigment density, pigment type content and light absorption efficiency, when found at different light intensities (**McCloskey and Muscatine, 1984; Gatusso, 1985**). These cooperative strategies make unique these symbiotic animals, indicating that the contribution of both partners to photoacclimation is more complex than in free-living algae. While the natural high light conditions have demonstrated to induce a robust photoprotection mechanism in shallow water colonies, the description has been less detailed in mesophotic colonies. A change in the light regime during three days was also tested, in order to provide information on the flexibility of the photosynthetic machinery, and the capacity of the symbiotic algae to acclimate.

My contribution to this submitted manuscript consisted in the experimental design of the measurement, the data acquisition during the manipulation of the corals, the analysis of the data, and the writing of the manuscript.

Shallow and mesophotic colonies of the coral *Stylophora pistillata* share regulatory strategies of photosynthetic electron transport but differ in their sensitivity to light

Authors:

Stephane Roberty [1][*][†], Félix Vega de Luna [2][†], Mattia Pierangelini [2], Julie Bomhals [1], Jean-Christophe Plumier [1], Oren Levy [3], Pierre Cardol [2][*]

Affiliations:

[1] InBioS–Animal Physiology, University of Liège, 4000 Liège, Belgium

[2] InBioS–Genetic and Physiology of Microalgae, University of Liège, 4000 Liège, Belgium

[3] The Mina and Everard Goodman Faculty of Life Sciences, Bar–Ilan University, Ramat Gan, Israel

[*] Corresponding authors: SR, sroberty@uliege.be; PC, pierre.cardol@uliege.be

[†] These authors contributed equally to this paper.

Abstract

Acclimation of corals to light intensity is known to depend on multiple factors. The details of the functioning of the photosynthetic machinery and its involvement in the photoacclimation strategies will help to understand the plasticity of the photosynthetic process in corals and in the understanding of the processes where destructive reactive species are produced. In this work, we used shallow and mesophotic colonies of the depth-generalist coral *Stylophora pistillata* from the Northern Red Sea, to carry out joint measurements of oxygen exchange, and PSI and PSII quantum yields to disclose the use of alternative electron flows. Despite a lower photosynthetic activity in mesophotic colonies, we found similar capacities to re-route photosynthetically derived electrons towards oxygen, and to perform cyclic electron flow under high light intensity in both colony types. Shallow colonies displayed a higher dissipative activity but showed the involvement of plastoquinone with stromal reactions at low light intensity. We also observed that their photosynthetic machinery was able to

drive a higher number of electrons, but these features were decreased after the colonies were transferred to lower light intensities for three days. Mesophotic corals at high light intensity showed a strong photoinhibition, but their PSI activity was preserved.

Introduction

Dinoflagellates belonging to the Family Symbiodiniaceae (LaJeunesse et al. 2018) are capable to establish endosymbiotic relationships with diverse animal hosts, including Cnidaria, Porifera and Mollusca (Weber & Medina, 2012; Lesser et al. 2018). Such associations between Symbiodiniaceae and scleractinian hosts are key to the integrity and functioning of coral reef ecosystems worldwide (Hughes et al. 2017). During the last decades, changes of the coastal marine ecosystems due to anthropogenic activities have been causing major disruption of the endosymbiotic relationship between Symbiodiniaceae and their hosts, causing loss of coral reef ecosystems (Hughes et al. 2107; 2018). Following these disturbances, a plethora of studies have been carried out to disentangle the ecological and physiological functioning of Symbiodiniaceae, hosts and their mutual relationships (e.g., Suggett et al. 2017; Torda et al. 2017; Hughes et al. 2018; Comeau et al. 2019). Most of these studies investigated reef species occurring in the shallow parts of the coastal habitats, and only relatively fewer studies focused attention on reef species dwelling in the deeper mesophotic environment (>30 m) (e.g., Mass et al. 2007; Einbinder et al. 2016; Lesser et al. 2018; Shlesinger et al. 2018). This is a considerable lack if we consider the vertical connectivity between the deep and the shallow coral reef populations (van Oppen et al. 2011; Holstein et al. 2016; Lesser et al. 2018), and that mesophotic communities have been recognized as refuges for several coral species endangered at shallow levels (Laverick et al. 2018).

In tropical regions, scleractinian corals are key members of both shallow and mesophotic reef communities. In the Gulf of Eilat-Aqaba (GoEA; Northern Red Sea), the coral reef is distributed along the steep shoreline where it can reach depths higher than 100 m in the first kilometer from the coast (Eyal et al. 2019). Hence, in this area, the coral species distribution is dramatically influenced by light availability at the different depths (Tamir et al. 2019). The light penetration is considered to be high due to the low presence of light-absorbing particles in the water column, but with a marked seasonal change due to its northern position in the Red Sea (29° 30' N) (Dishon et al. 2012). From winter (December-January) to summer (June-July) the increase of global solar radiation accounts for up to two times at shallow depths, and more than five times at mesophotic depths (Stambler 2006; Dishon et al. 2012; Nir et al. 2014).

The stony coral *Stylophora pistillata*, described as a depth-generalist, is bathymetrically distributed from shallow water to the upper mesophotic zone (30 - 60 m) in this coral reef (Mass et al. 2007; Scucchia et al. 2021). As water absorb and remove wavelengths from the incident spectrum, causing an exponential decline with depth of light quantity and a selection towards shorter wavelengths (blue light spectrum, c.a. 490–450 nm; Dubinsky and Stambler 2009; Dishon et al. 2012; Eyal et al. 2019), ability of corals to grow in such bathymetrical regions may require changes in the Symbiodiniaceae species composition, their abundance within the host tissue, and physiological plasticity (Mass et al. 2007; Einbinder et al. 2016).

Several studies carried out in the GoEA showed that Symbiodiniaceae harbored by *S. pistillata* occurring at mesophotic depths possess higher contents of photosynthetic pigments and exhibit lower photosynthetic rates (Porter et al. 1984; Mass et al. 2007; Einbinder et al. 2009; Cohen and Dubinsky, 2015; Einbinder et al. 2016). This reflects photo-physiological important traits for the photoacclimation process, such as higher number of pigments (i.e. the antenna size) associated to the photosynthetic units (PSUs) and/or the amount of PSUs (i.e. the amount of photosystem I (PSI) and II (PSII) reaction centers) (Falkowski and Dubinsky, 1981; Chang et al. 1983; Falkowski and LaRoche, 1991; Iglesias-Prieto and Trench, 1994; Hennige et al. 2009), and the energetic connectivity between PSII and PSI reaction centers (Einbinder et al. 2016).

Presence of photosynthetic alternative electron flows (AEF) such as electron rerouting toward oxygen (e.g., Mehler reaction) or cyclic electron flow (CEF) around PSI have been documented to occur in isolated Symbiodiniaceae (Roberty et al. 2014; Aihara et al. 2016), where they contribute to photo-protection and to the balance of the energetic ratio between photo-produced ATP and NADPH (Miyake, 2010; Dang et al. 2019). However, AEF possess only a finite capacity for protection beyond which the electron transport chain becomes over-reduced, the rate of reactive oxygen species production at the level of PSII and PSI exceeds the capacity of the cellular antioxidant network, and significant damages to the photosynthetic apparatus occur. In the mutualistic relationship between cnidarians and their photosynthetic endosymbionts, the dysregulation of redox homeostasis is thought to lead to a series of events ending with the breakdown of the symbiosis (i.e., bleaching; Roberty and Plumier, 2022). There is little information currently available on the presence of AEF when Symbiodiniaceae are *in hospite* (Aihara et al. 2016; Vega de Luna et al. 2020) and if or how the occurrence of AEF plays a role in defining the overall hosts' capacity to acclimate to different light regimes, as those experienced by of corals' species capable of inhabiting both shallow waters and mesophotic depths. In this study, we first aimed to establish the occurrence of AEF of

99

Symbiodiniaceae species *in hospite*, and second, to determine how the physiological traits shape the response of AEF of corals (i.e., *S. pistillata*) inhabiting at different depths.

Methods

Biological material and experimental settings

Mature colonies of *S. pistillata* were collected by scuba diving on the reef in the Red Sea in front of the Inter-University Institute for Marine Sciences, Eilat, Israel (29°30' N, 34°55' E) in November 2019. Five different colonies located at least 10 m apart, to decrease the potential of sampling clonal genotypes, were collected at both shallow (10 m) and mesophotic depths (45 m). The daily maximum photosynthetic photon flux densities (PPFD) measured at these depths were about 500 and 20-25 µmol photons m^{-2} s^{-1}, respectively. Colonies were then placed individually in 20 L aquaria partially submerged in an outdoor water table and acclimated for two weeks prior to any experiments. Seawater at 25.4 ± 0.2 °C was continuously pumped into each flow-through aquarium. The water table was covered with a combination of shade nets and neutral density filters in order to mimic the light intensities experienced by the corals at their collection depths (max 500 ± 20 and 20 ± 1 µmol photons m^{-2} s^{-1} at 10 and 45 m, respectively). For the light acclimation experiment, five different colonies were freshly collected at 10 and 45 m and maintained in the same outdoor water table as described above. They were fragmented into 10 cm long branches and distributed in four different aquaria. Coral pieces were then exposed for 3 days to a natural circadian light cycle, with daily maximum light intensities of 10 (low light) and 1500 (high light) µmol photons m^{-2} s^{-1} (obtained by adjusting the number of layers of shade nets and neutral density filters). Seawater temperature (25.5 ± 0.6 °C) and ambient light inside the aquarium were monitored using HOBO data loggers (Onset, Bourne, MA, USA).

Symbiodiniaceae purification

Coral tissue was removed from the exoskeleton with an airbrush connected to a reservoir of 0.2 µm filtered seawater (FSW). The crude homogenate was then passed 10 times through a syringe (24G x 1" BD Microlance 3, BD, Spain) in order to lyse host cells and keep intact symbiont cells into the solution. After centrifugation (3,000 x *g*, 5 min), the supernatant was discarded and the pelleted Symbiodiniaceae were resuspended into 3 mL of FSW. 250 µL of this suspension was fixed with 25 µL of a 35 % formaldehyde solution and stored at 4 °C for cell counting. One mL of the suspension

was used to determine the chlorophyll content and the rest of the suspension was stored at -80 °C for HPLC analyses.

Symbiodiniaceae densities and chlorophyll content

Cell counting was carried out using a Z2 Beckman Coulter Counter (Brea, CA, USA) from an aliquot of the purified Symbiodiniaceae suspension. To determine the chlorophyll content, cells were collected by centrifugation (10,000 x g; 5 min), resuspended into 1 mL of ice-cold 100 % methanol in presence of 250 µL of glass beads (710-1,180 µm; Sigma-Aldrich), and disrupted by vortexing for 3 min and by sonication for 5 min into an ultrasound water bath (Ultrasonic Cleaner; model Y-008, USA) filled with ice-cold water. After sonication, the homogenate solution was centrifuged (10,000 x g, 5 min at 4 °C) and Chl-*a* and Chl-*c2* concentrations were determined by spectrophotometry according to the equations of Ritchie (2006) for dinophytes. Chl-*a* and Chl-*c2* concentrations determined with this protocol were used to calculate the oxygen exchange rates.

Coral surface was calculated from coral nubbins used for Symbiodiniaceae purification using the wax dipping method described in Stimson and Kinzie (1991).

Pigment profile analysis

Cells were collected from the frozen suspension by centrifugation (12,000 x g for 5 min), resuspended into 1 mL of ice-cold 100% methanol in presence of 250 µL of glass beads (710–1,180 µm; Sigma-Aldrich), lysed in a TissueLyser II (30 Hz, 5 min, 4°C; Qiagen), and centrifuged at 16,000 x g for 20 min at 4°C. As described by Roberty et al. (2020), pigments were then separated by reverse-phase HPLC, using Shimadzu Prominence HPLC system, comprising a DGU-20A5R Degassing Unit, a LC-20AT Liquid chromatograph, a SIL-20AC Autosampler, a CTO-10ASVP Column Oven and a SPD-M20A Diode Array Detector (Shimadzu, Japan). The HPLC column (Nova Pak C18, 60A column, 150 mm length and 4 µm pore size) was eluted with a mobile phase gradient (1 mL min-1) set to the following program : 0.5 min with a gradient from 100 % (v/v) solvent A (80 % [v/v] methanol and 20 % [v/v] 0.5 M ammonium acetate [pH 7]) to 100 % (v/v) solvent B (90 % [v/v] acetonitrile in water); then during 0.5 min with a gradient from 100 % (v/v) solvent B to 90 % (v/v) solvent B and 10 % (v/v) solvent C (ethyl acetate); 10 min with a gradient from 90 % (v/v) solvent B to 65 % (v/v) solvent B and from 10 % (v/v) solvent C to 35 % (v/v) solvent C; 1 min with a gradient from 65 % (v/v) solvent B to 55 % (v/v) solvent B and from 35 % (v/v) solvent C to 45 % (v/v) solvent C; 3 min with a gradient from 55 % (v/v) solvent B to 40 % (v/v) solvent B and from 45 % (v/v) solvent C to 60 % (v/v) solvent C; 5 min with a gradient from 40 % (v/v) solvent B to 0 % (v/v)

solvent B and from 60 % (v/v) solvent C to 100 % (v/v) solvent C; and finally during 2 min with a gradient from the latter solvent mixture to 100 % (v/v) solvent A. Absorbance chromatograms obtained at 430 nm and compared to elution profiles of pigment standards (DHI Lab, Horstholm, Denmark) to quantify pigment amounts. Acquisition and data treatment were performed using the Shimadzu LabSolutions software (Shimadzu, Japan). The values of pigment content obtained with this method are reported only in Table 1 and S1.

Spectroscopic measurements

For spectroscopic measurements, coral fragments of about 5 x 5 mm (Figure 1a) were cut from *S. pistillata* colonies with a Dremel 8220 (Dremel, USA) equipped with a diamond disk, as described in Vega de Luna et al. 2020. *In vivo* chlorophyll *a* fluorescence images were obtained using a SpeedZen imaging system (BeamBio/API, France) or a JTS-10 spectrophotometer (BioLogic, France) controlled by a custom-made unit (BeamBio/API, France) as previously described (Vega de Luna et al. 2019; 2020). Briefly, the maximum photochemical quantum yield of PSII (F_V/F_M) was measured after a dark adaptation of 15 min and calculated as $(F_M-F_O)/F_M$. After F_V/F_M determination, light saturation curves for photosynthesis were performed using the two instruments with different coral fragments. The PPFD (660 nm red LEDs) applied were 40, 130, 320, 570, 840 and 1000 µmol photons m^{-2} s^{-1} with the SpeedZen imaging system, and 90, 138, 220, 350, 680 and 1200 µmol photons m^{-2} s^{-1} with the JTS-10 spectrophotometer. The effective photochemical quantum yield of PSII (ϕPSII), the relative electron transfer rate through PSII (rETR-PSII) and the non-photochemical quenching (NPQ) were calculated at the end of each light step (3 min) as ϕPSII = $(F_M'-F_S)/F_M'$, $rETR_{PSII}$ = ϕPSII x PPFD, and NPQ = $(F_M-F_M')/F_M'$. The chlorophyll *a* fluorescence measurements carried out in the JTS-10 included a period of darkness of five seconds between the saturating pulse and the next illumination period, during which five fluorescence values was acquired every second.

The activity of PSI was assessed by the monitoring of changes in absorption in the near infrared region. Light-induced absorption changes of P_{700} were measured at 705 nm with a JTS-10 spectrophotometer (BioLogic, France) controlled by a custom-made unit (BeamBio/API, France) as previously described (Vega de Luna et al. 2020). Similarly, to chlorophyll *a* fluorescence measurements, a light saturation curve for photosynthesis, comprising the same irradiance steps and the same duration was conducted. The effective photochemical quantum yield of PSI (Y(I)), the quantum yield of non-photochemical energy dissipation due to donor side limitation (Y_{ND}) or due to acceptor side limitation (Y_{NA}), and the relative electron transfer rate through PSI ($rETR_{PSI}$) were calculated at the end of each light step as Y(I) = $(P_M'-P_S)/(P_M-P_0)$, Y(ND) = $(P_S-P_0)/(P_M-P_0)$, Y(NA)

= $(P_M-P_M')/(P_M-P_0)$, and $rETR_{PSI}$ = Y(I) x PPFD (Klughammer and Schreiber, 2008). Re-reduction rates of P_{700} after 30 s at 1200 µmol photons m^{-2} s^{-1} were monitored in the presence of 3-(3,4-dichlorophenyl)-1,1-dimethylurea (DCMU, 20 µM) to determine the non-photochemical reducing power capacity. Inhibitors were added 10 min before measurements (Dang et al. 2019) and all spectroscopic measurements were conducted at 26 °C. The $rETR_{PSII}$ and $rETR_{PSI}$ rates as a function of PPFD were fitted through the mathematical model of Webb et al. (1974), to calculate photosynthetic parameters as maximum $rETR_{PSII}$ and $rETR_{PSI}$.

Oxygen exchange

Simultaneously with chlorophyll *a* fluorescence measurements, rates of oxygen uptake in the dark (U_{OD}) and net oxygen evolution (V_{O2}) in the light were recorded with a FireSting O_2 optical oxygen sensor (Pyro Science, Germany) fitted to a temperature-controlled acrylic chamber (8 mL volume, 26 °C). Illumination was provided by the SpeedZen imaging system and data were normalized to the surface area of the coral fragment and the total chlorophyll content of the fragment. Gross oxygen evolution (E_O) was calculated as V_{O2} - U_{OD}. Oxygen evolution rates as a function of light intensity were fitted through the mathematical model of Webb et al. (1974), to calculate photosynthetic parameters as maximum photosynthetic rate (P max, E_O), maximum photosynthetic efficiency (α), and onset of light saturated photosynthesis (I_k = E_O/α).

Symbiodiniaceae diversity

Coral fragments of 1-2 cm long were taken from shallow and deep independent colonies (n = 3). They were washed with filtered sea water and coral tissues were extracted by airbrushing the fragments into sterile PBS. DNA from the microalgal fraction was then extracted by using a DNeasy Plant mini kit (QIAGEN) according to the manufacturer's instructions, with slight modifications. The symbiont-enriched pellets were resuspended in 400 µL of AP3 lysis buffer in presence of 500 µL of acid-washed and autoclaved glass beads (710–1,180 µm; Sigma-Aldrich) and vortexed for 2 minutes at 30 Hz with a TissueLyser II (QIAGEN). All DNA samples were quantified with a Synergy MX spectrophotometer and normalized to 1 ng µL-1 for subsequent PCR.

The PCR amplification of the ITS2 gene marker was performed using primers pair SYM_VAR_5.8S2 and SYM_VAR_REV with an Illumina MiSeq adapter sequence, and the reagents and conditions detailed in Hume et al. 2018. PCRs were run in triplicate per sample and PCR products were run on a QIAxcel Advanced Instrument (QIAGEN) before being pooled.

Pooled samples were cleaned with AMPure XP beads (Beckman Coulter, Brea, CA, USA). Nextera XT indexing and sequencing adapters were added via PCR (8 cycles, total PCR cycles for all samples = 35) following the manufacturer's instructions. The samples were then quantified on an Agilent 2100 Bioanalyzer (Agilent Technologies, USA) and pooled in equimolar ratios. The pooled library was sequenced with 10% phiX on the Illumina MiSeq platform with 2 x 250 bp read configuration.

After sequencing, the pair of demultiplexed .fastq.gz files outputted from the Illumina platform were submitted to SymPortal.org. This analytical framework uses next generation amplicon sequencing data to identify ITS2-type profiles representative of putative Symbiodiniaceae taxa (Hume et al. 2019).

Statistical analyses

Statistical analyses of the data were performed in SigmaPlot 11.0 (Systat Software, San José, CA, USA). The 'depth' effect was examined by performing t-Tests. If the normality and equality of variance assumptions were not met, the Mann-Whitney Rank Sum test was used. For the photoacclimation experiment, the 'time', 'depth', and 'time x depth' effects were examined by two-way repeated-measures ANOVA. When significant differences were obtained, the analysis was followed by the Tukey's test for all pairwise multiple comparisons. Differences were considered statistically significant when $P < 0.05$. All data were expressed as mean ± SD.

Results

Morphological traits and holobiont characteristics

The morphology, polyp and pigment densities in colonies of *S. pistillata* collected at shallow and upper mesophotic depths were notably different. Colonies collected at 10 m depth (i.e., shallow) had a hemispherical shape with thick branches, whereas colonies collected at 45 m depth (i.e. mesophotic) were more planar with thinner branches and a lower polyp density (Fig. S1; Table 1). The Symbiodiniaceae communities harboured by these coral colonies also differed (Fig. S2), being largely composed (> 90 %) of *Symbiodinium microadriaticum* (ITS2-type A1) in the shallow colonies and mainly (> 75 %) belonging to the genus *Cladocopium* (ITS2-type C72) in mesophotic colonies. Endosymbionts' cell diameter did not differ between both depths. Pigment content was about 50 % higher in the symbionts of mesophotic colonies (Table 1; $P < 0.05$), but the content of chlorophyll and carotenoids per surface was similar between colonies of the two depths due to the higher symbiont

cell density displayed in shallow colonies (Table S1). The similar Chl-c_2/a ratios observed (Table 1) suggest that the photosynthetic antenna type composition did not differ at the two depths investigated.

Table 1 | Comparison of key biomass algal symbiont parameters. Poly density and algal Cell density are reported per unit of coral surface, while algal pigment contents are expressed as per cell. Data are presented as mean ± SD and asterisks denote a statistical difference between groups (P<0.05).

	Shallow	Mesophotic
Polyp density (polyps cm^{-2})	51 ± 8	42 ± 8 *
Cell density (x10^5 cells cm^{-2})	8.2 ± 2.2 *	4.2 ± 0.8 *
Cell diameter (μm)	8.78 ± 0.08	8.82 ± 0.08
Chl-a (pg cell^{-1})	4.37 ± 1.22 *	6.95 ± 0.51 *
Chl-c_2 (pg cell^{-1})	0.77 ± 0.24 *	1.25 ± 0.21 *
Chl-c_2/a	0.18 ± 0.02	0.18 ± 0.02
Peridinin (pg cell^{-1})	2.24 ± 0.74 *	3.09 ± 0.44 *
Diadinoxanthin (pg cell^{-1})	0.56 ± 0.21	0.73 ± 0.13
β-carotene (pg cell^{-1})	0.04 ± 0.02 *	0.06 ± 0.01 *

Comparison of the photosynthetic efficiency and non-photochemical quenching

We then evaluated the photosynthetic activity of *S. pistillata* colonies through light-response curves. Maximum values of net oxygen exchange (V$_{O2}$) per coral surface area did not differ between both colony types (Fig. 1A). However, the gross oxygen evolution (E$_O$) normalized per chlorophyll content was lower in mesophotic colonies along the light curve (P<0.001; Table 2; Fig. 1B). This

difference resulted from a lower maximum efficiency of oxygen evolution and a lower respiratory activity of mesophotic colonies (Table 2).
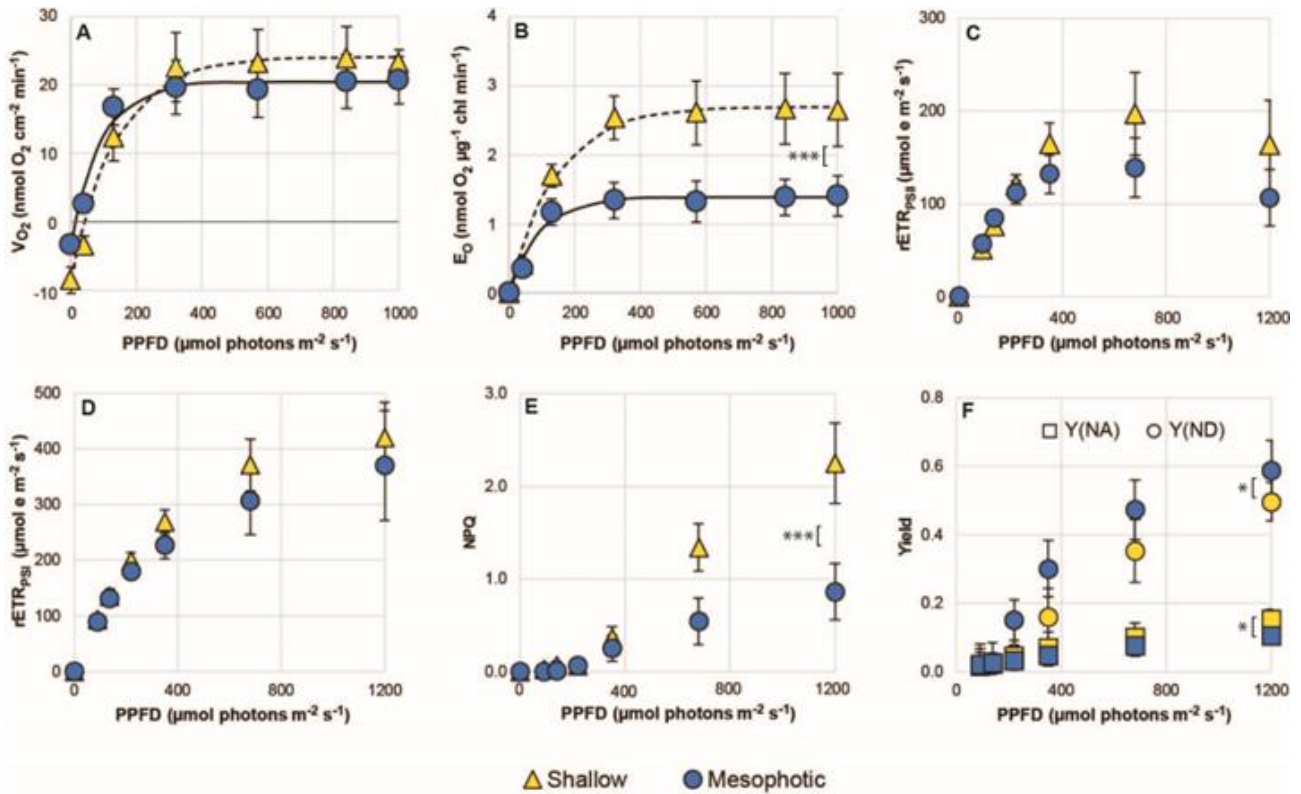
Figure 1 | Comparison of the photosynthetic efficiency and non-photochemical quenching between shallow and mesophotic colonies of *S. pistillata*. (A) Net oxygen evolution (VO$_2$) of the coral holobiont (nmol O$_2$ cm^{-2} min^{-1}). (B) Gross photosynthesis (E$_O$) per chlorophyll (nmol O$_2$ µg^{-1} chl min^{-1}). (C) Relative electron transport rates of photosystem II (rETR$_{PSII}$) and (D) photosystem I (rETR$_{PSI}$) as a function of PPFD. (E) Non-photochemical quenching of chlorophyll fluorescence (NPQ). (F) PSI quantum yield of non-photochemical energy dissipation due to acceptor side limitation (Y(NA)) or donor side limitation (Y(ND)). Data are mean ± SD, asterisks indicate statistically significant differences (*P<0.05; **P<0.01; ***P<0.001).

We also evaluated the electron transport activity of PSII by chlorophyll fluorescence (rETR$_{PSII}$). Shallow and mesophotic colonies had similar rETR$_{PSII}$ up to 220 µmol photons m^{-2} s^{-1}, but it was higher in shallow colonies at higher PPFD (P<0.01; Table 2; Fig. 1C). The relative electron transport through PSI (rETR$_{PSI}$), monitored by absorption changes of the PSI primary electron donor (P$_{700}$), also revealed similar maximum values for both colony types (Table 2, Fig. 1D), with no

difference in their response to light increases. This inconsistency between the PSI and PSII activities was further evaluated by comparing the quantum yield of non-photochemical energy dissipation for both photosystems. On the one hand, energy dissipation through the antenna of PSII (NPQ) was up to two times higher in shallow colonies compared to mesophotic ones at light intensities above 350 μmol photons m^{-2} s^{-1} (P<0.001; Fig. 1E), and the fraction of maximum NPQ reached at each light step was equivalent in both colonies. On the other hand, mesophotic corals had a higher energy dissipation due to PSI donor side limitation (Y(ND)) and a lower dissipation due to acceptor side limitation (Y(NA)) when exposed to increasing PPFD (Fig. 1F).

Table 2 | Comparison of key photosynthetic parameters. Values of Fv/Fm and rETR were obtained through chlorophyll a fluorescence in parallel of oxygen exchange rates during the light-dependent curves. Data are presented as mean $\pm$ SD and asterisks (*) denote a statistical difference between groups (P<0.05), double asterisk (**) denote P<0.001.

	Shallow	**Mesophotic**
F_V/F_M	0.61 ± 0.05 *	0.68 ± 0.03 *
Max $rETR_{PSII}$ (μmol e m^{-2} s^{-1})	188 ± 48 *	129 ± 29 *
Max $rETR_{PSI}$ (μmol e m^{-2} s^{-1})	444 ± 86	387 ± 129
Respiration (U_{OD}) (nmol O_2 cm^{-2} min^{-1})	8.4 ± 1.9 *	3.3 ± 1.1 *
Respiration Post-I (nmol O_2 cm^{-2} min^{-1})	14.4 ± 2.3	12.1 ± 3.0
Max E_O (nmol O_2 cm^{-2} min^{-1})	32.7 ± 5.5 *	23.8 ± 4.0 *
Max E_O (nmol O_2 μg^{-1} chl min^{-1})	2.7 ± 0.5 *	1.4 ± 0.3 *
α (pmol O_2 μg^{-1} chl) (μmol photons m^{-2})$^{-1}$	0.32 ± 0.02 *	0.25 ± 0.04 *
I_k (μmol photons m^{-2} s^{-1})	141 ± 20 *	92 ± 15 *
Ic (μmol photons m^{-2} s^{-1})	72 ± 55	32 ± 26
P_{700}^+ re-reduction rate (s^{-1})	25 ± 10	6 ± 2 **

Differences in alternative electron flow

To further characterize the photosynthetic activity in both coral colonies, we studied the main alternative electron flow (AEF) pathways. Because some AEF pathways involve only PSII (e.g., PTOX or PSII-CEF) while others involve only PSI (e.g. PSI-CEF) or both photosystems (e.g. the Mehler reaction), their occurrence can be deduced from joint measurements of ETR_{PSI}, ETR_{PSII} and O_2 evolution (Roberty et al. 2014).

A first comparison between E_O and $rETR_{PSII}$ showed a linear relationship at low PPFD, in both shallow and mesophotic colonies, with up to 2 and 1 nmol O_2 µg^{-1} chl min^{-1}, respectively. In the following higher light intensities we could observe a change of the initial linear trend (Figure 2A) for both colony types, turning to a higher electron transfer rate per oxygen evolved in comparison to the low PPFD phase. This was indicative of a re-routing of photosynthetically derived electrons towards O_2 (e.g. Mehler reaction) at high PPFD (Roberty et al. 2014, Dang et al. 2019). The fraction of oxygen uptake per electron transported in the light (calculated as $U_{OL}/rETR\ PSII$; see Dang et al. 2019) did not differ between shallow and mesophotic colonies, with values of 38 ± 10 and 45 ± 12 % at 850 µmol photons m^{-2} s^{-1}, respectively.
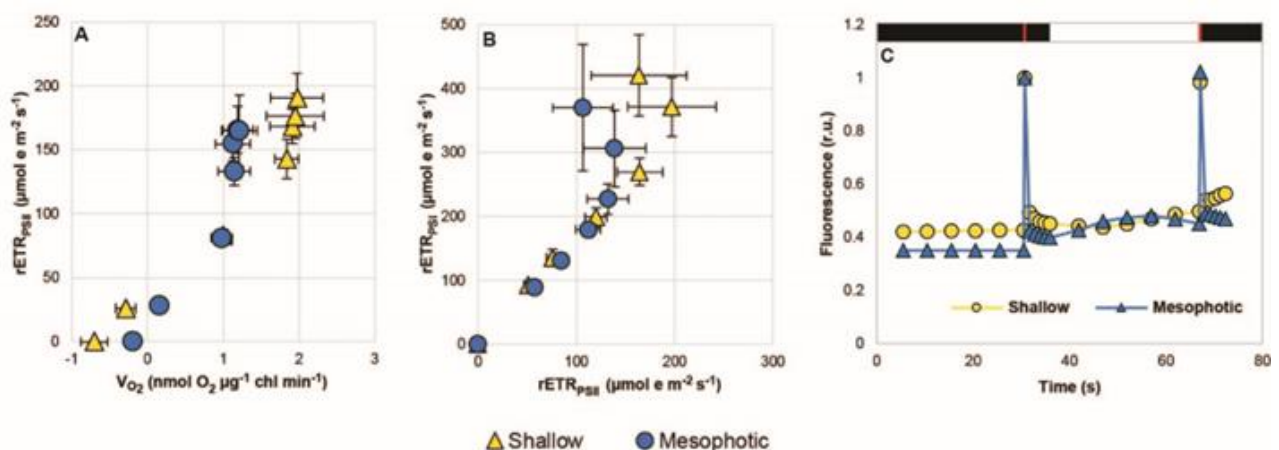
Figure 2 | Comparison of photosynthetic traits in shallow and mesophotic colonies of *S. pistillata*. (A) Comparison of VO$_2$ (nmol O$_2$ µg^{-1} chl min^{-1}) and $rETR_{PSII}$. (B) Relationship between $rETR_{PSI}$ and $rETR_{PSII}$. (C) Representative chlorophyll *a* fluorescence recording normalized to Fm value of shallow and mesophotic colonies. After 30 seconds of darkness (black bar over the plot) a pulse of saturating light was applied (red line), and chlorophyll *a* fluorescence was recorded in the next five seconds of

darkness. Low light intensity was switched on (empty bar) and after 30 s another saturating pulse of light was given. Chlorophyll *a* fluorescence was again recorded during the next five seconds in the darkness (black bar).

When comparing $rETR_{PSI}$ and $rETR_{PSII}$, a proportional increase was observed at low light intensities (up to 350 µmol photons m^{-2} s^{-1}) in both colony types (Fig. 2B). At higher PPFD, from 680 µmol photons m^{-2} s^{-1} for shallow colonies, and from 380 µmol photons m^{-2} s^{-1} for mesophotic colonies, there was a continued increase of $rETR_{PSI}$ in contrast to $rETR_{PSII}$. This result pointed out the existence of an AEF involving PSI (i.e., PSI-CEF). The maximum quantum yield of PSII (F_V/F_M), which is influenced by the redox state of its acceptor side (i.e., Q_A and the PQ pool), was found lower in shallow colonies than in mesophotic colonies (Table 2). Non-photochemical reduction of the PQ pool could also be evidenced by evaluating the kinetics of chlorophyll fluorescence changes after illumination (Reynolds et al. 2008; Claquin et al. 2021) which are characterized by several decay components; a fast component mainly driven by a redox equilibration of PQ with upstream redox centers in the milliseconds time range, and a slower decay component related to non-photochemical oxidation or reduction of PQ by stromal enzymes in the seconds time range (Gain et al. 2021). A post-illumination increase of chlorophyll fluorescence was observed only in shallow corals (Fig. 2C).

The capacity of electron driving towards PSI was finally evaluated through the re-reduction rate of P_{700} after its oxidation by a strong pulse of light in PSII-inhibited conditions (Nawrocki et al. 2019; Dang et al., 2019). Higher reducing rates were observed in shallow compared to mesophotic colonies (Table 2), confirming a higher reducing power capacity.

Impacts of light stress on photosynthetic traits

To compare the photosynthetic plasticity between shallow and mesophotic colonies, we next conducted a short light stress experiment with a freshly collected set of colonies. We set two light intensity conditions (natural light cycle with daily maximum PPFD 10 [LL] and 1500 [HL] µmol photons m^{-2} s^{-1}; Fig. S3) and exposed them for three days. No significant change in chlorophyll content was observed in shallow colonies at the end of both treatments. On the contrary, mesophotic colonies showed a ~65 % decrease when exposed to HL (Fig. 3A; P<0.05). We also observed an increase in the chl-c_2/a ratios in shallow and mesophotic colonies when exposed to HL (1.5 and 2.2-fold) (Fig. 3B; P<0.05 and P<0.001, respectively). Max E_O at the holobiont level decreased to 30% of the control when shallow colonies were exposed to low light conditions. In contrast, no change was observed during the HL treatment (Fig. 3C). In mesophotic colonies on the other hand, max Eo

was slightly less affected by the LL treatment, but it declined to 30 % at the end of the HL treatment (P<0.05; Fig. 3C). Respiratory rates did not change in both types of colonies (Fig. S4).
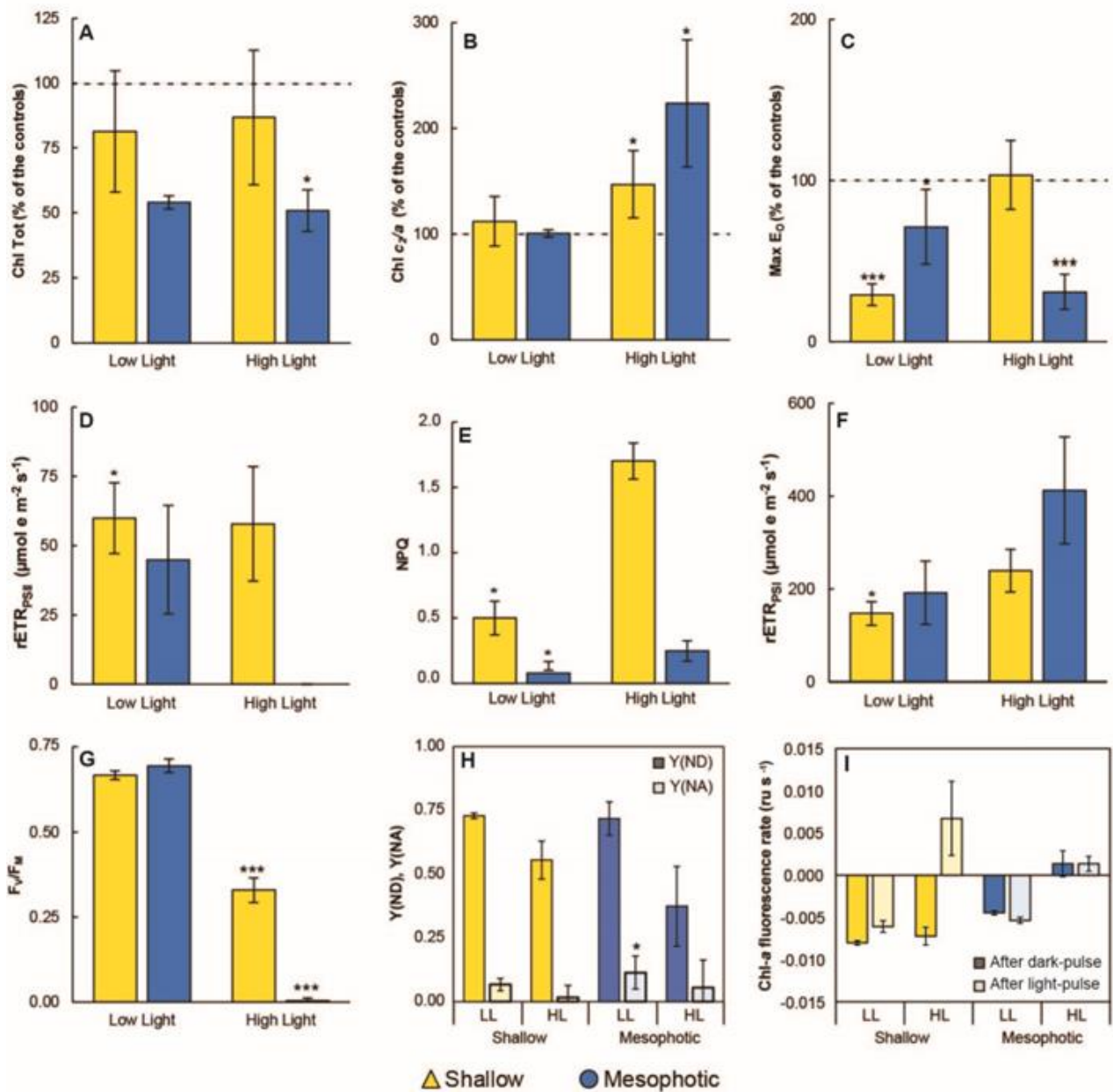
Figure 3 | Comparison of photosynthetic parameters in shallow and mesophotic colonies of *S. pistillata* exposed for 3 days to low and high PPFD. (A) Total chlorophyll content per coral surface area (in % of the controls). (B) Chlorophyll c_2/a ratio (in % of the controls). (C) Maximum gross photosynthesis (E_O) per coral surface area (in % of the controls). (D) Maximum relative electron transport rates of photosystem II (rETR$_{PSII}$). (E) Non-photochemical quenching of chlorophyll fluorescence (NPQ) measured at 1200 µmol photons m^{-2} s^{-1}. (F) Maximum relative electron transport rates of photosystem I

(rETR$_{PSI}$). (G) Maximum photochemical quantum yield (F$_V$/F$_M$). (H) PSI quantum yield of non-photochemical energy dissipation due to acceptor side limitation (YNA) or to donor side limitation (YND). (I) Post-illumination chlorophyll fluorescence rate. Chlorophyll fluorescence values were normalized to Fm, and the slope of the fluorescence recording in the post-illumination period was obtained between 1 and 5 s, from similar recording than Figure 2C. The rates are referred as those taken after the saturating pulse of light following the dark period (After dark-pulse), and as those rate after the saturating pulse of light following the period of 30 s of illumination (After light-pulse). Data are mean ± SD. Asterisks indicate statistically significant differences (*P<0.05; **P<0.01; ***P<0.001) between Days 0 and 3 for each treatment.

The LL treatment induced a decrease in rETR$_{PSI}$ and rETR$_{PSII}$ in both coral colonies (Fig 3D,F), which was consistent with the lower values observed for max Eo (Fig. 3C) and NPQ (Fig. 3E). The HL treatment had no impact on both rETR$_{PSI}$ and rETR$_{PSII}$ in shallow colonies. In contrast, the HL treatment resulted in a very low rETR$_{PSII}$ (P<0.05) but with a substantial rETR$_{PSI}$ remaining in mesophotic colonies (Fig. 3D,F). A ~40 % and >90 % decrease of F$_V$/F$_M$ was observed after the HL exposition in shallow and mesophotic colonies, respectively (P<0.001; Fig 3G). Max NPQ was not modified by the HL treatment in both colony types (Fig. 3E), but the LL exposition resulted in lower values for both colonies. Contrastingly, Y(NA) was not impacted by the light treatments in colonies from both depths but Y(ND) was increased due to LL in mesophotic colonies (P<0.05; Fig. 3H), most likely as a result of the impact on PSII activity.

Finally, we assessed the reducing power capacity by measuring the re-reduction rates of P$_{700}$ and we observed that it increased in both types of colony upon HL incubation but more prominently in mesophotic (P<0.01; by *ca*. 4 times) than in shallow colonies (P<0.01; by *ca*.1.5 times) (Fig. S5). In contrast, after the LL incubation, only shallow corals presented a marked decrease (P<0.001; by *ca*. 3 times). This effect was also evidenced in the post illumination chlorophyll fluorescence changes in shallow colonies, which after LL incubation lose its characteristic positive fluorescence increase, resembling the response of mesophotic corals in control conditions (Fig. 3I). In mesophotic colonies, the post illumination chlorophyll fluorescence did not change after the LL treatment, but it turned with a small positive change after the HL treatment due to the strong photoinhibition (Fig. 3I).

Discussion

The photosynthetic activity of *S. pistillata* colonies found at different depths was early recognized to be contrasting and influenced by light availability (Falkowski and Dubinsky, 1981). Comparatively, shallow colonies perform higher metabolic rates (Mass et al. 2007), but mesophotic colonies are able to thrive with a narrower light spectrum and lower light intensities (Mass et al. 2010). This photoacclimation capacity has its basis in a large set of features that have been described along decades, although the fine details of the photosynthetic electron transfer strategies have been barely described. Here, we analyzed shallow and mesophotic colonies to better understand their differences in photosynthetic strategies and the relevance of alternative photosynthetic electron pathways in response to changes in light intensity.

One main feature to take into consideration about *S. pistillata* residing in the Red Sea at shallow and mesophotic depths, is the genetic identity of its photosynthetic symbionts (Byler et al. 2013). Shallow colonies are populated by *S. microadriaticum* but by *Cladocopium sp*. in mesophotic colonies (Figure S2). This feature is present in other *Stylophora* species in the Red Sea (Arrigoni et al. 2016) and may become a relevant trait under changing environmental conditions, such as temperature and light, because they may conduct to different levels of sensitivity of the whole coral colony (Ezzat et al. 2017; Hennige et al. 2011; Hoadley et al. 2019; Voolstra et al. 2021). Despite the fact that *S. pistillata* is able to harbor two main symbiont species, transplantation experiments have shown that an adult colony contains only one main species and it hardly carry out a switch on symbiont genotype (Byler et al. 2013; Einbinder et al., 2016; Martinez et al. 2020). While opening more interesting questions, this also indicates that photoacclimation capacity to the different light environments must depend on the combination of host and symbiont genotype in this coral species. The condition of bearing a particular genotype, therefore, may not simply depend on average light availability at a particular depth, but it may also reflect the evolutionary history of *S. pistillata* in the characteristic light conditions of the Red Sea (Keshavmurthy et al. 2013).

The photosynthetic traits of the two main Symbiodiniaceae species harbored by *S. pistillata* were also contrasting (Table 1). The lower pigment content in *S. microadriaticum* was characteristic of its high light acclimation in shallow colonies, in comparison to *Cladocopium sp*. in mesophotic colonies (Dubinsky et al. 1984; Cohen and Dubinsky, 2015; Einbinder et al., 2016). Oxygen evolution capacity was also lower in mesophotic colonies (Figure 1B), suggesting differences in the photosynthetic unit content (Falkowski and Dubinsky, 1981; Hoogenboom et al. 2012). In our *S. pistillata* mesophotic corals the higher chlorophyll content together with the lower PSII activity,

indicate a relatively bigger antenna size, a phenomenon also observed in colonies found at 65 m depth (Einbinder et al., 2016). These features were indicative of classical photoacclimation strategies to low and high light conditions (Cardol et al. 2008; Ruban, 2009). Despite these differences, both photosynthetic symbionts in *S. pistillata* have shown comparable capacities to modulate their antenna size. Due to the northern position of the GoEA, in summer, when the light intensity is higher, mesophotic *S. pistillata* have shown smaller absorption cross sections (Einbinder et al., 2016). Shallow colonies, on the other hand, have shown capabilities to modify their chlorophyll abundance with respect to their photosynthetic reaction centers when found under different light regimes (Falkowski and Dubinsky, 1981). Antenna size modulation, thus, occurs in *S. pistillata* along the seasons following changes in light intensity. Contrastingly, the relative abundance of PSI with respect to PSII reaction centers have not been shown to vary in free living Symbiodiniaceae, such as *Symbiodinium* and *Breviolum*, when they are submitted to light changes (Hennige et al. 2009) or thermal stress (Dang et al. 2019). When in symbiosis, the content of reaction centers may show a similar absence of response, as no modifications in P_{700} content have been observed in shallow colonies after light changes (Falkowski and Dubinsky, 1981). Photosystem I roughly represent half of the total photosystems in many Symbiodiniaceae culture strains and in corals (Roberty et al. 2014; Dang et al., 2019; Vega de Luna et al. 2020). Downregulation or impairment to PSII reaction centers (photoinhibition) may account for transient variations in active photosystems stoichiometry, for example due to light conditions in summer (Winters et al. 2009).

We showed that *S. microadriaticum* in shallow colonies and *Cladocopium* sp. in mesophotic ones, have different capacities of PSII-driven electron transfer at saturating light intensities (Figure 1C), but similar capacity of PSI-driven electron transfer (Figure 1D; Table 2). This may have resulted from differences in the photosynthetic control of the Cytochrome b6f complex, which in mesophotic colonies could have caused a higher redox imbalance between the plastoquinone pool (PQ) at the PSII acceptor side, and the cytochrome c6 (Cytc6) at the PSI donor side (Figure 1F). A photosynthetic electron transfer imbalance in favour of PSI in both colony types indicated a comparable capacity to perform PSI-related cyclic electron flow (CEF), although evident at different light intensities (Figure 2B). This alternative electron flow has been shown to occur in *S. pistillata* and other shallow coral species (Hoogenboom et al. 2012; Vega de Luna et al. 2020). The activity of CEF is not limited by the Cytochrome b$_6$f complex (Alric, 2015), and it contributes to sustaining the trans-thylakoid proton gradient, which in turn allows ATP synthesis and induces NPQ (Miyake, 2010). The extent of NPQ is typically larger in shallow colonies in comparison to mesophotic colonies (Figure 1E; see for example Cohen and Dubinsky, 2015; Einbinder et al. 2016). In Symbiodiniaceae, this dissipation

mechanism comprises different factors from which a proton gradient-dependent mechanism is the main contributor under saturating light conditions (Hill et al. 2005; Kanazawa et al. 2014; Aihara et al. 2016). Although the molecular nature of this NPQ mechanism is not well understood in Symbiodiniaceae, it must largely rely on the dissipation capacity at the membrane embedded antenna chlorophyll *a*-chlorophyll c_2-peridinin protein complex (acpPC) (Kanazawa et al., 2014). It is typically more prominent in *Symbiodinium* than in *Cladocopium* or other Symbiodiniaceae genera (Reynolds et al. 2008), and it can be augmented after short temperature increases (Hill et al. 2005; Aihara et al. 2016).

When comparing the NPQ induction and the activity of both photosystems (Figure S6), we could not observe a linear relation for both coral colonies, as it has been shown for plants (Miyake et al. 2004). About half of NPQ extent already appeared when the relative activities of PSI and PSII remain proportional, but the second fraction of NPQ increase appeared concurrently with the relative increase of PSI to PSII activity in both colony types. This suggests that the fraction of energy dependent NPQ that was induced by CEF could be triggered through the same mechanism, although shallow colonies could contain a higher abundance of the quencher. Taking this into consideration, we hypothesize that CEF activity might have two different functions in the colonies of *S. pistillata*: it mainly contributes to the induction of NPQ in shallow colonies exposed to high light and would sustain ATP synthesis in mesophotic depths at lower light intensities. We also observed that both coral types had similar responses at performing linear electron transfer and oxygen evolution, indicating a comparable capacity for electron re-routing towards oxygen (Figure 2A; Table 2). This alternative electron pathway has not been found to correlate with tolerance to thermal stress (Dang et al. 2019), but it was described as the main mechanism of photoprotection in free living Symbiodiniaceae under high light conditions, where it may play a similar function as CEF (Roberty et al. 2014).

The redox state of the intersystem electron carriers was found to be in a more reduced state in shallow colonies after exposition to low light intensity or during dark acclimation, as evidenced by the post-illumination changes of chlorophyll *a* fluorescence (Figure 2C) and the higher re-reduction rate of $P_{700}+$ (Table 2). The non-photochemical reduction of the PQ pool in the darkness is a poorly understood phenomenon, but it may occur through the activity of an alternative type-II NAD(P)H-dehydrogenase (Ndh-2) of the chloro-respiratory pathway (Jans et al. 2008; Gain et al. 2021), which is present in Symbiodiniaceae (Roberty et al. 2014; Aihara et al. 2016). It has been proposed that the activation of the chloro-respiratory pathway in the darkness is induced by low oxygen levels, which

would be the cause of non-photochemical reduction of PQ in several coral species, having as a consequence the decrease of F_V/F_M in the range of minutes (Hill and Ralph, 2008; Reynolds et al. 2008; Claquin et al. 2021). Accordingly, during light to dark transitions, mitochondrial activity leads the coral tissue to hypoxia due to a limited diffusion of oxygen at the coral tissue boundary, as illustrated in the massive coral *Favia sp.*, where oxygen levels on its surface decreased to <2 % of air saturation after less than five minutes of darkness (Kühl et al. 1995). However, this hypoxia-induced model does not fit with our records where post-illumination chlorophyll fluorescence increase was observed in shallow colonies after five seconds of darkness (Figure 3C). The increase of chlorophyll fluorescence in the darkness in corals was initially shown to be induced by consecutive pulses of saturating light, and it was proposed to be genus specific in Symbiodiniaceae (Reynolds et al. 2008). However, it may rather be explained by a relatively lower capacity in *S. microadriaticum* in shallow colonies, and other high light acclimated Symbiodiniaceae species, to fix carbon at low light intensities (Ezzat et al. 2017). This would then reflect differences in the metabolic activity in the stroma, where the reducing power is found. In this respect, our shallow colonies showed higher respiration rates (Table 2 and Figure 1A) but the light-stimulated respiration rates were comparable with those of mesophotic colonies (Table 2). Alternatively, it can indicate differences at the level of the intersystem electron transfer components. It has been reported that mesophotic *S. pistillata* presented slower reoxidation of the plastoquinone at the acceptor side of PSII (Q_A) after a single pulse of saturating light (Einbinder et al., 2016), suggesting differences in the PQH_2 diffusion or in the activation of the Cytochrome b_6f complex with respect to shallow colonies. In other species, for example the coral *Acropora millepora* from the Great Barrier Reef, *Cladocopium sp.* maintained the redox state of the PQ pool constant even after hyperthermal stress induction, but it shifted to a more oxidized state after the photosynthetic efficiency was impaired (decrease of F_V/F_M) (Lutz et al. 2015). In this respect, no modifications in the active PQ pool content after light changes have been observed in plants, and it is postulated to be constant (Ksas et al. 2022). We do not rule out the existence of differences in the stoichiometric abundance of the photosynthetic components between *S. microadriaticum* and *Cladocopium sp.* in shallow and mesophotic colonies, respectively.

The higher P_{700} re-reduction rate in shallow colonies, with respect to mesophotic colonies (Table 2), can be used as evidence of the differences in the abundance of the photosynthetic electron carriers. This parameter is related to the capacity of the photosynthetic machinery to drive electrons towards PSI, and it might be influenced, at least during the measuring conditions, by the redox equilibration constant between Cytochrome b_6f complex, Cyt c_6 and P_{700} (Fan et al. 2016), and by the relative abundance of these components. This suggests that shallow colonies harbor a bigger pool of

intersystem electron carriers in comparison to mesophotic colonies, and that their PQ pool is more involved in non-photochemical reactions in the darkness and after illumination at low light intensity. These features would function as a strategy to face larger fluctuations of light in the shallow waters, promoting the conditions to sustain CEF at the beginning of illumination (Nawrocki et al. 2019), that in turn would activate the energy dependent NPQ dissipation mechanism.

We have shown the differences in AEFs prevailing in both shallow and mesophotic coral types. These AEFs are considered as important photoprotective mechanisms of the photosynthetic electron transfer chain under strong light conditions in green plants (Miyake, 2010; Chaux et al. 2015). Because of this, we evaluated the impact of changing the light regime on *S. pistillata* colonies. Three days after exposure to high light, the pigment content was diminished in mesophotic colonies (Figure 3A and B) but the ratio Chl-c_2/a was increased in both colony types, reflecting a decrease in the abundance of the peridinin-chlorophyll *a*-protein complex (PCP) in comparison to the acpPC in both colony types. This would reflect a differential degradation of the antennas in order to maintain the main light energy dissipation mechanism in both colony types upon high light conditions, as previously observed in other coral species (Hill et al. 2005). Mesophotic coral colonies displayed severe photoinhibition, reflected by the decrease in F_V/F_M (Figure 3G) and in the photosynthetic activity of oxygen evolution (Figure 3C). These colonies were unable to develop further changes in NPQ (Figure 3E), but surprisingly their PSI was maintained highly active (Figure 3F). Interestingly, this high light persistent PSI activity was accompanied by a decrease in the energy dissipation due to donor side limitation (Figure 3H), thus indicating that its activity involves CEF. It has been reported from cultures of the Symbiodiniaceae strain CS-156 isolated from the Hawaiian coral *Montipora verrucosa*, that after exposing the algae to bleaching conditions (i.e., high temperature and high light), it developed a non-photochemical quenching mechanism that diverted the energy trapped by PSII antenna towards PSI (Slavov et al. 2016). This so-called "spillover" mechanism was proposed to be based on the high efficiency of $P_{700}+$ to quench light energy, a process described to be present in several algal groups (Shimakawa and Miyake, 2018). The recent description of a low-resolution PSI-LHC complex structure of *Breviolum minutum*, proposed the possibility that this photosystem was the site of xanthophyll-dependent energy dissipation (Kato et al. 2020). It was found that the PSI light harvesting antenna associated diadinoxanthin as the second most abundant pigment after chlorophyll *a*, and it was converted to diatoxanthin after high light treatment (Kato et al. 2020).

The low light regime on the other hand, did not modify the pigment content or F_V/F_M (Figure 3A, B and G), but it induced a decrease in the photosynthetic capacity of both shallow and mesophotic

colonies (Figure 3C, D and F). A remarkable impact was observed in shallow colonies as a decrease in the NPQ extent and disappearance of the post-illumination chlorophyll fluorescence increase (Figure 3E and I), which then resembled those of the mesophotic colonies. The decrease of NPQ upon low light has been observed before (Cohen and Dubinsky, 2015), and it may reflect an increase of the light absorption capacity, as described for plants, where NPQ can be chemically inhibited (Osmond et al. 2022). This phenomenon is indicative of a fast acclimation to low light regime in shallow colonies of *S. pistillata*. Ultimately, the decrease of the $P_{700}+$ re-reduction rate in shallow colonies at low light treatment, indicated an overall change in the capacity of the photosynthetic machinery to withstand low light regimes.

We conclude that the photosynthetic strategies in shallow and mesophotic colonies of *S. pistillata* from the GoEA include the use of photosynthetic alternative electron pathways. Shallow colonies are able to display a higher NPQ capacity, but both colony types showed the enhanced use of Mehler-like reaction and CEF at saturating light intensities. Shallow colonies showed a higher abundance of the intersystem electron carriers, and it was accompanied by the involvement of the PQ pool with stromal reactions at low light intensities. However, these features were less evident after shallow corals were maintained for three days in low light conditions. In mesophotic colonies, the limited capacity for light energy dissipation and the lower efficiency to recycle the reducing power of the stroma towards the photosynthetic machinery, could have made them more susceptible during the high light treatment.

Acknowledgements

References

Aihara Y., Takahashi S. & Minagawa J. (2016) Heat induction of cyclic electron flow around photosystem I in the symbiotic dinoflagellate *Symbiodinium*. *Plant Physiology* **171**, 522–529.

Alric J. (2015) The plastoquinone pool, poised for cyclic electron flow? *Frontiers in plant science* **6**, 540.

Arrigoni R., Benzoni F., Terraneo T.I., Caragnano A. & Berumen M.L. (2016) Recent origin and semi-permeable species boundaries in the scleractinian coral genus *Stylophora* from the Red Sea. *Scientific Reports* **6** (1), 1-13.

Byler K.A., Carmi-Veal M., Fine M. & Goulet T.L. (2013) Multiple symbiont acquisition strategies as an adaptive mechanism in the coral *Stylophora pistillata*. *PLoS ONE* **8**, e59596.

Cardol P., Bailleul B., Rappaport F., Derelle E., Béal D., Breyton C., … Finazzi G. (2008) An original adaptation of photosynthesis in the marine green alga *Ostreococcus*. *Proceedings of the National Academy of Sciences* **105**, 7881–7886.

Chang S.S., Prézelin B.B. & Trench R.K. (1983) Mechanisms of photoadaptation in three strains of the symbiotic dinoflagellate *Symbiodinium microadriaticum*. *Marine Biology* **76**, 219–229.

Chaux F., Peltier G. & Johnson X. (2015) A security network in PSI photoprotection: Regulation of photosynthetic control, NPQ and O2 photoreduction by cyclic electron flow. *Frontiers in Plant Science* **6**, 875.

Claquin P., Rene-Trouillefou M., Lopez P.J., Japaud A., Bouchon-Navaro Y., Cordonnier S. & Bouchon C. (2021) Singular physiological behavior of the scleractinian coral *Porites astreoides* in the dark phase. *Coral Reefs* **40**, 139–150.

Cohen I. & Dubinsky Z. (2015) Long term photoacclimation responses of the coral *Stylophora pistillata* to reciprocal deep to shallow transplantation: Photosynthesis and calcification. *Frontiers in Marine Science* **2**, 45.

Comeau S., Cornwall C.E., DeCarlo T.M., Doo S.S., Carpenter R.C. & McCulloch M.T. (2019) Resistance to ocean acidification in coral reef taxa is not gained by acclimatization. *Nature Climate Change* **9**, 477–483.

Dang K. Van, Pierangelini M., Roberty S. & Cardol P. (2019) Alternative photosynthetic electron transfers and bleaching phenotypes upon acute heat stress in *Symbiodinium* and *Breviolum* spp. (Symbiodiniaceae) in culture. *Frontiers in Marine Science* **6**, 656.

Dishon G., Dubinsky Z., Fine M. & Iluz D. (2012) Underwater light field patterns in subtropical coastal waters: A case study from the Gulf of Eilat (Aqaba). *Israel Journal of Plant Sciences* **60**, 265–275.

Dubinsky Z., Falkowski P.G., Porter J.W. & Muscatine L. (1984) Absorption and utilization of radiant Energy by light- and shade-adapted colonies of the hermatypic coral *Stylophora pistillata*. *Proceedings of the Royal Society B: Biological Sciences* **222**, 203–214.

Dubinsky Z. & Stambler N. (2009) Photoacclimation processes in phytoplankton: Mechanisms, consequences, and applications. *Aquatic Microbial Ecology* **56**, 163–176.

Einbinder S., Gruber D.F., Salomon E., Liran O., Keren N. & Tchernov D. (2016) Novel adaptive photosynthetic characteristics of mesophotic symbiotic microalgae within the reef-building coral, *Stylophora pistillata*. *Frontiers in Marine Science* **3**, 195.

Einbinder S., Mass T., Brokovich E., Dubinsky Z., Erez J. & Tchernov D. (2009) Changes in morphology and diet of the coral *Stylophora pistillata* along a depth gradient. *Marine Ecology Progress Series* **381**, 167–174.

Eyal G., Tamir R., Kramer N., Eyal-Shaham L. & Loya Y. (2019) The Red Sea: Israel. In *Mesophotic Coral Ecosystems*. pp. 199–214. Springer Nature Switzerland.

Ezzat L., Fine M., Maguer J.F., Grover R. & Ferrier-Pagès C. (2017) Carbon and nitrogen acquisition in shallow and deep holobionts of the scleractinian coral *S. pistillata*. *Frontiers in Marine Science* **4**, 102.

Falkowski P.G. & LaRoche J. (1991) Acclimation to spectral irradiance in algae. *Journal of Phycology* **27**, 8–14.

Falkowski P.G. & Dubinsky Z. (1981) Light-shade adaptation of *Stylophora pistillata*, a hermatypic coral from the Gulf of Eilat. *Nature* **289**, 172–174.

Fan D.Y., Fitzpatrick D., Oguchi R., Ma W., Kou J. & Chow W.S. (2016) Obstacles in the quantification of the cyclic electron flux around Photosystem I in leaves of C3 plants. *Photosynthesis Research* **129**, 239–251.

Gain G., Vega de Luna F., Cordoba J., Perez E., Degand H., Morsomme P., … Cardol P. (2021) Trophic state alters the mechanism whereby energetic coupling between photosynthesis and respiration occurs in *Euglena gracilis*. *New Phytologist* **232**, 1603–1617.

Hennige S.J., Suggett D.J., Warner M.E., McDougall K.E. & Smith D.J. (2009) Photobiology of *Symbiodinium* revisited: Bio-physical and bio-optical signatures. *Coral Reefs* **28**, 179–195.

Hennige S.J., McGinley M.P., Grottoli A.G. & Warner M.E. (2011) Photoinhibition of *Symbiodinium* spp. within the reef corals *Montastraea faveolata* and *Porites astreoides*: Implications for coral bleaching. *Marine Biology* **158**, 2515–2526.

Hill R., Frankart C. & Ralph P.J. (2005) Impact of bleaching conditions on the components of non-photochemical quenching in the zooxanthellae of a coral. *Journal of Experimental Marine Biology and Ecology* **322**, 83–92.

Hill R. & Ralph P.J. (2008) Dark-induced reduction of the plastoquinone pool in zooxanthellae of scleractinian corals and implications for measurements of chlorophyll a fluorescence. *Symbiosis* **46**, 45–56.

Hoadley K.D., Lewis A.M., Wham D.C., Pettay D.T., Grasso C., Smith R., … Warner M.E. (2019) Host–symbiont combinations dictate the photo-physiological response of reef-building corals to thermal stress. *Scientific Reports* **9** (1), 1-15.

Holstein D.M., Paris C.B., Vaz A.C. & Smith T.B. (2016) Modeling vertical coral connectivity and mesophotic refugia. *Coral Reefs* **35**, 23–37.

Hoogenboom M.O., Campbell D.A., Beraud E., DeZeeuw K. & Ferrier-Pagès C. (2012) Effects of light, food availability and temperature stress on the function of photosystem II and photosystem I of coral symbionts. *PLoS ONE* **7**, e30167.

Hughes T.P., Barnes M.L., Bellwood D.R., Cinner J.E., Cumming G.S., Jackson J.B.C., … Scheffer M. (2017) Coral reefs in the Anthropocene. *Nature* **546**, 82–90.

Hughes T.P., Anderson K.D., Connolly S.R., Heron S.F., Kerry J.T., Lough J.M., … Wilson S.K. (2018) Spatial and temporal patterns of mass bleaching of corals in the Anthropocene. *Science* **359**, 1–4.

Hume B.C.C., Smith E.G., Ziegler M., Warrington H.J.M., Burt J.A., LaJeunesse T.C., … Voolstra C.R. (2019) SymPortal: A novel analytical framework and platform for coral algal symbiont next-generation sequencing ITS2 profiling. *Molecular Ecology Resources* **19**, 1063–1080.

Hume B.C.C., Ziegler M., Poulain J., Pochon X., Romac S., Boissin E., … Voolstra C.R. (2018) An improved primer set and amplification protocol with increased specificity and sensitivity targeting the *Symbiodinium* ITS2 region. *PeerJ* **6**, e4816.

Iglesias-Prieto R. & Trench R.K. (1994) Acclimation and adaptation to irradiance in symbiotic dinoflagellates. I. Responses of the photosynthetic unit to changes in photon flux density. *Marine Ecology Progress Series* **113**, 163–175.

Jans F., Mignolet E., Houyoux P.-A., Cardol P., Ghysels B., Cuiné S., … Franck F. (2008) A type II NAD(P)H dehydrogenase mediates light-independent plastoquinone reduction in the chloroplast of *Chlamydomonas*. *Proceedings of the National Academy of Sciences* **105**, 20546.

Kanazawa A., Blanchard G.J., Szabó M., Ralph P.J. & Kramer D.M. (2014) The site of regulation of light capture in *Symbiodinium*: Does the peridinin-chlorophyll a-protein detach to regulate light capture? *Biochimica et Biophysica Acta - Bioenergetics* **1837**, 1227–1234.

Kato H., Tokutsu R., Kubota-Kawai H., Burton-Smith R.N., Kim E. & Minagawa J. (2020) Characterization of a giant PSI supercomplex in the symbiotic dinoflagellate symbiodiniaceae. *Plant Physiology* **183**, 1725–1734.

Keshavmurthy S., Yang S.Y., Alamaru A., Chuang Y.Y., Pichon M., Obura D., … Chen C.A. (2013) DNA barcoding reveals the coral "laboratory-rat", *Stylophora pistillata* encompasses multiple identities. *Scientific Reports* **3** (1), 7.

Klughammer C. & Schreiber U. (2008) Saturation Pulse method for assessment of energy conversion in PS I. *PAM Application Notes* **1**, 11–14.

Ksas B., Alric J., Caffarri S. & Havaux M. (2022) Plastoquinone homeostasis in plant acclimation to light intensity. *Photosynthesis Research* **152**, 43–54.

Kühl M., Cohen Y., Dalsgaard T., Jorgensen B.B. & Revsbech N.P. (1995) Microenvironment and photosynthesis of zooxanthellae in scleractinian corals studied with microsensors for O2, pH and light. *Marine Ecology Progress Series* **117**, 159–172.

LaJeunesse T.C., Parkinson J.E., Gabrielson P.W., Jeong H.J., Reimer J.D., Voolstra C.R. & Santos S.R. (2018) Systematic revision of Symbiodiniaceae highlights the antiquity and diversity of coral endosymbionts. *Current Biology* **28**, 2570-2580.

Laverick J.H., Piango S., Andradi-Brown D.A., Exton D.A., Bongaerts P., Bridge T.C.L., … Rogers A.D. (2018) To what extent do mesophotic coral ecosystems and shallow reefs share species of conservation interest? A systematic review. *Environmental Evidence* **7**, 1–13.

Lesser M.P., Slattery M. & Mobley C.D. (2018) Biodiversity and functional ecology of mesophotic coral Reefs. *Annual Review of Ecology, Evolution, and Systematics* **49**, 49–71.

Lutz A., Raina J.B., Motti C.A., Miller D.J. & Van Oppen M.J.H. (2015) Host coenzyme Q redox state is an early biomarker of thermal stress in the coral *Acropora millepora*. *PLoS ONE* **10**, e0139290.

Martinez S., Kolodny Y., Shemesh E., Scucchia F., Nevo R., Levin-Zaidman S., … Mass T. (2020) Energy sources of the depth-generalist mixotrophic coral *Stylophora pistillata*. *Frontiers in Marine Science* **7**, 566663.

Mass T., Kine D.I., Roopin M., Veal C.J., Cohen S., Iluz D. & Levy O. (2010) The spectral quality of light is a key driver of photosynthesis and photoadaptation in *Stylophora pistillata* colonies from different depths in the Red Sea. *Journal of Experimental Biology* **213**, 4084–4091.

Mass T., Einbinder S., Brokovich E., Shashar N., Vago R., Erez J. & Dubinsky Z. (2007) Photoacclimation of *Stylophora pistillata* to light extremes: Metabolism and calcification. *Marine Ecology Progress Series* **334**, 93–102.

Miyake C. (2010) Alternative electron flows (water-water cycle and cyclic electron flow around PSI) in photosynthesis: Molecular mechanisms and physiological functions. *Plant and Cell Physiology* **51**, 1951–1963.

Miyake C., Shinzaki Y., Miyata M. & Tomizawa K.-I. (2004) *Enhancement of Cyclic Electron Flow Around PSI at High Light and its Contribution to the Induction of Non-Photochemical Quenching of Chl Fluorescence in Intact Leaves of Tobacco Plants. Plant and Cell Physiology* **45** (10), 1426-1433.

Nawrocki W.J., Bailleul B., Cardol P., Rappaport F., Wollman F.A. & Joliot P. (2019) Maximal cyclic electron flow rate is independent of PGRL1 in *Chlamydomonas*. *Biochimica et Biophysica Acta - Bioenergetics* **1860**, 425–432.

Nir O., Gruber D.F., Shemesh E., Glasser E. & Tchernov D. (2014) Seasonal mesophotic coral bleaching of *Stylophora pistillata* in the northern Red Sea. *PLoS ONE* **9**, e84968.

Osmond C.B., Chow W.S. & Robinson S.A. (2022) Inhibition of non-photochemical quenching increases functional absorption cross-section of photosystem II as excitation from closed reaction centres is transferred to open centres, facilitating earlier light saturation of photosynthetic electron transport. *Functional Plant Biology* **49**, 463–482.

Porter J.W., Muscatine L., Dubinsky Z. & Falkowski P.G. (1984) Primary production and photoadaptation in light- and shade-adapted colonies of the symbiotic coral, *Stylophora pistillata*. *Proceedings of the Royal Society B: Biological Sciences* **222**, 161–180.

Reynolds J.M., Bruns B.U., Fitt W.K. & Schmidt G.W. (2008) Enhanced photoprotection pathways in symbiotic dinoflagellates of shallow-water corals and other cnidarians. *Proceedings of the National Academy of Sciences* **105**, 13674–13678.

Ritchie R.J. (2006) Consistent sets of spectrophotometric chlorophyll equations for acetone, methanol and ethanol solvents. *Photosynthesis Research* **89**, 27–41.

Roberty S., Bailleul B., Berne N., Franck F. & Cardol P. (2014) PSI Mehler reaction is the main alternative photosynthetic electron pathway in *Symbiodinium* sp., symbiotic dinoflagellates of cnidarians. *New Phytologist* **204**, 81–91.

Roberty S., & Plumier J. C. (2022). Bleaching physiology: who's the 'weakest link'—host vs. symbiont? *Emerging Topics in Life Sciences*, **6**(1), 17-32.

Roberty, S., Beraud E., Grover R. & Ferrier-Pagès C. (2020) Coral productivity is co-limited by bicarbonate and ammonium availability. *Microorganisms* **8,** 640.

Ruban A. V. (2009) Plants in light. *Communicative and Integrative Biology* **2**, 50–55.

Scucchia F., Malik A., Putnam H.M. & Mass T. (2021) Genetic and physiological traits conferring tolerance to ocean acidification in mesophotic corals. *Global Change Biology* **27**, 5276–5294.

Shimakawa G. & Miyake C. (2018) Oxidation of P700 ensures robust photosynthesis. *Frontiers in Plant Science* **871**.

Shlesinger T., Grinblat M., Rapuano H., Amit T. & Loya Y. (2018) Can mesophotic reefs replenish shallow reefs? Reduced coral reproductive performance casts a doubt. *Ecology* **99**, 421–437.

Slavov C., Schrameyer V., Reus M., Ralph P.J., Hill R., Büchel C., … Holzwarth A.R. (2016) "Super-quenching" state protects *Symbiodinium* from thermal stress - Implications for coral bleaching. *Biochimica et Biophysica Acta - Bioenergetics* **1857**, 840–847.

Stambler N. (2006) Light and picophytoplankton in the Gulf of Eilat (Aqaba). *Journal of Geophysical Research: Oceans* **111**.

Stimson J. & Kinzie R.A. (1991) The temporal pattern and rate of release of zooxanthellae from the reef coral *Pocillopora damicornis* under nitrogen enrichment and control conditions. *Journal of Experimental Marine Biology and Ecology* **153**, 63–74.

Suggett D.J., Warner M.E. & Leggat W. (2017) Symbiotic dinoflagellate functional diversity mediates coral survival under ecological crisis. *Trends in Ecology and Evolution* **32**, 735–745.

Tamir R., Eyal G., Kramer N., Laverick J.H. & Loya Y. (2019) Light environment drives the shallow-to-mesophotic coral community transition. *Ecosphere* **10**, e02839.

Torda G., Donelson J.M., Aranda M., Barshis D.J., Bay L., Berumen M.L., … Munday P.L. (2017) Rapid adaptive responses to climate change in corals. *Nature Climate Change* **7**, 627–636.

Van Oppen M.J.H., Bongaerts P., Underwood J.N., Peplow L.M. & Cooper T.F. (2011) The role of deep reefs in shallow reef recovery: An assessment of vertical connectivity in a brooding coral from west and east Australia. *Molecular Ecology* **20**, 1647–1660.

Vega de Luna F., Córdoba-Granados J.J., Dang K. Van, Roberty S. & Cardol P. (2020) In vivo assessment of mitochondrial respiratory alternative oxidase activity and cyclic electron flow around photosystem I on small coral fragments. *Scientific Reports* **10** (1). 1-13.

Vega De Luna F., Dang K. Van, Cardol M., Roberty S. & Cardol P. (2019) Photosynthetic capacity of the endosymbiotic dinoflagellate *Cladocopium* sp. is preserved during digestion of its jellyfish host *Mastigias papua* by the anemone *Entacmaea medusivora*. *FEMS Microbiology Ecology* **95**, 1–7.

Voolstra C.R., Valenzuela J.J., Turkarslan S., Cárdenas A., Hume B.C.C., Perna G., … Barshis D.J. (2021) Contrasting heat stress response patterns of coral holobionts across the Red Sea suggest distinct mechanisms of thermal tolerance. *Molecular Ecology* **30**, 4466–4480.

Webb W.L., Newton M. & Starr D. (1974) Carbon Dioxide Exchange of *Alnus rubra*. *Oecologia* **17**(4), 281-291.

Weber M.X. & Medina M. (2012) The Role of microalgal symbionts (*Symbiodinium*) in holobiont physiology. In *Advances in Botanical Research*. pp. 119–140. Academic Press Inc.

Winters G., Beer S., Ben Zvi B., Brickner I. & Loya Y. (2009) Spatial and temporal photoacclimation of *Stylophora pistillata*: Zooxanthella size, pigmentation, location and clade. *Marine Ecology Progress Series* **384**, 107–119.

Supplementary Material

Figure S1 | *S. pistillata* colonies from shallow (left) and deep water (right).
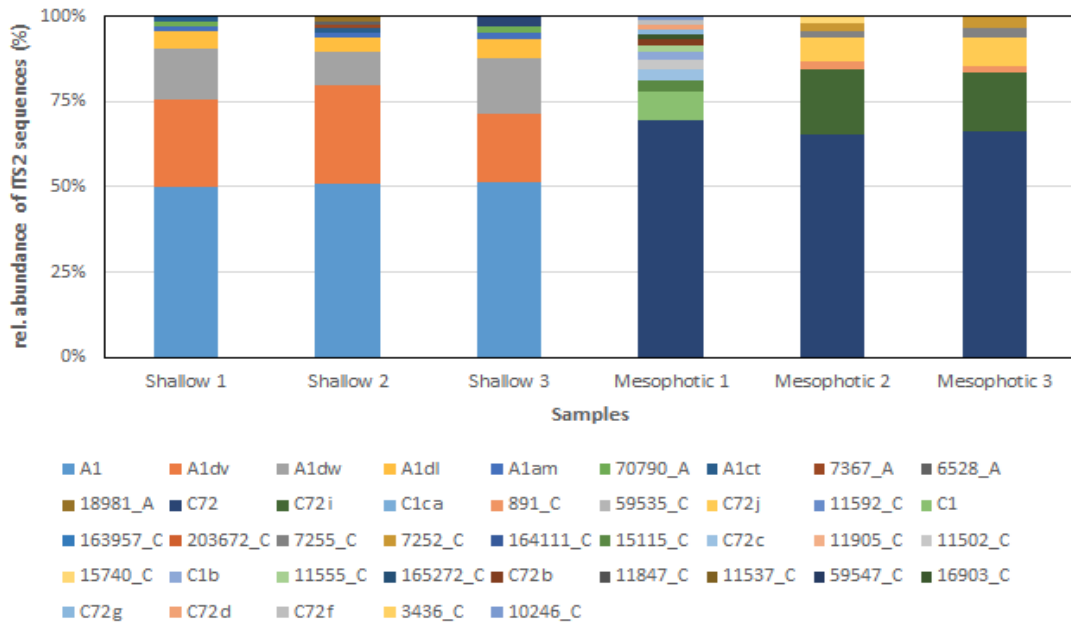
Figure S2 | Diversity of Symbiodiniaceae ITS2 sequences in shallow and deep colonies of *S. pistillata*. Recovered sequences representing less than 1% of the total abundance were excluded.
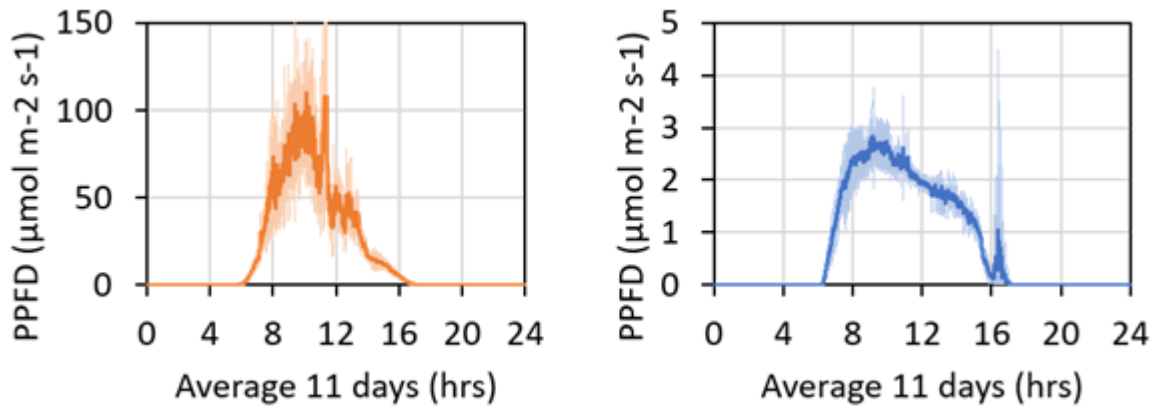
Figure S3 | Photosynthetic photon flux densities at which shallow (left) and mesophotic (right) coral colonies were maintained. The average of 11 consecutive days is shown and its standard deviation. Data acquisition was done every five seconds for the duration of the experiment.
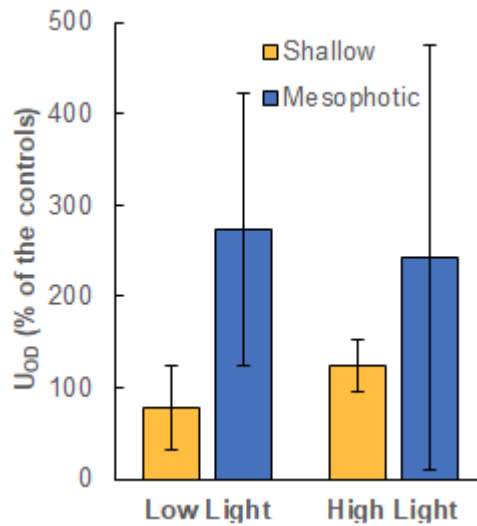
Figure S4 | Respiration rates per surface area of shallow and deep colonies of *S. pistillata*, after 3 days of treatment to low and high PPFD. Data are expressed as mean percentages ± SD of the control values (Day 0) (n=3). No statistical differences were found between Days 0 and 3 for each treatment.
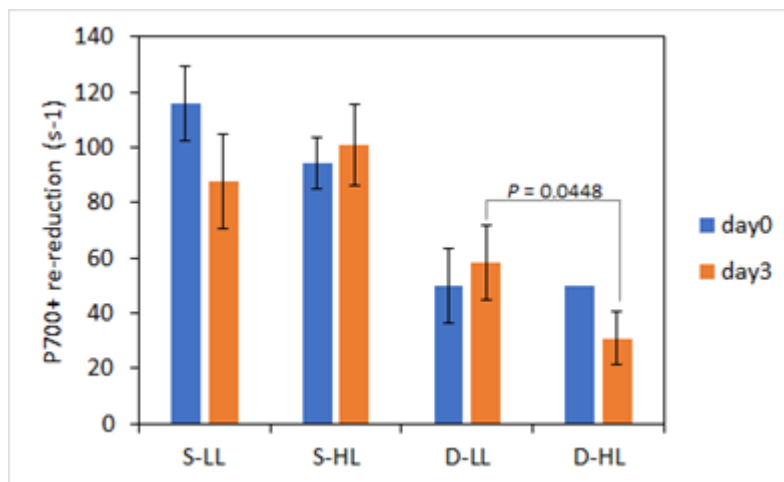
Figure S5 | Re-reduction rates of P$_{700}^+$ after 30 seconds of low PPFD (40 μmol photons m^{-2} s^{-1} and in the absence of DCMU). Data are expressed as mean percentages ± SD, (n=3).
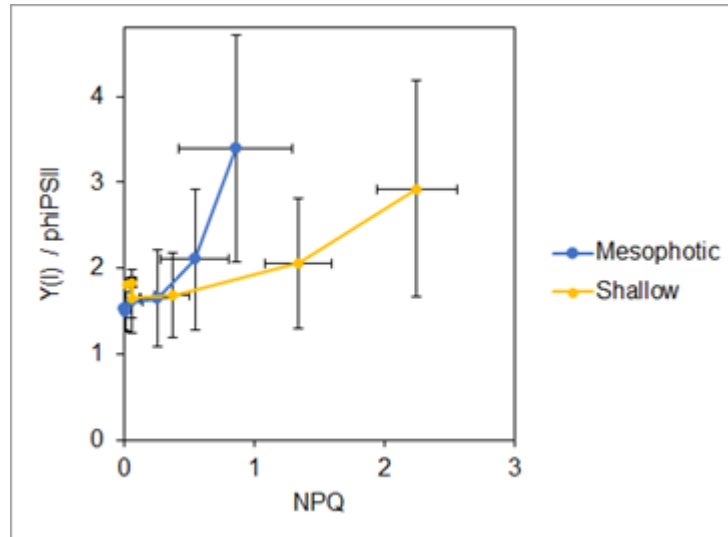
Figure S6 | Comparison between the PSI/PSII effective quantum yield and the induction of NPQ. Data are expressed as mean percentages ± SD.

Table S1| Pigment content per coral surface area

	Shallow	Mesophotic
Chl-a ($\mu g\ cm^{-2}$)	2.62 ± 0.71	2.50 ± 0.53
Chl-c_2 ($\mu g\ cm^{-2}$)	0.56 ± 0.15	0.52 ± 0.21
Peridinin ($\mu g\ cm^{-2}$)	1.66 ± 0.57	1.30 ± 0.32
Diadinoxanthin ($\mu g\ cm^{-2}$)	0.41 ± 0.14	0.31 ± 0.08
β-carotene ($\mu g\ cm^{-2}$)	0.03 ± 0.01	0.03 ± 0.01

CHAPTER 6   General discussion and conclusions

Spectroscopic methods were used to inform on the photosynthetic electron transfer activity prevailing in Symbiodiniaceae under a variety of conditions, during and after digestion of its jellyfish host by an aposymbiotic anemone predator (**Chapter 3**), during fragmentation of coral colonies (**Chapter 4**) and during the analysis of coral fragments collected from a reef (**Chapter 5**). Different aspects were analysed during these studies, and as a whole, they have provided new details on the features of the algal symbiont hosted by cnidarians. This general discussion is sorted by some aspects that were conclusive during this work.

Ecological role of the resistance of Symbiodiniaceae to digestion

Different studies have shown that Symbiodiniaceae is able to resist digestion by other animals (**Muller-Parker, 1984; Bachman and Muller-Parker, 2007; Castro-Sanguino and Sánchez, 2012**). This peculiar characteristic is also present in *Chlorella* harboured by the anemone *Anthopleura elegantissima*, when eaten by the sea star *Dermasterias imbricata* (**Bachman and Muller-Parker, 2007**). In those investigations, the resistance of Symbiodiniaceae to digestion and the dispersion by the animal predator is considered to have an ecological role in the maintenance of the algal reservoir in their communities. We also proposed that the survival of *Cladocopium sp.*, the algal symbiont of *M. papua*, to digestion could accomplish the same ecological role. This could be due to the particular conditions of the marine lakes and the conditions where *M. papua* achieve its life cycle. *M. papua* is not only found in marine lakes but also in some regions of the open ocean, although the peculiarities of its life cycle in these regions is not well described. Another consideration we can indicate, is the special conditions of culturing that *Cladocopium* species require (**Wang et al., 2021**), they have not been successfully cultivated in laboratories around the world, indicating the some factors may be present in the marine lake that favour its persistence to participate in the symbiotic association with *M. papua*.

In other studies, Symbiodiniaceae expelled from cnidarians during bleaching conditions were also found to be viable and photosynthetically active (**Ralph et al., 2001**). The capacity to acquire and fix inorganic carbon has been observed in freshly extracted Symbiodiniaceae from corals (**Streamer et al., 1993; Goiran et al., 1996**) and from the giant clam *Tridacna gigas* (Bivalvia, Mollusca) (**Leggat et al., 1999**). The fact that here we could record the photosynthetic activity along the process of digestion (**Chapter 3, Figure 2**), indicated that the physico-chemical conditions within the gastric cavity of the anemone allowed the transition from symbiotic to free living state.

When the algae were released from its host, we could also observe a difference in the spectrum of the light-induced absorption changes (also called electrochromic shift or ECS; **Chapter 3, Figure 4; Annex B, Figure 1**) above 540 nm, in proportion to the changes at 510 nm, the maximum positive peak. These changes are in accordance with other publications of ECS spectrum from these algae in free-living conditions (**Roberty et al., 2014**) and in symbiosis with corals (**Chapter 4, Figure 6**). Although no information is available on the causes of these differences, we can anticipate that this phenomenon can be related to morphological and functional changes in the photosynthetic machinery, such as the pigment array and content, the antenna type abundance or the distribution of the thylakoid membranes (**Bailleul et al., 2010**). The fact that we could observe these changes in ECS spectra when *Cladocopium* changed its life stage form, form symbiosis to free-living, and between free-living cultures of *Symbiodinium microadriaticum* and in symbiosis with *S. pistillata*, suggest that it is the phenomenon, although further experimental evidence might be conducted.

This can serve as another photosynthetic-related trait in *in vivo* studies of the adjustments that Symbiodiniaceae algae present between the free-living form and the one in symbiosis. The transition from symbiosis to free living is a process much less studied than the symbiosis forming phenomenon, however, both are clearly marked by changes in the osmotic environment (**Goiran et al., 1997; Mayfield and Gates, 2007**). These differences may be behind a rearrangement of the thylakoid structure, and constitute a good point to address the research.

Perspectives on a new strategy for the study of photosynthesis in corals

Different aspects of the photosynthetic activity were then explored in a different cnidarian model species, for which some considerations were taken. The photosynthetic parameters we obtained from corals could be done thanks to fragmentation (**Chapter 4**). Despite this being frequent in nature, it can be reasonably considered as a stressing condition. Coral fragments survival to these events is well known, and it is used as a propagation technique because their growth rate is usually higher than the one of non-fragmented corals (**Forsman et al., 2015; Barton et al., 2017**). We showed that coral fragments of *S. pistillata* were suitable for measurements and retained their photosynthetic capacity (**Chapter 4, Figure 1**). This strategy has the potential to reveal the contribution of the photosynthetic activity to the changes of growth rate due to fragmentation.

A comparison of some physiological parameters from recently obtained fragments with those reported in previous publications, indicated that they can represent the physiology of the coral colony (**Chapter 4, Figure 2**). With this as a starting point, we were able to monitor the redox state of the primary electron donor of PSI (**Chapter 4, Figure 1 c and f, and Figure 5**). Other instrumentation strategies have been used to study intact corals in *in vivo* conditions and in a non-intrusive manner.

For example with the use of submersible fluorometers or the use of light reflectance to deduce absorbance changes (**Szabó et al., 2017**). The advantages of our strategy include the possibility of using small fractions of corals, the acquisition of repeated observations on the same colony or coral branches, the use of a variety of metabolic inhibitors, and the feasibility of using different analytical instruments.

The photosynthetic activity of Symbiodiniaceae in symbiosis

The photosynthetic activity in symbiotic cnidarians is a process relying on the whole functioning of the holobiont, and as such, the activity of its algal symbionts under changing environmental conditions is better evaluated in symbiosis. We assessed different photosynthetic parameters by the use of light-response curves on coral fragments (**Chapter 4, Figure 3**). At saturating light conditions, where the light energy fluxes surpassed the CBB capacity, and we could compare different photosynthetic traits related to its regulation.

We can indicate, based on our results, that *S. pistillata* maintained in aquarium conditions and harbouring *S. microadriaticum*, did not make an evident use of WWC at saturating light intensities (**Chapter 4, Figure 3c**). This contrasted with cultured Symbiodiniaceae, including *Symbiodinium* species, that are able to reroute up to 50 % of photosynthetically-derived electrons to O_2 reduction through WWC (**Roberty et al., 2014; Dang et al., 2019**). The source of this discrepancy is not clear, mainly for the lack of information of different coral species, but it can be mentioned that it should rely on the metabolic differences experienced by the algae in each of both conditions. The activity of the WWC in cultured algae is seen as a photoprotection mechanism at saturating light intensities, while the corals maintained in aquarium conditions are able to make use of NPQ to dissipate light energy. While this must be taken carefully, we may also consider that both conditions might consist of optical conditions, and no stressing conditions should be displayed. It is also critical the consideration of the light conditions experienced by the alga in free-living and in symbiosis conditions. While the free-living form is subjected to the diffusion of light through the column of water, the algae immersed within the coral tissue may experience an enhanced light scattering and diffusion through the skeleton (**Enriquez et al., 2017; Kramer et al., 2022**). These differences, together with the biochemical detection of the molecular players of these alternative pathways, have the potential to be further explored.

Bleaching conditions (i.e. elevated temperature and high light intensity) leading to an increased oxidative stress, have been shown to lack a corresponding increase of the antioxidative system capacity, indicating that the Mehler reaction activity in Symbiodiniaceae was surpassed (**Roberty et al., 2015**). In the last decades there has been an increasing interest in the monitoring of ROS dynamics

in *in vivo* conditions along the holobiont surface (**Saragosti et al., 2010; Ousley et al., 2022**). These might include the proper determination of the light-dependent oxygen consuming pathways, such as the WWC, so the coupled monitoring of these features in corals might be a power strategy.

Physiological aspects of the photosynthetic activity of Symbiodiniaceae

A further characterisation of fine details occurring in the photosynthetic machinery of Symbiodiniaceae in symbiosis, were obtained through the comparison of multiple parameters obtained from joint measurements. Through the comparison of the relative activity of PSII and PSI and Chl *a* fluorescence analysis, we could observe that CEF and NPQ were present at saturating light intensities in *S. pistillata* maintained in aquarium conditions (**Chapter 4, Figure 3d and 7a**). The activity of CEF, by pumping H^+ into the thylakoid lumen, has shown to be involved in the activation of the photoprotection mechanisms, such as the xanthophyll cycle. With this information, an obvious step forward will be the demonstration of this correlation by the identification of the pigments involved (**Warner and Berry-Lowe, 2006**). We consider that different methodological strategies can be thereafter applied to provide information on the relevance of CEF and WWC under sub-saturating light conditions.

We could deduce that CEF activity was present in other corals collected from a reef in Palau, which harboured Symbiodiniaceae species from the *Durusdinium* genus (**Chapter 4, Figure 7b**). This contrasted with a previous hypothesis claiming that CEF activity could be clade-specific, and that it could not be developed at saturating light intensities in species from the *Durusdinium* genus (**Reynolds et al., 2008**). It is worth mentioning here that there are different methodological strategies that lead to deduce the activity of CEF (**Fan et al., 2016**) and so, contrasting results can originate from assumptions about the redox equilibration in the photosynthetic chain during *in vivo* measurements (**Dang et al., 2019**). With this we admit that the correct determination of absolute values of electron transfer rate are much more complex than what we have essayed here (**Szabó et al., 2014**), but it constitutes a good precedent for a more accurate evaluation of these relationships. Further research may also include the search of the molecular components, because some photosynthetic complexes might possess structural differences in comparison to their green counterpart. That is the case of the recently reported PSI complex (**Kato et al., 2020**), for which a further characterization is worth of a research line. As another case, some genes encoding external subunits of the Cytochrome b_6f complex (petM and petL) were absent from the plastid and nuclear genome of *Breviolum minutum* (**Mungpakdee et al., 2014**). The protein product of *petM* in *Arabidopsis* has shown to provide stabilization to the complex (**Lan et al., 2021**).

In contrast to cultures of Symbiodiniaceae, where NPQ values are usually low (c.a. 0.5; **Roberty et al., 2014**), in *S. pistillata* it is found to be more than four times higher at saturating light intensities (c.a. 2.1; **Chapter 4, Figure 3d**). This photoprotection mechanism was concurrent with the presence of CEF at those light levels (**Chapter 4**, **Figure 7a**). This relation was slightly different in corals collected from shallow depths in the reef, where they were also found to make use of WWC at saturating light intensities (**Chapter 5, Figure 2a**). Indeed, in these corals a fraction of NPQ was developed before the ratio of PSI to PSII activity was increased at saturating light intensity (**Chapter 5, Figure S6**). This indicated that *S. pistillata* harbouring *S. microadriaticum* and living in aquarium conditions (at 100 µmol photons m^{-2} s^{-1}) or at shallow depths (10 m) in the reef of the Gulf of Aqaba-Eilat, uses CEF to induce NPQ as a main photoprotection mechanism. When coral colonies of shallow depths were transferred to lower light intensities, they developed lower NPQ capacities (**Chapter 5, Figure 3e**), together with a decrease in the electron transfer capacity, larger in PSI than in PSII (**Chapter 5, Figure 3d and f**). In the case of *Cladocopium sp*. harboured by *S. pistillata* from mesophotic depths, the relation between CEF and NPQ could follow a similar pattern, but with a lower NPQ value (**Chapter 5, Figure 1e**). An incubation at high light intensity for three days could not induce a higher NPQ in coral colonies from mesophotic depths (**Chapter 5, Figure 3e**). Together, these indicated that the quencher could be less abundant in corals from mesophotic than from shallow depths.

We could also observe a higher participation of the PQ pool with non-photochemical reactions in shallow water colonies in comparison to mesophotic ones. The redox state of the PQ pool in oxygenic photosynthetic organisms is considered a key link between the energetic state in the chloroplast with a variety of cellular processes (**Alric, 2015**; **Nawrocki et al., 2015; Cheong et al., 2022**). Shallow corals exposed to lower light intensity, resulted in a lower participation of the PQ pool with stromal reactions, a lower maximum capacity of oxygen evolution and a higher PSI donor side limitation (**Chapter 5, Figure 3h and i**). When mesophotic coral colonies were exposed to a higher light intensity, an expected PSII photoinhibition was observed, but the remaining PSI was still active, most likely participating as a photoprotection mechanism (**Chapter 5, Fig. 3f**). Recently, a transcriptomic profile analysis from the Symbiodiniaceae symbiont *Cladocopium sp*. in the coral *Pavona decussata*, has shown a lower expression of key PSII subunits in comparison to PSI subunits during a coral bleaching event (**Zhang et al., 2022**). These authors suggested that a disbalance in the electron transfer along the photosynthetic chain could be related to oxidative stress. This contributes with our findings pointing out the participation of PSI in photoprotection.

The understanding of the photosynthetic electron transfer regulation in *in vivo* conditions is an open field for the development of new techniques and strategies (**Schansker, 2022**). Photosynthetic

alternative electron transfer continuously demonstrates to be linked to the photoprotection mechanisms in diverse species, such as the psychrophile species *Chlamydomonas priscuii* (**Stahl-Rommel et al., 2022**) or the plant *Triticum aestivum* under nutrient limiting conditions (**Filacek et al., 2022**). It was recently shown in the green microalga *Chlamydomonas reinhardtii* that the photosynthetic alternative electron pathways (CEF and WWC) contribute to the thylakoid lumen acidification promoting the energization important for the CCM activity (**Burlacot et al., 2022**). Because both WWC and CEF contribute to the increase of the *pmf*, a fine regulation must be present in order to regulate their concerted activity under the various adverse conditions for the photosynthetic electron transfer chain (**Shikanai and Yamamoto, 2017**).

Other perspectives and overview

A valuable consideration for the correct interpretation of the bioenergetic relations within photo-symbiotic cnidarians is the contribution of respiration, which in Symbiodiniaceae has shown to be coupled to the photosynthetic activity at different levels among species (**Pierangelini et al., 2020**). Oxygen uptake in the darkness has shown to be impacted upon acute heat stress in some Symbiodiniaceae species (**Dang et al., 2019**). In this sense, mitochondrial respiration has shown to be an important player in the photosynthetic process, contributing with ATP synthesis in a PGRL1 knockout mutant of *Chlamydomonas reinhardtii* (**Dang et al., 2014**) and in diatoms such as *Phaeodactylum tricornutum* (**Bailleul et al., 2015**). As a contribution to a parallel project, we have also shown in *Euglena gracilis*, a secondary green microalga, that the photosynthetic activity is coupled to mitochondrial respiration depending on its metabolic state (see **Annex A**). Upon addition of mitochondrial inhibitors to mixotrophically or photoautotrophically grown algae, different responses of the chloroplast stromal redox state could be observed (**Annex A, Figure 4 and 5**). These responses can also be monitored in coral fragments, with the potential to provide further details on their *in vivo* metabolic dynamics. Although the contribution of respiration to coral photosynthesis has been studied, the complexity of the bioenergetic relation between both partners has limited its advance (**Hawkins et al., 2016; Cunning et al., 2017**). We consider that the use of coral fragments can help to move forward the data acquisition of coral respiration. In this respect, we have shown that it is possible to determine the contribution of a CN resistant- but SHAM sensitive-oxygen consumption during dark respiration (**Chapter 4, Figure 4**). The study of coral respiration, and the identification of the algal and cnidarian contribution can help to better understand the diverse responses we have observed.

Other factors that can affect in a more direct way the photosynthetic activity of the algal symbiont are also of much interest. This is the case of the host-release factor. With the correct experimental

strategies, this has the potential to provide information on the flexibility and dynamism of the photosynthetic metabolism. Together with *in vivo* monitoring of the multiple photosynthetic traits, it will be possible to unveil the adaptations that Symbiodiniaceae uses to work as a photosynthetic symbiont.

ANNEX A_ Photosynthetic responses to changes in respiration in the secondary green alga *Euglena gracilis*

The microalga *E. gracilis* (Euglenozoa, Discoba) contains a secondary acquired chloroplast derived from green algae (**Jackson et al., 2018**). This organism is able to grow both in photoautotrophy, with light and CO_2 as energy and carbon sources, and in mixotrophy, with light and organic carbon sources, such as acetate or ethanol. Mixotrophic culturing conditions increased the growth and respiratory rates in this alga (**Annex A, Figure 1a**), leading to alter the proportion of the photosynthetic activity observed in autotrophic conditions (**Annex A, Figure 1b, 2 and 3**). With the use of the mitochondrial inhibitors antimycin-A (AA, inhibiting the activity of complex III), cyanide (KCN, inhibiting the activity of complex IV), and salicylhydroxamic acid (SHAM, inhibiting the activity of alternative oxidase), we monitored the responses of the trans-thylakoid electric field ($\Delta\Psi$) by ECS. We observed that $\Delta\Psi$ in dark acclimated cells was altered following mitochondrial inhibition (**Annex A, Figure 4a**). In order to evaluate the mitochondrial malate-aspartate shuttle of *E. gracilis* (**Uribe and Moreno-Sanchez, 1992**) we used the inhibitor aminooxyacetic acid (AOAA, an inhibitor of aspartate aminotransferase). We found that respiration in the dark was sensitive to this inhibitor in cells cultured in photoautotrophy and mixotrophy (**Annex A, Figure 4b**), but the photosynthetic activity was strongly affected in mixotrophic grown cells (**Annex A, Figure 4c**), suggesting a metabolic interaction through the malate-aspartate shuttle. We also monitored the thylakoid PQ pool redox state by Chl *a* fluorescence in the post-illumination period, and compared it with samples inhibited by octyl gallate (OG, inhibitor of PTOX). We observed a non-photochemical reduction of the PQ pool in the darkness, indicative of the chloroplast stromal reducing power accumulated during the light period (**Annex A, Figure 5a and b**). With the use of rotenone (Rot, inhibitor of mitochondrial complex I) we found that mitochondrial respiration is a key player in the consumption of reducing power produced in the light reactions in the chloroplast of this alga (**Annex A, Figure 5c**).

My contribution to this publication consisted in the experimental acquisition of photosynthetic activity, thylakoid proton motive force in the darkness by ECS, and the reducing power accumulation in the chloroplast in the presence of mitochondrial respiration through Chl *a* fluorescence (**Annex A, Figures 4 and 5**).

Publication title : Trophic state alters the mechanism whereby energetic coupling between photosynthesis and respiration occurs in *Euglena gracilis*.

Authors : Gwenaëlle Gain, Félix Vega de Luna, Javier Cordoba, Emilie Perez, Herve Degand, Pierre Morsomme, Marc Thiry, Denis Baurain, Mattia Pierangelini and Pierre Cardol.

Trophic state alters the mechanism whereby energetic coupling between photosynthesis and respiration occurs in *Euglena gracilis*

Gwenaëlle Gain[1]*, Félix Vega de Luna[1]*, Javier Cordoba[1], Emilie Perez[1], Hervé Degand[2], Pierre Morsomme[2], Marc Thiry[3], Denis Baurain[4], Mattia Pierangelini[1]† and Pierre Cardol[1]†

[1]InBioS – PhytoSYSTEMS, Laboratoire de Génétique et Physiologie des Microalgues, ULiège, Liège B-4000, Belgium; [2]Louvain Institute of Biomolecular Science and Technology (LIBST),

UCLouvain, Louvain-la-Neuve B-1348, Belgium; [3]Laboratoire de Biologie Cellulaire et Tissulaire, Giga-Neurosciences, ULiège, Liège B-4000, Belgium; [4]InBioS – PhytoSYSTEMS,

Eukaryotic Phylogenomics, ULiège, Liège B-4000, Belgium

Summary

- The coupling between mitochondrial respiration and photosynthesis plays an important role in the energetic physiology of green plants and some secondary-red photosynthetic eukaryotes (diatoms), allowing an efficient CO_2 assimilation and optimal growth.
- Using the flagellate *Euglena gracilis*, we first tested if photosynthesis–respiration coupling occurs in this species harbouring secondary green plastids (i.e. originated from an endosymbiosis between a green alga and a phagotrophic euglenozoan). Second, we tested how the trophic state (mixotrophy and photoautotrophy) of the cell alters the mechanisms involved in the photosynthesis–respiration coupling.
- Energetic coupling between photosynthesis and respiration was determined by testing the effect of respiratory inhibitors on photosynthesis, and measuring the simultaneous variation of photosynthesis and respiration rates as a function of temperature (i.e. thermal response curves). The mechanism involved in the photosynthesis–respiration coupling was assessed by combining proteomics, biophysical and cytological analyses.
- Our work shows that there is photosynthesis–respiration coupling and membrane contacts between mitochondria and chloroplasts in *E. gracilis*. However, whereas in mixotrophy adjustment of the chloroplast ATP/NADPH ratio drives the interaction, in photoautotrophy the coupling is conditioned by CO_2 limitation and photorespiration. This indicates that maintenance of photosynthesis–respiration coupling, through plastic metabolic responses, is key to *E. gracilis* functioning under changing environmental conditions.

Introduction

In photosynthetic organisms, it is a commonly accepted view that the ATP/NADPH ratio generated by photosynthetic linear electron flow is insufficient to sustain CO_2 import into the plastid and assimilation by the Calvin–Benson–Bassham cycle (Allen, 2002; Allen *et al.*, 2008; Bailleul *et al.*, 2015). In this respect, the activities of several plastid-localized alternative electron pathways (AEPs) contribute to establishing the proton motive force necessary to produce additional ATP without net NADPH generation. These AEPs include cyclic electron flow around photosystem II (PSII) (Feikema *et al.*, 2006) or around photosystem I (PSI) and the water-to-water cycles (i.e. flavodiiron proteins, Mehler-ascorbate peroxidase, plastoquinol terminal oxidase, oxygenase activity of RuBisCO (photorespiration)) that mediate electron

flow from oxidation of water to reduction of O_2 (Cardol *et al.*, 2011; McDonald *et al.*, 2011; Raven *et al.*, 2020).

Besides AEPs localized in the chloroplasts, optimization of ATP/NADPH budget can also rely on the sharing and rerouting of ATP and NADPH between chloroplasts and mitochondria. This has been shown in several species of photosynthetic eukaryotes, including flowering plants (Raghavendra & Padmasree, 2003; Noguchi & Yoshida, 2008), primary green algae (*Chlamydomonas reinhardtii*; Cardol *et al.*, 2003; Dang *et al.*, 2014) and complex algae bearing plastids of red origin such as the diatom *Phaeodactylum tricornutum* (Bailleul *et al.*, 2015; Murik *et al.*, 2019) or the dinoflagellate *Symbiodinium* sp. (Pierangelini *et al.*, 2020). It thus appears that the energetic chloroplast–mitochondrion coupling occurs in microalgal species with different evolutionary origins or from different ecological niches.

Euglena gracilis (Euglenozoa, Discoba, Excavata) is a unicellular photosynthetic eukaryote originating from an endosymbiosis

between a green alga (Pyramimonadales) and an ancient phagotrophic euglenozoan species (Turmel *et al.*, 2009; Jackson *et al.*, 2018). Lateral gene transfer events from other microorganisms (Novák Vanclová *et al.*, 2020) enriched the evolutionary history of Euglenoids with respect to the 'green' and 'red' primary algae. Because of this, *E. gracilis* has become increasingly relevant to understanding the changes that the 'green' secondary endosymbiosis has caused to both chloroplastic metabolism (Bennett *et al.*, 2012; Novák Vanclová *et al.*, 2020) and mitochondrial machinery (Perez *et al.*, 2014; Yadav *et al.*, 2017; Hammond *et al.*, 2020). *Euglena gracilis* chloroplast has three envelope membranes (Larkum *et al.*, 2007) and a reticulated mitochondrial network (Pellegrini, 1980). In relation to the respiratory apparatus, additional atypical domains have been found in complex I (CI) and complex IV (CIV) of the respiratory electron transport chain (Miranda-Astudillo *et al.*, 2018), and the Krebs cycle has an alternative pathway from 2-oxoglutarate to succinate (via 2-oxoglutarate decarboxylase) (Raven & Beardall, 2016). In the chloroplast, Shimakawa *et al.* (2017) suggested the possible presence of two (or more) AEP mechanisms, including an AEP with low affinity for O_2 (e.g. photorespiration). Yet, it is still not known whether, during evolution, *E. gracilis* retained the mechanisms connecting photosynthetic activity to respiration (e.g. NADPH and ATP exchange). The primary aim of our work is thus to investigate the chloroplast–mitochondrion energetic coupling in *E. gracilis*, thereby expanding on the role of chloroplast–mitochondrion coupling in regulating the cell ATP/NADPH budget in phylogenetically distant species (Wilken *et al.*, 2014), and thus on its possible multiple and independent appearances.

In addition to its key evolutionary history, *E. gracilis* represents an interesting model related to its ability to grow in the presence of both inorganic carbon (C_i) and organic carbon sources (e.g. acetate, ethanol) (Perez *et al.*, 2014). The presence of organic substrates promotes mixotrophic growth and may reduce the need for an active photosynthetic apparatus (Chapman *et al.*, 2015), for example, involving less pigments, RuBisCO, PSII or PSI biosynthesis (Wilken *et al.*, 2014; Kamalanathan *et al.*, 2017; Cecchin *et al.*, 2018), or a CO_2-concentrating mechanism activity (Polukhina *et al.*, 2016; Treves *et al.*, 2016). This shifts the role of photosynthesis from providing both carbon and energy to mainly providing energy (Wilken *et al.*, 2014). Contemporaneously to these alterations, organic substrates stimulate cell respiration (Perez *et al.*, 2014), potentially altering the mechanisms whereby the mitochondria interact with the chloroplasts. Our second aim is thus to determine how the cell trophic state influences the coupling and the exchange of metabolites between chloroplasts and mitochondria in *E. gracilis*.

Materials and Methods

Strain and culture conditions

Euglena gracilis strain (SAG 1224-5/25, obtained from the University of Göttingen (Sammlung von Algenkulturen, Germany), was grown under low photosynthetic photon flux density (PPFD) (LL, 50 μmol photons $m^{-2} s^{-1}$, white light-emitting diode (LED)) at 25°C in Tris-minimal-phosphate (TMP) liquid medium (Perez *et al.*, 2014). Unless specified, TMP + LL was chosen to set the photoautotrophic condition, whereas TMP added to acetate (17 mM) as an exogenous organic carbon source (i.e. Tris-acetate-phosphate, TAP) was chosen as the mixotrophic condition. The effects of different carbon sources (60 mM acetate, 22–220 mM ethanol, in combination with darkness or moderate PPFD (ML, 200 μmol photons $m^{-2} s^{-1}$), were tested after 48 h after their addition to TMP cells grown in LL. All media were supplemented with vitamins (biotin, 10^{-7}%; vitamin B12, 10^{-7}%; vitamin B1, 2×10^{-5}% (w/v); Perez *et al.*, 2014). For each experiment, cell concentration was determined with a Beckman Coulter Z2 Counter Analyser (Z2; Beckman, Indianapolis, IN, USA).

Oxygen exchange measurements

Rates of photosynthesis and dark respiration (R_d) were measured on exponentially growing cells using a Clark-type oxygen electrode (Hansatech, King's Lynn, UK). Briefly, cells were harvested from the culture by centrifugation (3500 *g*, 2 min), resuspended in fresh culture medium (TAP or TMP), and placed into the oxygen electrode chamber. For each measurement, temperature was kept at $25 \pm 1°C$. For cells grown photoautotrophically, 2 or 10 mM of $NaHCO_3$ was added during the experiment to guarantee a sufficient supply of C_i (Iglesias-Prieto *et al.*, 1992; Karsten & Holzinger, 2012). Respiration rates were measured after 5–10 min in the dark. Photosynthesis was measured under a red light source (provided by LED peaking at 660 nm; see figure legends for each PPFD and duration). Gross oxygen production (E_O) was calculated as the difference between net photosynthesis and R_d. To test the impact of respiratory inhibitors on photosynthesis, inhibitors of mitochondrial complexes were added at the beginning of the measurements. These included oligomycin (50 μM, blocking mitochondrial F_1F_O ATP synthase), antimycin A (AA, 10 μM, blocking CIII), rotenone (100 μM, blocking CI), potassium cyanide (KCN, 1 mM, blocking CIV) and salicylhydroxamic acid (SHAM, 1 mM, blocking mitochondrial alternative oxidase (AOX)) (Perez *et al.*, 2014). Stock solutions of oligomycin, AA, rotenone and SHAM were prepared in dimethyl sulfoxide. Stock solution of KCN was prepared in deionized water. Aminooxyacetic acid (AOAA, O-(carboxymethyl) hydroxylamine hemihydrochloride, 5 mM) was also used as an inhibitor of the aspartate aminotransferase (Cornell *et al.*, 1984) involved in the malate-aspartate shuttle. Aminooxyacetic acid was added to cells maintained in darkness for 2 min before measurements.

Thermal response curves (TRCs) were carried out as in Karsten & Holzinger (2012) and Pierangelini *et al.* (2020). *Euglena gracilis* was exposed to rising temperatures from 10 to 40°C. At each temperature, cells were initially incubated in the dark for 25 min, and the last 10 min of this incubation period was used to measure R_d. After the dark period, cells were exposed to a PPFD of 400 μmol photons $m^{-2} s^{-1}$ (LED light source peaking at 660 nm) for 10 min, with the final 5 min used to calculate $E_{O,max}$.

Growth

To determine the growth of *E. gracilis* under mixotrophic and photoautotrophic conditions in the absence or presence of respiratory inhibitors (rotenone (100 μM) and AA (10 μM)), batch cultures (25 ml of medium in a flask of 100 ml) were started with exponentially growing cells, at an initial cell concentration ≤ 4 × 10^4 cells ml^{-1}. Cell concentration was measured daily until the end of the exponential phase. Cell-specific division rate (μ) was calculated from the slope of the natural logarithm plot obtained from the exponential phase of the growth curve.

Spectroscopic measurements

Chlorophyll content Cells were harvested by centrifugation (2500 *g*, 1 min) and resuspended in cold 100% methanol. This suspension was then centrifuged (2500 *g*, 1 min) and the absorbance of the supernatant measured in a spectrophotometer (Lambda 265; Perkin Elmer, Waltham, MA, USA) at 665 and 652 nm. Total Chl($a + b$) concentration was calculated using equations for chlorophytes from Ritchie (2006). When needed, cells were resuspended in medium supplemented with ficoll 10% to a final Chl concentration of 10 μg ml^{-1}, and were dark-acclimated for at least 20 min with constant stirring.

Electrochromic shift The development of the light-induced thylakoid electric field ($\Delta\psi$) was followed *in vivo* by monitoring changes in absorption of membrane-embedded pigments (commonly referred to as electrochromic shift; ECS) (Bailleul *et al.*, 2010). Measurements were carried out with a Joliot-Type Spectrophotometer (JTS-10; Biologic, Seyssinet-Pariset, France) equipped with a white probing LED and interference filters (10 nm bandwidth). The ECS signal was recorded within the 440–600 nm region as the changes of absorption from a baseline in the darkness to the signal 150 μs after applying a saturating single turnover flash (duration *c.* 7 ns; Nd-YAG laser Minilite II, Continuum, Milpitas, CA, USA). The ECS spectrum response was similar for *E. gracilis* cells grown mixotrophically and photoautotrophically (Supporting Information Fig. S1a), with a maximum at 510 nm. The ECS at 510 nm was used to monitor the linearity of the signal increase (Fig. S1b) and the maximum electric field generated by a series of charge separations induced by the laser flash fired each 100 ms until the maximum signal was reached. When used, the mitochondrial respiratory inhibitors KCN (1 mM) and SHAM (1 mM) were added 1 min before measurements. The presence of mitochondrial inhibitors had only a minor effect on the signal increase corresponding to one charge separation (92 ± 4% and 85 ± 5% of the control values in photoautotrophic and mixotrophic conditions, respectively).

Chl*a* fluorescence Measurements were carried out in the JTS-10 spectrophotometer with a detecting probe providing short blue flashes (10 μs duration, 440–470 nm) and fluorescence was recorded after light was filtered by a long-pass filter (680 nm). Actinic light was provided by red LEDs (660 nm) either as a saturating pulse (9000 μmol photons $m^{-2} s^{-1}$ during 150 ms) or as

continuous illumination to maintain steady photosynthesis. The potential direct effect of inhibitors on photosynthetic electron transfer was monitored during the Chl fluorescence increase as a result of strong illumination (2750 μmol photons $m^{-2} s^{-1}$) during 500 ms followed by a 150 ms saturating pulse. Each inhibitor tested was added less than 2 min before the measurements to TAP or TMP dark-acclimated cells (Fig. S2). The impact of DCMU (3-(3,4-dichlorophenyl)-1,1-dimethylurea, 10 μM, prepared in methanol), and DBIMB (2,5-Dibromo-6-isopropyl-3-methyl-1,4-benzoquinone, 5 μM, prepared in ethanol) were evaluated as controls (Fig. S2).

Post-illumination Chl fluorescence recordings were obtained after 12 min of light acclimation in the JTS-10 (100 μmol photons $m^{-2} s^{-1}$) with constant stirring. Rotenone (100 μM), AOAA (5 mM) or sodium bicarbonate (10 mM) were added at the fourth minute of the light phase followed by the addition (or the absence in the case of control measurement) of octyl gallate (OG, 10 μM, prepared in dimethyl sulfoxide), blocking the plastidial terminal oxidase (PTOX). The changes of Chl fluorescence between 5 and 60 s of the post-illumination phase were calculated after normalization of the fluorescence traces by setting F_O to 1. At the end of the light phase, the nonphotochemical quenching of Chl fluorescence (NPQ, calculated as $(F_m - F_m')/F_m'$, where F_m is the maximum fluorescence of cells before illumination and F_m' is the maximum fluorescence before light is switched off) were very low and identical in the presence or absence of OG in mixotrophy or in photoautotrophy (Fig. S3) (two-way ANOVA; $P > 0.1$) so the contribution of NPQ relaxation to F_o changes (if any) should be negligible. Relative electron transport rate through PSII (rETR-PSII, μmol electrons $m^{-2} s^{-1}$) was calculated as PPFD × $(F_m' - F_s)/F_m'$, where F_s is the steady-state fluorescence of cells in the light.

Transmission electron microscopy (TEM)

In addition to the standard mixotrophic and photoautotrophic conditions under low light, *E. gracilis* cells were grown in photoautotrophy + 5% CO_2 : 95% air mixture bubbled in the culture. Cells were fixed for 60 min at room temperature in 2.5% glutaraldehyde in 0.1 M Sorensen's buffer (pH 7.4). After washing in Sorensen's buffer, cells were postfixed in 2% osmium tetroxide (CAS: 20816-12-0), dehydrated through graded ethanol-propylene oxide series and embedded in epoxy resin (SPI-PON 812; Spichem, West Chester, PA, USA). The resin was then polymerized at 60°C for 48 h. Ultrathin sections (80 nm) were mounted on colloidin-coated grids and stained with uranyl acetate and lead citrate before examination in a JEM 1400 transmission electron microscope at 80 kV.

Statistical analyses

Experiments were performed with at least three (unless otherwise stated) biological replicates. Comparisons between two treatments were made using two-tailed *t*-tests. When comparison involved more than two treatments, one-way ANOVA was used. Changes of parameters as a function of increasing temperature or

changes during exposure to respiratory inhibitors were tested using repeated-measures (RM) ANOVA. The variation among means in relation to treatments was tested by using two-way ANOVA. The analyses were performed using GRAPHPAD PRISM 5 (GraphPad Software, San Diego, CA, USA), setting the threshold of significance at 0.05.

Comparative proteomics

Preparation of protein samples In addition to the standard mixotrophic and photoautotrophic conditions under low light, we analysed mixotrophic cells under moderate light (TAP ML) and photoautotrophic cells in the presence of the 5% CO_2 : 95% air mixture bubbled in the culture (TMP CO_2). The membrane and soluble proteins were obtained as outlined in Remacle *et al.* (2006). All steps were performed at 4°C. Briefly, 20 µg of proteins (quantified by the Bradford assay (Bradford, 1976)) from each sample were precipitated in cold chloroform-methanol (Wessel & Flügge, 1984). Each sample was transferred to a 1.5 ml tube and adjusted to 100 µl with H_2O. Chloroform (100 µl) and methanol (400 µl) were added and the mixture vortexed for 30 s. Samples were then added with 300 µl of H_2O and the mixture was vortexed again for 30 s. Each sample was then centrifuged (4°C, 20 000 *g*, 15 min) and after removing the upper phase, 800 µl of methanol was added. The samples were then re-centrifuged (4°C, 20 000 *g*, 15 min), and the protein pellet vacuum-dried (SC 200 Savant Speed Vac Concentrator; Thermoscientific, Waltham, MA, USA) and then stored at −20°C. Before analysis, proteins were trypsin-digested according to Szopinska *et al.* (2011).

Shotgun proteomics and protein quantification Full details of this procedure, including comments about the total number of proteins identified, are given in Methods S1 and other supplementary materials. The relative abundance of proteins in each condition was determined using iTRAQ isobaric labelling. The iTRAQ marking was carried out according to the protocol supplied by the manufacturer (AB Sciex, Foster City, CA, USA). After isobaric labelling, the four samples were mixed and the mixture dried under vacuum in an SC 200 Savant Speed Vac concentrator. Sixteen micrograms1 of proteins for each labelled sample were then dissolved in 0.025% trifluoroacetic acid and 5% acetonitrile and subjected to reverse phase chromatography according to Szopinska *et al.* (2011), using an LC Ultimate nanochromatography system 3000 (Thermoscientific). The eluted peptides were analysed using an AB Sciex 4800 matrix-assisted laser desorption/ionization-time of flight MS as described in Szopinska *et al.* (2011). Each sample was analysed in three repetitions.

Peptides and proteins were inferred from the spectrum identification results using PEPTIDESHAKER v.1.16.43 (Vaudel *et al.*, 2015). Spectrum counting abundance indexes were estimated using the normalized spectrum abundance factor (Powell *et al.*, 2004) adapted for better handling of protein inference issues and peptide detectability. Finally, protein quantification was performed with REPORTER v.0.7.20 (beta). Normalized protein

abundance was then $\log_2$-transformed and significant changes ($P < 0.05$) between samples were computed using a linear model framework with LIMMA empirical Bayes approach (Kammers *et al.*, 2015; Ritchie *et al.*, 2015).

Results and Discussion

Mixotrophy increases the R_d : $E_{O,max}$ ratio

We compared dark respiration (R_d) to maximal gross oxygen evolution (E_O) of *E. gracilis* growing in the presence and absence of organic substrates. The total Chl concentration was 15.9 ± 1.8 pg per cell in mixotrophy with no significant difference with respect to cells in photoautotrophy (18.3 ± 4.3 pg Chl per cell; one-way ANOVA, $P = 0.20$) (Table 1), allowing us to express any metabolic activity on a cell or a Chl basis. In mixotrophy, the R_d : $E_{O,max}$ ratio for *E. gracilis* was significantly higher than in photoautotrophy (0.40 ± 0.03; one-way ANOVA, $P = 0.01$), probably because of the involvement of R_d in heterotrophic metabolism to provide the energy for biosynthesis (Geider & Osborne, 1989). These R_d : $E_{O,max}$ ratios in *E. gracilis* are in the range of values (0.1–0.5) previously reported for other microalgal species (Geider & Osborne, 1989; Raven & Beardall, 2016; Pierangelini *et al.*, 2019). We then investigated whether a sudden change in respiratory capacity was reflected by a change of photosynthesis in *E. gracilis*.

Reduction in photosynthetic performance following inhibition of mitochondrial respiration

We evaluated the impact of inhibition of the mitochondrial respiratory complexes (I, III and IV), mitochondrial AOX, and mitochondrial F_1F_O ATP synthase on R_d and E_O. In mixotrophy, addition of rotenone (blocking complex I), AA (blocking complex III), KCN (blocking complex IV), KCN + SHAM (blocking complex IV and AOX, respectively), or oligomycin (blocking mitochondrial F_1F_O ATP synthase) caused significant reductions in R_d (50%, 71%, 91%, 91%, 67%, respectively) (Fig. 1a), similar to those previously reported by Perez *et al.* (2014). The absence of effect of SHAM addition (Fig. 1a) or octyl gallate (Fig. S4) on KCN-resistant R_d indicated that the apparent capacity of AOX (SHAM-sensitive rate) is null or extremely low as previously reported (Castro-Guerrero *et al.*, 2004; Perez *et al.*, 2014; Krnáčová *et al.*, 2015). Conversely, the large KCN-sensitive respiration indicated a high capacity of the CIII + CIV pathway in mixotrophic conditions. In photoautotrophy, addition of rotenone and AA caused a 30–40% decline in R_d. Addition of every inhibitor (except SHAM) caused a significant decrease in $E_{O,max}$ (Fig. 1a). In mixotrophy, the R_d : $E_{O,max}$ ratio was not altered by the presence of rotenone, oligomycin, KCN or SHAM, reflecting the fact that the extent of the inhibition of $E_{O,max}$ was proportional to the inhibition of R_d (Fig. 1b). This ratio was, however, lower in presence of AA and KCN + SHAM as a result of a lesser inhibition of $E_{O,max}$ than R_d. In photoautotrophy, the R_d : $E_{O,max}$ ratio decreased by 20% (Fig. 1b). For cells in both trophic conditions, a linear relationship ($r^2 = 0.90$, $P = 0.0003$)

141

Table 1 Parameters extrapolated from the transmission electron micrographs of *Euglena gracilis* cells cultured in mixotrophy, photoautotrophy and photoautotrophy + 5% CO_2 (Figs 8, S7).

	Mixotrophy	Photoautotrophy	Photoautotrophy + 5% CO_2
Chl content (pg per cell)	15.9 (1.8)[a]	18.3 (4.3)[a]	20.5 (4.6)[a]
Cell length (μm)	13.8 (2.5)[a]	14.6 (2.6)[a]	14.2 (5.2)[a]
Mitochondrial section area (μm^2)	0.2 (0.04)[a]	0.3 (0.08)[a]	0.3 (0.07)[a]
Number of mitochondrial sections per cell	14.2 (4.3)[a]	7.7 (2.4)[b]	8.2 (5.7)[b]
Chloroplast section area (μm^2)	1.8 (0.6)[a]	3.4 (1.7)[ab]	3.7 (0.6)[b]
Number of chloroplastic section per cell	4.5 (1.4)[a]	5.9 (3.7)[a]	7.6 (3.8)[a]
Chloroplast/mitochondria total area ratio	3.0 (1.4)[a]	8.2 (3.0)[b]	9.6 (4.0)[b]
Mitochondrial sections in contact with chloroplast contact (%)	58 (25)[a]	78 (16)[a]	74 (16)[a]
Membrane contact sites length (μm)	0.50 (0.12)[a]	0.43 (0.10)[a]	0.55 (0.13)[a]
Pyrenoid/chloroplast section area	0.04 (0.03)[a]	0.07 (0.04)[a]	0.03 (0.01)[a]
Number of intrapyrenoid thylakoids	4.5 (0.5)[a]	3.4 (2.5)[a]	6.3 (3.6)[a]

Values in brackets represent SD. Different letters identify significantly different means (one-way ANOVA, $P < 0.05$) among treatments.

was found between the reduction of R_d and $E_{O,max}$ caused by the addition of respiratory inhibitors (Fig. 1c). Because there is no direct immediate effect of these inhibitors on Chl$a$ fluorescence induction curves (Fig. S2), the inhibition of $E_{O,max}$ thus resulted from indirect effects, very likely caused by direct inhibition of mitochondrial respiration. E_O was also measured at sub-saturating light intensities, and the general trends were similar (Fig. S5). However, differences in the extent of R_d and E_O inhibition between light intensities were observed (see legend text of Fig. S5 for details), and they might indicate the occurrence of either some compensatory/alternative pathways or various non-specific inhibitory effects (Roberty *et al.*, 2014). In two distant species, the diatom *P. tricornutum* and the green alga *C. reinhardtii*, the photosynthetic electron transfer rate also linearly followed changes in respiration upon inhibition of mitochondrial respiration (Cardol *et al.*, 2003; Bailleul *et al.*, 2015). In both species, the AOX has been identified as an electron sink for photosynthetic-reducing equivalents (Bailleul *et al.*, 2015; Kaye *et al.*, 2019). In *E. gracilis*, the apparent null capacity of AOX in mixotrophy (see earlier), but also in photoautotrophy (Fig. S5), rather suggests a strong dependence of photosynthetic electron transfer chain on mitochondrial respiratory electron flow coupled to ATP synthesis.

Similar changes of photosynthesis and respiration during rapid temperature exposure

In the next step, we tested the effect of rapid changes in temperature (from 10 to 40°C) on respiratory and photosynthetic capacities. We observed an overall similar increase of $E_{O,max}$ and R_d with temperature, whether cells were grown mixotrophically or photoautotrophically (e.g. about five times between 10°C and 35°C; t-test, $P < 0.01$) (Fig. 2a,b). This increase reflects the temperature sensitivity of electron-transport components and enzymatic machinery involved in both metabolic processes (Berry & Bjorkman, 1980; Atkin & Tjoelker, 2003). In agreement with the results reported in Fig. 1(b), the $R_d : E_{O,max}$ ratio for *E. gracilis* growing photoautotrophically was lower than for cells growing mixotrophically (Fig. 2c). These $R_d : E_{O,max}$ ratios were stable

from 10 to 35°C (one-way ANOVA; mixotrophy, $P = 0.67$; photoautotrophy, $P = 0.98$), which reflects the fact that both $E_{O,max}$ and R_d were equally sensitive to the increase of temperature, and indicative of a coupling between respiration and photosynthesis. By contrast, dissimilar temperature-dependent increases of photosynthesis and respiration (varying $R_d : E_{O,max}$) were observed in several other species of green algae (Padfield *et al.*, 2016; Schaum *et al.*, 2017; Pierangelini *et al.*, 2019), diatoms (Prelle *et al.*, 2019) and dinoflagellates (Pierangelini *et al.*, 2020), and these are an indication that photosynthesis may be less dependent on R_d in those species (Pierangelini *et al.*, 2020). Finally, in *E. gracilis*, the increase in $R_d : E_{O,max}$ at the high temperature tested (40°C) (Fig. 2c) could reflect the disruption of the photosynthesis–respiration coupling as a result of thermal stress, as was previously observed in dinoflagellates (Pierangelini *et al.*, 2020).

Parallel photosynthetic and respiratory capacities under different mixotrophic conditions

We then exposed photoautotrophic *E. gracilis* cells to changes in trophic conditions by modifying the light regime or adding an exogenous organic carbon source. Rates of R_d and E_O were measured after 36 h and are reported in Fig. 3(a). The presence and availability of different organic substrates (acetate or ethanol) caused a two- to 12-fold increase in the rates of R_d and E_O, in comparison to cells grown in photoautotrophic conditions. In agreement with the results reported in Fig. 1(c) for the $R_d : E_{O,max}$, the $R_d : E_O$ for cells growing mixotrophically was higher than that for cells growing photoautotrophically (Fig. 3b). Interestingly, despite the large changes in the rates of R_d and E_O, the $R_d : E_O$ ratio was similar under different organic substrates (one-way ANOVA, $P = 0.38$). This result again suggested that the coupling of the chloroplast with the mitochondrion is essential and has to be maintained regardless of the trophic conditions, to guarantee cell photosynthetic functioning. In relation to growth, in mixotrophy, addition of rotenone and AA caused *c.* 15% and 40% reductions of μ, respectively. When *E. gracilis* was grown photoautotrophically, μ was reduced *c.* 10% and 20% with rotenone and AA, respectively (Fig. S6). This μ reduction reflects
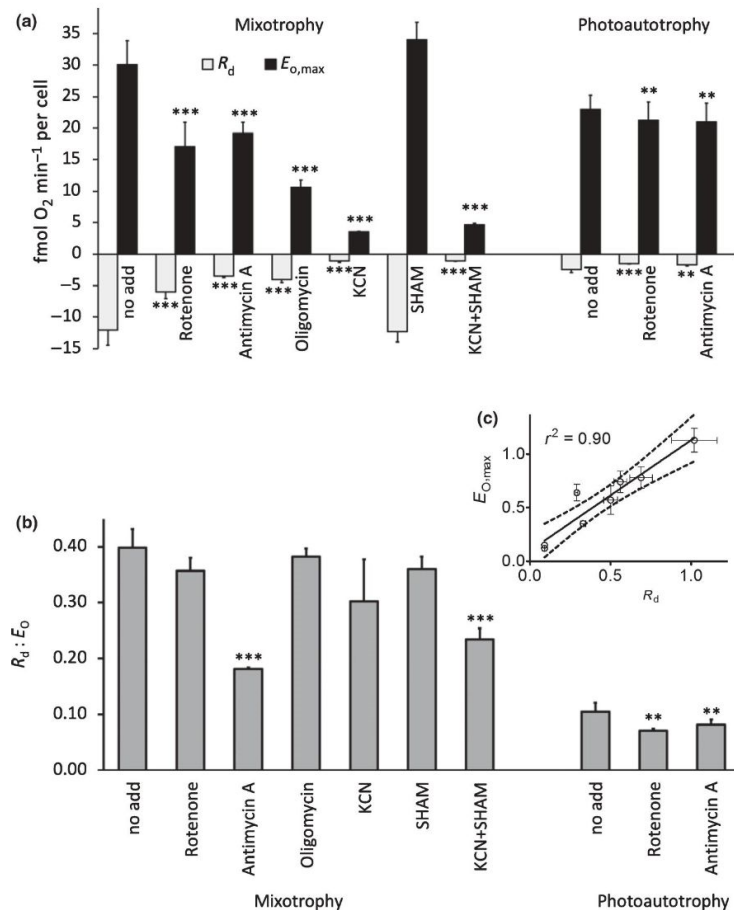
142

Fig. 1 Impact of mitochondrial respiratory inhibitors on dark respiration (R_d), gross maximal photosynthesis ($E_{O,max}$) (a), and $R_d : E_{O,max}$ ratios (b) in *Euglena gracilis* cultivated in mixotrophic and photoautotrophic conditions. All measurements were conducted in the presence of 10 mM $NaHCO_3$. A total of 10^6 cells ml^{-1} were adjusted in the oximeter chamber. Each light step (30, 103, and 571 μmol photons $m^{-2} s^{-1}$) was held for 5 min. Vertical bars indicate the standard deviation. **, $P < 0.05$; ***, $P < 0.01$; Student's t-test (values were compared with the E_O or R_d values of noninhibited cells (no add)). (c) Linear relationship ($r^2 = 0.90$, $P = 0.0003$) between $E_{O,max}$ and R_d in the presence of mitochondrial respiratory inhibitors for *E. gracilis* cultivated in mixotrophic and photoautotrophic conditions. All values were normalized to $E_{O,max}$ and R_d values in the absence of inhibitors. Vertical and horizontal bars indicate the standard deviation.

the involvement of the respiratory metabolism in the production (from carbohydrates produced during photosynthesis) of cellular metabolites used in the construction of cells (Falkowski *et al.*, 1985; Geider & Osborne, 1989).

Exchange of energy currency compounds between chloroplasts and mitochondria

As the interdependence between respiratory and photosynthetic activities often involves an energetic exchange between chloroplasts and mitochondria (Cardol *et al.*, 2009; Bailleul *et al.*, 2015), we determined whether ATP of mitochondrial origin could be imported into the chloroplasts. For dark-acclimated *E. gracilis* cells in both mixotrophic and photoautotrophic conditions, the maximum trans-thylakoid electric field ($\Delta\psi$, that can be built under a 10 Hz single-turnover flash train) was about 5 r.u. (threshold value corresponding to a membrane potential reference (Joliot & Joliot, 2008)). In the presence of mitochondrial inhibitors (AA or KCN+SHAM), $\Delta\psi$ increased to *c.* 6 and 8 r.u., respectively

(Fig. 4a). This indicated that the $\Delta\psi$ obtained in the absence of inhibitors was superimposed on a $\Delta\psi$ component present in the dark ($\Delta\psi_{dark}$, *c.* up to 3 r.u.), which is disrupted following the inhibition of mitochondrial respiratory electron transfer chain. In flowering plants and diatoms, it was proposed that the $\Delta\psi_{dark}$ was the result of hydrolysis of ATP imported from mitochondria by the chloroplastic ATP synthase (Joliot & Joliot, 2008; Bailleul *et al.*, 2015). Accordingly, we also conclude that the $\Delta\psi_{dark}$ in *E. gracilis* indicates export of ATP from mitochondria into the chloroplast. In this respect, an ATP/ADP translocase isoform has been identified in the chloroplast proteome of *E. gracilis* (Novák Vanclová *et al.*, 2020). Such ATP import may be useful during light exposure when ATP shortage occurs following the imbalance between the amount of ATP and NADPH produced by the activity of the photosynthetic electron transfer chain (Allen, 2002; Allen *et al.*, 2008; Bailleul *et al.*, 2015).

Previous studies (on diatoms, green algae and flowering plants) suggested that besides ATP, the energetic coupling between chloroplasts and mitochondria involves an exchange of reducing
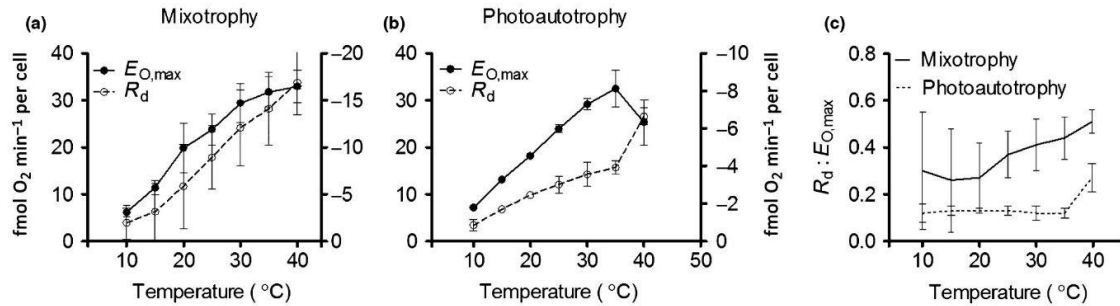
143

Fig. 2 Impact of change in temperature on gross maximal photosynthesis ($E_{O,max}$, left y-axis) and respiration (R_d, right y-axis) for *Euglena gracilis* cultivated in mixotrophic (a) and photoautotrophic (b) conditions. Measurements were conducted in the presence of 2 mM $NaHCO_3$. (c) $R_d : E_{O,max}$ ratios as a function of increasing temperature. The connecting line fits through the raw data. All measurements were performed for at least three independent culture replicates. Vertical bars indicate the standard deviation.
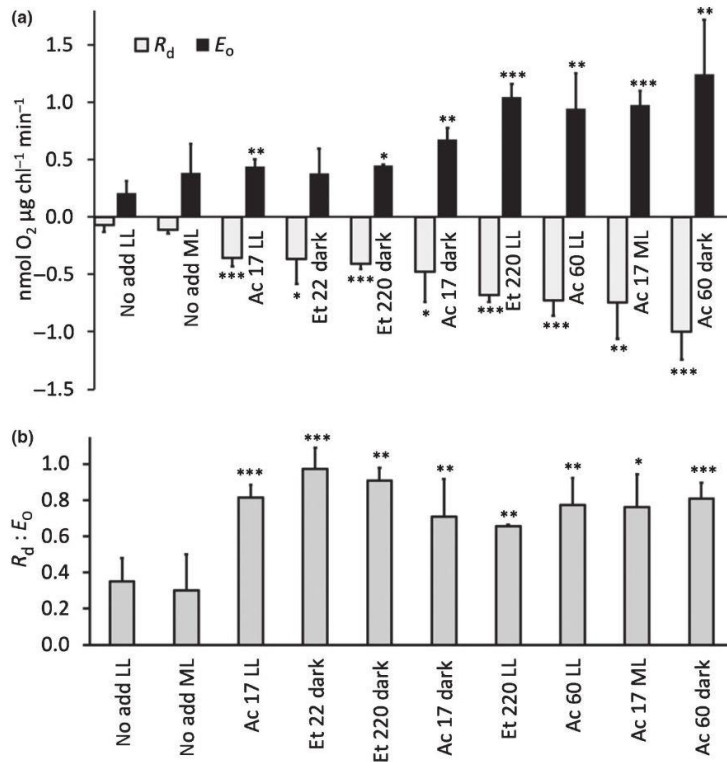
Fig. 3 Impact of addition of different organic carbon sources and/or variation in light intensity in culture on respiration (R_d), gross maximal photosynthesis ($E_{O,max}$) (a), and $R_d : E_{O,max}$ ratios (b) in *Euglena gracilis*. No add, no exogenous carbon source (TMP); Ac17, acetate 17 mM; Ac60, acetate 60 mM; Et22, ethanol 22 mM; Et220, ethanol 220 mM; LL, low light; ML, moderate light. No $NaHCO_3$ was added during the measurements. A total of 2×10^6 cells ml^{-1} were adjusted in the oximeter chamber. $E_{O,max}$ was measured during the last 3 min of 10 min illumination at 571 μmol photons $m^{-2} s^{-1}$. Measurements were performed for at least two independent culture replicates. Vertical bars indicate the standard deviation. *, $P < 0.1$; **, $P < 0.05$; ***, $P < 0.01$; Student's t-test (values were compared with the E_O or R_d control values of the photoautotrophic condition (no add LL)).

equivalents by the malate-aspartate shuttle (Cardol *et al.*, 2003; Allen *et al.*, 2008; Noguchi & Yoshida, 2008; Bailleul *et al.*, 2015). This shuttle system comprises two soluble enzymes in each compartment, a malate dehydrogenase and an aspartate aminotransferase. In *E. gracilis*, isoforms of malate dehydrogenase have been identified in the chloroplast and mitochondrial proteomes (Hammond *et al.*, 2020; Novák Vanclová *et al.*, 2020) and aspartate aminotransferase activity has been identified in both the

mitochondrial and chloroplastic fractions (Collins *et al.*, 1975). AOAA, an inhibitor of the aspartate aminotransferase (Cornell *et al.*, 1984), had an inhibitory effect of c. 40% and 70% on R_d and E_O, respectively, in mixotrophy (Fig. 4b,c) (t-test; R_d, $P = 0.04$; $E_{O,max}$, $P = 0.0001$). This indicated that exchange of reducing equivalents by malate-aspartate shuttle between cell compartments is critical in the interaction between photosynthesis and respiration in mixotrophic conditions. By contrast, in the
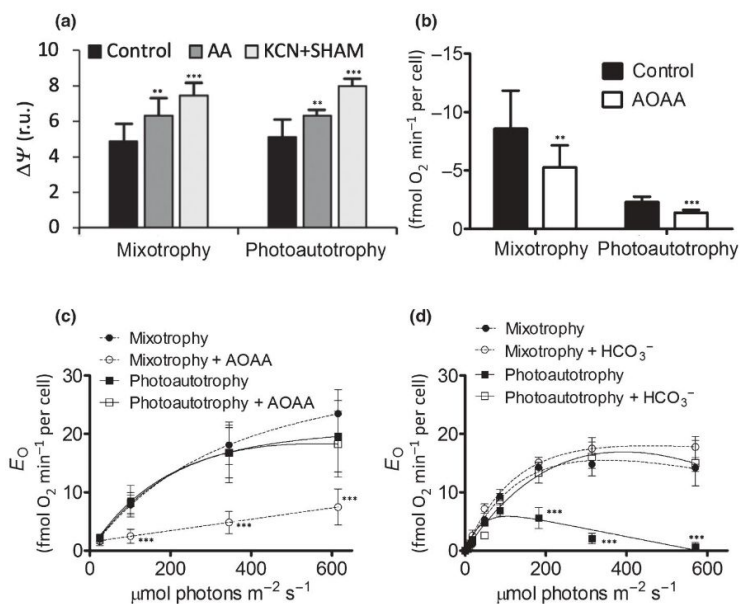
Fig. 4 (a) Impact of mitochondrial respiration inhibition (by potassium cyanide (KCN) and salicylhydroxamic acid (SHAM)), on the *Euglena gracilis* development of trans-thylakoid electric field ($\Delta\psi$) induced by a series of single turnover flashes. r.u., units relative to one charge separation of both photosystem I (PSI) and PSII monitored by electrochromic shift at 510 nm (Supporting Information Fig. S1). (b, c) Impact of aspartate aminotransferase inhibition by aminooxyacetic acid (AOAA) on dark respiration (R_d) and gross oxygen exchange rate (E_O) of *E. gracilis* cultivated in mixotrophic and photoautotrophic conditions. A total of 5×10^5 cells ml^{-1} were adjusted in the oximeter chamber. Each light step (photosynthetic photon flux density (PPFD) of 25, 100, 345 and 615 µmol photons $m^{-2} s^{-1}$) was held for 2 min. (d) *Euglena gracilis* E_O with and without addition of $NaHCO_3$ (10 mM) in mixotrophic and photoautotrophic conditions. A total of 2×10^6 cells ml^{-1} were adjusted in the oximeter chamber. Each light step (PPFD of 7, 18, 48, 86, 182, 314 and 570 µmol photons $m^{-2} s^{-1}$) was held for 5 min. All measurements were performed for at least three independent culture replicates. Vertical bars indicate the standard deviation. *, $P < 0.1$; **, $P < 0.05$; ***, $P < 0.01$; Student's *t*-test (values were compared with the values of control cells).

photoautotrophic condition, the absence of an effect of AOAA on photosynthesis (Fig. 4c) (*t*-test; $E_{O,max}$, $P = 0.73$) despite a 40% decrease of R_d (Fig. 4b) (*t*-test, $P = 0.003$) may indicate that exchange of reducing equivalents could occur through a different pathway (e.g. glycerol-3-phosphate shuttle (Shen *et al.*, 2003) or the glycolate/glycerate transporter involved in photorespiration (Dellero *et al.*, 2016)). Alternatively, this result suggests that in the photoautotrophic condition, ATP import or CO_2 availability in the chloroplast is limiting for photosynthesis, rather than the capacity to export reducing equivalents out of the chloroplast. To test this latter hypothesis, we assessed the photosynthetic activity in the presence and absence of extemporaneous $NaHCO_3$ addition (using a higher cell concentration in the oximeter chamber) during consecutive long steps of increasing light intensity. CO_2 limitation in the photoautotrophic condition was indicated by the progressive decrease of E_O in the absence of $NaHCO_3$ (from 16 to 2 fmol O_2 min^{-1} per cell at saturating light intensity) (two-way ANOVA, $P < 0.0001$), a decline that did not occur in mixotrophy (Fig. 4d).

In a next step, we probed the redox poise in the stroma in the light. In green plants, the accumulation of reducing power (i.e. reduced ferredoxin (Fd) or NADPH) in the stroma occurs notably under high light regime. As a consequence, post-illumination NADPH (or Fd) plastoquinone oxidoreductase activity leads to

nonphotochemical reduction of the plastoquinone pool in the dark. Therefore, the accumulation of reducing power can be evidenced as changes in the post-illumination fluorescence (Gotoh *et al.*, 2010). The use of an inhibitor of the plastoquinol terminal oxidase (PTOX), octyl gallate (Josse *et al.*, 2003), further reveals the extent of nonphotochemical reduction of the plastoquinone pool. In *E. gracilis*, in mixotrophic conditions, post-illumination Chl fluorescence increase was observed only in the presence of rotenone or AOAA (Fig. 5a,c). This indicates that reducing power is accumulated in the stroma when the mitochondrial respiration or the malate shuttle were inhibited. In photoautotrophic conditions, post-illumination increase in Chl fluorescence was observed even in the absence of rotenone or AOAA and was abolished in the presence of bicarbonate (Fig. 5b,c). These results reinforce the idea that the limiting step of photosynthetic electron transport is CO_2 availability in photoautotrophy, while balancing ATP/NADPH ratio is critical in mixotrophy.

Different mechanisms of chloroplast–mitochondrion energetic coupling in mixotrophy and photoautotrophy

We investigated the main responses of central carbon metabolism and electron transfer pathways in *E. gracilis* grown

Fig. 5 Influence of mitochondrial inhibitors and bicarbonate addition on the stromal reducing power in *Euglena gracilis*. Chlorophyll fluorescence of *E. gracilis* cells grown in mixotrophy (a) or photoautotrophy (b) was monitored during the post-illumination period in the absence (control) or presence of octyl gallate (OG; 10 μM). Time axis indicates the dark phase after 12 min of illumination. Chlorophyll fluorescence changes in the post-illumination phase were evaluated by the difference between fluorescence values at second 60 and 5 of this phase (c) in either the presence or absence of OG in addition to sodium bicarbonate (NaHCO$_3$; 10 mM), rotenone (Rot; 100 μM) or aminooxyacetic acid (AOAA; 5 mM). All measurements were performed for at least two independent culture replicates. Vertical bars indicate standard deviation. *, $P < 0.1$; **, $P < 0.05$; Student's *t*-test (values were compared with the values of cells without OG addition).
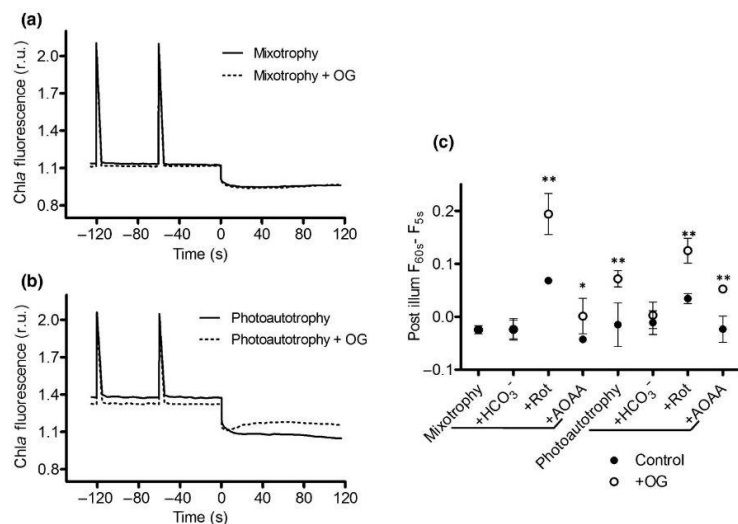
in mixotrophy or in photoautotrophy. iTRAQ-based comparative proteomics identified a total of 544 proteins, including several enzymes involved in the central carbon metabolism pathways (Krebs cycle, Calvin cycle, glycolysis, beta-oxidation of fatty acid, lipid synthesis, respiratory and photosynthetic electron transfer chains, etc.) (Table S1). Among them, 112 proteins showed a significant log$_2$-fold increase or decrease (in the ratio of normalized protein abundance) depending on the trophic state (Table S2). In the mixotrophic condition, among the 53 proteins involved in carbon metabolism and electron transfer, mitochondrial proteins were more abundant, while chloroplastic and cytoplasmic proteins (Calvin cycle, glycolysis, and AA biosynthesis pathways) were relatively less abundant (Fig. 6). This mirrors the higher R_d : $E_{O,max}$ ratio (Figs 1b, 3c). The TEM micrographs of *E. gracilis* (Figs 8, S7) also revealed a higher number of mitochondrial sections per cell in mixotrophy and larger individual chloroplastic section area in photoautotrophy (Table 1). This translated into a lower ratio (*c.* 60%) between total area of chloroplastic sections per cell relative to mitochondrial sections in mixotrophy (one-way ANOVA, $P < 0.01$) (Table 1). The absence of difference in the Chl content per cell suggests that the stroma is relatively larger in photoautotrophy. Among mitochondrial proteins, the ATP-dependent acetyl-CoA synthase (ACS, which converts acetate to acetyl-CoA) and bifunctional isocitrate lyase/malate synthase (ICL-MAS, which cleaves isocitrate into succinate and glyoxylate, and further synthesizes malate from glyoxylate and acetyl-CoA) were found to be more abundant in mixotrophy. This increase of ACS and ICL-MAS reflects a shift in the metabolism to assimilate acetate into 4C compounds by bypassing the two decarboxylating steps of the Krebs cycle. Several components of the respiratory chain CI, CII (succinate dehydrogenase), CIII, CIV and CV (F$_1$F$_O$ ATP synthase), along with the ADP/ATP translocase and the inorganic phosphate carrier, were also more

abundant in mixotrophy. This increase of ATP synthesis capacity by oxidative phosphorylation is in agreement with the higher respiratory rates in mixotrophy than in photoautotrophy (Figs 1a, 2, 4b), and may fuel anabolic reactions inside the mitochondria (e.g. for acetate assimilation), in the cytosol (e.g. neoglucogenesis) and/or in the chloroplast (e.g. for CO$_2$ assimilation). In *Chlorella sorokiniana*, mixotrophy was not associated with an increase in the transcript abundance of ICL and respiratory-chain components, but with an upregulation of glycolate oxidase and serine hydroxymethyltransferase (SHMT), two enzymes involved in photorespiration (Cecchin *et al.*, 2018). By contrast, mixotrophy in *E. gracilis* caused a decline in glycine cleavage system (P and H proteins) and SHMT. In *E. gracilis*, these proteins are present in the mitochondrial fractions (Hammond *et al.*, 2020) and participate in photorespiration by catalysing oxidative decarboxylation of glycine into serine. Only two photosynthetic electron transfer chain components (PSII H subunit and beta subunit of CF$_1$F$_O$ ATP synthase) were more abundant in mixotrophy (Fig. 6). These changes were not, however, accompanied by a difference in the $E_{O,max}$ between cells in mixotrophy and photoautotrophy (Figs 2, 4c,d) (provided that NaHCO$_3$ is added to the photoautotrophic cells during the measurement to limit RuBisCO oxygenase activity). On average, there is twice the number of pyrenoids (relative to the chloroplastic sections) in photoautotrophy than in mixotrophy or photoautotrophy + 5% CO$_2$ (Table 1). Although not statistically significant, this difference is supported by higher amounts of RuBisCO large subunit, Rubisco activase and RuBisCO large subunit-binding protein subunit beta specifically in photoautotrophy (Table S1). Altogether, this indicates that *E. gracilis* cells in photoautotrophy are more prone to photorespiration than when cells rely on an exogenous reduced carbon source (here acetate). Decarboxylating enzymes (isocitrate dehydrogenase and malic enzyme) are
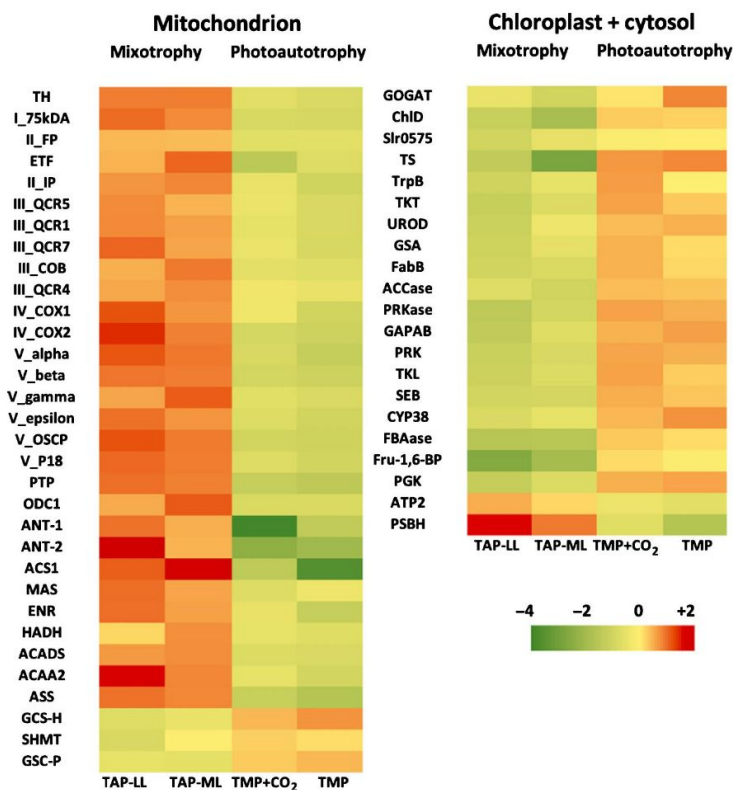
146

Fig. 6 Heat map generated from iTRAQ LC-MS quantitative proteomics analysis of *Euglena gracilis* cells in mixotrophic or photoautotrophic conditions. Only proteins participating in primary carbon metabolism and showing significant differences (log$_2$-fold change) in relative abundance between mixotrophic and photoautotrophic conditions are presented. Full datasets can be found in Supporting Information Tables S1, S2. Samples are arranged in columns, proteins in rows. Red shades, increased abundance; green shades, reduced abundance; yellow, median expression.

also more abundant specifically in TMP (Table S1). This may reflect the cellular need for CO$_2$ uptake and CO$_2$-concentrating mechanism activity (Giordano *et al.*, 2005). During photorespiration, RuBisCO oxygenase activity generates phosphoglycolate in addition to phosphoglycerate. Phosphoglycolate is converted to glycolate which can be imported into the mitochondrion in *E. gracilis* (Collins *et al.*, 1975). Glycolate dehydrogenase and glyoxylate-glutamate aminotransferase, two other photorespiratory enzymes which are usually localized in the peroxisome in other species, are also localized in the mitochondrion in *E. gracilis* and convert glycolate into glycine (Collins *et al.*, 1975; Horrum & Schwartzbach, 1980; Hammond *et al.*, 2020). Interestingly, glyoxylate-glutamate aminotransferase is not inhibited by AOAA (Horváth & Wanders, 1995). The lack of effect of AOAA addition on E_O specifically in photoautotrophy (Fig. 4c) is therefore in line with an active photorespiration, rather than an export of reducing equivalents through the malate shuttle that occurs in mixotrophy. Together with NADH produced by oxidation of glycine by glycine cleavage system and SHMT, glycolate oxidation may contribute directly to fuel mitochondrial electron transfer chain and ATP synthesis. This suggestion is in line with the observation that glycolate-dependent O$_2$ uptake by *E. gracilis* mitochondria is inhibited by AA or cyanide (Collins *et al.*, 1975). The negative impact of R_d

inhibition on E_O in photoautotrophic condition (Fig. 1a) could thus be caused by the loss of mitochondrial capacity to reoxidize NAD(P)H produced by photorespiratory enzymes inside the mitochondria. Concomitantly, the expected slowing down of the decarboxylative enzymes of the Krebs cycle and of photorespiration should limit the amount of CO$_2$ available for RuBisCO. A metabolic scheme summarizing how mitochondrial respiratory activity interacts with photosynthesis in mixotrophy and photoautotrophy in *E. gracilis* is presented in Fig. 7.

Membrane contact sites between chloroplasts and mitochondria

In diatoms, it has been suggested that the chloroplast–mitochondrion energetic coupling could be favoured by an intracellular placing of the mitochondrial network in close proximity to the single chloroplast (Prihoda *et al.*, 2012; Flori *et al.*, 2017). It was recently shown that the extent of chloroplast–mitochondrion physical interaction varies greatly among phytoplanktonic species of different lineages, being high in the diatom *P. tricornutum* and low in *Symbiodinium* sp. or *Nannochloropsis* sp. (Uwizeye *et al.*, 2021). In *E. gracilis*, TEM micrographs (Figs 8, S7) also showed that *c.* 60–80% of mitochondrial sections localize close to chloroplasts, often at margins of chloroplast sections,
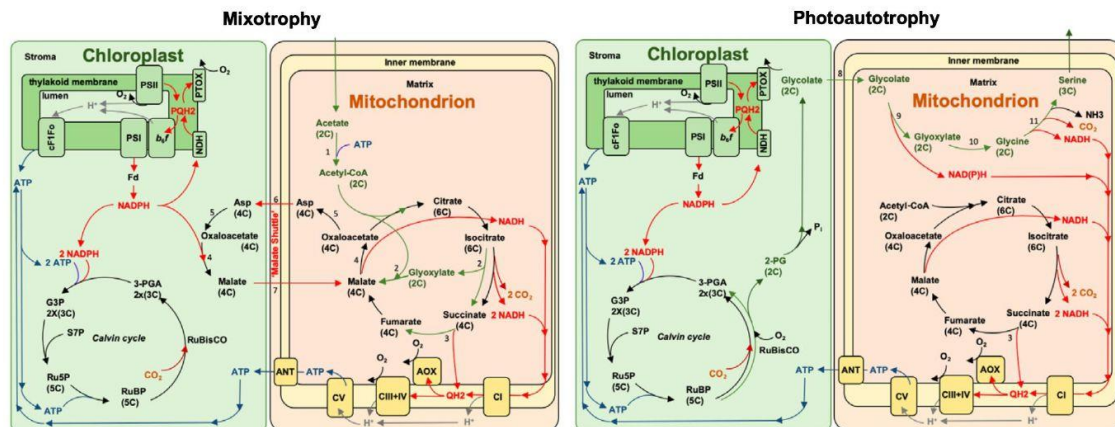
147

Fig. 7 Model of mitochondrial participation to photosynthesis regulation in mixotrophy and autotrophy in *Euglena gracilis*. Metabolic pathways reported in green are pathways with significant differences (log$_2$-fold change) in relative abundance between mixotrophic and photoautotrophic conditions (Fig. 5; Supporting Information Table S1). Red, blue, brown and grey arrows depict production/consumption of reducing equivalents (NAD(P)H, Quinone), ATP, carbon dioxide, and H$^+$, respectively. Only pathways mentioned in the text are depicted. ANT, adenine nucleotide translocator or ADP/ATP translocase; AOX, alternative oxidase; Asp, aspartate; G3P, glyceraldehyde 3-phosphate; Fd, ferredoxin; 2-PG, 2-phosphoglycolate; 3-PGA, 3-phosphoglycerate; NDH, putative NADPH plastoquinone reductase; PQH$_2$, plastoquinol; PTOX, plastidial alternative oxidase; QH$_2$, ubiquinol; Ru5P, ribulose-5-phosphate; RuBP, ribulose-1,5-bisphosphate; S7P, sedoheptulose 7-phosphate; 1, acetyl-CoA synthetase; 2, bifunctional isocitrate dehydrogenase / malate synthase; 3, succinate dehydrogenase (respiratory-chain complex II); 4, NAD(P)H-dependant malate dehydrogenase; 5, aspartate transaminase; 6, glutamate/aspartate transporter; 7 malate/oxoglutarate transporter; 8, glycolate/glycerate transporter; 9, glycolate dehydrogenase; 10, glutamate : glyoxylate aminotransferase; 11, glycine cleavage system + serine hydroxymethyltransferase.

with no difference among the mixotrophic, photoautotrophic and photoautotrophic + 5% CO$_2$ conditions (Table 1) (one-way ANOVA, $P = 0.18$). This confirmed previous observations that mitochondrial sections of *E. gracilis* tend to localize adjacent to the chloroplast in light-adapted cells (Wolken, 1967), but at the cell periphery in dark-adapted cells (Wolken, 1967; Pellegrini, 1980), which might relate to local concentration of oxygen (Wolken, 1967). The average distance between external membranes of chloroplasts and mitochondria was < 20–30 nm over 0.5 µm membrane segments (with no significant difference among conditions; one-way ANOVA, $P = 0.22$), and no outer membrane fusion between organelles was observed (Figs 8, S7). Such membrane contact sites (MCSs) have been described to create microdomains that favour exchange of molecules between endoplasmic reticulum and different organelles in the photosynthetic cell (Pérez-Sancho *et al.*, 2016). Thus, we suggest that ATP, ADP and reducing equivalents, along with other molecules (including, e.g., glycolate, glycerate, HCO$_3^-$), underlying the energetic coupling between respiration and photosynthesis, might be efficiently transported across MCSs between chloroplasts and mitochondria in *E. gracilis*. Protein tethering complexes are required for the establishment of MCSs between endoplasmic reticulum and different organelles (Helle *et al.*, 2013) but it is not known if chloroplast–mitochondrion MCSs also depend on such complexes in photosynthetic organisms. Because *E. gracilis* chloroplasts are surrounded by three membranes, rather than two as in green plants or four as in diatoms, it will be of interest to elucidate the configuration of the MCSs and the diversity of transporters.

Conclusions

Following the evolutionary course of *E. gracilis*, which consisted of the acquisition of photosynthesis by a heterotrophic ancestor (euglenozoan) from a eukaryotic donor (green alga), the activities of mitochondria and chloroplasts are intimately coupled. This ensures the cell has an export of reducing equivalents from the chloroplasts towards mitochondria and an import of ATP into the chloroplasts to sustain photosynthetic CO$_2$ fixation. Under the mixotrophic condition, the energetic coupling of *E. gracilis* is very similar to what is proposed to occur in diatoms, for which the main driver of this interaction is thought to be the adjustment of the ATP/NADPH ratio in the chloroplast (Bailleul *et al.*, 2015). By contrast, other photosynthetic organisms (and especially those bearing green plastids), may rely primarily on AEPs located in the chloroplasts for controlling the cellular ATP/NADPH budget (Scheibe, 2004; Roberty *et al.*, 2014; Raven *et al.*, 2020). In the green alga *C. reinhardtii*, mitochondrial cooperation supplies extra ATP for photosynthesis when the chloroplast capacity of AEPs to supply ATP for CO$_2$ assimilation is compromised (Dang *et al.*, 2014). Information on AEPs in *E. gracilis* in the literature is, however, still scarce (e.g. Shimakawa *et al.*, 2017). The linear relationship between PSI relative electron transport rate and PSI + PSII photochemical rate, their insensitivity to AA (Fig. S8a,b), and the very low photochemical rate (2.5 ± 1.4 s^{-1}) in the presence of DCMU suggest, however, that the cyclic electron flow around PSI is not prominent in *E. gracilis*. Similarly, the linear relationship between PSII relative electron transport rate and E_O (Fig. S8c) suggests that cyclic electron flow
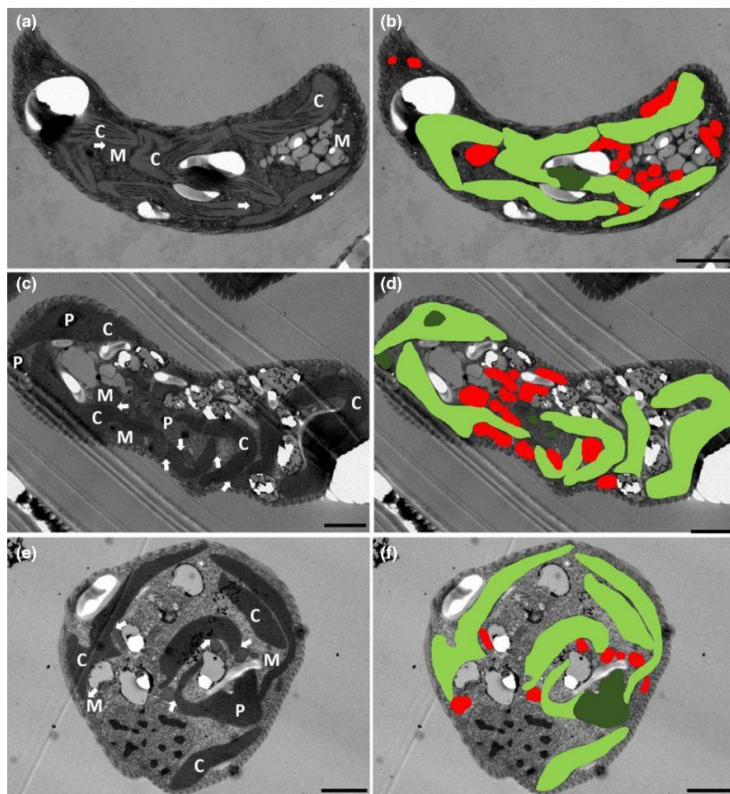
Fig. 8 Transmission electron micrographs illustrating subcellular organization of *Euglena gracilis* cultured in mixotrophy (a, b), photoautotrophy (c, d) and photoautotrophy + 5% CO_2 (e, f). Bars, 2 μm. (a, c, e) Arrows show the mitochondrial-chloroplastic contacts; C, chloroplast; M, mitochondrion; P, pyrenoid. (b, d, f) Cell compartments are highlighted in colour (chloroplasts in light green, pyrenoids in dark green and mitochondria in red).

around PSII does not occur. Overall, these findings reinforce the idea that the energetic coupling between chloroplasts and mitochondria is crucial in *E. gracilis*. The mechanisms whereby the energetic coupling between photosynthesis and respiration occurs vary in relation to the trophic state of the cell (mixotrophic vs photoautotrophic). Under the photoautotrophic condition, the ATP demand for photorespiration and the CO_2-concentrating mechanism takes precedence over the chloroplastic NADPH excess. In *E. gracilis*, as in diatoms, the evolutionary and physiological advantages and/or disadvantages of relying mainly on the chloroplast to mitochondrion coupling are not clear. Such strong chloroplast–mitochondrion interdependence could make these organisms sensitive to any impairment of the respiratory activity, which would cause negative consequences on the photosynthetic apparatus as well. Cell ability to ensure that photosynthesis–respiration coupling is maintained through plastic metabolic responses (as we have shown for mixotrophic vs photoautotrophic conditions in *E. gracilis*) is therefore key to guarantee cell functioning. In addition, the presence of AEP in the chloroplast could help cells to compensate for possible respiratory impairments. Further studies are required to establish the role of AEPs (if any) in the regulation of the cellular ATP/NADPH budget (e.g. during conditions impairing respiration) in species such as *E. gracilis* or *P. tricornutum* (diatom), characterized by having photosynthesis–respiration coupling as a major regulator of photosynthesis.

Author contributions

GG, FVdL, DB, MP and PC conceived the research. PM, HD, EP and JC carried out the proteomics analysis. MT performed the TEM analysis. GG, FVdL, EP, MP and PC performed the physiological analyses and analysed data. MP and PC wrote the manuscript. MP and PC share senior authorship. GG and FVdL

contributed equally to this work. All authors read and approved the manuscript.

ORCID

Denis Baurain (iD) https://orcid.org/0000-0003-2388-6185
Pierre Cardol (iD) https://orcid.org/0000-0001-9799-0546
Gwenaëlle Gain (iD) https://orcid.org/0000-0002-3871-3300
Pierre Morsomme (iD) https://orcid.org/0000-0001-7780-7230
Mattia Pierangelini (iD) https://orcid.org/0000-0002-6166-8472

Data availability

The data that support the findings of this study are available from the corresponding authors upon reasonable request. The data that supports the proteomics are available in the supplementary material.

References

Allen AE, LaRoche J, Maheswari U, Lommer M, Schauer N, Lopez PJ, Finazzi G, Fernie AR, Bowler C. 2008. Whole-cell response of the pennate diatom *Phaeodactylum tricornutum* to iron starvation. *Proceedings of the National Academy of Sciences, USA* **105**: 10438–10443.

Allen JF. 2002. Photosynthesis of ATP-electrons, proton pumps, rotors, and poise. *Cell* **110**: 273–276.

Atkin OK, Tjoelker MG. 2003. Thermal acclimation and the dynamic response of plant respiration to temperature. *Trends in Plant Science* **8**: 343–351.

Bailleul B, Berne N, Murik O, Petroutsos D, Prihoda J, Tanaka A, Villanova V, Bligny R, Flori S, Falconet D *et al.* 2015. Energetic coupling between plastids and mitochondria drives CO₂ assimilation in diatoms. *Nature* **524**: 366–369.

Bailleul B, Cardol P, Breyton C, Finazzi G. 2010. Electrochromism: a useful probe to study algal photosynthesis. *Photosynthesis Research* **106**: 179–189.

Bennett MS, Wiegert KE, Triemer RE. 2012. Comparative chloroplast genomics between *Euglena viridis* and *Euglena gracilis* (Euglenophyta). *Phycologia* **51**: 711–718.

Berry J, Bjorkman O. 1980. Photosynthetic response and adaptation to temperature in higher plants. *Annual Review of Plant Physiology* **31**: 491–543.

Bradford MM. 1976. A rapid and sensitive method for the quantitation of microgram quantities of protein utilizing the principle of protein-dye binding. *Analytical Biochemistry* **72**: 248–254.

Cardol P, Alric J, Girard-Bascou J, Franck F, Wollman FA, Finazzi G. 2009. Impaired respiration discloses the physiological significance of state transitions in *Chlamydomonas*. *Proceedings of the National Academy of Sciences, USA* **106**: 15979–15984.

Cardol P, Forti G, Finazzi G. 2011. Regulation of electron transport in microalgae. *Biochimica et Biophysica Acta (BBA)–Bioenergetics* **1807**: 912–918.

Cardol P, Gloire G, Havaux M, Remacle C, Matagne R, Franck F. 2003. Photosynthesis and state transitions in mitochondrial mutants of *Chlamydomonas reinhardtii* affected in respiration. *Plant Physiology* **133**: 2010–2020.

Castro-Guerrero NA, Krab K, Moreno-Sánchez R. 2004. The alternative respiratory pathway of *Euglena* mitochondria. *Journal of Bioenergetics and Biomembranes* **36**: 459–469.

Cecchin M, Benfatto S, Griggio F, Mori A, Cazzaniga S, Vitulo N, Delledonne M, Ballottari M. 2018. Molecular basis of autotrophic vs mixotrophic growth in *Chlorella sorokiniana*. *Scientific Reports* **8**: 1–13.

Chapman SP, Paget CM, Johnson GN, Schwartz JM. 2015. Flux balance analysis reveals acetate metabolism modulates cyclic electron flow and alternative glycolytic pathways in *Chlamydomonas reinhardtii*. *Frontiers in Plant Science* **6**: 474.

Collins N, Brown RH, Merrett MJ. 1975. Oxidative phosphorylation during glycollate metabolism in mitochondria from phototrophic *Euglena gracilis*. *Biochemical Journal* **150**: 373–377.

Cornell NW, Zuurendonk PF, Kerich MJ, Straight CB. 1984. Selective inhibition of alanine aminotransferase and aspartate aminotransferase in rat hepatocytes. *Biochemical Journal* **220**: 707–716.

Dang KV, Plet J, Tolleter D, Jokel M, Cuiné S, Carrier P, Auroy P, Richaud P, Johnson X, Alric J *et al.* 2014. Combined increases in mitochondrial cooperation and oxygen photoreduction compensate for deficiency in cyclic electron flow in *Chlamydomonas reinhardtii*. *Plant Cell* **26**: 3036–3050.

Dellero Y, Jossier M, Schmitz J, Maurino VG, Hodges M. 2016. Photorespiratory glycolate–glyoxylate metabolism. *Journal of Experimental Botany* **67**: 3041–3052.

Falkowski PG, Dubinsky Z, Wyman K. 1985. Growth-irradiance relationships in phytoplankton. *Limnology and Oceanography* **30**: 311–321.

Feikema WO, Marosvölgyi MA, Lavaud J, Van Gorkom HJ. 2006. Cyclic electron transfer in photosystem II in the marine diatom *Phaeodactylum tricornutum*. *Biochimica et Biophysica Acta (BBA)–Bioenergetics* **1757**: 829–834.

Flori S, Jouneau PH, Bailleul B, Gallet B, Estrozi LF, Moriscot C, Bastien O, Eicke S, Schober A, Bártulos CR *et al.* 2017. Plastid thylakoid architecture optimizes photosynthesis in diatoms. *Nature Communications* **8**: 1–9.

Geider RJ, Osborne BA. 1989. Respiration and microalgal growth: a review of the quantitative relationship between dark respiration and growth. *New Phytologist* **112**: 327–341.

Giordano M, Beardall J, Raven JA. 2005. CO₂ concentrating mechanisms in algae: mechanisms, environmental modulation, and evolution. *Annual Review of Plant Biology* **56**: 99–131.

Gotoh E, Matsumoto M, Ogawa KI, Kobayashi Y, Tsuyama M. 2010. A qualitative analysis of the regulation of cyclic electron flow around photosystem I from the post-illumination chlorophyll fluorescence transient in *Arabidopsis*: a new platform for the in vivo investigation of the chloroplast redox state. *Photosynthesis Research* **103**: 111–123.

Hammond MJ, Nenarokova A, Butenko A, Zoltner M, Dobáková EL, Field MC, Lukeš J. 2020. A uniquely complex mitochondrial proteome from *Euglena gracilis*. *Molecular Biology and Evolution* **37**: 2173–2191.

Helle SC, Kanfer G, Kolar K, Lang A, Michel AH, Kornmann B. 2013. Organization and function of membrane contact sites. *Biochimica et Biophysica Acta (BBA)–Molecular Cell Research* **1833**: 2526–2541.

Horrum MA, Schwartzbach SD. 1980. Nutritional regulation of organelle biogenesis in *Euglena*: repression of chlorophyll and NADP-glyceraldehyde-3-phosphate dehydrogenase synthesis. *Plant Physiology* **65**: 382–386.

Horváth VAP, Wanders RJ. 1995. Aminooxy acetic acid: a selective inhibitor of alanine: glyoxylate aminotransferase and its use in the diagnosis of primary hyperoxaluria type I. *Clinica Chimica Acta* **243**: 105–114.

Iglesias-Prieto R, Matta JL, Robins WA, Trench RK. 1992. Photosynthetic response to elevated temperature in the symbiotic dinoflagellate *Symbiodinium microadriaticum* in culture. *Proceedings of the National Academy of Sciences, USA* **89**: 10302–10305.

Jackson C, Knoll AH, Chan CX, Verbruggen H. 2018. Plastid phylogenomics with broad taxon sampling further elucidates the distinct evolutionary origins and timing of secondary green plastids. *Scientific Reports* **8**: 1–10.

Joliot P, Joliot A. 2008. Quantification of the electrochemical proton gradient and activation of ATP synthase in leaves. *Biochimica et Biophysica Acta (BBA)–Bioenergetics* **1777**: 676–683.

Josse EM, Alcaraz JP, Labouré AM, Kuntz M. 2003. In vitro characterization of a plastid terminal oxidase (PTOX). *European Journal of Biochemistry* **270**: 3787–3794.

Kamalanathan M, Dao LHT, Chaisutyakorna P, Gleadow R, Beardall J. 2017. Photosynthetic physiology of *Scenedesmus* sp. (Chlorophyceae) under photoautotrophic and molasses-based heterotrophic and mixotrophic conditions. *Phycologia* **56**: 666–674.

Kammers K, Cole RN, Tiengwe C, Ruczinski I. 2015. Detecting significant changes in protein abundance. *EuPA Open Proteomics* **7**: 11–19.

Karsten U, Holzinger A. 2012. Light, temperature, and desiccation effects on photosynthetic activity, and drought-induced ultrastructural changes in the green alga *Klebsormidium dissectum* (Streptophyta) from a high alpine soil crust. *Microbial Ecology* **63**: 51–63.

Kaye Y, Huang W, Clowez S, Saroussi S, Idoine A, Sanz-Luque E, Grossman AR. 2019. The mitochondrial alternative oxidase from *Chlamydomonas*

reinhardtii enables survival in high light. *Journal of Biological Chemistry* **294**: 1380–1395.

Krnáčová K, Rýdlová I, Vinarčíková M, Krajčovič J, Vesteg M, Horváth A. 2015. Characterization of oxidative phosphorylation enzymes in *Euglena gracilis* and its white mutant strain W$_{gm}$ZOfIL. *FEBS Letters* **589**: 687–694.

Larkum AW, Lockhart PJ, Howe CJ. 2007. Shopping for plastids. *Trends in Plant Science* **12**: 189–195.

McDonald AE, Ivanov AG, Bode R, Maxwell DP, Rodermel SR, Hüner NP. 2011. Flexibility in photosynthetic electron transport: the physiological role of plastoquinol terminal oxidase (PTOX). *Biochimica et Biophysica Acta (BBA)– Bioenergetics* **1807**: 954–967.

Miranda-Astudillo HV, Yadav KNS, Colina-Tenorio L, Bouillenne F, Degand H, Morsomme P, Boekema EJ, Cardol P. 2018. The atypical subunit composition of respiratory complexes I and IV is associated with original extra structural domains in *Euglena gracilis*. *Scientific Reports* **8**: 1–13.

Murik O, Tirichine L, Prihoda J, Thomas Y, Araújo WL, Allen AE, Fernie AR, Bowler C. 2019. Downregulation of mitochondrial alternative oxidase affects chloroplast function, redox status and stress response in a marine diatom. *New Phytologist* **221**: 1303–1316.

Noguchi K, Yoshida K. 2008. Interaction between photosynthesis and respiration in illuminated leaves. *Mitochondrion* **8**: 87–99.

Novák Vanclová AM, Zoltner M, Kelly S, Soukal P, Záhonová K, Füssy Z, Ebenezer TE, Lacová Dobáková E, Eliáš M, Lukeš J *et al.* 2020. Metabolic quirks and the colourful history of the *Euglena gracilis* secondary plastid. *New Phytologist* **225**: 1578–1592.

Padfield D, Yvon-Durocher G, Buckling A, Jennings S, Yvon-Durocher G. 2016. Rapid evolution of metabolic traits explains thermal adaptation in phytoplankton. *Ecology Letters* **19**: 133–142.

Pellegrini M. 1980. Three-dimensional reconstruction of organelles in *Euglena gracilis* Z.I. Qualitative and quantitative changes of chloroplasts and mitochondrial reticulum in synchronous photoautotrophic culture. *Journal of Cell Science* **43**: 137–166.

Perez E, Lapaille M, Degand H, Cilibrasi L, Villavicencio-Queijeiro A, Morsomme P, González-Halphen D, Field MC, Remacle C, Baurain D *et al.* 2014. The mitochondrial respiratory chain of the secondary green alga *Euglena gracilis* shares many additional subunits with parasitic Trypanosomatidae. *Mitochondrion* **19**: 338–349.

Pérez-Sancho J, Tilsner J, Samuels AL, Botella MA, Bayer EM, Rosado A. 2016. Stitching organelles: organization and function of specialized membrane contact sites in plants. *Trends in Cell Biology* **26**: 705–717.

Pierangelini M, Glaser K, Mikhailyuk T, Karsten U, Holzinger A. 2019. Light and dehydration but not temperature drive photosynthetic adaptations of basal streptophytes (*Hormidiella*, *Streptosarcina* and *Streptofilum*) living in terrestrial habitats. *Microbial Ecology* **77**: 380–393.

Pierangelini M, Thiry M, Cardol P. 2020. Different levels of energetic coupling between photosynthesis and respiration do not determine the occurrence of adaptive responses of Symbiodiniaceae to global warming. *New Phytologist* **228**: 855–868.

Polukhina I, Fristedt R, Dinc E, Cardol P, Croce R. 2016. Carbon supply and photoacclimation cross talk in the green alga *Chlamydomonas reinhardtii*. *Plant Physiology* **172**: 1494–1505.

Powell DW, Weaver CM, Jennings JL, McAfee KJ, He Y, Weil PA, Link AJ. 2004. Cluster analysis of mass spectrometry data reveals a novel component of SAGA. *Molecular and Cellular Biology* **24**: 7249–7259.

Prelle LR, Graiff A, Gründling-Pfaff S, Sommer V, Kuriyama K, Karsten U. 2019. Photosynthesis and respiration of Baltic Sea benthic diatoms to changing environmental conditions and growth responses of selected species as affected by an adjacent peatland (Hütelmoor). *Frontiers in Microbiology* **10**: 1500.

Prihoda J, Tanaka A, de Paula WB, Allen JF, Tirichine L, Bowler C. 2012. Chloroplast-mitochondria cross-talk in diatoms. *Journal of Experimental Botany* **63**: 1543–1557.

Raghavendra AS, Padmasree K. 2003. Beneficial interactions of mitochondrial metabolism with photosynthetic carbon assimilation. *Trends in Plant Science* **8**: 546–553.

Raven JA, Beardall J. 2016. Dark respiration and organic carbon loss. In: Borowitzka M, Beardall J, Raven J, eds. *The physiology of microalgae. Developments in applied phycology*. Cham, Switzerland: Springer, 129–140.

Raven JA, Beardall J, Quigg A. 2020. Light-driven oxygen consumption in the water-water cycles and photorespiration, and light stimulated mitochondrial respiration. In: Larkum A, Grossman A, Raven J, eds. *Photosynthesis in algae: biochemical and physiological mechanisms*. Cham, Switzerland: Springer, 161–178.

Remacle C, Cardol P, Coosemans N, Gaisne M, Bonnefoy N. 2006. High-efficiency biolistic transformation of *Chlamydomonas* mitochondria can be used to insert mutations in complex I genes. *Proceedings of the National Academy of Sciences, USA* **103**: 4771–4776.

Ritchie ME, Phipson B, Wu DI, Hu Y, Law CW, Shi W, Smyth GK. 2015. limma powers differential expression analyses for RNA-sequencing and microarray studies. *Nucleic Acids Research* **43**: e47.

Ritchie RJ. 2006. Consistent sets of spectrophotometric chlorophyll equations for acetone, methanol and ethanol solvents. *Photosynthesis Research* **89**: 27–41.

Roberty S, Bailleul B, Berne N, Franck F, Cardol P. 2014. PSI Mehler reaction is the main alternative photosynthetic electron pathway in *Symbiodinium* sp., symbiotic dinoflagellates of cnidarians. *New Phytologist* **204**: 81–91.

Schaum CE, Barton S, Bestion E, Buckling A, Garcia-Carreras B, Lopez P, Lowe L, Pawar S, Smirnoff N, Trimmer M *et al.* 2017. Adaptation of phytoplankton to a decade of experimental warming linked to increased photosynthesis. *Nature Ecology & Evolution* **1**: 1–7.

Scheibe R. 2004. Malate valves to balance cellular energy supply. *Physiologia Plantarum* **120**: 21–26.

Shen W, Wei Y, Dauk M, Zheng Z, Zou J. 2003. Identification of a mitochondrial glycerol-3-phosphate dehydrogenase from *Arabidopsis thaliana*: evidence for a mitochondrial glycerol-3-phosphate shuttle in plants. *FEBS Letters* **536**: 92–96.

Shimakawa G, Matsuda Y, Nakajima K, Tamoi M, Shigeoka S, Miyake C. 2017. Diverse strategies of O$_2$ usage for preventing photo-oxidative damage under CO$_2$ limitation during algal photosynthesis. *Scientific Reports* **7**: 1–9.

Szopinska A, Degand H, Hochstenbach JF, Nader J, Morsomme P. 2011. Rapid response of the yeast plasma membrane proteome to salt stress. *Molecular & Cellular Proteomics* **10**: M111-009589.

Treves H, Raanan H, Kedem I, Murik O, Keren N, Zer H, Berkowicz SM, Giordano M, Norici A, Shotland Y *et al.* 2016. The mechanisms whereby the green alga *Chlorella ohadii*, isolated from desert soil crust, exhibits unparalleled photodamage resistance. *New Phytologist* **210**: 1229–1243.

Turmel M, Gagnon MC, O'Kelly CJ, Otis C, Lemieux C. 2009. The chloroplast genomes of the green algae *Pyramimonas*, *Monomastix*, and *Pycnococcus* shed new light on the evolutionary history of prasinophytes and the origin of the secondary chloroplasts of euglenids. *Molecular Biology and Evolution* **26**: 631–648.

Uwizeye C, Decelle J, Jouneau P, Flori S, Gallet B, Keck JB, Dal Bo D, Moriscot C, Seydoux C, Chevalier F *et al.* 2021. Morphological bases of phytoplankton energy management and physiological responses unveiled by 3D subcellular imaging. *Nature Communications* **12**: 1–12.

Vaudel M, Burkhart JM, Zahedi RP, Oveland E, Berven FS, Sickmann A, Martens L, Barsnes H. 2015. PeptideShaker enables reanalysis of MS-derived proteomics data sets. *Nature Biotechnology* **33**: 22–24.

Wessel DM, Flügge UI. 1984. A method for the quantitative recovery of protein in dilute solution in the presence of detergents and lipids. *Analytical Biochemistry* **138**: 141–143.

Wilken S, Schuurmans JM, Matthijs HC. 2014. Do mixotrophs grow as photoheterotrophs? Photophysiological acclimation of the chrysophyte *Ochromonas danica* after feeding. *New Phytologist* **204**: 882–889.

Wolken JJ. 1967. *Euglena: an experimental organism for biochemical and biophysical studies, 2nd edn.* New York, NY, USA: Appleton-Century-Crofts.

Yadav KS, Miranda-Astudillo HV, Colina-Tenorio L, Bouillenne F, Degand H, Morsomme P, González-Halphen D, Boekema EJ, Cardol P. 2017. Atypical composition and structure of the mitochondrial dimeric ATP synthase from *Euglena gracilis*. *Biochimica et Biophysica Acta (BBA)–Bioenergetics* **1858**: 267–275.

Supporting Information

Additional Supporting Information may be found online in the Supporting Information section at the end of the article.

151

Fig. S1 Electrochromic shift spectrum and linearity in *Euglena gracilis* cultivated mixotrophically and photoautotrophically.

Fig. S2 Impact of inhibitors on Chl fluorescence in *Euglena gracilis* cultured in mixotrophy and in photoautotrophy.

Fig. S3 NPQ in *Euglena gracilis* cells grown in mixotrophy or in photoautotrophy.

Fig. S4 Impact of octyl gallate (OG) and salicylhydroxamic acid (SHAM) on dark respiration (R_d) in *Euglena gracilis* cultivated in mixotrophic and photoautotrophic conditions.

Fig. S5 Impacts of the inhibitors of mitochondrial respiratory complexes (I, III, IV), ATP synthase and AOX on respiratory (R_d) and photosynthetic gross oxygen evolution (E_O) rates for *Euglena gracilis* cultivated in mixotrophic and photoautotrophic conditions.

Fig. S6 (a) End of exponential phase of batch cultures of *Euglena gracilis* cultivated in mixotrophic (TAP) and photoautotrophic (TMP) conditions, and in the presence of rotenone (Rot, 100 μM) or antimycin A (AA, 10 μM).

Fig. S7 Transmission electron micrographs illustrating subcellular organization of *Euglena gracilis* cultured in mixotrophy, photoautotrophy and photoautotrophy + 5% CO_2.

Fig. S8 Relationship between PSI relative electron transport rate and PSI + PSII photochemical rate, and relationship between PSII relative electron transport rate and E_O in *Euglena gracilis* cultivated in mixotrophic and photoautotrophic conditions.

Method S1 Detailed procedure of the proteomics analysis.

Table S1 Table containing the 544 proteins identified in *Euglena gracilis*, including several enzymes involved in the central carbon metabolism pathways.

Table S2 Table containing 112 proteins showing significant $\log_2$-fold increase or decrease (in ratio of normalized protein abundance) depending on the trophic state in *Euglena gracilis*.

Please note: Wiley Blackwell are not responsible for the content or functionality of any Supporting Information supplied by the authors. Any queries (other than missing material) should be directed to the *New Phytologist* Central Office.

About *New Phytologist*

- *New Phytologist* is an electronic (online-only) journal owned by the New Phytologist Foundation, a **not-for-profit organization** dedicated to the promotion of plant science, facilitating projects from symposia to free access for our Tansley reviews and Tansley insights.

- Regular papers, Letters, Viewpoints, Research reviews, Rapid reports and both Modelling/Theory and Methods papers are encouraged. We are committed to rapid processing, from online submission through to publication 'as ready' via *Early View* – our average time to decision is <26 days. There are **no page or colour charges** and a PDF version will be provided for each article.

- The journal is available online at Wiley Online Library. Visit **www.newphytologist.com** to search the articles and register for table of contents email alerts.

- If you have any questions, do get in touch with Central Office (np-centraloffice@lancaster.ac.uk) or, if it is more convenient, our USA Office (np-usaoffice@lancaster.ac.uk)

- For submission instructions, subscription and all the latest information visit **www.newphytologist.com**

152

ANNEX B   Extended ECS spectra of Figure 4a from Chapter 3

The ECS spectra from *Cladocopium* in symbiosis with *M. papua* and in the gastric cavity of *E. medusivora* after 24 h of feeding, was reported in the Figure 4a of the Chapter 3. This data was published without the ECS values at 546 and 554 nm, that are included in this Figure below. The data was published like this because we were interested at showing the development of ECS at 510 nm as an indicative of the energization of the thylakoid membranes upon a saturating flash of light.
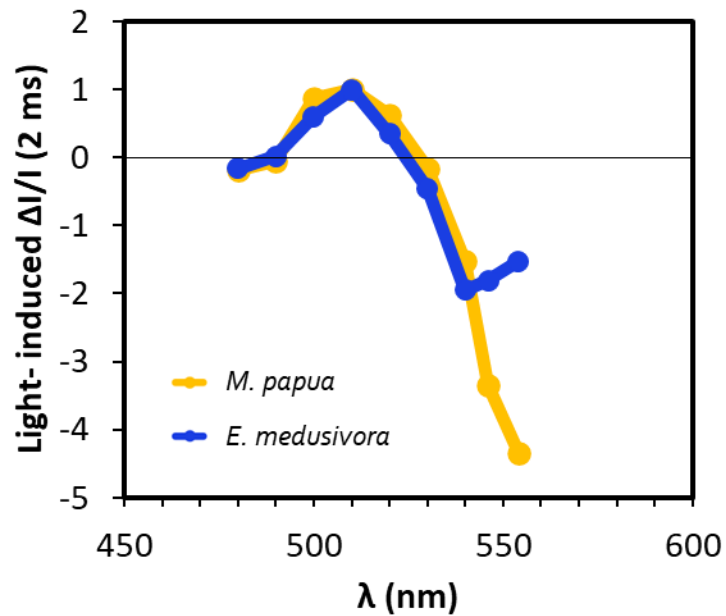

Figure 1. Electrochromic shift (ECS) spectra acquired upon 4 ms of illumination, from *Cladocopium* in symbiosis with *M. papua* and in the gastric cavity of *E. medusivora* after 24 h of feeding.

REFERENCES

Abrego D., Ulstrup K.E., Willis B.L. & Van Oppen M.J.H. (2008) Species-specific interactions between algal endosymbionts and coral hosts define their bleaching response to heat and light stress. *Proceedings of the Royal Society B: Biological Sciences* **275**, 2273–2282.

Aihara Y., Maruyama S., Baird A.H., Iguchi A., Takahashi S. & Minagawa J. (2019) Green fluorescence from cnidarian hosts attracts symbiotic algae. *Proceedings of the National Academy of Sciences of the United States of America* **116**, 2118–2123.

Aihara Y., Takahashi S. & Minagawa J. (2016) Heat induction of cyclic electron flow around photosystem I in the symbiotic dinoflagellate *Symbiodinium. Plant Physiology* **171**, 522–529.

Alboresi A., Storti M. & Morosinotto T. (2019) Balancing protection and efficiency in the regulation of photosynthetic electron transport across plant evolution. *New Phytologist* **221**, 105–109.

Alric J. (2014) Redox and ATP control of photosynthetic cyclic electron flow in Chlamydomonas reinhardtii: (II) Involvement of the PGR5-PGRL1 pathway under anaerobic conditions. *Biochimica et Biophysica Acta - Bioenergetics* **1837**, 825–834.

Alric J. (2015) The plastoquinone pool, poised for cyclic electron flow? *Frontiers in Plant Science* **6**, 1–4.

Anderson S.L. & Burris J.E. (1987) Role of glutamine synthetase in ammonia assimilation by symbiotic marine dinoflagellates (zooxanthellae). *Marine Biology* **94**, 451–458.

Aranda M., Li Y., Liew Y.J., Baumgarten S., Simakov O., Wilson M.C., … Voolstra C.R. (2016) Genomes of coral dinoflagellate symbionts highlight evolutionary adaptations conducive to a symbiotic lifestyle. *Scientific Reports* **6**, 1–15.

Arossa S., Klein S.G., Parry A.J., Aranda M. & Duarte C.M. (2022) Assessing Magnesium Chloride as a Chemical for Immobilization of a Symbiotic Jellyfish (Cassiopea sp.). *Frontiers in Marine Science* **9**, 1–9.

Arrigoni R., Benzoni F., Terraneo T.I., Caragnano A. & Berumen M.L. (2016) Recent origin and semi-permeable species boundaries in the Scleractinian coral genus *Stylophora* from the Red Sea. *Scientific Reports* **6**.

Asada K., Allen J., Foyer C.H. & Matthijs H.C.P. (2000) The water-water cycle as alternative photon and electron sinks. *Philosophical Transactions of the Royal Society B: Biological Sciences* **355**, 1419–1431.

Bachman S. & Muller-Parker G. (2007) Viable algae released by the seastar *Dermasterias imbricata* feeding on the symbiotic sea anemone *Anthopleura elegantissima*. *Marine Biology* **150**, 369–375.

Bailleul B., Berne N., Murik O., Petroutsos D., Prihoda J., Tanaka A., … Finazzi G. (2015) Energetic coupling between plastids and mitochondria drives CO 2 assimilation in diatoms. *Nature* **524**, 366–369.

Bailleul B., Cardol P., Breyton C. & Finazzi G. (2010) Electrochromism: A useful probe to study algal photosynthesis. *Photosynthesis Research* **106**, 179–189.

Baker N.R. (2008) Chlorophyll fluorescence: A probe of photosynthesis in vivo. *Annual Review of Plant Biology* **59**, 89–113.

Barbeitos M.S., Romano S.L. & Lasker H.R. (2010) Repeated loss of coloniality and symbiosis in Scleractinian corals. *Proceedings of the National Academy of Sciences* **107**, 11877–11882.

Barbrook A.C., Voolstra C.R. & Howe C.J. (2014) The chloroplast genome of a *Symbiodinium* sp. clade C3 isolate. *Protist* **165**, 1–13.

Barott K.L., Venn A.A., Perez S.O., Tambutteeé S., Tresguerres M. & Somero G.N. (2015) Coral host cells acidify symbiotic algal microenvironment to promote photosynthesis. *Proceedings of the National Academy of Sciences of the United States of America* **112**, 607–612.

Barton J.A., Willis B.L. & Hutson K.S. (2017) Coral propagation: a review of techniques for ornamental trade and reef restoration. *Reviews in Aquaculture* **9**, 238–256.

Belgio E., Santabarbara S., Bína D., Trsková E., Herbstová M., Kaňa R., … Prášil O. (2017) High photochemical trapping efficiency in Photosystem I from the red clade algae *Chromera velia* and *Phaeodactylum tricornutum*. *Biochimica et Biophysica Acta - Bioenergetics* **1858**, 56–63.

Berges J.A., Charlebois D.O., Mauzerall D.C. & Falkowski P.G. (1996) Differential effects of nitrogen limitation on photosynthetic efficiency of photosystems I and II in microalgae. *Plant Physiology* **110**, 689–696.

Berner T., Baghdasarian G. & Muscatine L. (1993) Repopulation of a sea anemone with symbiotic dinoflagellates: Analysis by in vivo fluorescence. *Journal of Experimental Marine Biology and Ecology* **170**, 145–158.

Bertucci A., Tambutté É., Tambutté S., Allemand D. & Zoccola D. (2010) Symbiosis-dependent gene expression in coral-dinoflagellate association: Cloning and characterization of a P-type H+-ATPase gene. *Proceedings of the Royal Society B: Biological Sciences* **277**, 87–95.

Bhagooli R. (2013) Inhibition of Calvin-Benson cycle suppresses the repair of photosystem II in *Symbiodinium*: Implications for coral bleaching. *Hydrobiologia* **714**, 183–190.

Bi Y., Wang F. & Zhang W. (2019) Omics analysis for dinoflagellates biology research. *Microorganisms* **7**, 1–25.

Biel K.Y., Gates R.D. & Muscatine L. (2007) Effects of free amino acids on the photosynthetic carbon metabolism of symbiotic dinoflagellates. *Russian Journal of Plant Physiology* **54**, 171–183.

Bieri T., Onishi M., Xiang T., Grossman A.R. & Pringle J.R. (2016) Relative contributions of various cellular mechanisms to loss of algae during cnidarian bleaching. *PLoS ONE* **11**, 1–24.

Biquand E., Okubo N., Aihara Y., Rolland V., Hayward D.C., Hatta M., … Takahashi S. (2017) Acceptable symbiont cell size differs among cnidarian species and may limit symbiont diversity. *ISME Journal* **11**, 1702–1712.

Boldt L., Yellowlees D. & Leggat W. (2012) Hyperdiversity of Genes Encoding Integral Light-Harvesting Proteins in the Dinoflagellate *Symbiodinium* sp. *PLoS ONE* **7**, 1–13.

Bollati E., D'Angelo C., Alderdice R., Pratchett M., Ziegler M. & Wiedenmann J. (2020) Optical Feedback Loop Involving Dinoflagellate Symbiont and Scleractinian Host Drives Colorful Coral Bleaching. *Current Biology* **30**, 2433-2445.e3.

Bonente G., Pippa S., Castellano S., Bassi R. & Ballottari M. (2012) Acclimation of Chlamydomonas reinhardtii to different growth irradiances. *Journal of Biological Chemistry* **287**, 5833–5847.

Bosch T.C.G. & Miller D.J. (2016) The holobiont imperative: Perspectives from early emerging animals. *The Holobiont Imperative: Perspectives from Early Emerging Animals*, 1–155.

Brading P., Warner M.E., Smith D.J. & Suggett D.J. (2013) Contrasting modes of inorganic carbon acquisition amongst *Symbiodinium* (Dinophyceae) phylotypes. *New Phytologist* **200**, 432–442.

Brown B.E. (1997) Coral bleaching: Causes and consequences. *Coral Reefs* **16**, 129–138.

Brown B.E., Ambarsari I., Warner M.E., Fitt W.K., Dunne R.P., Gibb S.W. & Cummings D.G. (1999) Diurnal changes in photochemical efficiency and xanthophyll concentrations in shallow water reef corals : evidence for photoinhibition and photoprotection. *Coral Reefs* **18**, 99–105.

Burlacot A., Dao O., Auroy P., Cuiné S., Li-Beisson Y. & Peltier G. (2022) Alternative photosynthesis pathways drive the algal CO2-concentrating mechanism. *Nature* **605**, 366–371.

Burriesci M.S., Raab T.K. & Pringle J.R. (2012) Evidence that glucose is the major transferred metabolite in dinoflagellate-cnidarian symbiosis. *Journal of Experimental Biology* **215**, 3467–3477.

Byler K.A., Carmi-Veal M., Fine M. & Goulet T.L. (2013) Multiple Symbiont Acquisition Strategies as an Adaptive Mechanism in the Coral *Stylophora pistillata*. *PLoS ONE* **8**.

Camaya A.P. (2020) Stages of the symbiotic zooxanthellae–host cell division and the dynamic role of coral nucleus in the partitioning process: a novel observation elucidated by electron microscopy. *Coral Reefs* **39**, 929–938.

Campoy A.N., Addamo A.M., Machordom A., Meade A., Rivadeneira M.M., Hernández C.E. & Venditti C. (2020) The Origin and Correlated Evolution of Symbiosis and Coloniality in Scleractinian Corals. *Frontiers in Marine Science* **7**, 1–13.

Cardol P., Bailleul B., Rappaport F., Derelle E., Bé al D., cile Breyton C., … Finazzi G. (2008) *An original adaptation of photosynthesis in the marine green alga Ostreococcus*.

Cardol P., Forti G. & Finazzi G. (2011) Regulation of electron transport in microalgae. *Biochimica et Biophysica Acta - Bioenergetics* **1807**, 912–918.

Castro-Sanguino C. & Sánchez J.A. (2012) Dispersal of *Symbiodinium* by the stoplight parrotfish *Sparisoma viride*. *Biology Letters* **8**, 282–286.

Cheong K.Y., Jouhet J., Maréchal E. & Falkowski P.G. (2022) The redox state of the plastoquinone (PQ) pool is connected to thylakoid lipid saturation in a marine diatom. *Photosynthesis Research*.

Claquin P., Rene-Trouillefou M., Lopez P.J., Japaud A., Bouchon-Navaro Y., Cordonnier S. & Bouchon C. (2021) Singular physiological behavior of the scleractinian coral *Porites astreoides* in the dark phase. *Coral Reefs* **40**, 139–150.

Cohen I. & Dubinsky Z. (2015) Long term photoacclimation responses of the coral *Stylophora pistillata* to reciprocal deep to shallow transplantation: Photosynthesis and calcification. *Frontiers in Marine Science* **2**.

Colley N.J. & Trench R.K. (1985) Cellular events in the reestablishment of a symbiosis between a marine dinoflagellate and a coelenterate. *Cell and Tissue Research* **239**, 93–103.

Colombo M., Suorsa M., Rossi F., Ferrari R., Tadini L., Barbato R. & Pesaresi P. (2016) Photosynthesis control: An underrated short-term regulatory mechanism essential for plant viability. *Plant Signaling and Behavior* **11**, 1–6.

Crawley A., Kline D.I., Dunn S., Anthony K. & Dove S. (2010) The effect of ocean acidification on symbiont photorespiration and productivity in *Acropora formosa*. *Global Change Biology* **16**, 851–863.

Crossland C.J., Hatcher B.G. & Smith S. V. (1991) Role of coral reefs in global ocean production. *Coral Reefs* **10**, 55–64.

Crossland C.J., Barnes D.J. & Borowitzka M.A. (1980) Diurnal Lipid and Mucus Production in Coral. *Marine Biology* **60**, 81–90.

Cruz S., Dionísio G., Rosa R.U.I., Calado R., Cruz S., Dionísio G., … Calado R. (2012) Linked references are available on JSTOR for this article : Anesthetizing Solar-Powered Sea Slugs for Photobiological Studies. **223**, 328–336.

Cui G., Liew Y.J., Konciute M.K., Zhan Y., Hung S.H., Thistle J., … Aranda M. (2022) Nutritional control regulates symbiont proliferation and life history in coral-dinoflagellate symbiosis. *BMC Biology* **20**, 1–16.

Cunning R., Muller E.B., Gates R.D. & Nisbet R.M. (2017) A dynamic bioenergetic model for coral-*Symbiodinium* symbioses and coral bleaching as an alternate stable state. *Journal of Theoretical Biology* **431**, 49–62.

Curien G., Flori S., Villanova V., Magneschi L., Giustini C., Forti G., … Finazzi G. (2016) The water to water cycles in microalgae. *Plant and Cell Physiology* **57**, 1354–1363.

Dang K. Van, Pierangelini M., Roberty S. & Cardol P. (2019) Alternative Photosynthetic Electron Transfers and Bleaching Phenotypes Upon Acute Heat Stress in *Symbiodinium* and *Breviolum* spp. (Symbiodiniaceae) in Culture. *Frontiers in Marine Science* **6**.

Dang K. Van, Plet J., Tolleter D., Jokel M., Cuiné S., Carrier P., … Peltier G. (2014) Combined increases in mitochondrial cooperation and oxygen photoreduction compensate for deficiency in cyclic electron flow in *Chlamydomonas reinhardtii*. *Plant Cell* **26**, 3036–3050.

Dani V., Priouzeau F., Mertz M., Mondin M., Pagnotta S., Lacas-Gervais S., … Sabourault C. (2017) Expression patterns of sterol transporters NPC1 and NPC2 in the cnidarian–dinoflagellate symbiosis. *Cellular Microbiology* **19**.

Davis G.A. & Kramer D.M. (2020) Optimization of ATP Synthase c–Rings for Oxygenic Photosynthesis. *Frontiers in Plant Science* **10**, 1–13.

Davy S.K., Allemand D. & Weis V.M. (2012) Cell Biology of Cnidarian-Dinoflagellate Symbiosis. *Microbiology and Molecular Biology Reviews* **76**, 229–261.

Decelle J., Carradec Q., Pochon X., Henry N., Romac S., Mahé F., … de Vargas C. (2018) Worldwide Occurrence and Activity of the Reef-Building Coral Symbiont *Symbiodinium* in the Open Ocean. *Current Biology* **28**, 3625-3633.e3.

Djeghri N., Pondaven P., Stibor H. & Dawson M.N. (2019) Review of the diversity, traits, and ecology of zooxanthellate jellyfishes. *Marine Biology* **166**, 1–19.

Dorrell R.G. & Howe C.J. (2015) Integration of plastids with their hosts: Lessons learned from dinoflagellates. *Proceedings of the National Academy of Sciences of the United States of America* **112**, 10247–10254.

Dungan A.M., Maire J., Perez-Gonzalez A., Blackall L.L. & van Oppen M.J.H. (2022) Lack of evidence for the oxidative stress theory of bleaching in the sea anemone, *Exaiptasia diaphana*, under elevated temperature. *Coral Reefs* **41**, 1161–1172.

Emery M.A., Dimos B.A. & Mydlarz L.D. (2021) Cnidarian Pattern Recognition Receptor Repertoires Reflect Both Phylogeny and Life History Traits. *Frontiers in Immunology* **12**.

Fabina N.S., Putnam H.M., Franklin E.C., Stat M. & Gates R.D. (2012) Transmission Mode Predicts Specificity and Interaction Patterns in Coral-*Symbiodinium* Networks. *PLoS ONE* **7**, 1–9.

Falkowski P.G., Dubinsky Z., Muscatine L. & Porter J.W. (1984) Light and the Bioenergetics of a Symbiotic Coral. *BioScience* **34**, 705–709.

Fan D.Y., Fitzpatrick D., Oguchi R., Ma W., Kou J. & Chow W.S. (2016) Obstacles in the quantification of the cyclic electron flux around Photosystem I in leaves of C3 plants. *Photosynthesis Research* **129**, 239–251.

Ferrier-Pagès C., Martinez S., Grover R., Cybulski J., Shemesh E. & Tchernov D. (2021) Tracing the trophic plasticity of the coral-dinoflagellate symbiosis using amino acid compound-specific stable isotope analysis. *Microorganisms* **9**, 1–16.

Filacek A., Zivcak M., Barboricova M., Misheva S.P., Pereira E.G., Yang X. & Brestic M. (2022) Diversity of responses to nitrogen deficiency in distinct wheat genotypes reveals the role of alternative electron flows in photoprotection. *Photosynthesis Research 2022*, 1–18.

Fitt W.K. & Trench R.K. (1983) The Relation of Diel Patterns of Cell Division To Diel Patterns of Motility in the Symbiotic Dinoflagellate *Symbiodinium microadriaticum* Freudenthal in Culture. *New Phytologist* **94**, 421–432.

Fitzgerald L.M. & Szmant A.M. (1997) Biosynthesis of "essential" amino acids by scleractinian corals. *Biochemical Journal* **322**, 213–221.

Forsman Z.H., Page C.A., Toonen R.J. & Vaughan D. (2015) Growing coral larger and faster: Micro-colony-fusion as a strategy for accelerating coral cover. *PeerJ* **2015**.

Foyer C., Furbank R., Harbinson J. & Horton P. (1990) The mechanisms contributing to photosynthetic control of electron transport by carbon assimilation in leaves. *Photosynthesis Research* **25**, 83–100.

Fransolet D., Roberty S. & Plumier J.C. (2012) Establishment of endosymbiosis: The case of cnidarians and *Symbiodinium*. *Journal of Experimental Marine Biology and Ecology* **420**–**421**, 1–7.

Furla P., Richier S. & Allemand D. (2011) Physiological adaptation to symbiosis in cnidarians. In *Coral Reefs: An Ecosystem in Transition*. (eds Z. Dubinsky & N. Stambler), pp. 187–195.

Gates R.D., Baghdasarian G. & Muscatine L. (1992) Temperature stress causes host cell detachment in symbiotic cnidarians: implications for coral bleaching. *Biological Bulletin* **182**, 324–332.

Gates R.D., Hoegh-Guldberg O., McFall-Ngai M.J., Bil K.Y. & Muscatine L. (1995) Free amino acids exhibit anthozoan "host factor" activity: They induce the release of photosynthate from symbiotic dinoflagellates in vitro. *Proceedings of the National Academy of Sciences of the United States of America* **92**, 7430–7434.

Genty B., Briantais J.M. & Baker N.R. (1989) The relationship between the quantum yield of photosynthetic electron transport and quenching of chlorophyll fluorescence. *Biochimica et Biophysica Acta - General Subjects* **990**, 87–92.

Goiran C., Allemand D. & Galgani I. (1997) Transient Na+ stress in symbiotic dinoflagellates after isolation from coral-host cells and subsequent immersion in seawater. *Marine Biology* **129**, 581–589.

Goiran C., Al-Moghrabi S., Allemand D. & Jaubert J. (1996) Inorganic carbon uptake for photosynthesis by the symbiotic coral/dinoflagellate association: I. Photosynthetic performances of symbionts and dependence on sea water bicarbonate. *Journal of Experimental Marine Biology and Ecology* **199**, 207–225.

Gold D.A., Grabenstatter J., De Mendoza A., Riesgo A., Ruiz-Trillo I. & Summons R.E. (2016) Sterol and genomic analyses validate the sponge biomarker hypothesis. *Proceedings of the National Academy of Sciences of the United States of America* **113**, 2684–2689.

González-Pech R.A., Stephens T.G., Chen Y., Mohamed A.R., Cheng Y., Shah S., … Chan C.X. (2021) Comparison of 15 dinoflagellate genomes reveals extensive sequence and structural divergence in family Symbiodiniaceae and genus *Symbiodinium*. *BMC Biology* **19**, 1–22.

Goss R. & Lepetit B. (2015) Biodiversity of NPQ. *Journal of Plant Physiology* **172**, 13–32.

Hambleton E.A., Jones V.A.S., Maegele I., Kvaskoff D., Sachsenheimer T. & Guse A. (2019) Sterol transfer by atypical cholesterol-binding NPC2 proteins in coral-algal symbiosis. *eLife* **8**, 1–26.

Harriott V. (1985) Mortality rates of scleractinian corals before and during a mass bleaching event. *Marine Ecology Progress Series* **21**, 81–88.

Hawkins T.D., Hagemeyer J.C.G., Hoadley K.D., Marsh A.G. & Warner M.E. (2016) Partitioning of respiration in an animal-algal symbiosis: Implications for different aerobic capacity between *Symbiodinium* spp. *Frontiers in Physiology* **7**.

Hennige S.J., Suggett D.J., Warner M.E., McDougall K.E. & Smith D.J. (2009) Photobiology of *Symbiodinium* revisited: Bio-physical and bio-optical signatures. *Coral Reefs* **28**, 179–195.

Hertle A.P., Blunder T., Wunder T., Pesaresi P., Pribil M., Armbruster U. & Leister D. (2013) PGRL1 Is the Elusive Ferredoxin-Plastoquinone Reductase in Photosynthetic Cyclic Electron Flow. *Molecular Cell* **49**, 511–523.

Hill R., Larkum A.W.D., Prášil O., Kramer D.M., Szabó M., Kumar V. & Ralph P.J. (2012) Light-induced dissociation of antenna complexes in the symbionts of scleractinian corals correlates with sensitivity to coral bleaching. *Coral Reefs* **31**, 963–975.

Hill R., Larkum A., Frankart C., Kühl M. & Ralph P. (2004) Loss of Functional Photosystem II Reaction Centres in Zooxanthellae of Corals Exposed to Bleaching {…}. *Photosynthesis Research*, 59–72.

Hill R., Szabó M., Rehman A.U., Vass I., Ralph P.J. & Larkum A.W.D. (2014) Inhibition of photosynthetic CO_2 fixation in the coral *Pocillopora damicornis* and its relationship to thermal bleaching. *Journal of Experimental Biology* **217**, 2150–2162.

Hoegh-Guldberg O. & Jones R.J. (1999) Photoinhibition and photoprotection in symbiotic dinoflagellates from reef-building corals. *Marine Ecology Progress Series* **183**, 73–86.

Hughes D.J., Giannini F.C., Ciotti A.M., Doblin M.A., Ralph P.J., Varkey D., … Suggett D.J. (2021) Taxonomic Variability in the Electron Requirement for Carbon Fixation Across Marine Phytoplankton. *Journal of Phycology* **57**, 111–127.

Hughes T.P., Anderson K.D., Connolly S.R., Heron S.F., Kerry J.T., Lough J.M., ... Wilson S.K. (2018) Spatial and temporal patterns of mass bleaching of corals in the Anthropocene. *Science* **359**, 80–83.

Hume B.C.C., Ziegler M., Poulain J., Pochon X., Romac S., Boissin E., ... Voolstra C.R. (2018) An improved primer set and amplification protocol with increased specificity and sensitivity targeting the Symbiodinium ITS2 region. *PeerJ* **2018**.

Huot Y. & Babin M. (2010) *Chlorophyll a Fluorescence in Aquatic Sciences: Methods and Applications*.

Iglesias-Prieto R., Govind N.S. & Trench R.K. (1991) Apoprotein composition and spectroscopic characterization of the water-soluble peridinin-chlorophyll a-proteins from three symbiotic dinoflagellates. *Proceedings of the Royal Society B: Biological Sciences* **246**, 275–283.

Iglesias-Prieto R., Matta J.L., Robins W.A. & Trench R.K. (1992) Photosynthetic response to elevated temperature in the symbiotic dinoflagellate *Symbiodinium microadriaticum* in culture. *Proceedings of the National Academy of Sciences of the United States of America* **89**, 10302–10305.

Ishida K.I. & Green B.R. (2002) Second- and third-hand chloroplasts in dinoflagellates: Phylogeny of oxygen-evolving enhancer 1 (PsbO) protein reveals replacement of a nuclear-encoded plastid gene by that of a haptophyte tertiary endosymbiont. *Proceedings of the National Academy of Sciences of the United States of America* **99**, 9294–9299.

Ishikawa M., Shimizu H., Nozawa M., Ikeo K. & Gojobori T. (2016) Two-step evolution of endosymbiosis between hydra and algae. *Molecular Phylogenetics and Evolution* **103**, 19–25.

Jackson C., Knoll A.H., Chan C.X. & Verbruggen H. (2018) Plastid phylogenomics with broad taxon sampling further elucidates the distinct evolutionary origins and timing of secondary green plastids. *Scientific Reports* **8**, 1–10.

Janouškovec J., Horák A., Oborník M., Lukeš J. & Keeling P.J. (2010) A common red algal origin of the apicomplexan, dinoflagellate, and heterokont plastids. *Proceedings of the National Academy of Sciences of the United States of America* **107**, 10949–10954.

Jenks A. & Gibbs S.P. (2000) IMMUNOLOCALIZATION AND DISTRIBUTION OF FORM II RUBISCO IN THE PYRENOID AND CHLOROPLAST STROMA OF *AMPHIDINIUM CARTERAE* AND FORM I RUBISCO IN THE SYMBIONT-DERIVED PLASTIDS OF *PERIDINIUM FOLIACEUM* (DINOPHYCEAE). *Journal of Phycology* **36**, 127–138.

Jiang J., Zhang H., Kang Y., Bina D., Lo C.S. & Blankenship R.E. (2012) Characterization of the peridinin-chlorophyll a-protein complex in the dinoflagellate *Symbiodinium*. *Biochimica et Biophysica Acta - Bioenergetics* **1817**, 983–989.

Jiang J., Zhang H., Orf G.S., Lu Y., Xu W., Harrington L.B., … Blankenship R.E. (2014) Evidence of functional trimeric chlorophyll a/c2-peridinin proteins in the dinoflagellate *Symbiodinium*. *Biochimica et Biophysica Acta - Bioenergetics* **1837**, 1904–1912.

Jiang P.L., Pasaribu B. & Chen C.S. (2014) Nitrogen-deprivation elevates lipid levels in *Symbiodinium* spp. by lipid droplet accumulation: Morphological and compositional analyses. *PLoS ONE* **9**.

Jinkerson R.E., Russo J.A., Newkirk C.R., Kirk A.L., Chi R.J., Martindale M.Q., … Xiang T. (2022) Cnidarian-Symbiodiniaceae symbiosis establishment is independent of photosynthesis. *Current Biology* **32**, 2402-2415.e4.

Johnson J.E. & Berry J.A. (2021) The role of Cytochrome b 6f in the control of steady-state photosynthesis: a conceptual and quantitative model. *Photosynthesis Research* **148**, 101–136.

Johnson X., Vandystadt G., Bujaldon S., Wollman F.A., Dubois R., Roussel P., … Béal D. (2009) A new setup for in vivo fluorescence imaging of photosynthetic activity. *Photosynthesis research* **102**, 85–93.

Kagatani K., Nagao R., Shen J.R., Yamano Y., Takaichi S. & Akimoto S. (2022) Excitation relaxation dynamics of carotenoids constituting the diadinoxanthin cycle. *Photosynthesis Research*.

Kanazawa A., Blanchard G.J., Szabó M., Ralph P.J. & Kramer D.M. (2014) The site of regulation of light capture in *Symbiodinium*: Does the peridinin-chlorophyll a-protein detach to regulate light capture? *Biochimica et Biophysica Acta - Bioenergetics* **1837**, 1227–1234.

Kanazawa A., Neofotis P., Davis G.A., Fisher N. & Kramer D.M. (2020) Diversity in photoprotection and energy balancing in terrestrial and aquatic phototrophs. In *Photosynthesis in Algae:*

Biochemical and Physiological Mechanisms. (eds A.W.D. Larkum, A.R. Grossman & J.A. Raven), pp. 299–327. Spring Cham.

Kanazawa A., Ostendorf E., Kohzuma K., Hoh D., Strand D.D., Sato-Cruz M., … Kramer D.M. (2017) Chloroplast ATP synthase modulation of the thylakoid proton motive force: implications for photosystem I and photosystem II photoprotection. *Frontiers in Plant Science* **8**, 1–12.

Karako-Lampert S., Zoccola D., Salmon-Divon M., Katzenellenbogen M., Tambutté S., Bertucci A., … Levy O. (2014) Transcriptome analysis of the scleractinian coral *Stylophora pistillata*. *PLoS ONE* **9**.

Kato H., Tokutsu R., Kubota-Kawai H., Burton-Smith R.N., Kim E. & Minagawa J. (2020) Characterization of a giant PSI supercomplex in the symbiotic dinoflagellate symbiodiniaceae. *Plant Physiology* **183**, 1725–1734.

Kawaida H., Ohba K., Koutake Y., Shimizu H., Tachida H. & Kobayakawa Y. (2013) Symbiosis between hydra and chlorella: Molecular phylogenetic analysis and experimental study provide insight into its origin and evolution. *Molecular Phylogenetics and Evolution* **66**, 906–914.

Kayal E., Bentlage B., Sabrina Pankey M., Ohdera A.H., Medina M., Plachetzki D.C., … Ryan J.F. (2018) Phylogenomics provides a robust topology of the major cnidarian lineages and insights on the origins of key organismal traits. *BMC Evolutionary Biology* **18**.

Kemp D.W., Hernandez-Pech X., Iglesias-Prieto R., Fitt W.K. & Schmidt G.W. (2014) Community dynamics and physiology of *Symbiodinium* spp. before, during, and after a coral bleaching event. *Limnology and Oceanography* **59**, 788–797.

Khorobrykh S., Havurinne V., Mattila H. & Tyystjärvi E. (2020) Oxygen and ROS in photosynthesis. *Plants* **9**, 1–61.

Kitajima M. & Butler W.L. (1975) Quenching of Chlorophyll fluorescence and primary photochemistry in chloroplasts by Dibromothymoquinone. *Biochimica et Biophysica Acta* **376**, 105–115.

Klueter A., Crandall J.B., Archer F.I., Teece M.A. & Coffroth M.A. (2015) Taxonomic and environmental variation of metabolite profiles in marine dinoflagellates of the genus *Symbiodinium*. *Metabolites* **5**, 74–99.

Klughammer C. & Schreiber U. (2008) Saturation Pulse method for assessment of energy conversion in PS I. *PAM Application Notes* **1**, 11–14.

Klughammer C. & Schreiber U. (2016) Deconvolution of ferredoxin, plastocyanin, and P700 transmittance changes in intact leaves with a new type of kinetic LED array spectrophotometer. *Photosynthesis Research* **128**, 195–214.

Kopp C., Domart-Coulon I., Escrig S., Humbel B.M., Hignette M. & Meibom A. (2015) Subcellular investigation of photosynthesis-driven carbon assimilation in the symbiotic reef coral *Pocillopora damicornis*. *mBio* **6**.

Kowalczyk N., Rappaport F., Boyen C., Wollman F.A., Collén J. & Joliot P. (2013) Photosynthesis in *Chondrus crispus*: The contribution of energy spill-over in the regulation of excitonic flux. *Biochimica et Biophysica Acta - Bioenergetics* **1827**, 834–842.

Kozuleva M., Petrova A., Milrad Y., Semenov A., Ivanov B., Redding K.E. & Yacoby I. (2021) Phylloquinone is the principal Mehler reaction site within photosystem I in high light. *Plant Physiology* **186**, 1848–1858.

Kramer N., Guan J., Chen S., Wangpraseurt D. & Loya Y. (2022) Morpho-functional traits of the coral *Stylophora pistillata* enhance light capture for photosynthesis at mesophotic depths. *Communications Biology* **5**.

LaJeunesse T.C. (2002) Diversity and community structure of symbiotic dinoflagellates from Caribbean coral reefs. *Marine Biology* **141**, 387–400.

LaJeunesse T.C., Fitt W.K. & Schmidt G.W. (2010) The reticulated chloroplasts of zooxanthellae (*Symbiodinium*) and differences in chlorophyll localization among life cycle stages. *Coral Reefs* **29**, 627–627.

LaJeunesse T.C. (2005) "Species" radiations of symbiotic dinoflagellates in the Atlantic and Indo-Pacific since the Miocene-Pliocene transition. *Molecular Biology and Evolution* **22**, 570–581.

LaJeunesse T.C. (2017) Validation and description of *Symbiodinium microadriaticum*, the type species of *Symbiodinium* (Dinophyta). *Journal of Phycology* **53**, 1109–1114.

LaJeunesse T.C., Parkinson J.E., Gabrielson P.W., Jeong H.J., Reimer J.D., Voolstra C.R. & Santos S.R. (2018) Systematic Revision of Symbiodiniaceae Highlights the Antiquity and Diversity of Coral Endosymbionts. *Current Biology* **28**, 2570–2580.

Lampert K.P. (2016) *Cassiopea* and Its Zooxanthellae. In *The Cnidaria, Past, Present and Future*. (eds S. Goffredo & Z. Dubinsky), pp. 415–423.

Lawrenz E., Silsbe G., Capuzzo E., Ylöstalo P., Forster R.M., Simis S.G.H., … Suggett D.J. (2013) Predicting the Electron Requirement for Carbon Fixation in Seas and Oceans. *PLoS ONE* **8**.

Leggat W., Badger M.R. & Yellowlees D. (1999) Evidence for an inorganic carbon-concentrating mechanism in the symbiotic dinoflagellate *Symbiodinium* sp. *Plant Physiology* **121**, 1247–1255.

Leggat W., Whitney S. & Yellowlees D. (2004) Is coral bleaching due to the instability of the zooxanthellae dark reactions? *Symbiosis* **37**, 137–153.

Lehnert E.M., Mouchka M.E., Burriesci M.S., Gallo N.D., Schwarz J.A. & Pringle J.R. (2014) Extensive differences in gene expression between symbiotic and aposymbiotic cnidarians. *G3: Genes, Genomes, Genetics* **4**, 277–295.

Lesser M.P. (1997) Oxidative stress causes coral bleaching during exposure to elevated temperatures. *Coral Reefs* **16**, 187–192.

Lesser M.P. (1996) Elevated temperatures and ultraviolet radiation cause oxidative stress and inhibit photosynthesis in symbiotic dinoflagellates. *Limnology and Oceanography* **41**, 271–283.

Levy S., Elek A., Grau-Bové X., Menéndez-Bravo S., Iglesias M., Tanay A., … Sebé-Pedrós A. (2021) A stony coral cell atlas illuminates the molecular and cellular basis of coral symbiosis, calcification, and immunity. *Cell* **184**, 2973-2987.e18.

Lewis L.A. & Muller-Parker G. (2004) Phylogenetic placement of "zoochlorellae" (Chlorophyta), algal symbiont of the temperate sea anemone Anthopleura elegantissima. *Biological Bulletin* **207**, 87–92.

Lilley R.M., Ralph P.J. & Larkum A.W.D. (2010) The determination of activity of the enzyme Rubisco in cell extracts of the dinoflagellate alga *Symbiodinium* sp. by manganese

chemiluminescence and its response to short-term thermal stress of the alga. *Plant, Cell and Environment* **33**, 995–1004.

Loussert-Fonta C., Toullec G., Paraecattil A.A., Jeangros Q., Krueger T., Escrig S. & Meibom A. (2020) Correlation of fluorescence microscopy, electron microscopy, and NanoSIMS stable isotope imaging on a single tissue section. *Communications Biology* **3**, 1–10.

Lu Y., Jiang J., Zhao H., Han X., Xiang Y. & Zhou W. (2020) Clade-Specific Sterol Metabolites in Dinoflagellate Endosymbionts Are Associated with Coral Bleaching in Response to Environmental Cues. *mSystems* **5**.

Lyndby N.H., Rädecker N., Bessette S., Søgaard Jensen L.H., Escrig S., Trampe E., … Meibom A. (2020) Amoebocytes facilitate efficient carbon and nitrogen assimilation in the *Cassiopea*-Symbiodiniaceae symbiosis: Nutrient transport in Cassiopea. *Proceedings of the Royal Society B: Biological Sciences* **287**.

Maas D.L., Capriati A., Ahmad A., Erdmann M. V., Lamers M., de Leeuw C.A., … Becking L.E. (2020) Recognizing peripheral ecosystems in marine protected areas: A case study of golden jellyfish lakes in Raja Ampat, Indonesia. *Marine Pollution Bulletin* **151**, 110700.

Malone L.A., Proctor M.S., Hitchcock A., Hunter C.N. & Johnson M.P. (2021) Cytochrome b6f – Orchestrator of photosynthetic electron transfer. *Biochimica et Biophysica Acta - Bioenergetics* **1862**, 148380.

Maor-Landaw K., van Oppen M.J.H. & McFadden G.I. (2020) Symbiotic lifestyle triggers drastic changes in the gene expression of the algal endosymbiont *Breviolum minutum* (Symbiodiniaceae). *Ecology and Evolution* **10**, 451–466.

Martin L.E., Dawson M.N., Bell L.J. & Colin P.L. (2006) Marine lake ecosystem dynamics illustrate ENSO variation in the tropical western Pacific. *Biology Letters* **2**, 144–147.

Maruyama S., Shoguchi E., Satoh N. & Minagawa J. (2015) Diversification of the light-harvesting complex gene family via intra- and intergenic duplications in the coral symbiotic alga *Symbiodinium*. *PLoS ONE* **10**.

Mashini A.G., Oakley C.A., Grossman A.R., Weis V.M. & Davy S.K. (2022) Immunolocalization of Metabolite Transporter Proteins in a Model Cnidarian-Dinoflagellate Symbiosis. *Applied and Environmental Microbiology* **88**.

Mathiot C. & Alric J. (2021) Standard units for ElectroChromic Shift measurements in plant biology. *Journal of Experimental Botany* **72**, 6467–6473.

Maxwell K. & Johnson G.N. (2000) Chlorophyll fluorescence-a practical guide. *Journal of Experimental Botany* **51**, 659–668.

Mayfield A.B. & Gates R.D. (2007) Osmoregulation in anthozoan-dinoflagellate symbiosis. *Comparative Biochemistry and Physiology - A Molecular and Integrative Physiology* **147**, 1–10.

Mayfield A.B., Hsiao Y.Y., Chen H.K. & Chen C.S. (2014) Rubisco Expression in the Dinoflagellate *Symbiodinium* sp. Is Influenced by Both Photoperiod and Endosymbiotic Lifestyle. *Marine Biotechnology* **16**, 371–384.

McCloskey L.R., Muscatine L. & Wilkerson F.P. (1994) Daily photosynthesis, respiration, and carbon budgets in a tropical marine jellyfish (Mastigias sp.). *Marine Biology* **119**, 13–22.

Medrano E., Merselis D.G., Bellantuono A.J. & Rodriguez-Lanetty M. (2019) Proteomic basis of symbiosis: A heterologous partner fails to duplicate homologous colonization in a novel cnidarian-symbiodiniaceae mutualism. *Frontiers in Microbiology* **10**, 1–15.

Mies M., Güth A.Z., Castro C.B., Pires D.O., Calderon E.N., Pompeu M. & Sumida P.Y.G. (2018) Bleaching in reef invertebrate larvae associated with *Symbiodinium* strains within clades A–F. *Marine Biology* **165**, 1–9.

Mies M., Sumida P.Y.G., Rädecker N. & Voolstra C.R. (2017) Marine invertebrate larvae associated with *Symbiodinium*: A mutualism from the start? *Frontiers in Ecology and Evolution* **5**.

Minagawa J. (2011) State transitions-the molecular remodeling of photosynthetic supercomplexes that controls energy flow in the chloroplast. *Biochimica et Biophysica Acta - Bioenergetics* **1807**, 897–905.

Mohamed A.R., Cumbo V., Harii S., Shinzato C., Chan C.X., Ragan M.A., … Miller D.J. (2016) The transcriptomic response of the coral *Acropora digitifera* to a competent *Symbiodinium* strain: The symbiosome as an arrested early phagosome. *Molecular Ecology* **25**, 3127–3141.

Mohammad Aslam S., Patil P.P., Vass I. & Szabó M. (2022) Heat-Induced Photosynthetic Responses of Symbiodiniaceae Revealed by Flash-Induced Fluorescence Relaxation Kinetics. *Frontiers in Marine Science* **9**, 1–12.

Muller-Parker G. (1984) Dispersal of Zooxanthellae on Coral Reefs by Predators on Cnidarians. *Biological Bulletin* **167**, 159–167.

Mungpakdee S., Shinzato C., Takeuchi T., Kawashima T., Koyanagi R., Hisata K., … Shoguchi E. (2014) Massive gene transfer and extensive RNA editing of a symbiotic dinoflagellate plastid genome. *Genome Biology and Evolution* **6**, 1408–1422.

Muscatine L., Falkowski P.G., Porter J.W. & Dubinsky Z. (1984) Fate of photosynthetic fixed carbon in light- and shade-adapted colonies of the symbiotic coral *Stylophora pistillata*. *Proceedings of the Royal Society B: Biological Sciences* **222**, 181–202.

Naumann M.S., Haas A., Struck U., Mayr C., el-Zibdah M. & Wild C. (2010) Organic matter release by dominant hermatypic corals of the Northern Red Sea. *Coral Reefs* **29**, 649–659.

Naumann M.S., Richter C., Mott C., El-Zibdah M., Manasrah R. & Wild C. (2012) Budget of coral-derived organic carbon in a fringing coral reef of the Gulf of Aqaba, Red Sea. *Journal of Marine Systems* **105**–**108**, 20–29.

Nawrocki W.J., Bailleul B., Picot D., Cardol P., Rappaport F., Wollman F.A. & Joliot P. (2019) The mechanism of cyclic electron flow. *Biochimica et Biophysica Acta - Bioenergetics* **1860**, 433–438.

Nawrocki W.J., Buchert F., Joliot P., Rappaport F., Bailleul B. & Wollman F.A. (2019) Chlororespiration controls growth under intermittent light. *Plant Physiology* **179**, 630–639.

Nawrocki W.J., Tourasse N.J., Taly A., Rappaport F. & Wollman F.A. (2015) The plastid terminal oxidase: Its elusive function points to multiple contributions to plastid physiology. *Annual Review of Plant Biology* **66**, 49–74.

Niedzwiedzki D.M., Jiang J., Lo C.S. & Blankenship R.E. (2014) Spectroscopic properties of the Chlorophyll a-Chlorophyll c 2-Peridinin-Protein-Complex (acpPC) from the coral symbiotic dinoflagellate Symbiodinium. *Photosynthesis Research* **120**, 125–139.

Niedzwiedzki D.M., Magdaong N.C.M., Su X. & Liu H. (2022) Biochemical and spectroscopic characterizations of the oligomeric antenna of the coral symbiotic Symbiodiniaceae *Fugacium kawagutii*. *Photosynthesis Research*.

Norris B.J. & Miller D.J. (1994) Nucleotide sequence of a cDNA clone encoding the precursor of the peridinin-chlorophyll a-binding protein from the dinoflagellate *Symbiodinium* sp. *Plant Molecular Biology* **24**, 673–677.

Oakley C.A., Ameismeier M.F., Peng L., Weis V.M., Grossman A.R. & Davy S.K. (2016) Symbiosis induces widespread changes in the proteome of the model cnidarian Aiptasia. *Cellular Microbiology* **18**, 1009–1023.

Oakley C.A., Schmidt G.W. & Hopkinson B.M. (2014) Thermal responses of *Symbiodinium* photosynthetic carbon assimilation. *Coral Reefs* **33**, 501–512.

Osinga R., Schutter M., Griffioen B., Wijffels R.H., Verreth J.A.J., Shafir S., … Lavorano S. (2011) The Biology and Economics of Coral Growth. *Marine Biotechnology* **13**, 658–671.

Ousley S., de Beer D., Bejarano S. & Chennu A. (2022) High-Resolution Dynamics of Hydrogen Peroxide on the Surface of Scleractinian Corals in Relation to Photosynthesis and Feeding. *Frontiers in Marine Science* **9**, 1–14.

Peers G. & Price N.M. (2006) Copper-containing plastocyanin used for electron transport by an oceanic diatom. *Nature* **441**, 341–344.

Peltier G., Aro E.M. & Shikanai T. (2016) NDH-1 and NDH-2 Plastoquinone Reductases in Oxygenic Photosynthesis. *Annual Review of Plant Biology* **67**, 55–80.

Peltier G. & Schmidt G.W. (1991) Chlororespiration: An adaptation to nitrogen deficiency in *Chlamydomonas reinhardtii*. *Proceedings of the National Academy of Sciences of the United States of America* **88**, 4791–4795.

Peng S.E., Wang Y.B., Wang L.H., Chen W.N.U., Lu C.Y., Fang L.S. & Chen C.S. (2010) Proteomic analysis of symbiosome membranes in cnidaria - Dinoflagellate endosymbiosis. *Proteomics* **10**, 1002–1016.

Pernice M., Meibom A., Van Den Heuvel A., Kopp C., Domart-Coulon I., Hoegh-Guldberg O. & Dove S. (2012) A single-cell view of ammonium assimilation in coral-dinoflagellate symbiosis. *ISME Journal* **6**, 1314–1324.

Pfündel E.E., Klughammer C., Meister A. & Cerovic Z.G. (2013) Deriving fluorometer-specific values of relative PSI fluorescence intensity from quenching of F0 fluorescence in leaves of Arabidopsis thaliana and Zea mays. *Photosynthesis Research* **114**, 189–206.

Pierangelini M., Thiry M. & Cardol P. (2020) Different levels of energetic coupling between photosynthesis and respiration do not determine the occurrence of adaptive responses of Symbiodiniaceae to global warming. *New Phytologist* **228**, 855–868.

Pochon X. & LaJeunesse T.C. (2021) *Miliolidium* n. gen, a New Symbiodiniacean Genus Whose Members Associate with Soritid Foraminifera or Are Free-Living. *Journal of Eukaryotic Microbiology* **68**, 1–9.

Polívka T. & Hofmann E. (2014) Structure-Function Relatioship in Peridinin-Chlorophyll Proteins. In *The Structural Basis of Biological Energy Generation, Advances in Photosynthesis and Respiration*. (ed M.F. Hofmann-Marriott), pp. 39–58. Springer Dordrecht.

Putnam H.M., Barott K.L., Ainsworth T.D. & Gates R.D. (2017) The Vulnerability and Resilience of Reef-Building Corals. *Current Biology* **27**, R528–R540.

Quigley K.M., Willis B.L. & Kenkel C.D. (2019) Transgenerational inheritance of shuffled symbiont communities in the coral *Montipora digitata*. *Scientific Reports* **9**, 1–11.

Ralph P.J. & Gademann R. (2005) Rapid light curves: A powerful tool to assess photosynthetic activity. *Aquatic Botany* **82**, 222–237.

Ralph P.J., Gademann R. & Larkum A.W.D. (2001) Zooxanthellae expelled from bleached corals at 33°C are photosynthetically competent. *MARINE ECOLOGY PROGRESS SERIES Mar Ecol Prog Ser Published* **Vol. 220:**, 164–168.

Raven J.A., Suggett D.J. & Giordano M. (2020) Inorganic carbon concentrating mechanisms in free-living and symbiotic dinoflagellates and chromerids. *Journal of Phycology* **56**, 1377–1397.

Reaka-Kudla M.L. (1997) The Global Biodiversity of Coral Reefs: A comparison with Rain Forests. In *Biodiversity II: Understanding and Protecting Our Biological Resources*. pp. 83–108.

Rees T.A.V. (1991) Are symbiotic algae nutrient deficient? *Proceedings of the Royal Society B: Biological Sciences* **243**, 227–233.

Reich H.G., Robertson D.L. & Goodbody-Gringley G. (2017) Do the shuffle: Changes in *Symbiodinium* consortia throughout juvenile coral development. *PLoS ONE* **12**, 1–18.

Reynolds J.M.C., Bruns B.U., Fitt W.K. & Schmidt G.W. (2008) Enhanced photoprotection pathways in symbiotic dinoflagellates of shallow-water corals and other cnidarians. *Proceedings of the National Academy of Sciences of the United States of America* **105**, 17206.

Richier S., Furla P., Plantivaux A., Merle P.L. & Allemand D. (2005) Symbiosis-induced adaptation to oxidative stress. *Journal of Experimental Biology* **208**, 277–285.

Roberty S., Fransolet D., Cardol P., Plumier J.C. & Franck F. (2015) Imbalance between oxygen photoreduction and antioxidant capacities in *Symbiodinium* cells exposed to combined heat and high light stress. *Coral Reefs* **34**, 1063–1073.

Roberty S., Bailleul B., Berne N., Franck F. & Cardol P. (2014) PSI Mehler reaction is the main alternative photosynthetic electron pathway in *Symbiodinium* sp., symbiotic dinoflagellates of cnidarians. *New Phytologist* **204**, 81–91.

Roberty S., Béraud E., Grover R. & Ferrier-Pagès C. (2020) Coral productivity is co-limited by bicarbonate and ammonium availability. *Microorganisms* **8**.

Robison J.D. & Warner M.E. (2006) Differential impacts of photoacclimation and thermal stress on the photobiology of four different phylotypes of *Symbiodinium* (Pyrrhophyta). *Journal of Phycology* **42**, 568–579.

Roháček K. & Barták M. (1999) Technique of the modulated chlorophyll fluorescence: Basic concepts, useful parameters, and some applications. *Photosynthetica* **37**, 339–363.

Rodríguez-Román A. & Iglesias-Prieto R. (2005) Regulation of photochemical activity in cultured symbiotic dinoflagellates under nitrate limitation and deprivation. *Marine Biology* **146**, 1063–1073.

Roth M.S. (2014) The engine of the reef: Photobiology of the coral-algal symbiosis. *Frontiers in Microbiology* **5**, 1–22.

Rowan R. (2004) Thermal adaptation in reef coral symbionts. *Nature* **430**, 2004–2004.

Rowan R., Whitney S.M., Fowler A. & Yellowlees D. (1996) Rubisco in marine symbiotic dinoflagellates: Form II enzymes in eukaryotic oxygenic phototrophs encoded by a nuclear multigene family. *Plant Cell* **8**, 539–553.

Ruban A. V. & Wilson S. (2021) The mechanism of non-photochemical quenching in plants: Localization and driving forces. *Plant and Cell Physiology* **62**, 1063–1072.

Rydzy M., Tracz M., Szczepaniak A. & Grzyb J. (2021) Insights into the structure of rubisco from dinoflagellates-in silico studies. *International Journal of Molecular Sciences* **22**.

Saragosti E., Tchernov D., Katsir A. & Shaked Y. (2010) Extracellular production and degradation of superoxide in the coral *Stylophora pistillata* and cultured *Symbiodinium*. *PLoS ONE* **5**, 1–10.

Schansker G. (2022) Determining photosynthetic control, a probe for the balance between electron transport and Calvin–Benson cycle activity, with the DUAL-KLAS-NIR. *Photosynthesis Research* **153**, 191–204.

Schreiber U. (2017) Redox changes of ferredoxin, P700, and plastocyanin measured simultaneously in intact leaves. *Photosynthesis Research* **134**, 343–360.

Schubert N. & García-Mendoza E. (2008) Photoinhibition in red algal species with different carotenoid profiles. *Journal of Phycology* **44**, 1437–1446.

Shahhosseiny M.H., Mostafavi P.G., Fatemi S.M.R. & Karimi E. (2011) Clade identification of symbiotic zooxanthellae of dominant Scleractinian coral species of intertidal pools in Hengam Island. *African Journal of Biotechnology* **10**, 1502–1506.

Shikanai T. & Yamamoto H. (2017) Contribution of Cyclic and Pseudo-cyclic Electron Transport to the Formation of Proton Motive Force in Chloroplasts. *Molecular Plant* **10**, 20–29.

Shimakawa G., Shoguchi E., Burlacot A., Ifuku K., Che Y., Kumazawa M., … Nakanishi S. (2022) Coral symbionts evolved a functional polycistronic flavodiiron gene. *Photosynthesis Research* **151**, 113–124.

Shoguchi E., Beedessee G., Hisata K., Tada I., Narisoko H., Satoh N., … Shinzato C. (2021) A New Dinoflagellate Genome Illuminates a Conserved Gene Cluster Involved in Sunscreen Biosynthesis. *Genome biology and evolution* **13**, 1–7.

Silverstein R.N., Correa A.M.S. & Baker A.C. (2012) Specificity is rarely absolute in coral–algal symbiosis: Implications for coral response to climate change. *Proceedings of the Royal Society B: Biological Sciences* **279**, 2609–2618.

Slavov C., Schrameyer V., Reus M., Ralph P.J., Hill R., Büchel C., … Holzwarth A.R. (2016) "Super-quenching" state protects Symbiodinium from thermal stress - Implications for coral bleaching. *Biochimica et Biophysica Acta - Bioenergetics* **1857**, 840–847.

Smith D.J., Suggett D.J. & Baker N.R. (2005) Is photoinhibition of zooxanthellae photosynthesis the primary cause of thermal bleaching in corals? *Global Change Biology* **11**, 1–11.

Sproles A.E., Kirk N.L., Kitchen S.A., Oakley C.A., Grossman A.R., Weis V.M. & Davy S.K. (2018) Phylogenetic characterization of transporter proteins in the cnidarian-dinoflagellate symbiosis. *Molecular Phylogenetics and Evolution* **120**, 307–320.

Stahl-Rommel S., Kalra I., D'Silva S., Hahn M.M., Popson D., Cvetkovska M. & Morgan-Kiss R.M. (2022) Cyclic electron flow (CEF) and ascorbate pathway activity provide constitutive photoprotection for the photopsychrophile, *Chlamydomonas* sp. UWO 241 (renamed *Chlamydomonas priscuii*). *Photosynthesis Research* **151**, 235–250.

Stambler N. (2011) Zooxanthellae: The yellow Symbionts Inside Animals. In *Coral Reefs: An Ecosystem in Transition*. pp. 1–552.

Starzak D.E., Quinnell R.G., Nitschke M.R. & Davy S.K. (2014) The influence of symbiont type on photosynthetic carbon flux in a model cnidarian-dinoflagellate symbiosis. *Marine Biology* **161**, 711–724.

Stochaf W.R. & Grossman A.R. (1997) DIFFERENCES IN THE PROTEIN PROFILES OF CULTURED AND ENDOSYMBIOTIC *SYMBIODINIUM* SP . (PYRROPHYTA) FROM THE ANEMONE *AIPTASIA PALLIDA* (ANTHOZOA). *Journal of Phy* **33**, 44–53.

Strand D.D., Fisher N. & Kramer D.M. (2017) The higher plant plastid NAD(P)H dehydrogenase-like complex (NDH) is a high efficiency proton pump that increases ATP production by cyclic electron flow. *Journal of Biological Chemistry* **292**, 11850–11860.

Streamer M., McNeil Y.R. & Yellowlees D. (1993) Photosynthetic carbon dioxide fixation in zooxanthellae. *Marine Biology* **115**, 195–198.

Suggett D.J., Goyen S., Evenhuis C., Szabó M., Pettay D.T., Warner M.E. & Ralph P.J. (2015) Functional diversity of photobiological traits within the genus *Symbiodinium* appears to be governed by the interaction of cell size with cladal designation. *New Phytologist* **208**, 370–381.

Suggett D.J., MacIntyre H.L., Kana T.M. & Geider R.J. (2009) Comparing electron transport with gas exchange: Parameterising exchange rates between alternative photosynthetic currencies for eukaryotic phytoplankton. *Aquatic Microbial Ecology* **56**, 147–162.

Suggett D.J., Warner M.E., Smith D.J., Davey P., Hennige S. & Baker N.R. (2008) Photosynthesis and production of hydrogen peroxide by *Symbiodinium* (Pyrrhophyta) phylotypes with different thermal tolerances. *Journal of Phycology* **44**, 948–956.

Supasri K.M., Kumar M., Mathew M.J., Signal B., Padula M.P., Suggett D.J. & Ralph P.J. (2021) Evaluation of Filter, Paramagnetic, and STAGETips Aided Workflows for Proteome Profiling of Symbiodiniaceae Dinoflagellate. *Processes* **9**, 1–18.

Swain T.D., Westneat M.W., Backman V. & Marcelino L.A. (2018) Phylogenetic analysis of symbiont transmission mechanisms reveal evolutionary patterns in thermotolerance and host specificity that enhance bleaching resistance among vertically transmitted *Symbiodinium*. *European Journal of Phycology* **53**, 443–459.

Szabo M., Larkum A.W.D. & Vass I. (2020) A Review: The role of Reactive Oxygen Species in Mass Coral Bleaching. In *Photosynthesis in Algae: Biochemical and Physiological Mechanisms*. (eds A.W.D. Larkum, A.R. Grossman & J.A. Raven), pp. 459–488. Springer Cham.

Szabó M., Larkum A.W.D., Suggett D.J., Vass I., Sass L., Osmond B., … Chow W.S. (2017) Non-intrusive Assessment of Photosystem II and Photosystem I in Whole Coral Tissues. *Frontiers in Marine Science* **4**.

Takahashi S. & Murata N. (2006) Glycerate-3-phosphate, produced by CO2 fixation in the Calvin cycle, is critical for the synthesis of the D1 protein of photosystem II. *Biochimica et Biophysica Acta - Bioenergetics* **1757**, 198–205.

Takahashi S., Whitney S., Itoh S., Maruyama T. & Badger M. (2008) Heat stress causes inhibition of the de novo synthesis of antenna proteins and photobleaching in cultured *Symbiodinium*. *Proceedings of the National Academy of Sciences of the United States of America* **105**, 4203–4208.

Tambutté S., Holcomb M., Ferrier-Pagès C., Reynaud S., Tambutté É., Zoccola D. & Allemand D. (2011) Coral biomineralization: From the gene to the environment. *Journal of Experimental Marine Biology and Ecology* **408**, 58–78.

Tamir R., Eyal G., Kramer N., Laverick J.H. & Loya Y. (2019) Light environment drives the shallow-to-mesophotic coral community transition. *Ecosphere* **10**.

Tchernov D., Gorbunov M.Y., De Vargas C., Yadav S.N., Milligant A.J., Häggblom M. & Falkowski P.G. (2004) Membrane lipids of symbiotic algae are diagnostic of sensitivity to thermal bleaching in corals. *Proceedings of the National Academy of Sciences of the United States of America* **101**, 13531–13535.

Tian L., Xu P., Chukhutsina V.U., Holzwarth A.R. & Croce R. (2017) Zeaxanthin-dependent nonphotochemical quenching does not occur in photosystem i in the higher plant *Arabidopsis thaliana*. *Proceedings of the National Academy of Sciences of the United States of America* **114**, 4828–4832.

Tikhonov A.N. (2014) The cytochrome b6f complex at the crossroad of photosynthetic electron transport pathways. *Plant Physiology and Biochemistry* **81**, 163–183.

Tikkanen M., Grieco M., Nurmi M., Rantala M., Suorsa M. & Aro E.M. (2012) Regulation of the photosynthetic apparatus under fluctuating growth light. *Philosophical Transactions of the Royal Society B: Biological Sciences* **367**, 3486–3493.

Tivey T.R., Parkinson J.E. & Weis V.M. (2020) Host and symbiont cell cycle coordination is mediated by symbiotic state, nutrition, and partner identity in a model cnidarian-dinoflagellate symbiosis. *mBio* **11**, 1–17.

Tóth S.Z., Schansker G. & Strasser R.J. (2007) A non-invasive assay of the plastoquinone pool redox state based on the OJIP-transient. *Photosynthesis Research* **93**, 193–203.

Tresguerres M., Barott K.L., Barron M.E., Deheyn D.D., Kline D.I. & Linsmayer L.B. (2017) Acid-Base Balance and Nitrogen Excretion in Invertebrates. *Acid-Base Balance and Nitrogen Excretion in Invertebrates*, 193–218.

Turnham K.E., Wham D.C., Sampayo E. & LaJeunesse T.C. (2021) Mutualistic microalgae co-diversify with reef corals that acquire symbionts during egg development. *ISME Journal* **15**, 3271–3285.

Ulstrup K.E., Hill R. & Ralph P.J. (2005) Photosynthetic impact of hypoxia on in hospite zooxanthellae in the scleractinian coral Pocillopora damicornis. *Marine Ecology Progress Series* **286**, 125–132.

Uribe A. & Moreno-Sánchez R. (1992) Energy-dependent reactions supported by several substrates in coupled *Euglena gracilis* mitochondria. *Plant Science* **86**, 21–32.

van Oppen M.J.H., Baker A.C., Coffroth M.A. & Willis B.L. (2009) Bleaching Resistance and the Role of Algal Endosymbionts. In *Coral Bleaching. Patterns, Processes, Causes and Consequences*. (eds M.J.H. van Oppen & J.M. Lough), pp. 83–102. Springer-Verlag Berlin Heiderlberg.

van Oppen M.J.H. & Lough J.M. (2018) *Coral Bleaching: Patterns, Processes, Causes and Consequences*. (eds M.J.H. van Oppen & J.M. Lough), Springer.

Vega De Luna F., Dang K. Van, Cardol M., Roberty S. & Cardol P. (2019) Photosynthetic capacity of the endosymbiotic dinoflagellate *Cladocopium* sp. is preserved during digestion of its jellyfish host *Mastigias papua* by the anemone *Entacmaea medusivora*. *FEMS Microbiology Ecology* **95**, 1–7.

Viola S., Sellés J., Bailleul B., Joliot P. & Wollman F.A. (2021) In vivo electron donation from plastocyanin and cytochrome c6 to PSI in Synechocystis sp. PCC6803. *Biochimica et Biophysica Acta - Bioenergetics* **1862**.

Wakefield T.S., Farmer M.A. & Kempf S.C. (2000) Revised description of the fine structure of in situ "Zooxanthellae" genus *Symbiodinium*. *Biological Bulletin* **199**, 76–84.

Wang D.Z., Dong H.P., Li C., Xie Z.X., Lin L. & Hong H.S. (2011) Identification and characterization of cell wall proteins of a toxic dinoflagellate *Alexandrium catenella* using 2-D DIGE and MALDI TOF-TOF mass spectrometry. *Evidence-based Complementary and Alternative Medicine* **2011**.

Wang J.T. & Douglas A.E. (1998) Nitrogen recycling or nitrogen conservation in an alga-invertebrate symbiosis? *Journal of Experimental Biology* **201**, 2445–2453.

Wang J., Chen J., Wang S., Li F., Fu C. & Wang Y. (2021) Monoclonal Culture and Characterization of Symbiodiniaceae C1 Strain From the Scleractinian Coral *Galaxea fascicularis*. *Frontiers in Physiology* **11**, 1–10.

Warner M.E. & Berry-Lowe S. (2006) Differential xanthophyll cycling and photochemical activity in symbiotic dinoflagellates in multiple locations of three species of Caribbean coral. *Journal of Experimental Marine Biology and Ecology* **339**, 86–95.

Witt H.T. (1979) Energy conversion in the functional membrane of photosynthesis. Analysis by light pulse and electric pulse methods. The central role of the electric field. *BBA Reviews On Bioenergetics* **505**, 355–427.

Witt H., Bordignon E., Carbonera D., Dekker J.P., Karapetyan N., Teutloff C., … Schlodder E. (2003) Species-specific differences of the spectroscopic properties of P700: Analysis of the influence of non-conserved amino acid residues by site-directed mutagenesis of photosystem I from Chlamydomonas reinhardtii. *Journal of Biological Chemistry* **278**, 46760–46771.

Wooldridge S.A. (2013) Breakdown of the coral-algae symbiosis: Towards formalising a linkage between warm-water bleaching thresholds and the growth rate of the intracellular zooxanthellae. *Biogeosciences* **10**, 1647–1658.

Xiang T., Jinkerson R.E., Clowez S., Tran C., Krediet C.J., Onishi M., … Grossman A.R. (2018) Glucose-induced trophic shift in an endosymbiont dinoflagellate with physiological and molecular consequences. *Plant Physiology* **176**, 1793–1807.

Xiang T., Lehnert E., Jinkerson R.E., Clowez S., Kim R.G., DeNofrio J.C., … Grossman A.R. (2020) Symbiont population control by host-symbiont metabolic interaction in Symbiodiniaceae-cnidarian associations. *Nature Communications* **11**, 1–9.

Xu Y., Zhang J., Huang H., Yuan X., Zhang J. & Ge J. (2022) Coral Symbiosis Carbon Flow: A Numerical Model Study Spanning Cellular to Ecosystem Levels. *Frontiers in Marine Science* **9**, 1–19.

Yamashita H., Kobiyama A. & Koike K. (2009) Do Uric Acid Deposits in Zooxanthellae Function as Eye-Spots? *PLoS ONE* **4**.

Yamashita H. & Koike K. (2015) Biology of Symbiotic Dinoflagellates (Symbiodinium) in Corals. In *Marine Protists: Diversity and Dynamics*. (eds S. Ohtsuka, T. Suzaki, T. Horiguchi, N. Suzuki & F. Not), pp. 421–439. Springer Tokyo.

Yoon H.S., Hackett J.D. & Bhattacharya D. (2018) A single origin of the peridinin- and fucoxanthin-containing plastids in dinoflagellates through tertiary endosymbiosis. *Proceedings of the National Academy of Sciences* **99**, 11724–11729.

Zhang Y., Ip J.C.H., Xie J.Y., Yeung Y.H., Sun Y. & Qiu J.W. (2022) Host–symbiont transcriptomic changes during natural bleaching and recovery in the leaf coral *Pavona decussata*. *Science of the Total Environment* **806**, 150656.